THE UNIVERSITY OF ASTON IN BIRMINGHAM

A FORCED AIR CONVECTION METHOD FOR NON-CONTACT TEMPERATURE MEASUREMENT OF SURFACES

A Thesis Submitted for the Degree of

DOCTOR OF PHILOSOPHY

by

IAN ROBERT FOTHERGILL M.Sc., M.Inst.P.

Physics Department
May 1974

ABSTRACT

Methods of non-contact temperature measurement have been examined; emphasis being placed on radiation pyrometry. Such methods are vulnerable to emissivity errors unless blackbody emitters are involved. There are however several ways of minimizing these errors and the underlying theoretical principles of the major ones have been discussed.

The author has developed a non-contact temperature measuring technique employing forced air convection to avoid emissivity errors.

The technique exploits the phenomenon of heat transfer between a surface and air flowing over it when a temperature differential exists between the two. Two modes of temperature measurement have been examined, one involving initially unheated air and the other pre-heated air.

In the former case the surface temperature is predicted from the temperature increase of the air passing over it.

The pre-heated air mode, however, involves identifying a state of zero nett heat transfer between the surface and the air when the latter temperature is adjusted until it equals that of the former. Under these conditions the surface temperature may be inferred directly from a measurement of the air temperature.

This latter mode has been applied successfully to temperature measurement of surfaces of cylindrical geometry.

Since a requirement for temperature measurement of plane surfaces is widespread, most of the thesis has been devoted to applying the forced air convection principle (using both pre-heated and initially unheated air modes) to plane surfaces. It has involved

a detailed theoretical and experimental investigation of the flow and temperature characteristics necessary for a successful implementation of the principle. On the basis of these investigations recommendations have been made for the design of instruments to measure the temperature of plane surfaces. One such instrument employing the initially unheated air mode has been constructed and installed on a strip annealing line for measuring the temperature (up to 550^{o}C) of moving aluminium strip.

CONTENTS

CHAPTER 1

INTRODUCTION

A knowledge of the temperature of surfaces is desirable in fields ranging from medicine to metallurgy. The purpose to which this knowledge is put, of course, depends upon the particular type of surface involved. For example, in metallurgy the metallurgical and mechanical properties of a specimen are usually dependent upon the temperature to which it has been elevated, thus a knowledge of the temperature is necessary for controlling these properties.

In the extrusion of aluminium and its alloys, the surface temperature increases with extrusion speed and surface damage results if this temperature exceeds a critical value. A continuous measurement of the temperature would permit maximum production rates to be achieved consistent with no surface damage[1,2].

At the other extreme, in medicine, research is currently being undertaken in an attempt to correlate small 'hot spots' on the skin surface with the incidence of tumours below the skin at these sites. This work is particularly applicable to breast cancer. The technique employed for this purpose is called medical thermography and involves measuring the infra-red radiation from the site under investigation. However, medical thermography is not confined to detection of breast cancer, there being many other physiological and diagnostic applications[3,4,5].

Other requirements for temperature measurement are found in the manufacturing and processing of such materials as wood, plastics, paper, textiles, rubber and glass, this list being by no means exhaustive.

In the field of heat transfer a knowledge of surface temperature is often necessary in calculating heat transfer coefficients.

TEMPERATURE MEASUREMENT OF SURFACES

Temperature measurement of surfaces falls broadly into two categories:

(1) Contact temperature measurement.

(2) Non-contact temperature measurement.

Apart from a few general comments on methods falling within the former category, no further consideration will be given to contact temperature measurement.

Contact Temperature Measurement

Various contact methods are available to measure surface temperature. They differ in principle usually in the particular temperature dependent parameter they exploit.

One of the commonest methods, the thermocouple, exploits the thermoelectric e.m.f. generated between dissimilar metals with junctions at different temperatures. Such methods usually have fairly high accuracies 1 or 2% and can be used within a temperature range of -200°C to +1100°C.

Resistance thermometers exploit the change in resistance with temperature. Their accuracy is usually higher than that of the thermocouple, but their upper range is somewhat lower, i.e. approx. 600°C.

Resistance thermometry includes metals, an important example of which is platinum, as well as thermistors.

In both the thermocouple and resistance methods the actual physical form of the sensor is based on the particular requirement. For

example it can be in the form of wire, strip or a thin film.

Certain materials suddenly melt at accurately predictable temperatures, (within 1% of nominal value). Examples of these materials are certain crayons, paints, papers and pellets[6,7]. Some of these materials may be used at up to 1500°C and down to 40°C.

Other methods exploit the sudden change in colour of a substance at a known temperature[7]. The range of such methods may be as large as 40°C-1400°C with accuracies of up to 2% in some cases.

All the above methods involve contact with the surface whose temperature is to be measured. Three undesirable effects arise from this:

(1) There will always be some finite thermal capacity associated with the sensor which will distort the temperature profiles in the contact zone. If the thermal capacity and thermal conductivity of the test surface is high, this effect is usually small.

A method of minimising the temperature profile distortion caused by the sensor is to use a thermally compensated device. This involves heating the sensor externally until no heat flow from the surface is detected. Clearly the procedure is not appropriate to all the methods described above.

(2) Unless an intimate contact between the surface and sensor exists errors will arise from thermal gradients across the contact zone due to the finite thermal resistance of this zone.

(3) In order to minimize the effect described in (2), surface damage by the sensor often results.

For surfaces moving relative to the sensor, e.g. a rubbing thermocouple, (2) and (3) usually become more significant.

The techniques discussed so far have all involved extracting heat from the surface. Other methods exploit temperature dependent parameters within the material itself, e.g. thermal expansion, resistivity, hardness elastic modulus.

NON-CONTACT TEMPERATURE MEASUREMENT

The main purpose of these methods is to avoid some of the undesirable

effects common to many of the contact methods, i.e. perturbation of the surface temperature profiles, surface damage, errors due to poor surface contact, difficulty of implementation for moving surfaces, the necessity for very close contact.

As with the contact methods the non-contact methods exploit some parameter which is a function of temperature. However in most cases this parameter is not a unique function of temperature and is influenced by other surface parameters.

Amongst the non-contact methods those exploiting the E.M.R. emitted from a heated surface are probably the commonest. It is therefore, appropriate to examine these techniques in some detail, but before doing so a brief review of other non-contact methods will be made.

Electromagnetic Effects

The magnitude of eddy currents induced in a metal body by an alternating magnetic field will depend upon the magnetic and electrical properties of the metal[8]. In general, these properties will vary with the temperature of the body. Now the coil impedance will be a function of the magnetic and electrical properties of the metal and hence of the temperature.

If a high frequency field is used, (say 100 KHz), the eddy currents will be localized near the surface of the metal due to the skin effect, thus the phenomenon provides a method of near-surface temperature measurement without making contact.

Unfortunately the coil impedance is very sensitive to spacing between itself and the body. However, methods have been devised to minimize this effect. Such a technique, of course, is not absolute and requires calibration for each type of metal involved.

Methods Exploiting the Temperature Dependence of the Elastic Constants of the Test Specimen

The velocity of sound in a solid is a function of the elastic constants and density of the solid.

For example, the velocity, c, of a compressional sound wave in an extended medium, (i.e. dimensions much greater than the sound wavelength) is given by:

$$c = \left[\frac{E(1-\mu)}{\rho(1+\mu)(1-2\mu)}\right]^{\frac{1}{2}} \quad \ldots\ldots\ldots\ldots\ldots\ldots\ldots\ldots\ldots\ldots \quad (1)$$

where E = Young's modulus

μ = Poisson's ratio

ρ = density

If on the other hand a compressional wave is propagated down say a thin rod whose diameter is very much less than the wavelengths, then the velocity becomes:

$$c = \left[\frac{E}{\rho}\right]^{\frac{1}{2}} \quad \ldots\ldots\ldots\ldots\ldots\ldots\ldots\ldots\ldots\ldots\ldots\ldots \quad (2)$$

The elastic constants in (1) and (2) depend upon the temperature of the solid and the net effect of this is to make the velocity temperature dependent.

Experiments by the author have shown that when a 5 Mg Hz pulsed ultrasonic wave was propagated into the end of an accurately machined aluminium bar of dimensions considerably greater than the sound wavelength in the medium (so that equation (1) applies), the velocity is indeed a function of temperature. The velocity was measured using a pulse echo technique together with a knowledge of the bar dimensions.

It was found that the velocity varied inversely as the temperature.

Further experiments indicated that the velocity was a function of the type of alloy and indeed even varied by significant amounts between different samples of the same alloy at the same temperature. Thus the

technique was considered unsuitable for production purposes.

Strictly speaking, this technique does not measure surface temperature but due to the high thermal conductivity of aluminium the results would have indicated, fairly closely, the surface temperature.

It is interesting to note that although the experiments described involved making contact between the transducer Pb zirconate titanate and the surface, it has been found possible to generate ultrasonic waves in metal solids by electromagnetic induction[9], thus making it a true non-contact method.

Another interesting application of this technique, although not strictly non-contact surface temperature measurement is in ultrasonic thermometry where a compressional wave is propagated down a wire or thin rod sensor, and the wave velocity measured (see equation (2)) by pulse echo techniques. The wave velocity in the sensor will be a function of its temperature and hence that of the environment in which it is situated[10].

A Method Involving Free Convection Currents in Air

This method is similar in principle to the thermally compensated thermocouple. This latter consists of a thermocouple with a small auxiliary heater. Facilities are provided to detect heat flow between the junction and the test surface and the heater current is adjusted until the flow becomes zero. Under these conditions, neglecting losses, the thermocouple junction will be at the surface temperature. Up to this balance condition there is heat transfer between the junction and surface by conduction.

Fig. 1 shows a schematic diagram of the natural convection method[11].

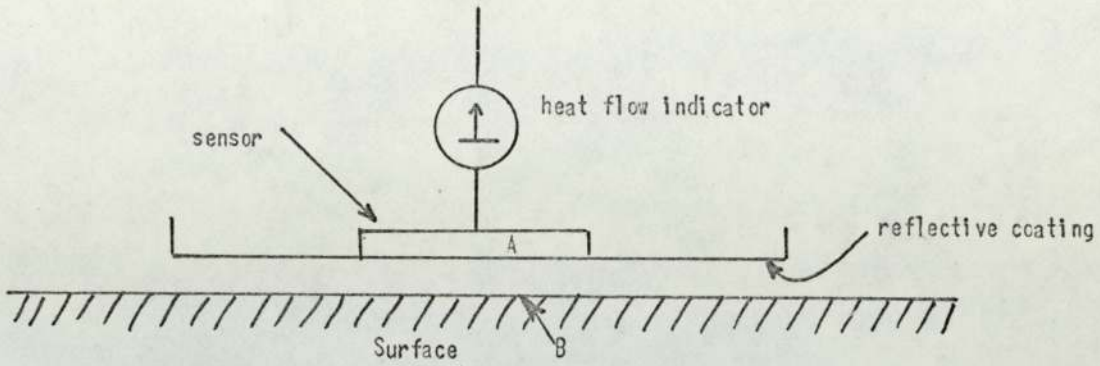

Fig. 1. Natural Convection Method

In this case heat transfer is by natural convection and to a lesser extent radiation (because of the reflective coating).

If A and B are very close, i.e. of the order of 2 mm and a temperature differential exists between them, then a finite heat flow will be indicated. By changing the temperature of A in such a direction to reduce the heat flow a balance condition can be achieved when A = B in which case the heat flow will be zero.

For separations much greater than 2 mm radiation effects are bound to manifest themselves due to extraneous sources and a departure from almost pure black body conditions at balance. Also for those wider separations free convective air currents become very turbulent resulting in a certain amount of air cooling and considerable instability of heat transfer. The net result of the above is to introduce large errors into the measurements. Nevertheless in applications where close proximity is permissible this is a very useful technique.

Other Techniques

If a 'Molecular beam' of potassium or rubidium atoms is made to impinge on a surface then the velocity distribution of the reflected atoms will be a function of the surface temperature[12].

The technique is emissivity independent and has no perturbating effect on the surface. Accuracies as high as 1% have been claimed over a temperature range 200°C-2700°C.

The technique is fairly elaborate, making it unsuitable for most production purposes but it could well have numerous laboratory applications.

The mean temperature of heat exchanger tubes has been determined by measuring their thermal expansion[13].

This technique could have other applications where the thermal expansion coefficient of the body is known and accurate measurements of linear dimensions can be made (or inferred).

The thermal expansion method only measures surface temperature if the body is isothermal.

METHODS EXPLOITING THE ELECTROMAGNETIC RADIATION EMITTED BY A HEATED BODY

Various methods have been devised to exploit the radiant energy from a hot body in temperature measurement. Before considering any particular method it is appropriate to present a few of the fundamental expressions on which all these methods are based.

The emissive power of a black body is a unique function of temperature and is given by:

$$E_B = \sigma T^4 \quad \ldots\ldots\ldots\ldots\ldots\ldots\ldots\ldots\ldots\ldots\ldots\ldots \quad (3)$$

where σ is Stefan's constant and T is the absolute temperature.

This is known as Stefan Boltzman's Law. In general the emissive power of a real emitter is less that that of a black body at the same temperature and is given by:

$$E_R = \varepsilon\sigma T^4 \quad \ldots\ldots\ldots\ldots\ldots\ldots\ldots\ldots\ldots\ldots\ldots\ldots \quad (4)$$

where ε is a constant of the emitting surface called the emissivity

and always lies between 0 and 1, where the highest value corresponds to a black body.

The energy emitted by a black body per unit area per unit time in the wavelength range λ to $\lambda+d\lambda$ is given by Plank's expression:

$$E_\lambda d\lambda = C_1 \lambda^{-5}\left[\exp\left(\frac{C_2}{\lambda T}\right) - 1\right]^{-1} d\lambda \quad \ldots\ldots\ldots\ldots\ldots\ldots\ldots\ldots \quad (5)$$

where C_1 and C_2 are the first and second radiation constants respectively.

The rate of emission of a non-black body in a limited wavelength range is a function of its temperature and spectral emissivity. The latter is a function of wavelength, the temperature and the nature of the surface involved[14]. Figs. 2 and 3 show the spectral emissivity for polished and roughened aluminium. Thus it is important to examine the significance of emissivity in temperature measurement using different radiation techniques.

The Total Radiation Pyrometer

This method measures the radiation received over the complete range of wavelengths.

Neglecting any re-emission or reflection of radiation from the detector the net rate of energy collection for a black body is aT^4 and for a non-black body of emissivity ε is εaT^4 where a is a constant which absorbs Stefan's constant (see equations (3) and (4)).

Thus if the pyrometer is calibrated against a black body emitter (i.e. $\varepsilon=1$) the apparent (indicated) temperature T_A of the non-black body will be related to the true temperature T by:

$$T_A^4 = \varepsilon T^4 \quad \ldots\ldots\ldots\ldots\ldots\ldots\ldots\ldots\ldots\ldots\ldots\ldots\ldots\ldots \quad (6)$$

giving a fractional error in temperature measurement of:

$$\frac{T-T_A}{T} = 1 - \varepsilon^{\frac{1}{4}} \quad \ldots\ldots\ldots\ldots\ldots\ldots\ldots\ldots\ldots\ldots\ldots\ldots\ldots \quad (7)$$

showing that the error varies as the fourth root of the total emissivity.

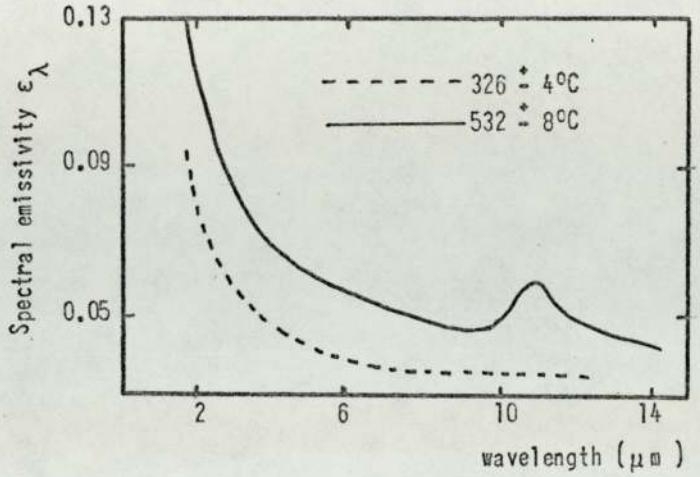

Fig. 2. Variation of spectral emissivity with wavelength for polished aluminium

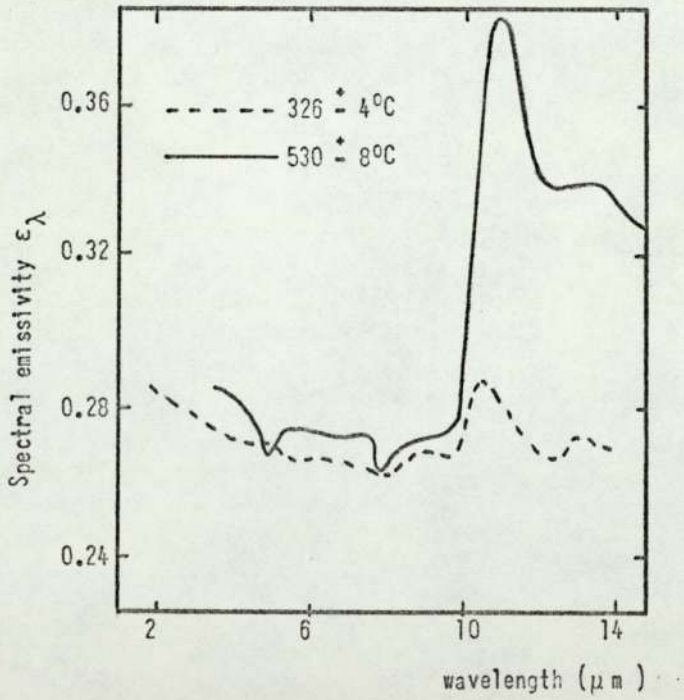

Fig. 3. Variation of spectral emissivity with wavelength for roughened aluminium

Partial Radiation Pyrometers

As the name suggests these methods measure radiation from a limited range of wavelengths. Rewriting equation (5) gives:

$$E_\lambda d\lambda = C_1 \lambda^{-5} \left[\exp\left(\frac{C_2}{\lambda T}\right) - 1 \right]^{-1} d\lambda \quad \ldots\ldots\ldots\ldots\ldots\ldots\ldots\ldots \quad (5)$$

The variation of E_λ with λ for a number of temperatures is shown in Fig. 4.

This spectral distribution of energy does not imply necessarily that the device output will follow the same trend. This will only happen if the response R_λ is constant for all wavelengths.

In general the output is given by:

$$S = b \int_0^\infty R_\lambda E_\lambda d\lambda \quad \ldots\ldots\ldots\ldots\ldots\ldots\ldots\ldots\ldots\ldots\ldots\ldots \quad (8)$$

(b = constant), provided S is linearly related to detected energy.

A typical spectral response is shown in Fig. 5 for a Mullard 615V lead sulphide photoconductive cell.

It has been shown experimentally by Harner and Watts[16] that S can be expressed in the following form for this type of detector:

$$S = cT^n \quad \ldots\ldots\ldots\ldots\ldots\ldots\ldots\ldots\ldots\ldots\ldots\ldots\ldots\ldots\ldots\ldots \quad (9)$$

where c is constant and n, which varies with temperature lies between 8 and 12.

If the pyrometer is again calibrated against a black body and subsequently used to measure the temperature of a surface of emissivity ε at temperature T then the apparent temperature T_A will be less than the true one T and is given by:

$$T_A^{\,n} = \varepsilon T^n \quad \ldots\ldots\ldots\ldots\ldots\ldots\ldots\ldots\ldots\ldots\ldots\ldots\ldots\ldots\ldots\ldots \quad (10)$$

giving a fractional error in temperature measurement of:

$$\frac{T - T_A}{T} = 1 - \varepsilon^{1/n} \quad \ldots\ldots\ldots\ldots\ldots\ldots\ldots\ldots\ldots\ldots\ldots\ldots\ldots\ldots\ldots\ldots \quad (11)$$

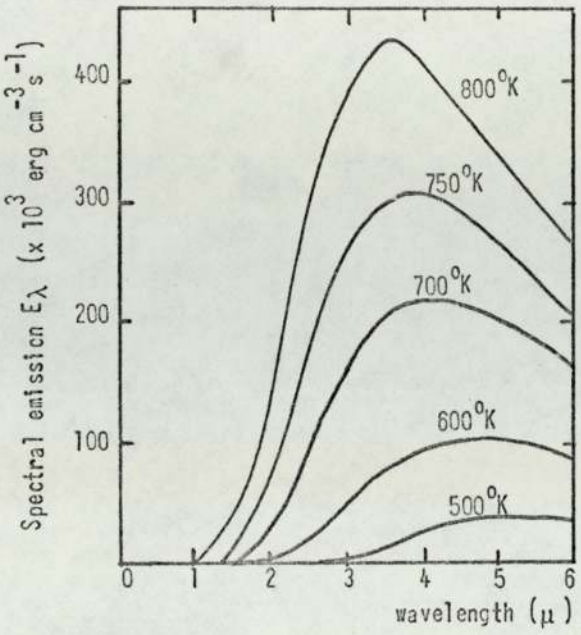

Fig. 4. Variation of energy emission with wavelength

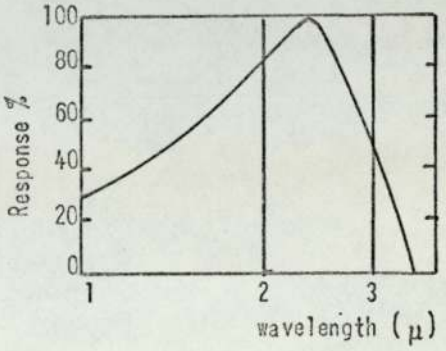

Fig. 5. Spectral response of lead sulphide cell

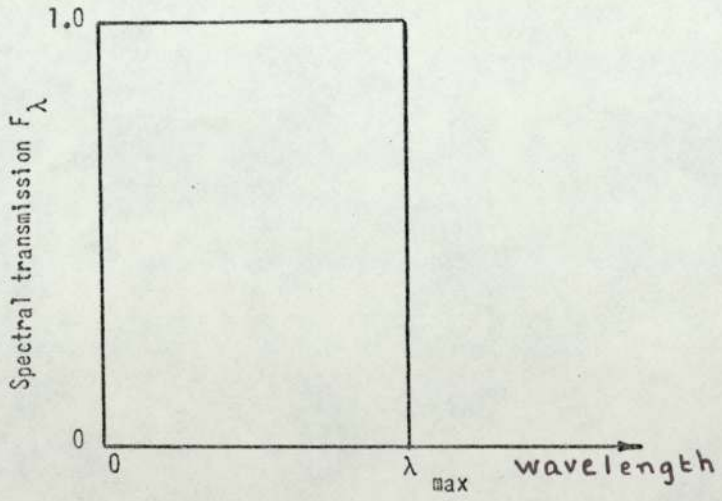

Fig. 6. Assumed transmission for sharp cut-off filter

Since $\varepsilon<1$ then $\varepsilon^{1/n}$ approaches 1 as n approaches ∞, thus the higher the value of n the lower the emissivity error. For a lead sulphide cell pyrometer the emissivity errors are therefore lower than for a total radiation pyrometer since n is higher in the former case.

An examination of Fig. 4 will indicate that the emission rate varies more rapidly with λ for the shorter wavelengths than for the longer ones.

Fig. 5 shows that the wavelength cut-off for a lead sulphide cell lies at about 3-3.5 μ hence a large proportion of the measured energy lies within the shorter wavelengths giving rise to the large values of n.

A similar result to the above can be obtained using filters with a long wavelength cut-off, λ max. The smaller the value of λ max. the higher the value of n. Thus for low emissivity errors the pyrometer must be insensitive to the longer wavelength.

Table 1 shows the approximate values of n for cut-off filters within a temperature range 500-750°C[15].

TABLE 1

λ max.	500°C	600°C	700°C	750°C
5.0	7.4	6.4	6.0	
4.5	7.6	7.0	6.2	
4.0	8.4	7.6	6.8	6.6
3.5	9.8	8.2	7.4	7.4
3.0	11.2	9.0	8.2	8.0
2.5		10.6	9.6	9.4
2.0		12.4	12.4	11.4

Monochromatic 'Brightness' Radiation Pyrometer

This technique measures the radiant energy in a very narrow band

of wavelengths defined by filters and the spectral response of the detector.

The emissivity errors can be determined in a similar manner to those in the total and partial radiation pyrometers when the device is calibrated against a black body.

Rewriting once again Plank's equation:

$$E_\Lambda d\Lambda = C_1 \Lambda^{-5} \left[\exp\left(\frac{C_2}{\Lambda T}\right) - 1\right]^{-1} d\Lambda \quad \ldots\ldots\ldots\ldots\ldots\ldots\ldots \quad (5)$$

Now in the normal wavelength and temperature ranges encountered in radiation pyrometry, $\exp \frac{C_2}{\Lambda T} \gg 1$ and equation (5) reduces to Wein's law:

$$E_\Lambda d\Lambda = C_1 \Lambda^{-5} \left[\exp \frac{C_2}{\Lambda T}\right]^{-1} d\Lambda \quad \ldots\ldots\ldots\ldots\ldots\ldots\ldots\ldots \quad (12)$$

Thus although not quite so rigorous as Plank's expression, equation (12) is sufficiently rigorous to permit its use in some of the derivations to follow.

Using Wein's law the rate of emission per unit area in a wavelength range Λ-Λ+$d\Lambda$ from a body at temperature T but with emissivity ε_Λ is:

$$\varepsilon_\Lambda E_\Lambda d\Lambda = \varepsilon_\Lambda C_1 \Lambda^{-5} \left[\exp \frac{C_2}{\Lambda T}\right]^{-1} d\Lambda \quad \ldots\ldots\ldots\ldots\ldots\ldots\ldots \quad (13)$$

The right-hand side of (13) may be written in terms of an apparent temperature T_A thus:

$$C_1 \varepsilon_\Lambda \Lambda^{-5} \left[\exp \frac{C_2}{\Lambda T}\right]^{-1} = C_1 \Lambda^{-5} \left[\exp \frac{C_2}{\Lambda T_A}\right]^{-1} \quad \ldots\ldots\ldots\ldots\ldots \quad (14)$$

on simplifying and taking logs (14) becomes:

$$\frac{1}{T} - \frac{1}{T_A} = \frac{\Lambda}{C_2} \log_e \varepsilon_\Lambda \quad \ldots\ldots\ldots\ldots\ldots\ldots\ldots\ldots\ldots\ldots \quad (15)$$

It is interesting to note that the difference in the reciprocals of the true and apparent temperatures is now proportional to the log. of the spectral emissivity making uncertainties in emissivity estimates

less significant than in the other cases discussed. Also the error again decreases as Λ decreases.

If in Planck's equation (5) $\log_e E_\Lambda$ is plotted against $\log_e T$, for fixed wavelengths, a series of almost straight lines emerge, each corresponding to a different wavelength. This gives justification for expressing the output once again in the form:

$$S = \text{const. } T^n \quad \ldots\ldots\ldots\ldots\ldots\ldots\ldots\ldots\ldots\ldots\ldots\ldots \quad (16)$$

where n is the slope of these curves and varies with Λ.

The corresponding fractional error in temperature measurement is thus:

$$\frac{T-T_A}{T} = 1 - \varepsilon^{1/n} \quad \ldots\ldots\ldots\ldots\ldots\ldots\ldots\ldots\ldots\ldots\ldots\ldots \quad (17)$$

It is found that n increases as the operating wavelength decreases this being consistent with the predictions from equation (15). Also at a given wavelength n decreases as T increases. A partial radiation pyrometer with a uniform response and a cut-off at Λ max. (see Fig.6) in general gives slightly higher values of n than a monochromatic pyrometer operating at Λ max. The former is also more sensitive of course because it gathers more radiation.

The Two Colour Pyrometer

This is a further attempt to reduce emissivity errors by measuring the ratio of the intensities from two adjacent wavelengths[17]. So long as the spectral emissivity is the same or is in a constant ratio for the two wavelengths then the ratio R will be a unique function of temperature.

Consider two adjacent wavelengths Λ_1 and Λ_2 with band widths $d\Lambda_1$ and $d\Lambda_2$ and spectral emissivities ε_{Λ_1} and ε_{Λ_2} respectively, then

the ratio of the spectral intensities will be given by:

$$R = \frac{\varepsilon_{\lambda_1}}{\varepsilon_{\lambda_2}} \left(\frac{\lambda_2}{\lambda_1}\right)^5 \frac{\left[\exp\left(\frac{C_2}{\lambda_2 T}\right) - 1\right] d\lambda_1}{\left[\exp\left(\frac{C_2}{\lambda_1 T}\right) - 1\right] d\lambda_2} \quad \ldots\ldots\ldots\ldots\ldots\ldots\ldots \quad (18)$$

which is independent of emissivity so long as $\frac{\varepsilon_{\lambda_1}}{\varepsilon_{\lambda_2}}$ is constant.

For most pyrometer applications (18) may again be simplified to:

$$R = \frac{\varepsilon_{\lambda_1}}{\varepsilon_{\lambda_2}} \left(\frac{\lambda_2}{\lambda_1}\right)^5 \frac{\left[\exp \frac{C_2}{\lambda_2 T}\right]}{\left[\exp \frac{C_2}{\lambda_1 T}\right]} \frac{d\lambda_1}{d\lambda_2} \quad \ldots\ldots\ldots\ldots\ldots\ldots\ldots \quad (19)$$

Using (19) the value of $\frac{1}{T} - \frac{1}{T_A}$ may again be easily obtained giving an indication of the error in apparent temperature when the pyrometer is calibrated against a black body.

Writing the right-hand side of (19) in terms of the apparent temperature T_A the following relationship results:

$$\frac{\left[\exp \frac{C_2}{\lambda_2 T_A}\right]}{\left[\exp \frac{C_2}{\lambda_1 T_A}\right]} = \frac{\varepsilon_{\lambda_1}}{\varepsilon_{\lambda_2}} \frac{\left[\exp \frac{C_2}{\lambda_2 T}\right]}{\left[\exp \frac{C_2}{\lambda_1 T}\right]} \quad \ldots\ldots\ldots\ldots\ldots\ldots\ldots \quad (20)$$

which on simplifying and taking logs of both sides gives:

$$\frac{1}{T} - \frac{1}{T_A} = \frac{\lambda_1 \lambda_2}{C_2(\lambda_2 - \lambda_1)} \log_e \frac{\varepsilon_1}{\varepsilon_2} \quad \ldots\ldots\ldots\ldots\ldots\ldots\ldots \quad (21)$$

It has been found by Reynolds[18] that for aluminium at 700°K the errors of a two colour pyrometer would be less than 13°K for a typical rough surface for almost any choice of the pair of operating wavelengths. But for a polished surface the errors are likely to be in excess of 30°K. Thus the surface roughness has a profound effect on the accuracy

of this pyrometer. Further, from experimental work performed there is no evidence to suggest that a two-colour pyrometer will be any less emissivity independent than a suitably chosen monochromatic instrument. However, more experimental results would be desirable to confirm this assumption.

Ackerman[19] has made a comparison between a two-colour pyrometer operating at $\lambda_1 = 0.65\ \mu$ and $\lambda_2 = 0.51\ \mu$, a monochromatic brightness pyrometer operating at 0.65 μ and a 'total' radiation pyrometer 0-10 μ each used to indicate the temperature of induction heated brass billets with abrasively cleaned surfaces. Each pyrometer was calibrated against a black body. The data from these tests is shown in Table 2.

TABLE 2

COMPARISON OF THE ERRORS OF THREE RADIATION PYROMETERS USED TO MEASURE THE TEMPERATURE OF INDUCTION HEATED BRASS

Alloy	Temp. range	Errors		
		Two colour °C	Total radn. °C	Monochromatic 'brightness' °C
		+ve	-ve	-ve
Cartridge Brass	750-880	85/55	170/133	/10
Trumpet Brass	800-900	31/17	175/113	/8
Phosphorised Admiralty Brass	750-800	82/62	190/140	/17
Arsenical Admiralty Brass	750-830	95/81	127/92	/23
10% Cupro-Nickel Brass	760-1000	14/4	10/10	/4
Aluminium Brass	760-920	70/130	170/200	/33

The left-hand figure in each column shows the error in deg. C immediately after the billet reached the control temperature; the right-hand figure shows the error after about three minutes at equilibrium temperature. These differential errors in each pair of

readings are due mainly to progressive oxidation of the alloys. The single readings for the monochromatic pyrometer corresponds to the measurement being made after 3 minutes at a steady temperature. It is seen from Table 2 that the monochromatic 'brightness' pyrometer suffers the least error.

Having examined the theory of one or two common forms of radiation pyrometer and assessed briefly their susceptibility to emissivity errors, a somewhat different approach to overcoming these emissivity errors will now be made.

Multiple Reflection Methods

It has been indicated that a black body emitter has an emissivity of unity and will emit radiation at rate given by:

$$E = \sigma A T^4 \quad \ldots\ldots\ldots\ldots\ldots\ldots\ldots\ldots\ldots\ldots\ldots\ldots\ldots\ldots\ldots\ldots \quad (22)$$

where σ is Stefan's constant and A is area.

Thus the emission per unit area from a black body is a unique function of temperature.

The multiple reflection methods are an attempt to reduce emissivity errors by effecting partial black body conditions.

It is not intended to pursue these methods in great detail, but a few of the general principles will be discussed with the aid of Fig. 7.

By inducing the radiation from the emitter to undergo multiple reflections between itself and an unheated plane parallel reflector the effective emissivity of the surface may be increased.

Assume each surface to act as a specular reflector. Let ε_s be the emissivity of the emitter, r_s the specular reflectivity of the emitter and R_s the specular reflectivity of the reflector. Then the effective emissivity after n reflection is given by:

$$\varepsilon_{eff} = \varepsilon_s [1 + r_s R_s + (r_s R_s)^2 \ldots\ldots\ldots (r_s R_s)^n] \quad \ldots\ldots\ldots\ldots\ldots\ldots \quad (23)$$

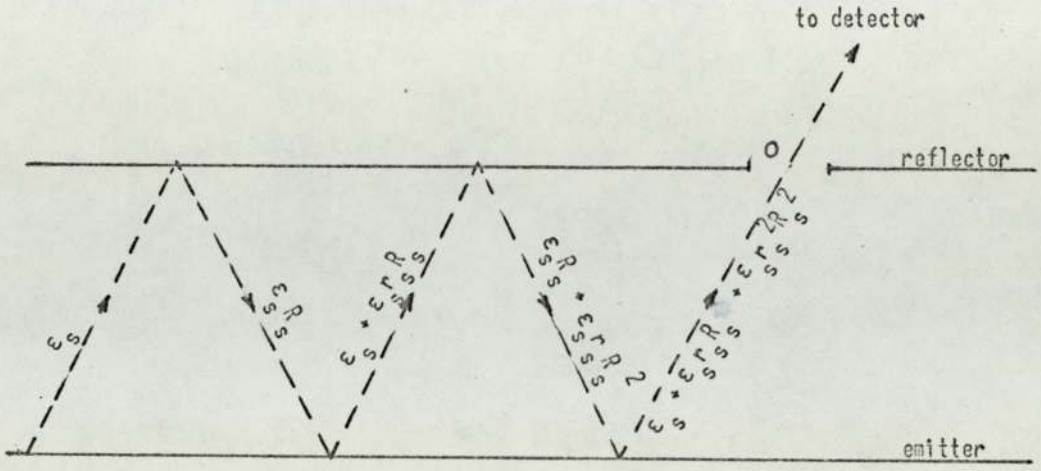

Fig. 7. Principle of reflection methods

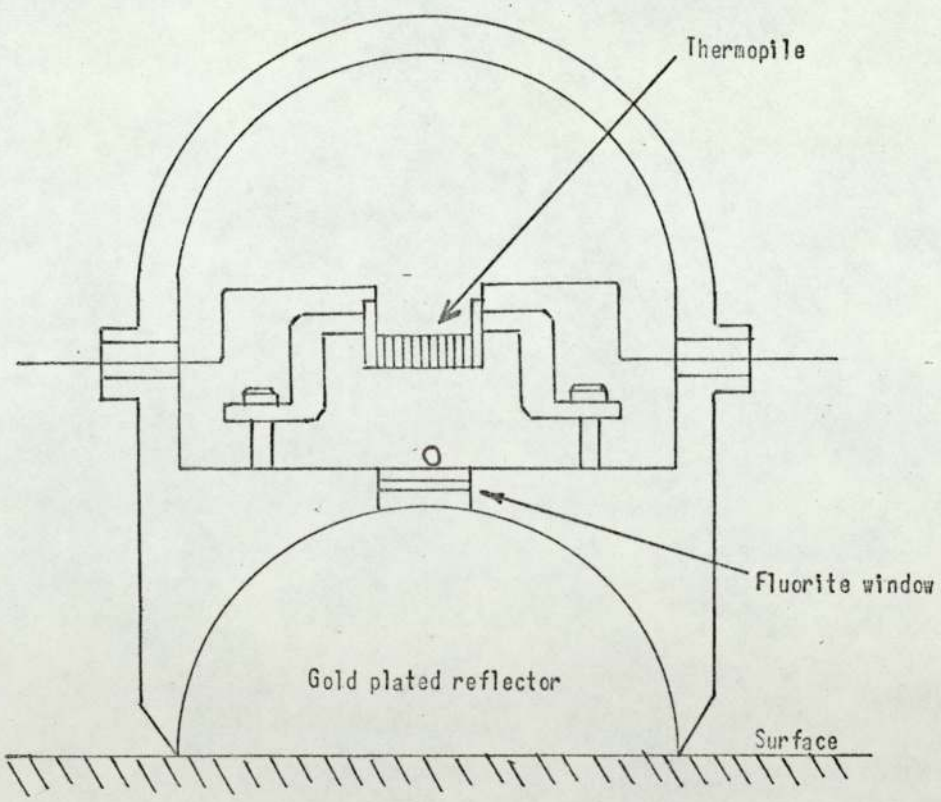

Fig. 8. The Land Surface Pyrometer

If n is large then:

$$\varepsilon_{eff} \rightarrow \frac{\varepsilon_s}{[1-r_s R_s]} \quad \ldots\ldots\ldots\ldots\ldots\ldots\ldots\ldots\ldots\ldots\ldots\ldots\ldots\ldots\ldots\ldots \quad (24)$$

A similar expression to (24) may be derived if the reflectivities are assumed perfectly diffuse thus:

$$\varepsilon_{eff} \rightarrow \frac{\varepsilon_d}{[1-r_d R_d]} \quad \ldots\ldots\ldots\ldots\ldots\ldots\ldots\ldots\ldots\ldots\ldots\ldots\ldots\ldots\ldots\ldots \quad (25)$$

where r_d, R_d and ε_d are the diffuse reflection and emission coefficients.

Despite the formulae for specular and diffuse reflections being mathematically identical their effective emissivities will in general differ.

Usually a real surface will reflect both specularly and diffusely but the relative significance of each is often uncertain, thus making an estimate of effective emissivity difficult.

Nevertheless the nett effect of these reflections is to augment the total emissivity of the emitter such that the radiation finally emerging through an aperture O and passing to the detector will be closer to black body radiation than if the reflector were absent.

The Land Surface Pyrometer

The above treatment was very simplified and applies to parallel surfaces, nevertheless it demonstrates the beneficial effects of multiply reflected radiation in that it increases the effective emissivity of the emitter.

The land pyrometer[20] is a method exploiting multiply reflected radiation not from a parallel reflector but from a gold plated hemisphere (see Fig.8).

This hemisphere is placed on or near the surface and a small hole allows multiply reflected radiation to leak out and activate a detector.

The reflector gives protection from the surroundings and as a result of internal reflections emission through O is almost black body radiation.

Typical hemispherical diameters vary from about $\frac{1}{2}$ in. - 3 in.

Errors in measurement for emissivities of 0.9 and 0.5 have been found to be 1°C and 8°C respectively for a surface at 1100°C.

This device has a slight perturbing effect on the surface since for a temperature of 1000°C surface temperature elevations of 20°C and 40°C for reflector diameters of $\frac{1}{2}$ in. and 2 in. have been observed.

The Reflecting Wedge Radiation Pyrometer

The multiple reflection method may be exploited in a different way from the above. In this case the reflector takes the form of a plane surface inclined to the emitter surface forming a wedge (see Fig.9).

Reynolds[21] describes such a system with a reflector consisting of highly polished aluminium plate inclined at an angle of 10° to the emitter surface. The radiation undergoes a series of reflections before entering the aperture of a total radiation pyrometer.

It can be shown that black body conditions can be approximated to even closer by heating the reflector to a temperature close to that of the emitter.

It was found that with this system calibration curves for specimens of total emissivity, 0.89, 0.28 and 0.17 coincided within ± 4°C over the temperature range 200-450°C. However the geometry of the system was found, experimentally, to be critical.

An Emissivity Compensated Pyrometer

This method due to Kelsall, exploits specular reflection from the specimen[22]. Fig. 10 shows the principles on which the method

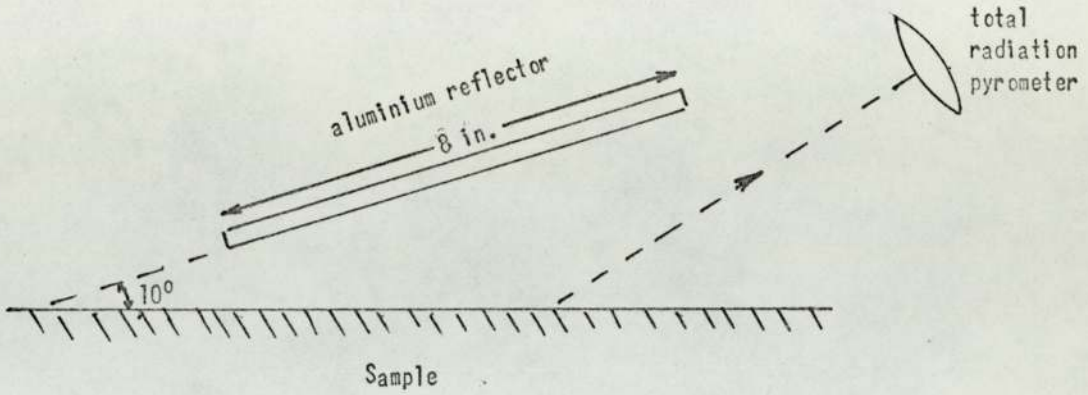

Fig. 9. Arrangement of reflecting wedge method

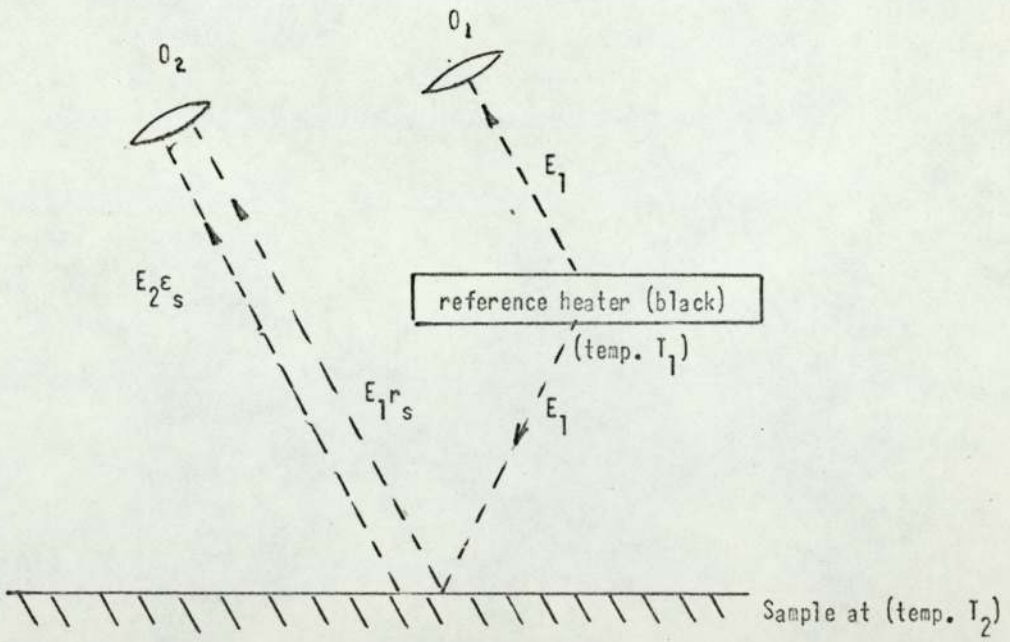

Fig. 10. Principle of Kelsall's method

is based. The nomenclature used in the simplified discussion to follow is defined in the diagram.

A black body reference heater emits radiant energy E_1 part of which passes through the right-hand optical system O_1. However part is specularly reflected from the sample, so augmenting the direct emitted radiation from the sample and the resultant radiation $E_2\varepsilon_s+E_1r_s$ passes through the left-hand optical system O_2.

By adjusting T_1 until the direct emission from the reference source becomes equal to the combined emitted and reflected radiation from the sample, the temperature of the sample may be determined by measuring T_1. This is shown in the following relationships:

$$E_1r_s+E_2\varepsilon_s = E_1 \quad \ldots\ldots\ldots\ldots\ldots\ldots\ldots\ldots\ldots\ldots\ldots\ldots\ldots\ldots \quad (26)$$

Now from Kirchhoff's law:

$$r_s+\varepsilon_s = 1 \quad \text{(for specular reflections)} \quad \ldots\ldots\ldots\ldots\ldots\ldots \quad (27)$$

thus $E_1[1-\varepsilon_s]+E_2\varepsilon_s = E_1$

giving $E_1 = E_2$

thus when an energy balance occurs the temperature of the reference source will be equal to the sample temperature.

This comparison between reference and sample signals is made by subjecting the signals alternatively to a lead sulphide detector.

It has been assumed that the reflected radiation is purely specular but in practice there will be a diffusely reflected component. Kelsall considers the error arising from this effect to be small however. His argument is that a surface which reflects fairly diffusely usually has a high emissivity and vice-versa.

Tests on many surfaces at 200°C gave an accuracy of $\pm$10°C, but for aluminium and brass with emissivities less than 0.2 errors of up to 30°C were observed.

A Method Employing Polarized Radiation

The main disadvantage of Kelsall's method described above was that it could not accommodate diffusely reflected radiation from the sample.

Murry[23] has developed a method similar in some respects to Kelsalls except that instead of examining the reflected plus emitted radiation for intensity he examined it for polarization.

Arago[24] found that the light emitted in an oblique direction from a heated surface was polarized. This phenomenon is exploited in Murry's method.

The radiation emitted by a metal has the dominant component $E_{\parallel}$ in the plane of incidence and the lesser component $E_{\perp}$ perpendicular to this plane.

Consider unpolarized black body radiation reflected from the sample surface (Fig.11). Since Kirchhoff's laws still apply to separate components of polarization, the reflected radiation will be polarized with the dominant component $E_{\perp}$ perpendicular to the plane of incidence and the lesser component $E_{\parallel}$ parallel to this plane.

If the beam now passes through a rotating analyzer then the emergent radiation will consist of an alternating component and a steady component. This is due to the resultant vector of the two elliptically polarized beams varying with angular displacement.

If the sample is initially hotter than the black body then the sum of the vectors parallel to the plane of incidence $E_{\parallel}$ will be greater than the sum of those perpendicular to this plane $E_{\perp}$. If the black body is heated until the sum of the two values of $E_{\perp}$ equals the sum of the two values of $E_{\parallel}$ then the alternating component will disappear leaving a steady radiation level.

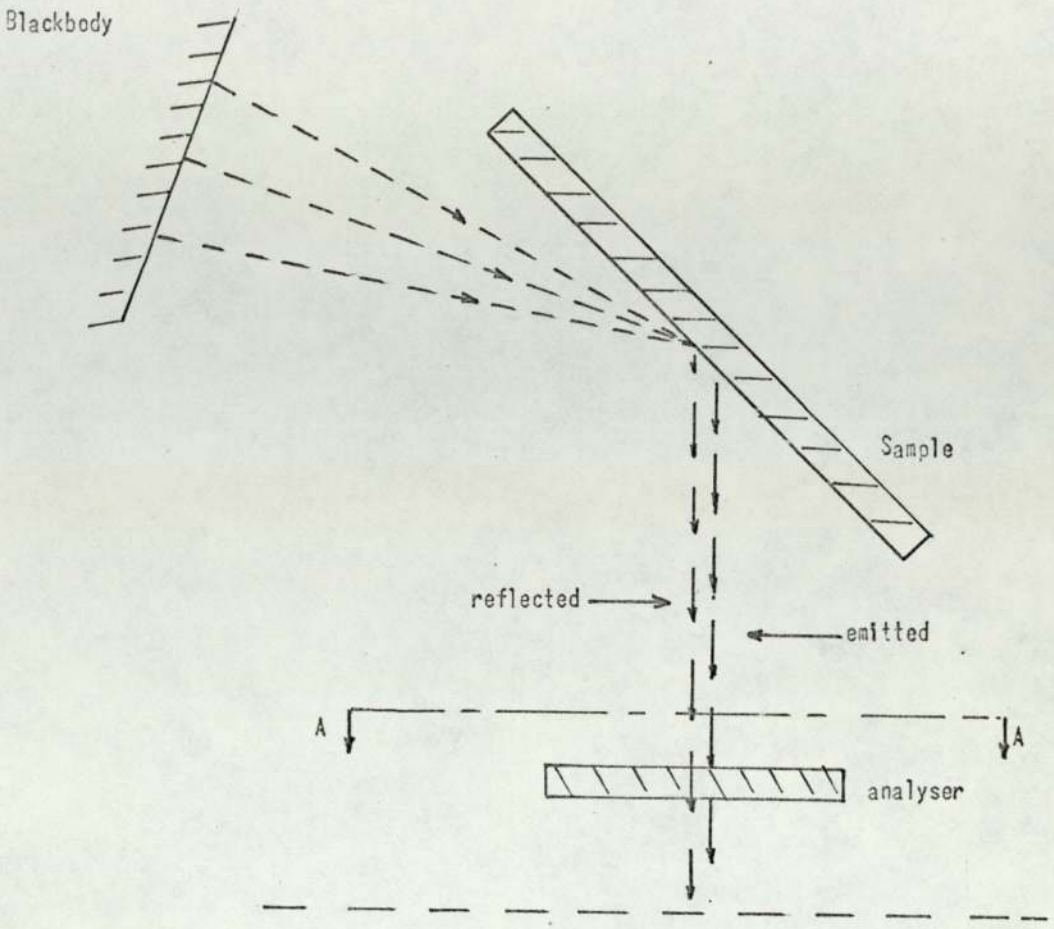

Plan view of optical system looking down on plane of incidence

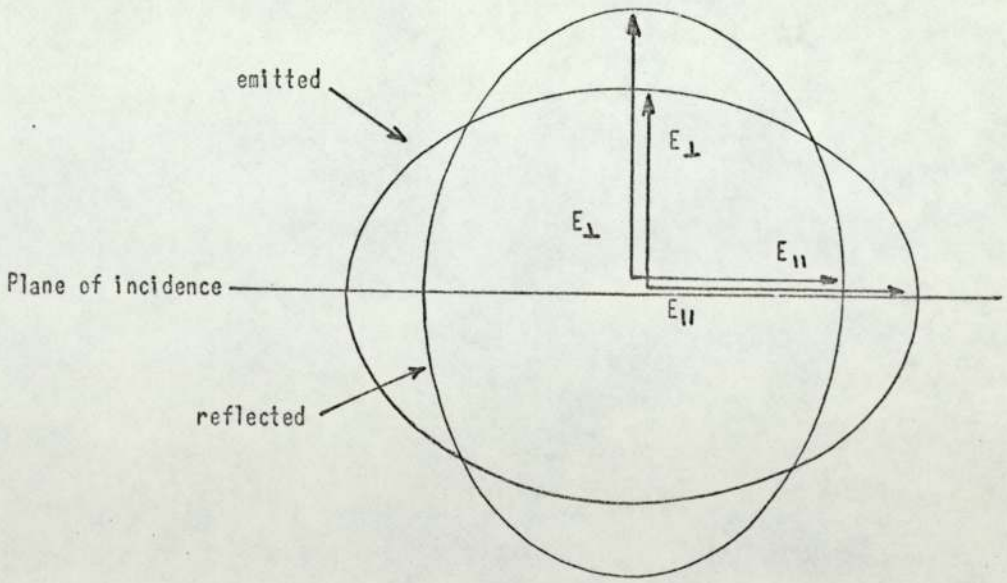

Section A – A through plane of incidence

Fig. 11. The polarization of emitted and reflected radiation

Under these conditions the sample temperature will be equal to that of the black body reference source.

An automatic pyrometer based on the above principle has been constructed. In measurements up to 450°C on metallic surfaces with emissivities of 0.05-0.47 the difference between sample and reference temperatures at balance was found to lie within $\pm$2% with no emissivity corrections.

The theory indicated that for out of balance conditions the device becomes sensitive to $\varepsilon_p - \varepsilon_s$ where ε_p is the emissivity of the sample corresponding to the radiation polarized parallel to the plane of incidence and ε_s that perpendicular to the plane of incidence.

If the sample is viewed in a direction normal to the plane of incidence or if the sample exhibits no polarization (which would be true for a black body or a surface which acts as a completely diffuse reflector), then the method will not work.

The Disappearing Filament Brightness Pyrometer

No discussion of radiation pyrometry would be complete without a brief mention of the disappearing filament pyrometer[25,26].

In this type of pyrometer the operator compares the brightness of the surface with that of an electrically heated filament. This comparison can be made manually with the aid of the human eye or automatically with the aid of photon detectors. A simplified schematic diagram of an arrangement with which to perform this comparison manually is shown in Fig. 12.

S = surface whose temperature is to be measured.

O_2 = objective lens.

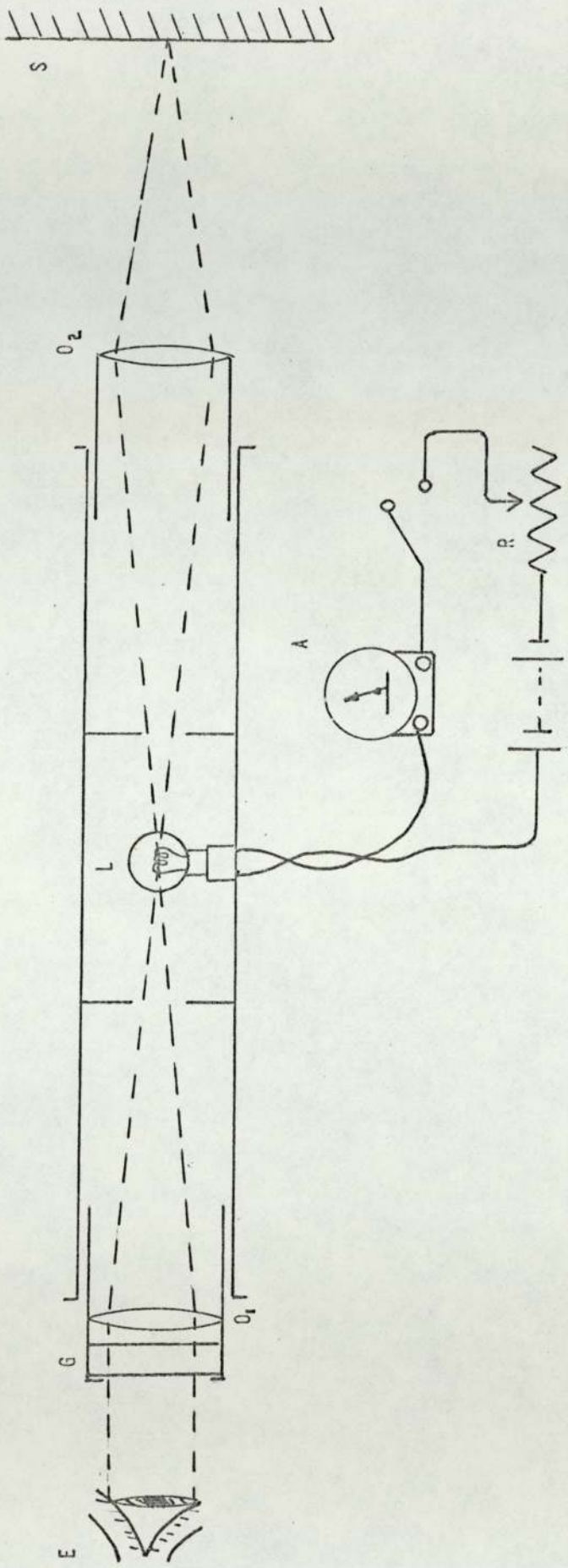

Fig. 12. The Disappearing Filament Brightness Pyrometer

L = pyrometer lamp.

O_1 = eye piece lens.

G = red filter.

E = eye.

A = ammeter.

R = rheostat.

In most instruments a comparison is made in a narrow wavelength band at about 0.65 μ in the red part of the spectrum using a filter between the observer's eye and both sources. The use of this filter permits a good photometric comparison to be made. It also permits a more reliable extension of the instruments range to be made (with the aid of absorbing glass or a rotating sector to cut down the source intensity).

In operation the objective is adjusted until an image of the source is produced in the plane of the lamp filament. By varying the current through the filament its temperature may be adjusted until it becomes indistinguishable from the superimposed image of the surface. At this balance point the surface temperature is read from the previously calibrated current setting. Alternatively a balance can be made by keeping the filament temperature constant (and hence its brightness) and adjusting the observed brightness of the surface by means of a suitably calibrated optical filter.

This type of pyrometer is subject to the same type of emissivity errors present in the other pyrometers discussed.

If a small cavity can be found, or produced on the sample surface then approximate black body radiation will emerge and the emissivity errors will be correspondingly reduced.

The disappearing filament pyrometer operated manually as indicated

above has a range from about 760°C upwards. Below this temperature there is insufficient emission of visible light for satisfactory measurements.

In order to extend the temperature measuring range down to lower values and to overcome human error associated with visual comparisons instruments employing photoelectric detectors have been developed[27,28].

Harmer and Watts[16] have developed a device employing a lead sulphide cell as a null detector. Radiation from the specimen is chopped at 800 Hz and passes through a glass lens where it is focussed onto the cell. A reference signal from a tungsten filament lamp is also chopped at the same frequency but is 180° out of phase with the sample signal.

If the sample and reference signals are unequal resulting from a difference in brightness, then an alternating signal will result from the photocell. This will be passed into an amplifier followed by a phase sensitive detector which automatically adjusts the lamp current until the error signal disappears.

From a knowledge of the lamp current at balance the temperature of the specimen may be deduced.

Various ranges are available in this instrument, the lowest one being 150°C-400°C and the response time is less than 0.1 second.

The range of the instrument may be extended to 1600°C by using stops in the sample beam. The range could have been increased by increasing the lamp temperature but this would have shortened its life.

The comparison method discussed above is no more immune to emissivity errors than the other methods employing lead sulphide photoconductive cells. It has been shown that the output S from such a cell varies rapidly with temperature giving a relationship of the

form:

$$S \propto T^n$$

where n is of the order of 10-12 at low temperatures. Thus any emissivity errors that do exist will be low for this cell.

However one advantage the comparison method has over the others is that because it is a null method it is not affected by the large temperature coefficient of sensitivity of the lead sulphide cell (approx. 7% per degree change in cell temperature) since the cell is only utilized in identifying a balance between the reference and sample signals. With those methods involving absolute measurements with the cell this large temperature coefficient of sensitivity could introduce significant errors unless measures were taken to stabilize the cell temperature.

The theory, principles and limitations of different types of radiation pyrometer have briefly been examined.

It has not been possible to discuss in detail the numerous variations of each type of instrument and indeed it would be inappropriate to do so in this thesis.

The spectral emissivity of surfaces varies with wavelength as well as temperature. In the metal fabricating industry, for example, a knowledge of the spectral emissivities of metal undergoing rolling, extrusion, drawing or casting is extremely incomplete hence a realistic comparison between the performance of the different types of pyrometer cannot be made. Thus in choosing a particular type of pyrometer one must be guided to a certain extent by the conclusions drawn from the theoretical discussions given. Other factors, of a more practical nature, must of course be taken into account when making a final choice. For example the electronic hardware associated with the two colour

pyrometer is very much more complex than that associated with a monochromatic or total radiation pyrometer. Thus the former will be more susceptible to failure, unreliability and inconsistency. Also, because of this complexity the cost of such an instrument will be correspondingly higher than the other total and monochromatic types.

CHAPTER 2

A METHOD OF TEMPERATURE MEASUREMENT EMPLOYING FORCED AIR CONVECTION

Most of the last chapter was devoted to examining different methods of exploiting electromagnetic radiation emitted from an incandescent surface, in temperature measurement. Emphasis was placed on assessing the influence and minimizing the effects of emissivity in these methods.

The method to be discussed below and in subsequent sections is a departure from the above approach employing electromagnetic radiation and exploits forced air convection in an attempt to eliminate emissivity errors.

Before extending the method to the temperature measurement of plane surfaces its application to cylindrical rods will first be discussed.

Simplified Theory of Forced Air Convection Method

If a jet of cold air is blown across a hot body and the air temperature is measured on either side of the body in the direction of the jet (see Fig. 13) then there will exist a difference, in temperature between the two measurements due to transfer of heat to the air from the body with T_2 being greater than T_1.

If precautions are taken to minimize the temperature gradients in the jet due to entrainment of cold air, then as the jet temperature is increased this temperature difference will decrease. When this difference becomes zero the air and body temperatures will be equal. Thus by measuring the air temperature under these balance conditions the body temperature can be determined without making contact.

This phenomenon was exploited in the temperature measurement

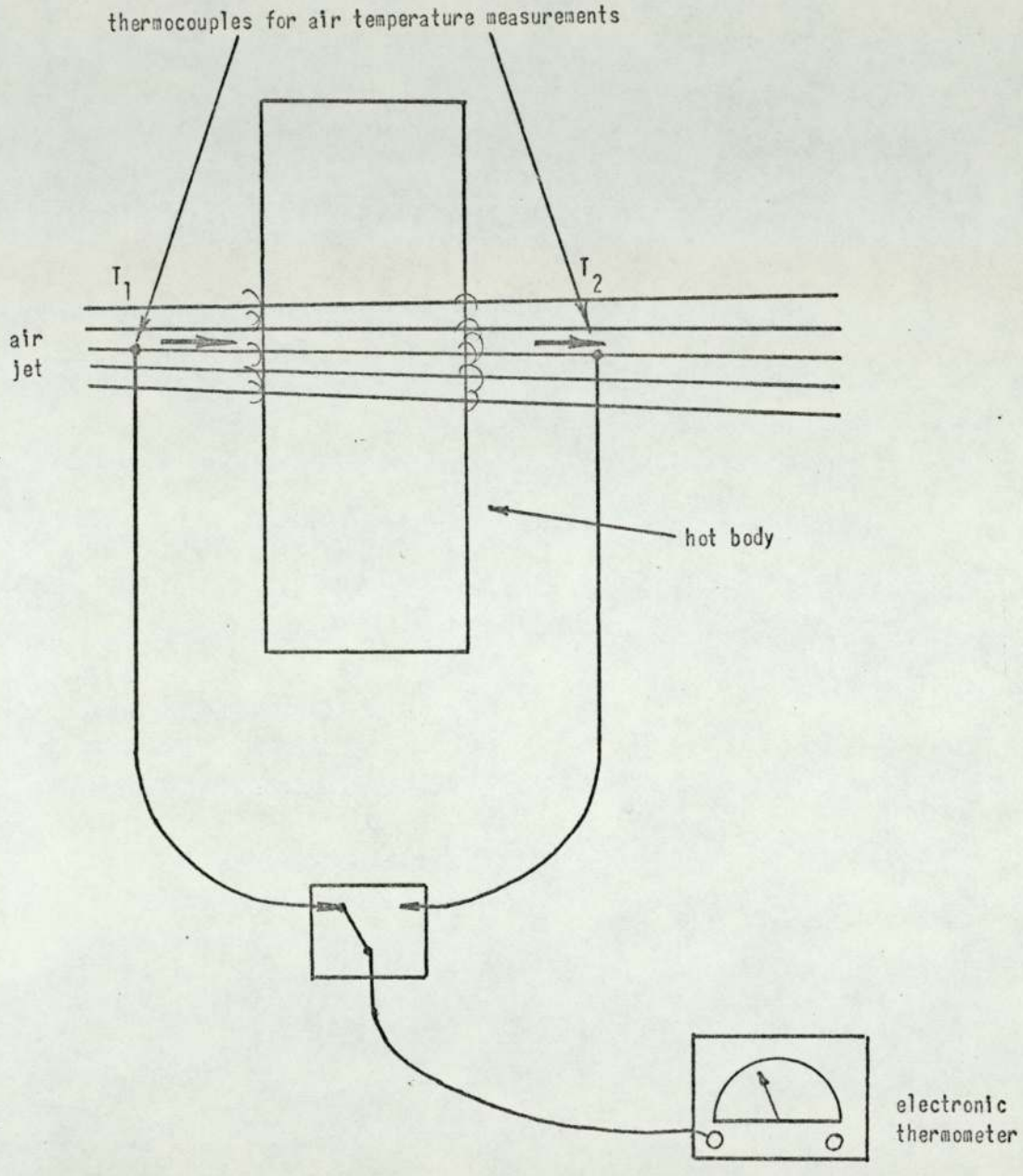

Fig. 13. Temperature difference created by heat transfer from a hot body to a jet of air blown across it

of 9 mm diameter metal rod.

The device constructed for this purpose is shown in Fig. 14 together with the experimental arrangement used for assessing its performance.

The device fabricated from aluminium consisted of an annular cavity sealed at both ends with an inner diameter 40 mm, an outer diameter 60 mm and a length of 230 mm.

Lying concentric with the device was a 9 mm diameter copper rod, (chosen for its high thermal conductivity), the temperature of which was to be measured. The rod was heated by two small cylindrical ovens placed at either end and the temperatures T_3 and T_4 at two different locations along its length, were measured with the aid of thermocouples C and D respectively.

Air was introduced into the cavity, via tubes, at either end and made to circulate round the cavity before finally emerging through a series of 6 mm diameter holes in the inner thin aluminium wall. The purpose of the cavity will be described later.

On passing into the inner tube the air circulated round the rod and in so doing extracted heat from the latter (if the rod was hotter than the air). Two thermocouples A and B placed at different locations along the length of this tube indicated respective temperatures T_1 and T_2. Since the air temperature was proportional to both the temperature difference between itself and the rod, and the time it had been exposed to the rod, T_1 was greater than T_2 (if the air had been hotter than the rod, then T_2 would have been greater than T_1).

On reducing the temperature differential between the rod and the air, a smaller value of (T_1-T_2) resulted, until when the rod and air temperatures became equal, a state of zero nett heat transfer

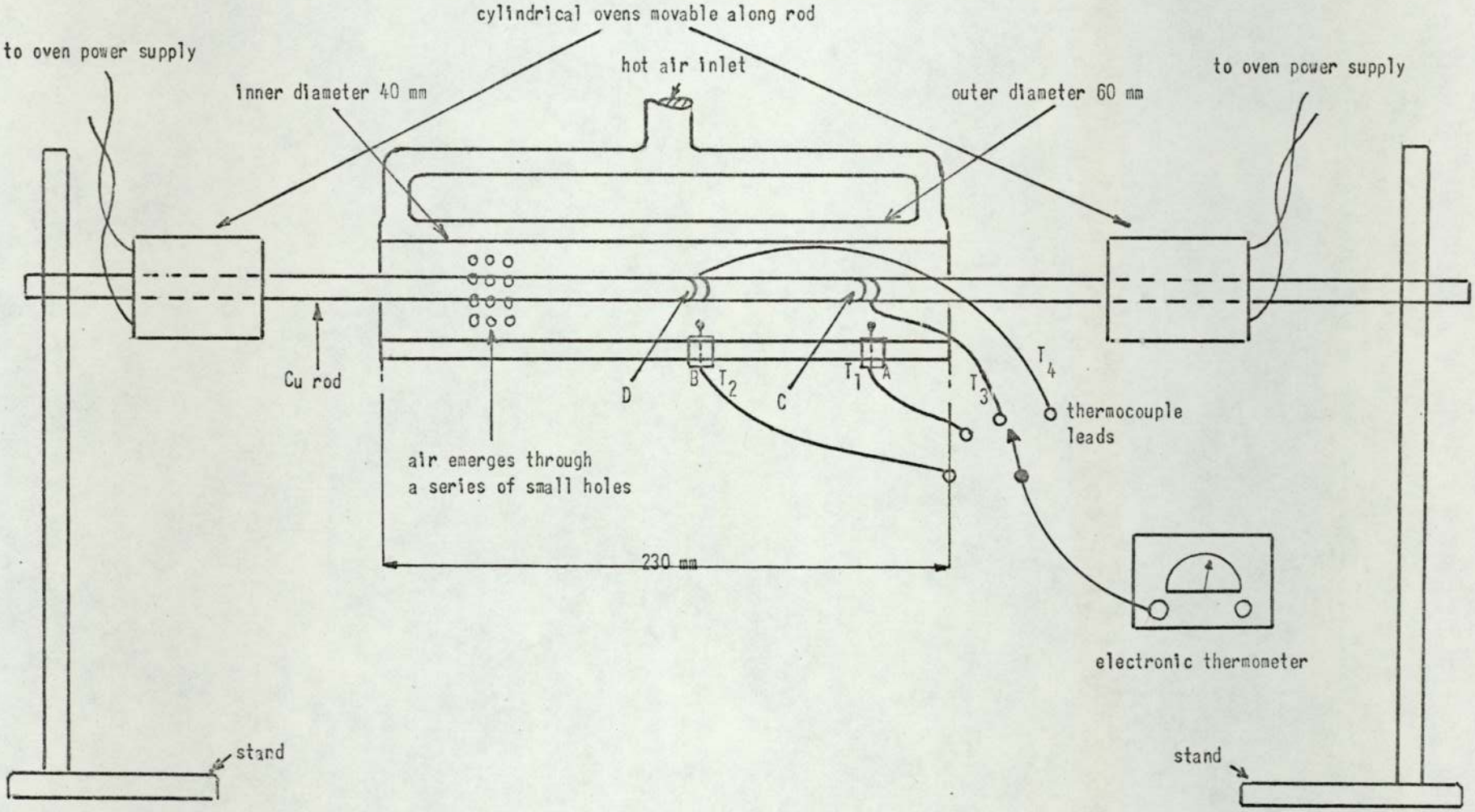

Fig. 14. Temperature measurement of copper rod

between the two was obtained. Under these conditions T_1 equalled T_2.

The purpose of the surrounding annular cavity was to maintain the walls of the inner tube at the temperature of the air in this tube, when zero nett heat transfer conditions between the rod and air prevailed.

Clearly this equality between the inner wall and air temperatures could not exist when the air and rod temperatures were unequal, since there would be heat transfer between the latter, the effect of which would be to create a temperature differential between T_1 and T_2, and hence between the air in the cavity and that in the inner tube. The inner wall temperature was a function of both these air temperatures.

In order to measure the rod temperature, therefore, the air temperature was adjusted, before introduction into the device, until T_1 equalled T_2 and under these zero nett heat transfer conditions the rod temperature was inferred directly from a measurement of either T_1 or T_2.

The sensitivity of the device was proportional to the displacement of A and B. That part of the inner tube to the left of the series of holes was not redundant as might appear, since it had the effect of precluding entrainment of cold air into the sensitive region of the device. The results of tests performed with this device are shown in Table 3.

The Dynamic Measurement of 9 mm Continuously Cast Aluminium Rod

The device discussed in the last section measured the temperature of stationary 9-mm diameter rod. However, another device based on this design was developed (though at the time of writing has not yet been installed), to measure the temperature of 9-mm diameter

TABLE 3

RESULTS OF EXPERIMENTS USING A 9-mm DIAMETER CYLINDRICAL COPPER ROD

T_1	T_2	T_3	T_4	$T_1 - T_2$
48.0	40.0	200.0	195.5	8.0
56.0	48.5	203.0	198.0	7.5
62.0	55.0	202.0	195.5	7.0
73.0	67.0	196.0	194.0	6.0
80.0	74.0	195.0	192.0	6.0
91.0	85.5	203.0	200.0	5.5
100.0	95.0	205.0	200.0	5.0
110.0	105.3	203.0	198.0	4.7
120.0	115.5	204.0	201.0	4.5
132.0	128.0	204.0	201.0	4.0
140.0	136.2	204.0	200.5	3.8
151.0	148.0	202.5	199.5	3.0
160.0	157.2	202.0	199.0	2.8
166.0	164.0	201.0	199.5	2.0
170.0	168.1	201.0	199.5	1.9
176.0	174.5	201.0	200.0	1.5
180.0	178.8	201.0	200.0	1.2
183.0	182.0	201.0	200.0	1.0
189.0	188.1	201.0	201.0	0.9
190.0	189.2	201.5	201.5	0.8
195.0	194.8	202.0	203.0	0.2
199.0	198.9	203.0	204.0	0.1
203.5	203.5	204.2	205.6	0
205.0	205.0	204.5	206.0	0
206.0	206.0	204.8	206.0	0
206.9	207.0	204.8	206.1	-0.1
207.5	207.8	204.2	205.9	-0.3

continuously cast aluminium rod as it emerged from the mill from which it was formed. Since rod speeds of the order of 1500 ft per/min. were involved during production, it was necessary to modify the design of the original device slightly, as well as add some peripheral equipment in order to accommodate the somewhat more demanding conditions under which it was to operate.

Plates 1 and 2 show the final rig. In this case the device was in two identical halves which swung away from the rod when the temperature was not required to be measured and was replaced by two graphite guides. The rod itself was restrained from moving in a plane normal to its axis by means of two sets of roller guides placed at either end of the device.

All the mechanical operations of the rig, e.g. closing and opening the guides, or closing or opening the two halves of the device, were performed with the aid of pneumatics. Interlocks were provided in order to prevent certain operations being performed accidentally, e.g. if the two halves of the device were closed, then without these interlocks it would have been possible to swing the graphite guides together, the result of which would have been to damage the device.

The air temperatures were measured with the aid of two sets of four thermocouples, each set located symmetrically in a plane normal to the axis of the device, the two planes lying at different positions along the axis.

By measuring the temperature with four thermocouples instead of one (as for the original design) at each of the two axial locations, a more accurate average air temperature could be measured. The effect of any slight lateral movement of the rod which might occur would also be accommodated.

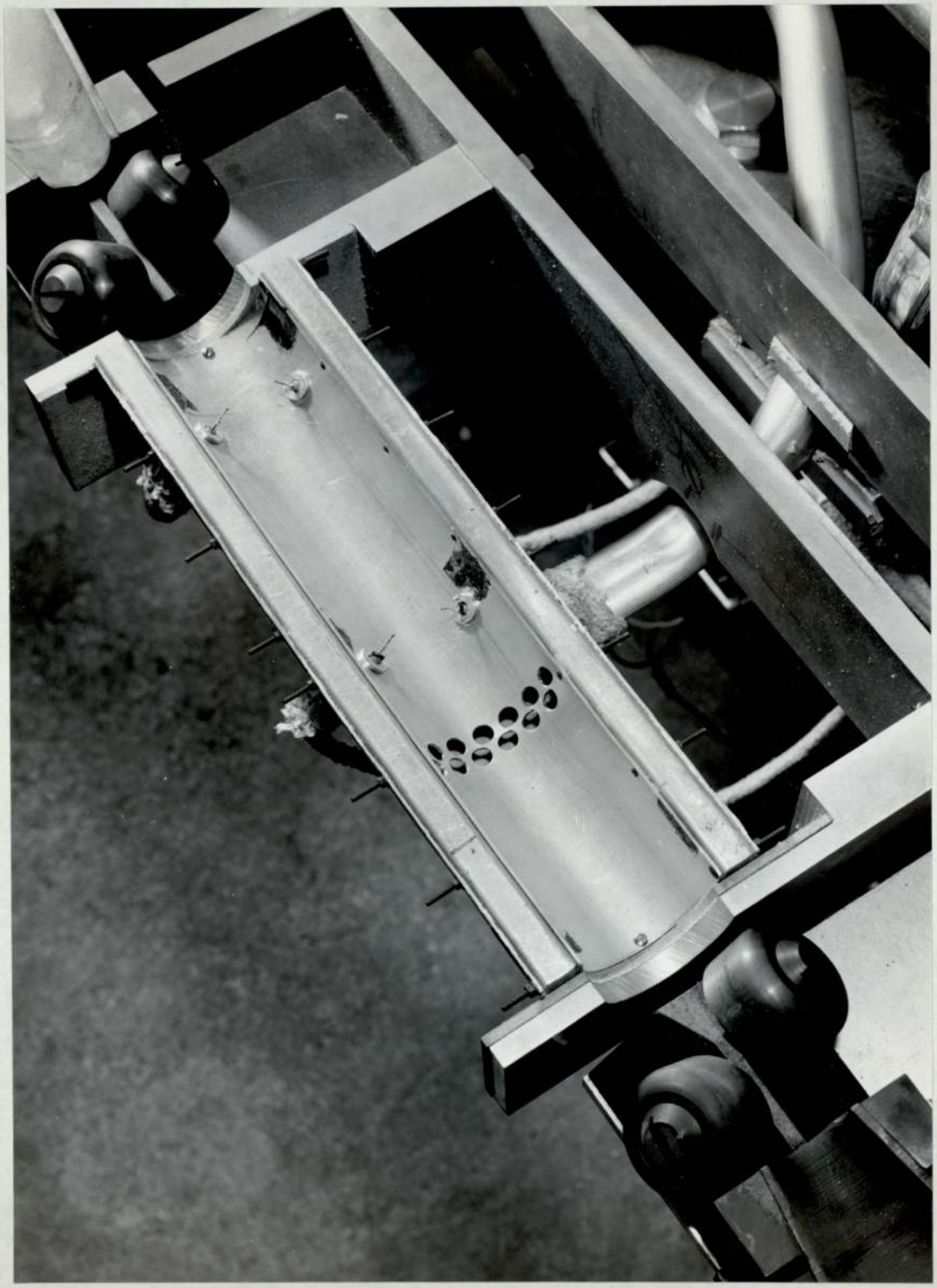

Plate 1. Temperature measurement of moving rod showing device in open position.

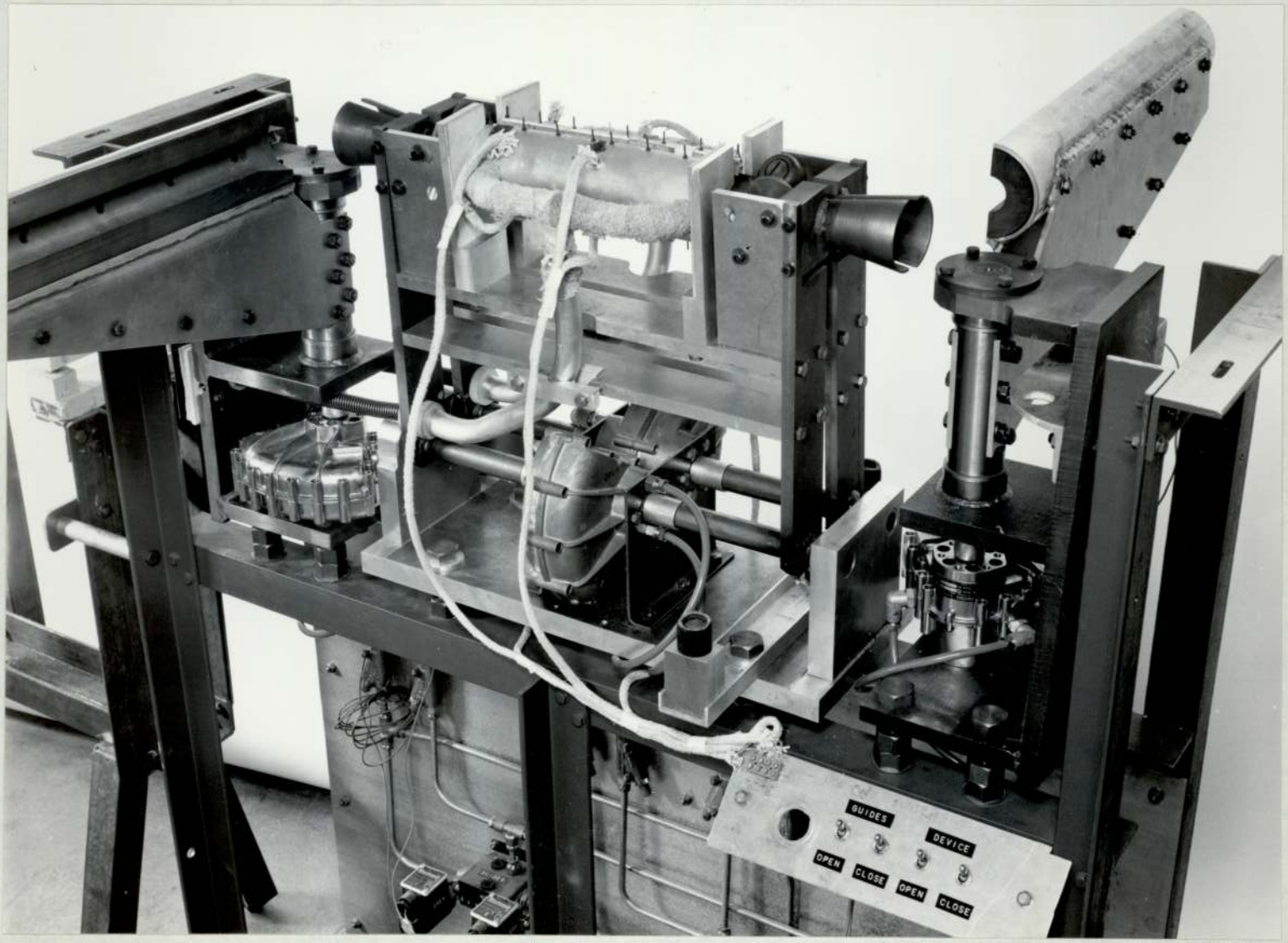

Plate 2. Rig for temperature measurement of moving rod showing guides open and the two halves of the device together.

CHAPTER 3

THE APPLICATION OF THE FORCED AIR CONVECTION METHOD TO PLANE SURFACES

Having demonstrated the potential of the forced air convection method for surfaces of cylindrical geometry the possibility of its exploitation in the temperature measurement of plane surfaces will now be examined.

Due to the different surface geometry a different geometrical arrangement of the measuring system would have to be adopted for plane surfaces, (unless their lateral dimensions were sufficiently small to permit a design similar to the above to be used).

The forced air convection method necessarily involves the measurement of air temperature after it has been in contact with the surface whose temperature is to be measured. Since the most convenient way of delivering air to a surface is by impinging a jet onto the surface it is appropriate to examine whether any of the characteristics of the subsequent flow patterns may be exploited in temperature measurement.

THE WALL JET

In 1956 Glauert published a paper which dealt with the theory of flow resulting from a jet, consisting of a fluid similar to that of its surroundings, impinging normally onto a plane surface[29]. He termed this flow pattern a 'Wall jet' and predicted various characteristics of the jet in his paper.

When a round free jet impinges normally onto a plane surface the fluid (air in this case) moves out radially from the origin

(stagnation point). Glauert showed that this flow condition had characteristics similar to a boundary layer in the inner wall region, and characteristics similar to a free jet in the outer regions.

Fig. 15 shows Glauert's predicted velocity profile through the thickness of the wall jet together with that derived experimentally by Bakke[30].

The vertical axis indicates the velocity, U, expressed in terms of the maximum, U_m. The horizontal axis indicates the displacement, y, normal to the surface expressed in terms of δ where δ is the value of y at which $U = \frac{U_m}{2}$.

Theory predicts that exact similarity of flow does not exist at all distances from the origin, i.e. if $U_m \propto R^a$ and $\delta \propto R^b$, then a and b vary slightly. However, the variation of a and b was so small as to be undetectable experimentally.

Figs. 16 and 17 show a plot of Log. δ vs. Log. R and Log. U_m vs. Log. R respectively as obtained by Bakke[30]. Note in Bakke's experiments the peak velocity of the free jet as it emerged from the pipe from which it originated was 34 m per second.

One possible way of exploiting this wall jet flow condition would be to place two thermal sensors in the wall jet at different radial distances from the origin. It will be shown in the theory section that the temperature of the wall jet increases with R so long as the temperature of the free jet at impingement is less than the surface temperature. Assume for the moment, that heat transfer only takes place between the wall jet and the surface and the effects of entrainment of cooler air into the wall jet and free jet are negligible. Then if a temperature differential exists between the impinging free jet and the surface then the two thermal sensors will indicate

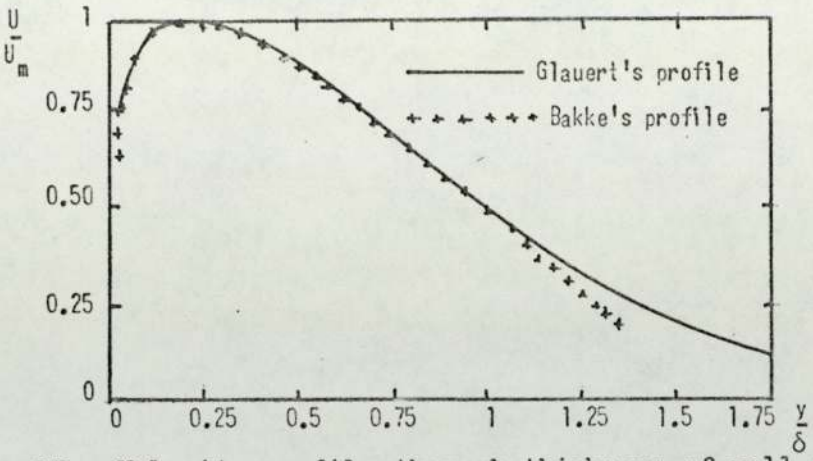

Fig. 15. Velocity profile through thickness of wall jet

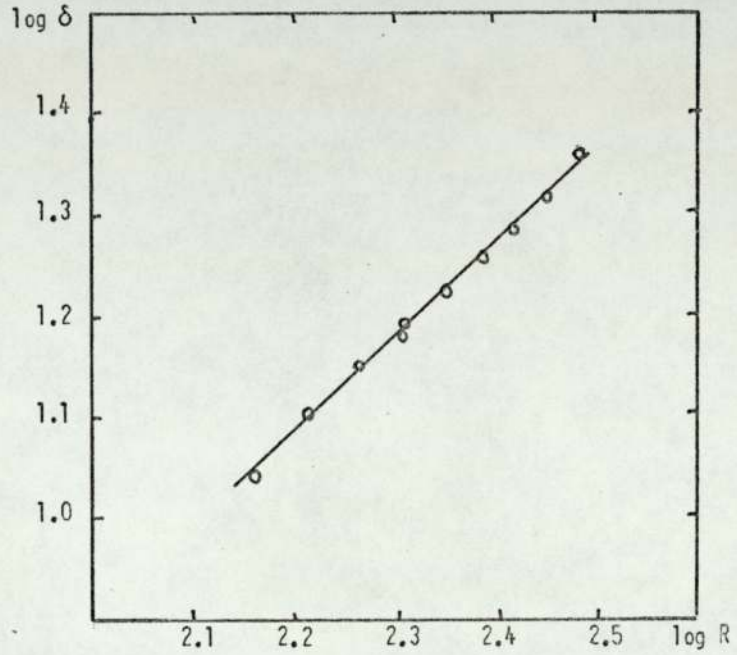

Fig. 16. Variation of wall jet width with distance from origin

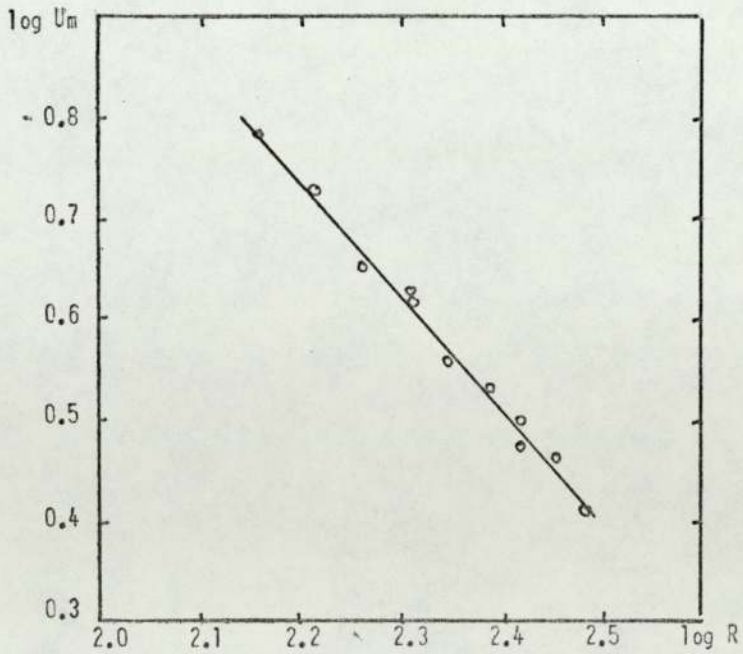

Fig. 17. Variation of maximum velocity of wall jet with distance from origin

different temperatures. If the free jet temperature is adjusted until it equals that of the surface then under the assumptions made there will be zero nett heat transfer between the wall jet and surface and the two thermal sensors will indicate the same temperature, this being the free jet and surface temperature.

Bakke's experiments were performed for radial distances ranging from 143 mm to 303 mm and wall jet thicknesses at these points were found to be 11 and 23 mm respectively.

Consider a design exploiting these wall jet characteristics. In order to keep its dimensions within practical limits the thermal sensors may conceivably be placed at locations with radial distances from the origin of say 5 cm and 10 cm. Extrapolating Bakke's best fit plot back to these values of R (see Fig.16) the 10 cm wall jet thickness would be approximately 7.9 mm and the 5 cm wall jet thickness would be approximately 4.2 mm. This procedure assumes of course that similarity exists for these smaller radial distances. Nevertheless even if a departure from similarity did occur the results drawn from this extrapolation will not be very different from the true values. The main implication of these results is that the thermal sensors would have to be placed very close to the surface (for practical radial distances) in order to exploit the wall jet temperature characteristics.

Another important characteristic relevant to the wall jet exploitation is its steep temperature gradient normal to the surface[31]. (This gradient, of course, depends upon the surface and air temperatures involved.) The effect of this would be to make the thermal sensor's location in this direction very critical.

Thus both these characteristics, i.e. very small wall jet

thicknesses for practical values of R and steep temperature gradients normal to the surface would make a temperature measuring method, involving temperature measurements at different radial locations in the wall jet, impracticable.

Note the increase of wall jet thickness and the decrease in maximum velocity with R as well as the steep temperature gradient normal to the surface are due mainly to the effects of turbulent mixing with air in the regions adjacent to the wall jet. Thus the original assumptions made at the beginning of this section have been proved to be invalid, i.e. entrainment effects are significant.

In view of the somewhat unfavourable characteristics associated with the wall jet it was decided to synthesize a different flow condition involving two wall jets but with characteristics conceivably, more suitable for exploitation in temperature measurement employing forced air convection.

This new flow condition will subsequently be referred to as a WIS jet where WIS is an acronym for 'wall jet impingement synthesis'.

THE WIS JET - A FLOW CONDITION RESULTING FROM THE IMPINGEMENT OF TWO IDENTICAL AXIALLY SYMMETRIC WALL JETS

Suppose two identical round free jets with axes O_1 and O_2 impinge normally onto a surface (lying in the xy plane) forming their respective wall jets (see Fig.18). The two wall jets will move out radially from their respective origins and impinge along a line AA'. This line may be visualized as an imaginary barrier.

Consider two fluid elements in the wall jets O_1ab and O_2ab. If these elements were in isolation then a possible flow pattern (in the yz plane) resulting from their impingement would be as indicated in

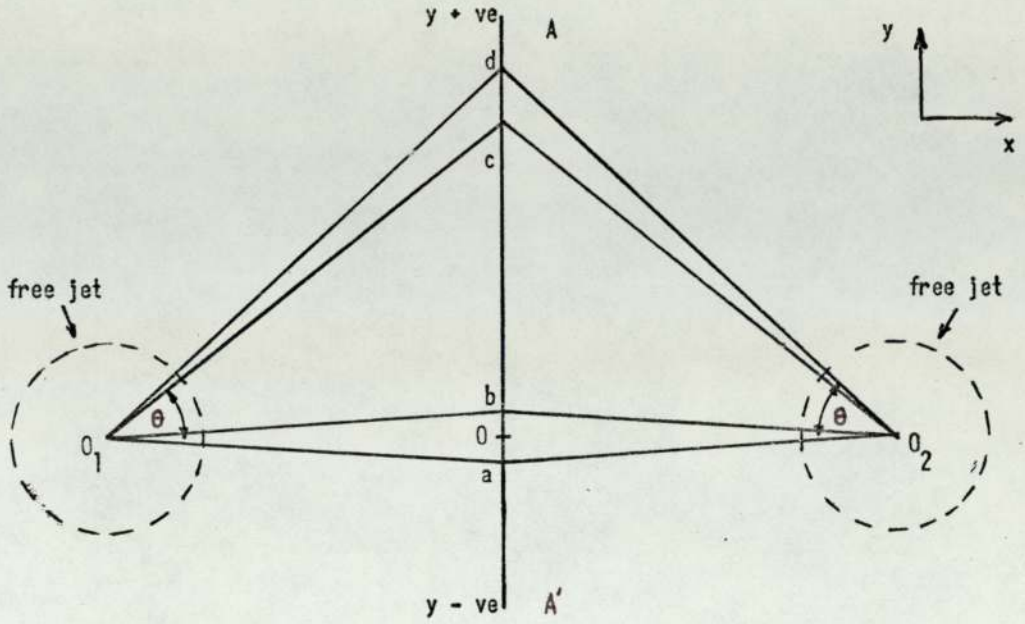

Fig. 18. The impingement of two identical wall jets

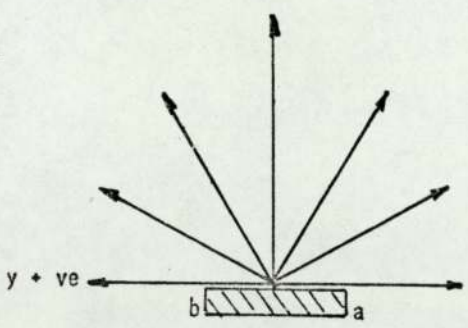

Fig. 19. Postulated flow resulting from the impingement of two fluid elements at y = 0 cm

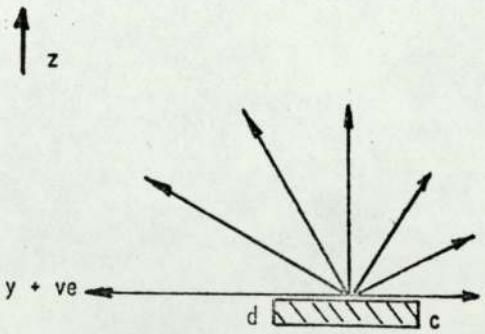

Fig. 20. Postulated flow resulting from the impingement of two fluid elements at y > 0 cm

Fig. 19. The vectors indicate the velocity and direction of flow. They need not, and probably will not be equal in magnitude, but they will form a symmetrical distribution. An almost identical flow pattern would result from the impingement of corresponding fluid elements, (if these were in isolation), adjacent to O_1ab and O_2ab.

If now the latter fluid elements are considered in situ, i.e. bounded by fluid on both sides, then after impingement the fluid must escape, but any tendency for escape in the y direction (+ve. or -ve.) will be opposed since adjacent fluid elements would behave in an almost identical manner. The only path which would not present this type of opposition would be one in the vertical direction. Thus for wall jet fluid elements lying close to O_1OO_2 the flow after impingement would be away from the surface in the z direction.

Consider the fluid elements O_1cd and O_2cd at an angle θ to O_1OO_2. In this case there is a significant residual y component of flow. If the maximum wall jet velocity just prior to impingement is U_r then this component will be proportional to $U_r \sin \theta$. The corresponding x component will be proportional to $U_r \cos \theta$. If the elements O_1cd and O_2cd were in isolation, then after impingement an asymmetrical flow pattern similar to that indicated in Fig.20 would result.

In situ these fluid elements will be bounded by almost identical fluid elements. The resultant component of flow after impingement would not in this case be normal to the surface in the z direction but would have a y component, which would have the effect of deflecting this resultant from the vertical.

Let the resultant velocity vector make an angle α with the vertical. Then as y increases θ will increase and hence $U_r \sin \theta$ will increase relative to $U_r \cos \theta$. The result of this is that α will

increase with y and approach $\frac{\pi}{2}$ as y approaches ∞.

Fig. 21 indicates the general flow characteristics based on the above model.

It has been shown experimentally that the WIS jet is fairly turbulent having a turbulent velocity profile similar to the mean velocity profile (see results of flow studies). The effect of this turbulence would be to modify the above characteristics, i.e. broaden the WIS jet as it moved away from the surface. Furthermore, since the maximum wall jet velocity varies almost linearly with $\frac{1}{r}$ the WIS jet should broaden as y increases.

It can be seen from the above that because a large proportion of fluid moves away from the surface after impingement the heat transfer between the WIS jet and surface will be small. There will, of course, be some diffusion and turbulent mixing.

It is likely that due to impingement, the fluid in the WIS jet close to the surface will be partially stagnated resulting in a low heat transfer rate between the WIS jet and surface under the jet.

It may be concluded, therefore, that because of the above and also the fact that for practical values of free jet spacing and θ, the surface area covered by the WIS jet will be much smaller than that covered by the constituent wall jets, the heat transfer between the WIS jet and surface will be much less than that between the constituent wall jets and the surface.

Having made a prediction of the general flow structure of the WIS jet on the basis of a simple model it is appropriate to consider its temperature characteristics. Since these will be related to the temperature characteristics of the constituent wall jets a theoretical examination of the latter will first be made.

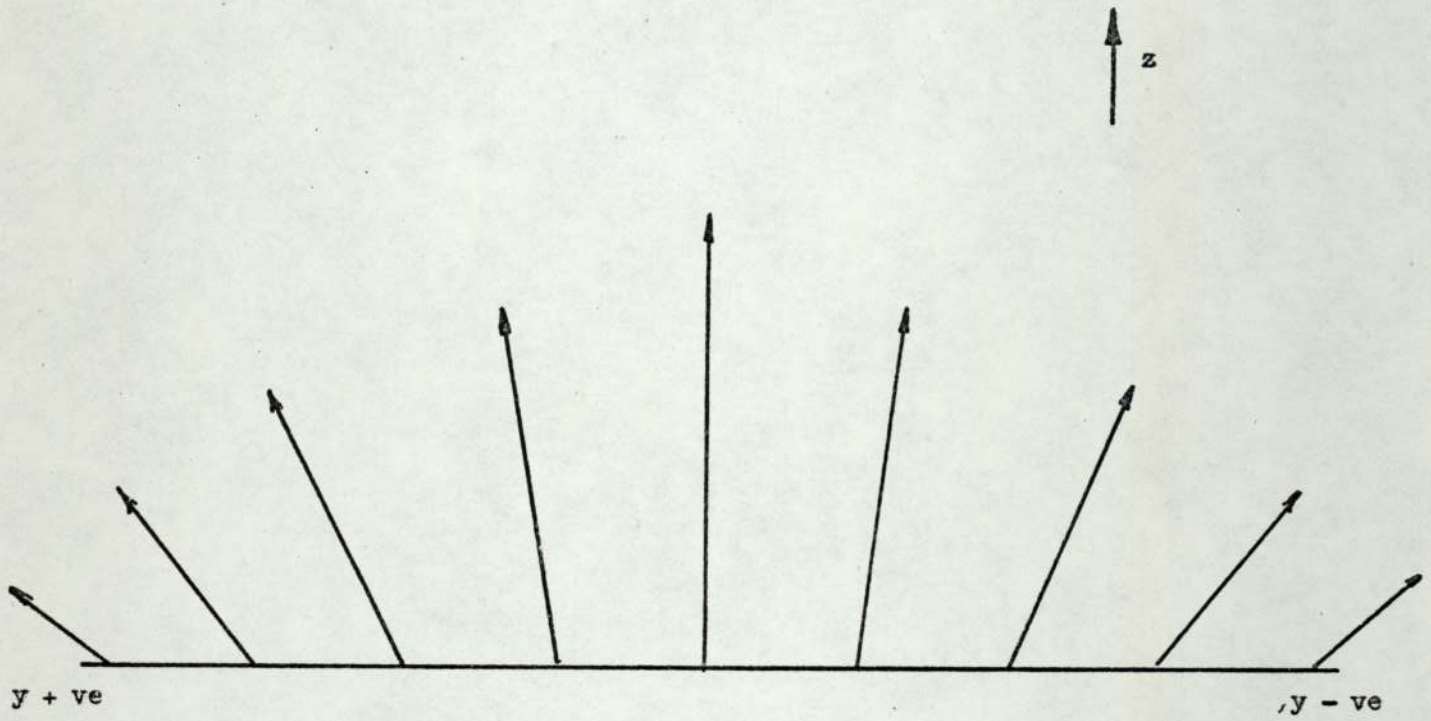

Fig. 21. Postulated flow in the yz plane resulting from the impingement of two identical wall jets

CHAPTER 4

THEORY

PREDICTION OF THE RADIAL VARIATION OF TEMPERATURE IN A WALL JET

Consider a round jet of air impinging normally onto a surface and forming a wall jet, (see section on the 'Wall Jet') and Figs. 22 and 23.

It will be assumed that the wall jet is manifest at a radial distance R_2 with its axis coinciding with the axis of the free jet.

For the moment the effects of entrainment and radiation will be neglected.

Consider a heat balance over an annular element of width δr and radius r.

Rate of heat gain by the air in moving across the element

$$= mc_p \frac{dT_r}{dr} . \delta r \quad \ldots\ldots\ldots\ldots\ldots\ldots\ldots\ldots\ldots\ldots\ldots\ldots \quad (28)$$

where m = mass flow rate at the beginning of the wall jet region.

c_p = specific heat of the air at const. pressure (assumed constant[32])

T_r = mean temperature of the wall jet at a radial distance r.

Let T_s be the temperature of the surface. Then the heat flow rate from the surface within the element of width δr at r is given by:

$$h_r 2\pi r \delta r (T_s - T_r) \quad \ldots\ldots\ldots\ldots\ldots\ldots\ldots\ldots\ldots\ldots\ldots\ldots \quad (29)$$

where h_r is the local heat transfer coefficient at r.

Equating (28) and (29) gives:

$$mc_p \frac{dT_r}{dr} . \delta r = h_r 2\pi r \delta r (T_s - T_r) \quad \ldots\ldots\ldots\ldots\ldots\ldots\ldots\ldots \quad (30)$$

Integrating (30) between R_2 and R:

$$mc_p \int_{T_2}^{T_R} \frac{dT_r}{(T_s - T_r)} = 2\pi \int_{R_2}^{R} r . h_r dr \quad \ldots\ldots\ldots\ldots\ldots\ldots\ldots \quad (31)$$

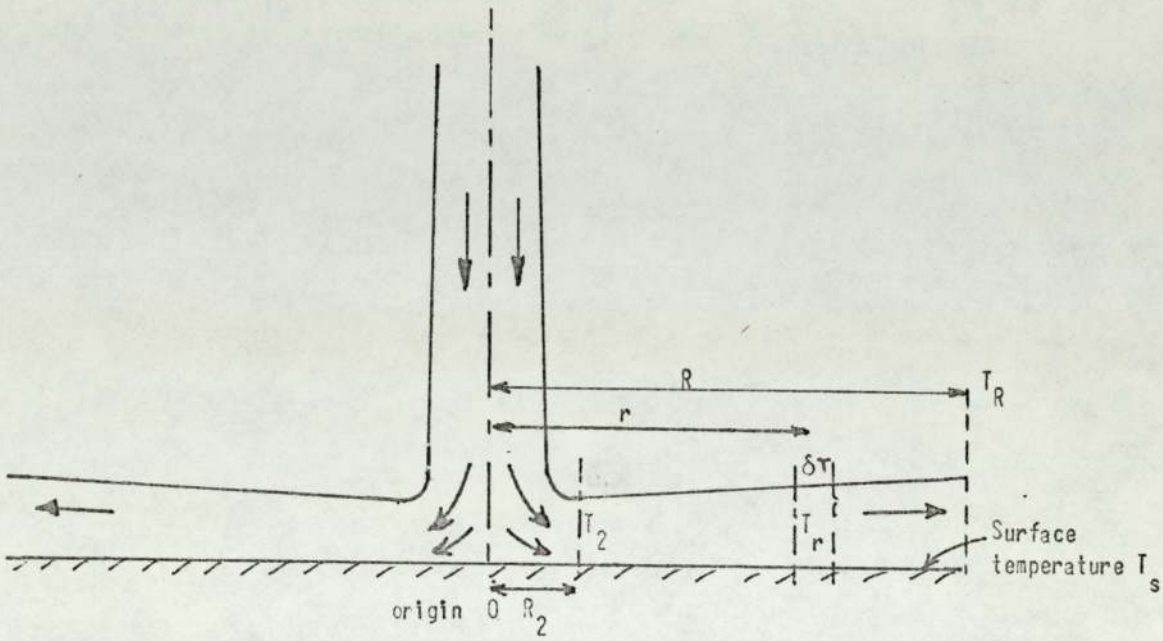

Fig. 22. Section through free jet and wall jet axis

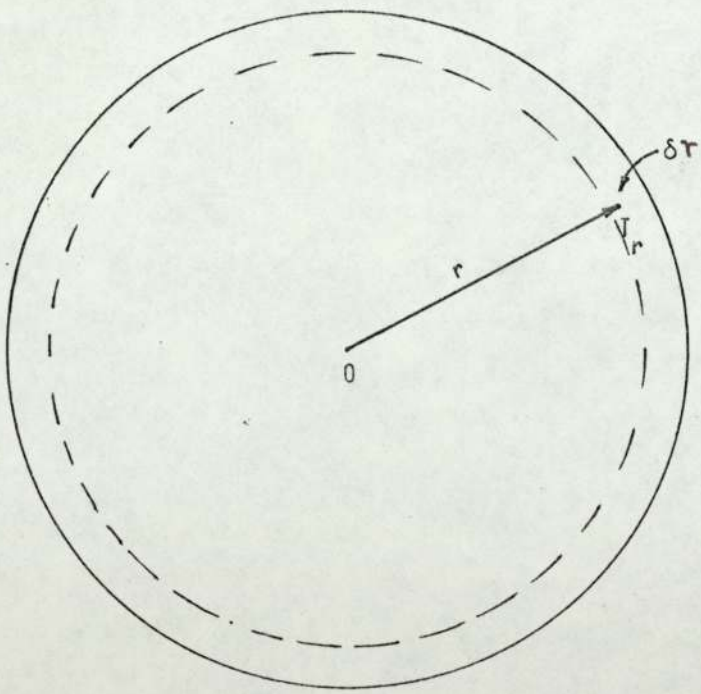

Fig. 23. Plan view of wall jet

Thus: $$\text{Log}_e \frac{(T_s-T_R)}{(T_s-T_2)} = \frac{-2\pi}{mc_p} \int_{R_2}^{R} r.h_r dr \quad \ldots\ldots\ldots\ldots\ldots\ldots \quad (32)$$

The right-hand integral cannot be integrated directly without a knowledge of the functional relationship between h_r and r[33,34,35].

Two relationships will be considered:

(1) $h_r = K$ where K is constant.

(2) $h_r = \frac{K'}{r}$ where K' is a different constant.

performing the integration for each case gives:

for $h_r = K$

$$\text{Log}_e \frac{(T_s-T_R)}{(T_s-T_2)} = \frac{-\pi K}{mc_p} [R^2-R_2^2] \quad \ldots\ldots\ldots\ldots\ldots\ldots\ldots \quad (33)$$

and for $h_r = \frac{K'}{r}$

$$\text{Log}_e \frac{(T_s-T_R)}{(T_s-T_2)} = \frac{-2\pi K'}{mc_p} [R-R_2] \quad \ldots\ldots\ldots\ldots\ldots\ldots\ldots \quad (34)$$

Let ${}_K T_R$ be the value of T_R corresponding to $h_r = K$

and ${}_{K'} T_R$ be the value of T_R corresponding to $h_r = \frac{K'}{r}$,

then solving for ${}_K T_R$ from (33):

$${}_K T_R = T_s - (T_s-T_2) \exp \frac{-\pi K}{mc_p} [R^2-R_2^2] \quad \ldots\ldots\ldots\ldots\ldots\ldots \quad (35)$$

and for ${}_{K'} T_R$ from (34):

$${}_{K'} T_R = T_s - (T_s-T_2) \exp \frac{-2\pi K'}{mc_p} [R-R_2] \quad \ldots\ldots\ldots\ldots\ldots\ldots \quad (36)$$

It can be seen from (35) and (36) that when $R = R_2$, then ${}_K T_R = T_2 = {}_{K'} T_R$ also when R approaches ∞ then both ${}_K T_R$ and ${}_{K'} T_R$ approach T_s.

Without a knowledge of K and K' the exact relationship between ${}_K T_R$ and R, and that between ${}_{K'} T_R$ and R cannot be deduced.

For the purpose of this analysis, however, it is sufficient to display their general trends. (See Fig.24)

Note the wall jet ceases to exist for values of $R < R_2$.

THE TEMPERATURE CHARACTERISTICS OF A WIS JET

Consider two identical round free jets impinging normally onto a surface and forming their respective wall jets. When these wall jets impinge they form a WIS jet. As has been shown in the section on WIS jets this particular type of flow has a three dimensional structure. It has also been shown that the proportion of fluid, within the WIS jet, which actually flows along the surface in the y direction (y+ve or y-ve) is small compared with the total flow of the WIS jet, i.e. most of the flow is away from the surface, the actual flow direction being a function of y (see Fig.21).

The area occupied by that part of the WIS jet in contact with the surface is small compared with the total area covered by the constituent-free jets (the relative areas are of course a function of the free jet spacing but for practical spacings the above statement is true).

From the above two statements it may be concluded that the heat transferred from the surface to the WIS jet itself is negligible compared with the heat transferred to the corresponding wall jets.

For this reason the temperature variation in the y direction along the WIS jet will be assumed to be solely a function of the temperature characteristics of the constituent wall jets.

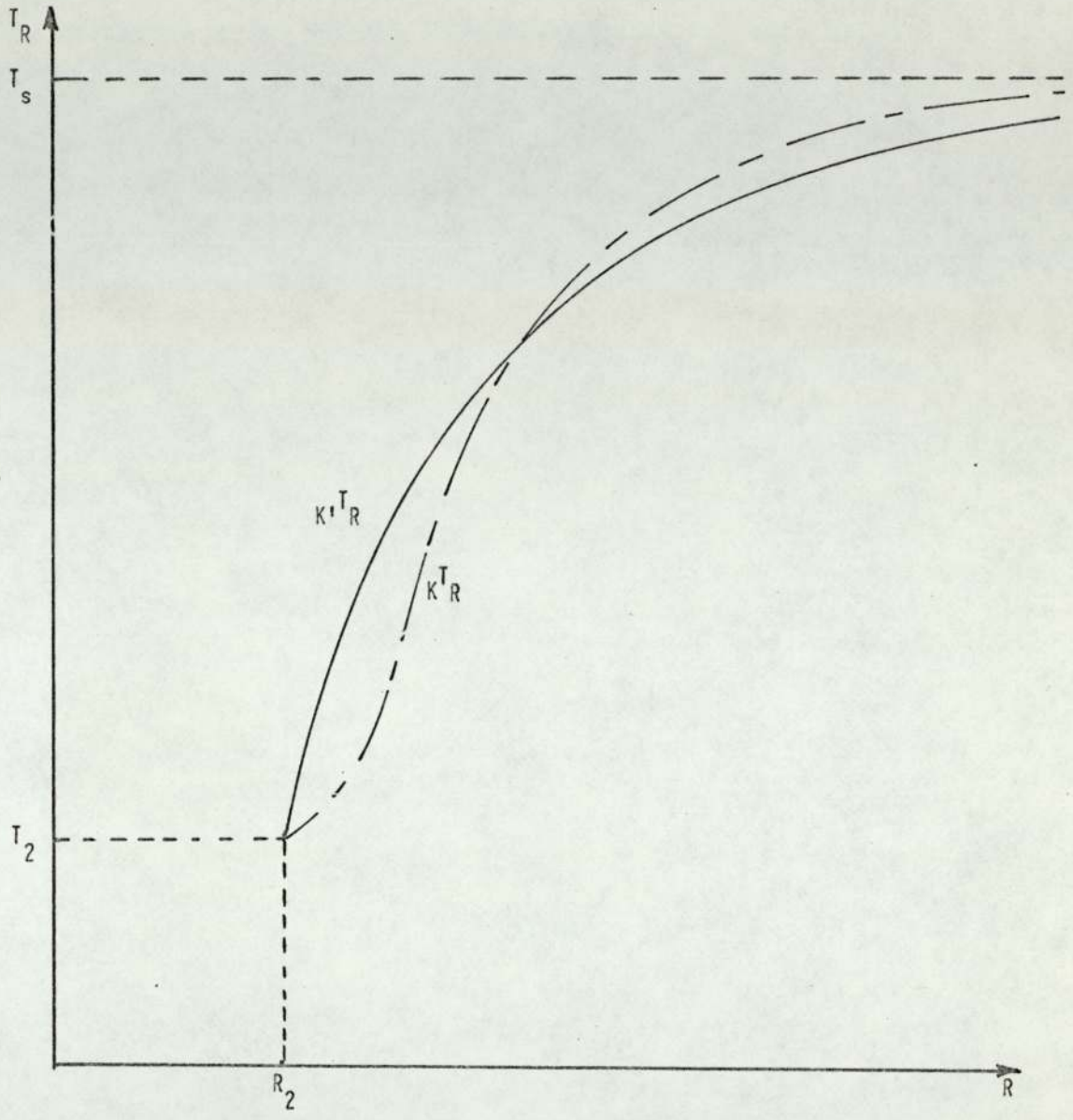

Fig. 24. Variation of mean wall jet temperature T_R with distance R from the origin for heat transfer coefficients h_r = K (corresponding to KT_R) and $h_r = \frac{K'}{r}$ (corresponding to $K'T_R$)

THE VARIATION OF WIS JET TEMPERATURE IN THE y DIRECTION

Equations (35) and (36) express the dependence of wall jet temperature on R for $h_r = K$ and $h_r = \frac{K'}{r}$ respectively. It is the purpose of this section to derive relationships expressing the variation of wall jet temperature in the y direction just prior to impingement.

Using the nomenclature of Fig.25 :

$$R^2 = x^2+y^2$$

For the moment x will be assumed constant.

Thus (35) becomes:

$$_K T_y = T_s - (T_s-T_2) \exp \frac{-\pi K}{mc_p} [x^2+y^2-R_2^2] \quad \ldots\ldots\ldots\ldots\ldots\ldots \quad (37)$$

and (36) becomes

$$_{K'}T_y = T_s - (T_s-T_2) \exp \frac{-2\pi K'}{mc_p} [(x^2+y^2)^{\frac{1}{2}} - R_2] \quad \ldots\ldots\ldots\ldots \quad (38)$$

differentiating (37) w.r.t. y

$$\frac{\partial}{\partial y} (_K T_y) = \frac{2y\pi K}{mc_p} (T_s-T_2) \exp \frac{-\pi K}{mc_p} [x^2+y^2-R_2^2] \quad \ldots\ldots\ldots\ldots \quad (39)$$

differentiating (38) w.r.t. y

$$\frac{\partial}{\partial y} (_{K'}T_y) = \frac{2y\pi K'}{mc_p} \frac{(T_s-T_2)}{(x^2+y^2)^{\frac{1}{2}}} \exp \frac{-2\pi K'}{mc_p} [(x^2+y^2)^{\frac{1}{2}} - R_2] \ldots\ldots\ldots \quad (40)$$

It can be seen from (39) and (40) that as x increases (y remaining constant) the gradients decrease. Thus it would be expected that a close free jet spacing should give rise to a WIS jet with a steeper y temperature gradient than a large free jet spacing.

It can also be seen that the gradients approach 0 as y approaches 0 and y approaches ∞, a result which is not surprising on purely physical grounds.

THE THEORY OF SURFACE TEMPERATURE PREDICTION USING THE FORCED AIR CONVECTION METHOD

It is the purpose of this section to show how the temperature

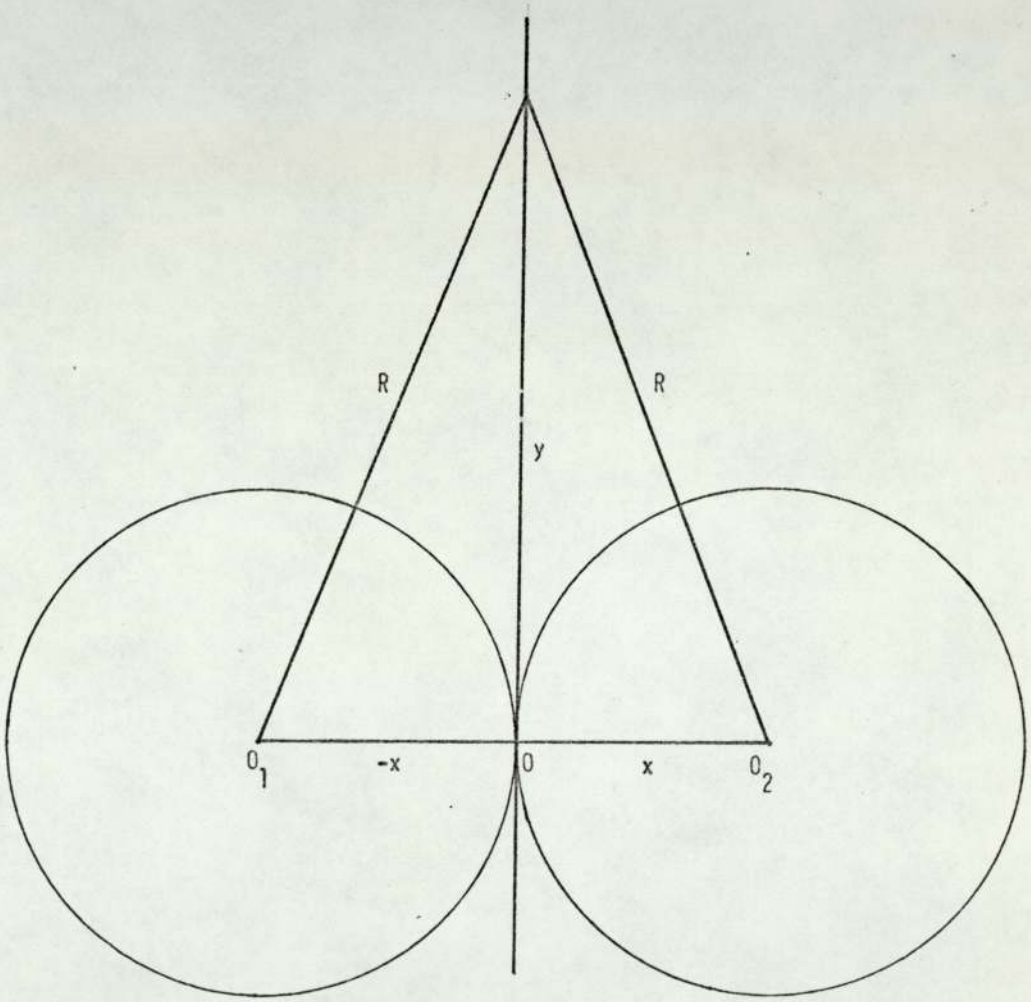

Fig. 25. Impingement of two identical wall jets

characteristics of the wall and WIS jets may be exploited in the prediction of surface temperature.

It is more convenient to examine the processes involved in terms of temperatures and temperature differences rather than energy transfer since the latter approach would necessitate a comprehensive knowledge of all the mechanisms involved, and the relative significance of the individual variables.

All the methods of prediction to be examined will involve either two or three free jets, these latter being either heated or unheated depending on the mode of operation employed, i.e. a surface temperature prediction need not necessarily involve identifying a state of zero nett heat transfer between the surface and the air blowing over it.

In the last section relationships were derived expressing the variation of wall jet temperature with radial distance from the origin (centre of the free jet impingement area). It was shown that the wall jet temperature increased with R (becoming asymptotic for $T_R = T_s$), irrespective of the form of a heat transfer coefficient, h, chosen.

The wall jet temperature at R_2 will differ from the corresponding free jet temperature (or some mean value) by an amount proportional to the heat transfer coefficient of the free jet. Suppose the free jet mean temperature at impingement is T_F.

Let $T_F - T_2 = \delta T_{F2}$ ..... (41)

then ${}_K T_R$ and ${}_{K'} T_R$ may be related to the free jet temperature by replacing T_2 in (35) and (36) by $T_F - \delta T_{F2}$.

Methods of Surface Temperature Prediction Using Two Free Jets

This section will be divided into two parts. The first part will

involve air temperature measurement in a plane drawn through the axes of the free jets and parallel to these jets. This will be referred to as the horizontal plane. (Fig. 26). The second part will involve air temperature measurement in a plane normal to the latter, parallel to the axes of the free jets and passing through a point midway between the free jet axes. This will be referred to as the vertical plane.

METHOD INVOLVING AIR TEMPERATURE MEASUREMENTS IN THE HORIZONTAL PLANE

Nomenclature

T_R = mean temperature of the wall jet at a radial distance R from the origin.

${}_sT_F$ = axial free jet temperature close to the surface S.

${}_oT_F$ = axial free jet temperature close to the orifice plate.

δT_F = ${}_oT_F - {}_sT_F$

${}_sT_W$ = WIS jet temperature at a point in the middle of the WIS jet close to the surface.

T_W = WIS jet temperature at a point in the middle of the WIS jet close to the orifice plate.

δT_W = ${}_sT_W - T_W$

δT_{sw} = ${}_sT_W - {}_sT_F$

T_s = surface temperature.

d = surface (S) - orifice plate (P_o) spacing.

T_e = the air temperature in those regions surrounding the jets.

Consider two identical round free jets impinging normally onto a surface and forming corresponding wall jets. These wall jets will flow over the surface and impinge forming a WIS jet midway between the two free jets.

The following assumptions will be made at this stage:

(1) $T_s \geq {}_sT_F > T_e$

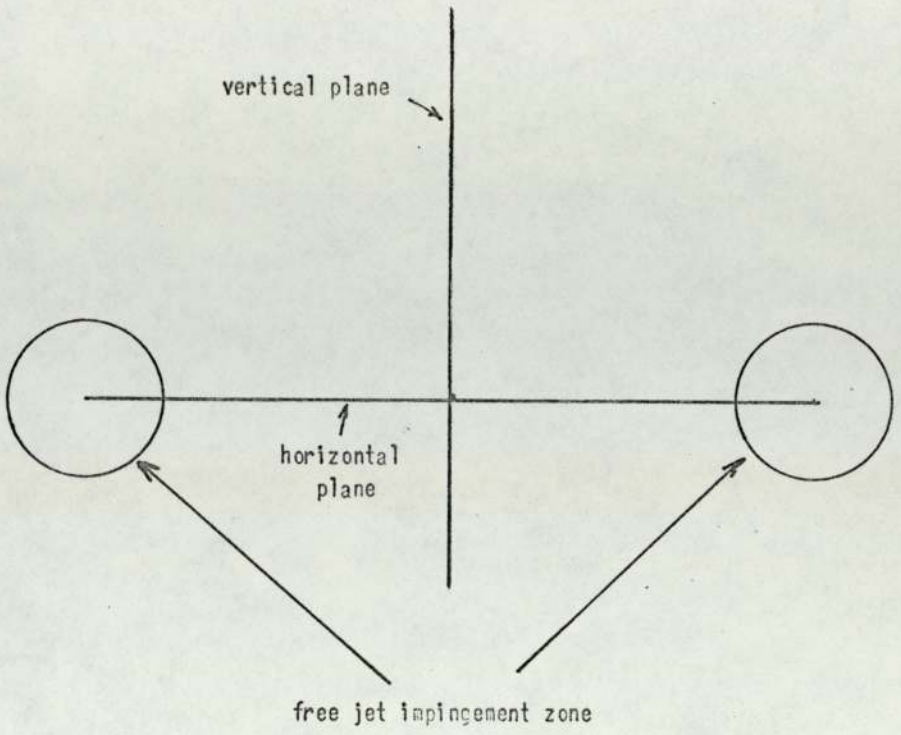

Fig. 26. Horizontal and vertical planes

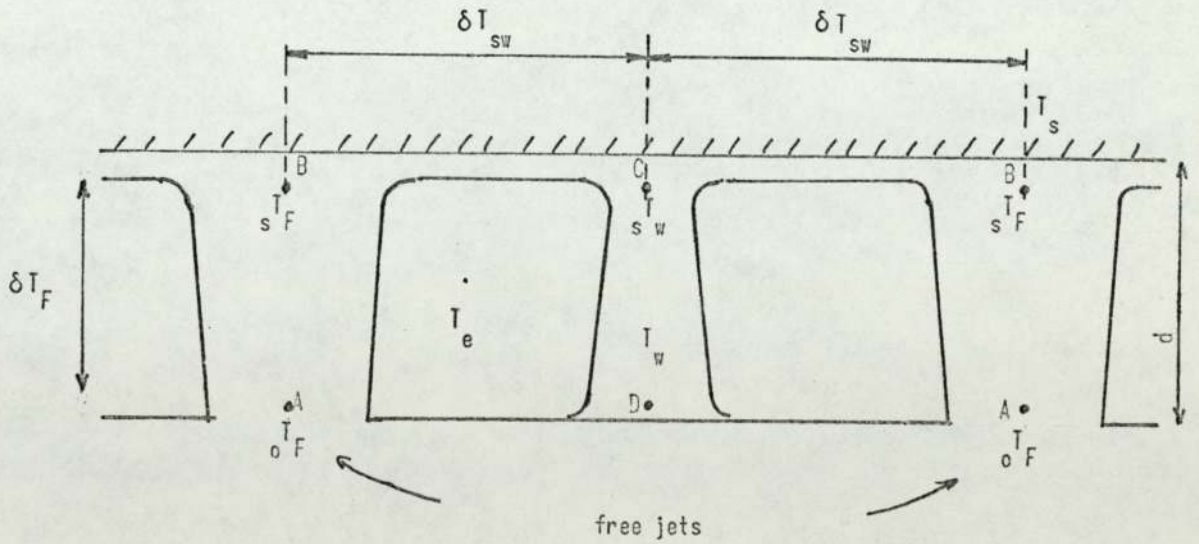

Fig. 27. Method involving two free jets and air temperature measurements in the horizontal plane

(2) Transverse temperature gradients in the free jets are negligible at locations close to P_o and close to S.

(3) Radiation effects are negligible.

(4) Cooling of the wall jets by entrainment of cooler air is negligible.

(5) T_e is the same for the free and WIS jets.

The significance of (3) and (4) will be examined later.

The variation in air temperature from the point A just outside the orifice from which it emerges, to a point D in the WIS jet close to the orifice plate will now be examined.

Using the nomenclature in the Fig. 27:

$$T_w = {}_oT_F - \delta T_F + \delta T_{sw} - \delta T_w \quad \ldots\ldots\ldots\ldots\ldots\ldots\ldots\ldots \quad (42)$$

From (42)

$$T_w - {}_oT_F = \delta T_{sw} - (\delta T_F + \delta T_w) \quad \ldots\ldots\ldots\ldots\ldots\ldots\ldots \quad (43)$$

Now it can be seen directly from equation (35) that

$$K T_R - T_2 = (T_s - T_2)\left[1 - \exp \frac{-\pi K}{mc_p}(R^2 - R_2^2)\right] \quad \ldots\ldots\ldots\ldots \quad (44)$$

a similar expression may be obtained from equation (36).

Since it has been assumed that transverse temperature gradients in the free jets close to S are zero it follows that δT_{F2} will equal zero and hence $T_F = {}_sT_F = T_2$. Thus δT_{sw} is in fact equal to $K T_R - T_2$ (or $K' T_R - T_2$) under these circumstances, i.e.

$$\delta T_{sw} \propto (T_s - T_2) \text{ or } (T_s - {}_sT_F) \quad \ldots\ldots\ldots\ldots\ldots\ldots\ldots\ldots \quad (45)$$

(Note T_2 only equals ${}_sT_F$ when $\delta T_{F2} = 0$ nevertheless even if δT_{F2} were finite δT_{sw} would still be a function of $(T_s - T_2)$ or $(T_s - {}_sT_F)$ (see equation (41)).

If temperature attenuation along the free and WIS jets were zero, i.e. $\delta T_F = \delta T_w = 0$ then (43) would become:

$$T_w - {}_oT_F = \delta T_{sw} \quad \ldots\ldots\ldots\ldots\ldots\ldots\ldots\ldots\ldots\ldots\ldots\ldots\ldots\ldots \quad (46)$$

Equation (46) is appropriate to conditions close to S. However, it can be seen from (43) that in a practical situation where air temperature must be measured at locations away from the surface, i.e. A and D then $T_w - {}_oT_F$ becomes a function of the temperature attentuation in the free jets[36,37,38,39] and WIS jet.

It is important, therefore to examine which factors influence δT_F and δT_w.

In general δT_F and δT_w will increase with d, δT_F will increase with $({}_oT_F - T_e)$ and δT_w will increase with $({}_sT_w - T_e)$.

If free jets at temperature T_e are used, i.e ${}_oT_F = T_e$ then $\delta T_F = 0$ and (40) becomes:

$$T_w - {}_oT_F = \delta T_{sw} - \delta T_w \quad \ldots\ldots\ldots\ldots\ldots\ldots\ldots\ldots\ldots\ldots \quad (47)$$

Now ${}_sT_w$ is proportional to ${}_oT_F$ as well as T_s thus by decreasing ${}_oT_F$, ${}_sT_w$ will also be reduced resulting in smaller value of $({}_sT_w - T_e)$ and hence δT_w. Thus the value of δT_w in (47) will be somewhat lower for unheated free jets than for heated ones.

The nett effect of using unheated free jets is therefore to reduce the significance of δT_F and δT_w in equation (43). An important consequence of this is that T_w becomes less sensitive to d.

The use of cold air of course, increases the temperature differential $T_s - {}_oT_F$ and hence $T_w - {}_oT_F$ the result being that surface temperature predictions based on $T_w - {}_oT_F$ will be more sensitive to T_s than if heated free jets (still cooler than T_s) had been employed.

Method Using Heated 'Free' Jets

Assuming, for the moment, δT_F and δT_w to be zero then:

$$T_w - {}_oT_F = \delta T_{sw} \quad \ldots\ldots\ldots\ldots\ldots\ldots\ldots\ldots\ldots\ldots \quad (48)$$

If ${}_oT_F$ is increased until ${}_oT_F = T_w$ then δT_{sw} will equal zero, i.e. a state of zero nett heat transfer (Z.N.H.T.) between the wall jet and S will exist.

The implication of this is that the temperature of the free jets will be equal to T_s. Thus by measuring the temperature of the free jets and/or the WIS jets at balance the value of T_s may be obtained directly.

In practice δT_F and δT_w will not be zero and it is appropriate to examine, therefore, the accuracy of prediction in this case. From (43):

$$T_w - {}_oT_F = \delta T_{sw} - (\delta T_F + \delta T_w) \quad \ldots\ldots\ldots\ldots\ldots\ldots\ldots\ldots \quad (43)$$

Suppose $\delta T_{sw} = \delta T_F + \delta T_w$ $\quad \ldots\ldots\ldots\ldots\ldots\ldots\ldots\ldots\ldots\ldots\ldots\ldots \quad (49)$

then $T_w = {}_oT_F$ and a balance will be indicated between thermal sensors placed at A and D. However, δT_F and δT_w are finite and additive, thus δT_{sw} must be finite.

Thus a balance under these conditions is <u>not</u> indicative of a state of (Z.N.H.T.) between the surface and the air blowing over it (the wall jet) and consequently ${}_oT_F$ and T_w will not equal T_s.

So long as ${}_sT_F < T_s$ then ${}_sT_w$ will never reach T_s (for practical free jet spacing, i.e. $R < \infty$) and since $T_w < {}_sT_w$ by an amount δT_w then T_w will always be less than T_s.

Thus the temperatures of the free and WIS jets measured under balance conditions will be less than T_s.

A true Z.N.H.T. condition would require ${}_oT_F - T_w$ to equal $\delta T_F + \delta T_w$ (resulting from a zero value of δT_{sw}).

It can be seen therefore that the difference between T_s and ${}_oT_F$ or T_w at balance will increase with δT_F and δT_w.

Thus to implement a method of surface temperature prediction using the Z.N.H.T. approach when two free jets are employed and measurements are made in the horizontal plane, it is necessary to keep δT_F and δT_W as low as possible.

Entrainment Effects in the Wall Jet

It was assumed at the beginning of this section that cooling of the wall jet by entrainment of colder air from the adjacent regions was negligible. It is appropriate to examine however, just what effect entrainment would have if this assumption were not justified.

It has been seen that δT_{sw} represents the increase in the temperature of air flowing over the surface, this increase being due to heat transfer from the surface to air (assuming ${}_sT_F < T_s$). Entrainment from adjacent cooler regions would oppose this increase, resulting in a reduced value of δT_{sw}. Let the value with entrainment be ${}_{en}\delta T_{sw}$.

Now $\quad \delta T_W \propto ({}_sT_W - T_e)$ .... (50)

thus if ${}_sT_W - T_e >> \delta T_{sw} - {}_{en}\delta T_{sw}$ then the effect of wall jet entrainment on δT_W will be negligible.

Let $\delta T_{sw} - {}_{en}\delta T_{sw} = {}_{en}\delta T$ .... (51)

from (43)

$${}_eT_W - {}_oT_F = {}_{en}\delta T_{sw} - (\delta T_F + \delta T_W) \quad \text{.................................} \quad (52)$$

where ${}_eT_W$ corresponds to the WIS jet temperature with wall jet entrainment.

Substituting from (51):

$${}_eT_W - {}_oT_F = (\delta T_{sw} - {}_{en}\delta T) - \delta T_F - \delta T_W \quad \text{.......................} \quad (53)$$

which shows that the existence of wall jet entrainment tends to

exaggerate the effect of finite temperature attenuation along the free and WIS jets. $_{en}\delta T$ will increase with $_{o}T_F$ and T_s but is not likely to be as sensitive to d as δT_F and δT_w (note if $_{o}T_F = T_e$ then $\delta T_F = 0$).

Entrainment Effects in the Heated Free Jet Mode

It must be remembered that in (53) δT_{sw} is not the actual temperature difference between $_{s}T_F$ and $_{s}T_w$ but is the difference which would exist in the absence of wall jet entrainment. It can be seen from (53) that if:

$$(\delta T_{sw} - {}_{en}\delta T) = \delta T_F + \delta T_w$$

a balance will be indicated between thermal sensors placed at A and D (see Fig. 27). However, under these conditions $(\delta T_{sw} - {}_{en}\delta T)$ would be finite and positive thus $_{e}T_w$ would be less than T_s and so also would be $_{o}T_F$.

If it were possible to reduce δT_F and δT_w to zero and yet still keep $_{en}\delta T$ finite and positive, it would be necessary to reduce $_{o}T_F$ to a value less than T_s in order to achieve a balance betwen $_{o}T_F$ and $_{e}T_w$.

It is interesting to note that if R approaches ∞ in equations (35) and (36) $_{K}T_R$ and $_{K'}T_R$ approach T_s. However, these equations were derived neglecting wall jet entrainment effects and if these effects are included then neither $_{K}T_R$ nor $_{K'}T_R$ would reach T_s as R approached ∞.

RADIATION EFFECTS IN A SYSTEM USING TWO FREE JETS

Up to now heat transfer by radiation has been neglected. It is appropriate, however, to discuss the effect it would have on surface temperature prediction if it were significant compared to the

convective heat transfer discussed so far.

In both the heated and unheated free jet modes of operation the measuring sensors (thermo-couples) have been located at point A($T.C_A$) in the free jets and point D($T.C_D$) in the WIS jet.

The following discussion will relate to the two dimensional configuration indicated in Fig.28 .

It will be assumed throughout that gas radiation is negligible and that the convective heat transfer to the thermo-couple is the same for the WIS jets and free jets*.

Unheated Free Jets

Reference to Fig.28 will indicate that $T.C_A$ will receive direct and multiply reflected radiation from S in an angle θ_A. Since $T.C_A$ lies directly over the free jet orifice very little reflected radiation from the orifice plate will be received. A small proportion of radiation (direct and reflected) from S will pass through the orifice and be reflected by the baffle plate in the device. However, very little of this reflected radiation will be intercepted by $T.C_A$.

The angle subtended by S at D, i.e. θ_D will be greater than θ_A thus $T.C_D$ will receive more direct and multiply reflected radiation from S than $T.C_A$. Furthermore $T.C_D$ lies directly over a reflector, the orifice plate, and will thus receive radiation reflected from the orifice plate.

The nett effect of the above is, therefore, to make $T.C_D$ more sensitive to radiation than $T.C_A$. Thus the temperature differential

---

* This assumption is not completely justified since it is likely that the convective heat transfer coefficient of the free jet is different from the WIS jet. The significance of this effect will be dealt with in a later section.

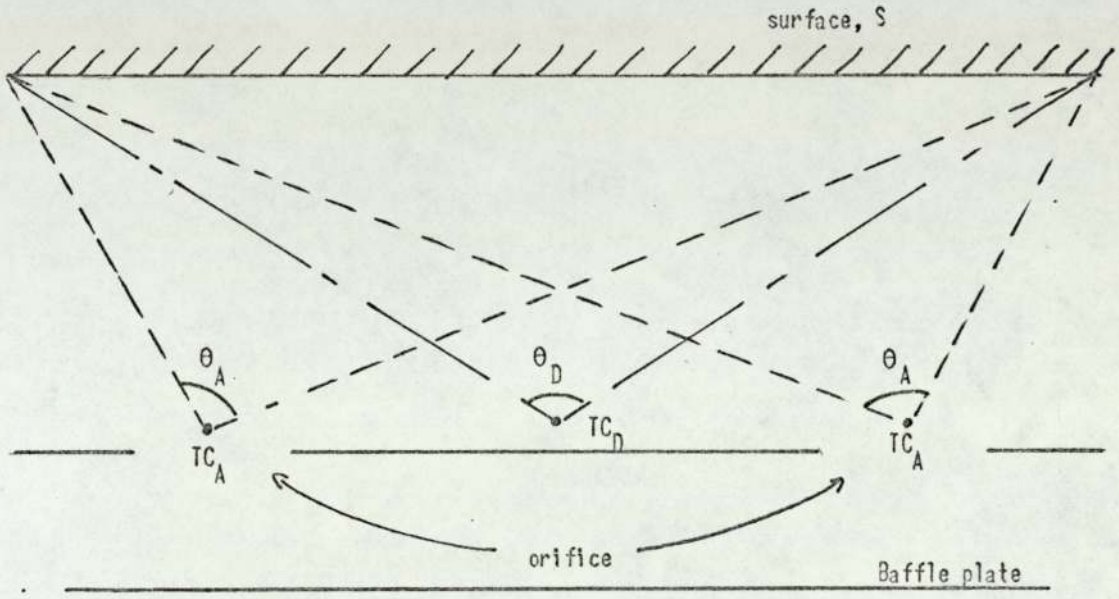

Fig. 28. Geometrical radiation effects in the two free jet method involving air temperature measurements in the horizontal plane

between $T.C_A$ and $T.C_D$ will contain a radiation contribution and the predicted temperature will thus be a function of emissivity. This temperature differential will, of course, be higher than it would have been in the absence of radiation effects.

By extending the above reasoning to the true three dimensional configuration the same general conclusions as above will be drawn.

Heated Free Jets (Under Z.N.H.T. Conditions)

In this case partial black body conditions will prevail, the departure from perfect black body conditions resulting from radiation leakage from between the two plates.

$T.C_A$ will receive almost black body radiation from the orifice together with direct and multiply reflected radiation from S contained in the angle θ_A.

$T.C_D$ will receive a little more direct and multiply reflected radiation from S contained in an angle θ_D together with direct and multiply reflected radiation from the orifice plate over which $T.C_D$ lies. Since the surface emissivity of the orifice plate will be somewhat less than 1 (maybe 0.1 it is possible and indeed likely that $T.C_D$ will receive slightly less total radiation than $T.C_A$.

Suppose δT_F, δT_W and $_{en}\delta T$ are zero then without radiation effects the temperature of the WIS and free jets at balance would be equal to T_s. However, with radiation effects the temperature of $T.C_D$ would probably be less than that of $T.C_A$ under these zero nett heat transfer conditions at the surface and in order to regain a balance between $T.C_A$ and $T.C_D$ the free jet temperature $_oT_F$ must be reduced, giving rise to a value of $_oT_F$ (or T_W) at balance less than T_s.

METHOD INVOLVING AIR TEMPERATURE MEASUREMENTS IN THE VERTICAL PLANE

Nomenclature:

T_w = WIS jet temperature at a point 'a' in the middle of the WIS jet in the horizontal plane and close to the orifice plate.

$_yT_w$ = WIS jet temperature at a point 'b' in the middle of the WIS jet in the vertical plane close to the orifice plate and displaced from 'a' by a distance y.

$_{ys}T_w$ = WIS jet temperature at a point, 'c', in the middle of the WIS jet in the vertical plane close to S and displaced from the horizontal plane by a distance y.

$_sT_w$ = WIS jet temperature at a point, 'd', in the middle of the WIS jet close to S and lying in the horizontal plane.

$$_y\delta T_w = {}_{ys}T_w - {}_yT_w$$

$$\delta T_{Rsw} = {}_{ys}T_w - {}_sT_F$$

$$\delta T_{sw} = {}_sT_w - {}_sT_F$$

Any other nomenclature used in this section has been defined previously or will be defined in the text.

It has been shown in equations (37) and (38) that if $T_s > T_2$ (the air temperature at the start of the wall jet) then $_KT_y$ and $_{K'}T_y$ will increase with y (neglecting entrainment and radiation effects) and also with T_s.

Using the nomenclature of Fig.29 the temperature differential between c and d will be equal to:

$$_{ys}T_w - {}_sT_w \quad \ldots\ldots\ldots\ldots\ldots\ldots\ldots\ldots\ldots\ldots\ldots\ldots\ldots\ldots\ldots\ldots\ldots\ldots \quad (54)$$

Assuming again no transverse temperature gradients in the free jets close to S and the orifice plate then:

$$T_2 = {}_sT_F \quad \ldots\ldots\ldots\ldots\ldots\ldots\ldots\ldots\ldots\ldots\ldots\ldots\ldots\ldots\ldots\ldots\ldots\ldots \quad (55)$$

and reference to (39) and (40) will show that the temperature gradient in the y direction in the WIS jets will decrease as $_sT_F$

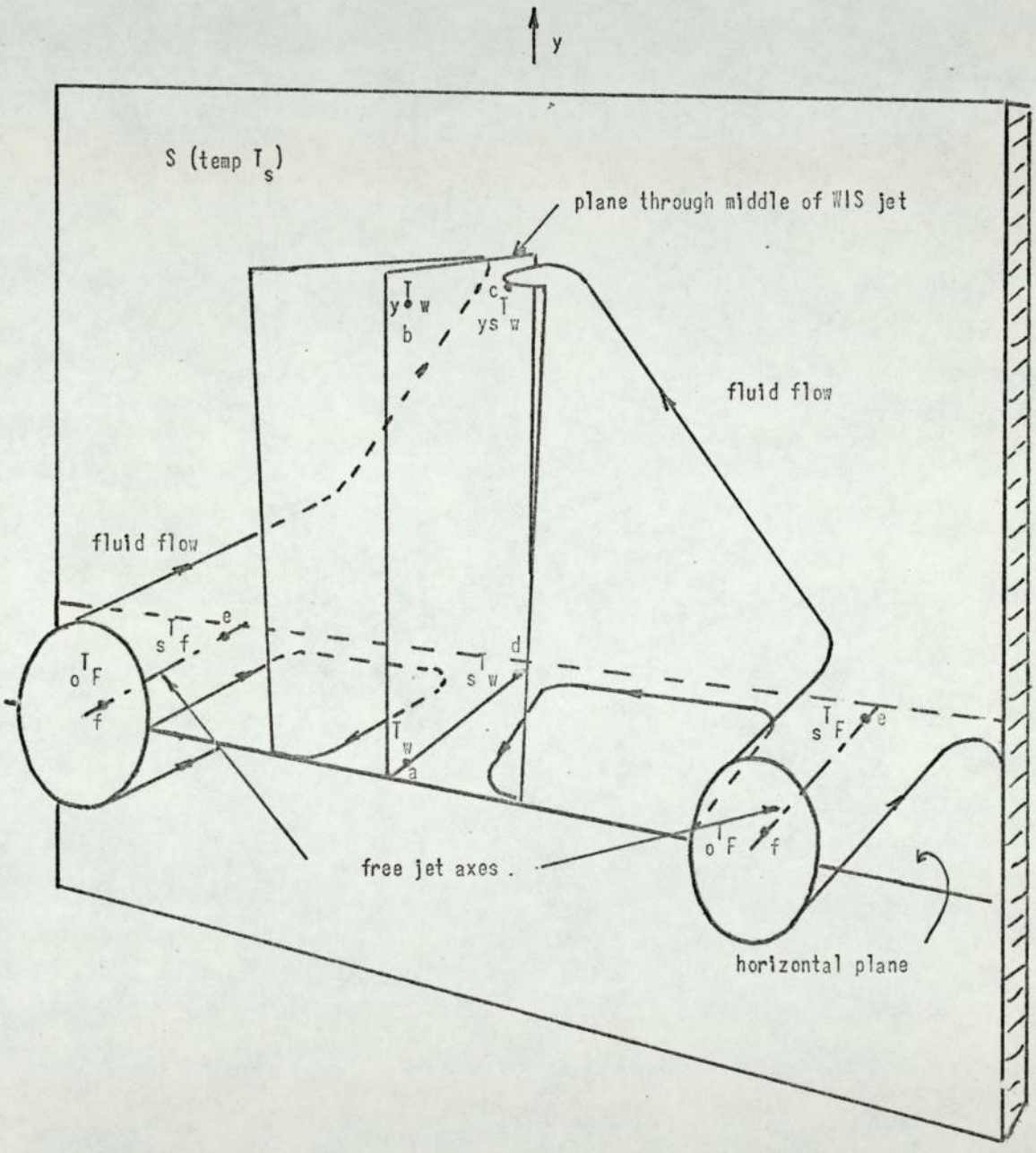

Fig. 29. Method involving two free jets and air temperature measurements in the vertical plane

approaches T_s this gradient becoming zero for ${}_sT_F = T_s$.

It can be seen, therefore, that ${}_{ys}T_w - {}_sT_w$ is proportional to $T_s - {}_sT_F$ and is thus potentially capable of being exploited in surface temperature prediction.

For the moment the effects of entrainment in the wall jet will be neglected. Radiation effects will also be neglected.

The variation of air temperature round the paths fecb and feda will now be examined.

Path fecb

$$ {}_yT_w = {}_oT_F - \delta T_F + \delta T_{Rsw} - {}_y\delta T_w \quad \ldots\ldots (56) $$

$$ \text{or} \quad {}_yT_w - {}_oT_F = \delta T_{Rsw} - \delta T_F - {}_y\delta T_w \quad \ldots\ldots (57) $$

Path feda

$$ T_w = {}_oT_F - \delta T_F + \delta T_{sw} - \delta T_w \quad \ldots\ldots (58) $$

$$ \text{or} \quad T_w - {}_oT_F = \delta T_{sw} - \delta T_F - \delta T_w \quad \ldots\ldots (59) $$

Combining (57) and (59) the following relationship is obtained:

$$ {}_yT_w - \delta T_{Rsw} + {}_y\delta T_w = T_w - \delta T_{sw} + \delta T_w \quad \ldots\ldots (60) $$

$$ \text{or} \quad {}_yT_w - T_w = (\delta T_{Rsw} - \delta T_{sw}) + (\delta T_w - {}_y\delta T_w) \quad \ldots\ldots (61) $$

It can be seen from (61) that the δT_F and ${}_oT_F$ terms have disappeared. Reference to (37) and (38) however will indicate that δT_{Rsw} and δT_{sw} are both exponential functions of $T_s - ({}_oT_F - \delta T_F)$ where $({}_oT_F - \delta T_F) = T_2$ under the assumptions made. Thus ${}_yT_w - T_w$ is dependent upon ${}_oT_F$ and δT_F.

It can also be seen from (61) that ${}_yT_w - T_w$ involves the difference between the WIS jet attenuations along cb and da, thus the effect of these attenuations should be reduced. If $\delta T_w = {}_y\delta T_w$ then the sensitivity of ${}_yT_w - T_w$ to WIS jet attenuation would disappear.

Unheated Free Jets

For unheated jets at a temperature T_e, δT_F will be zero as was the case for measurements in the horizontal plane.

If $\delta T_w - {}_y\delta T_w$ is finite implying that the WIS jet attenuations along da and cb are unequal then for a given value of $T_s - {}_sT_F$, ${}_yT_w - T_w$ will be dependent on d. (i.e. δT_w and ${}_y\delta T_w$ are proportional to d). The extent of this dependence will increase with $\delta T_w - {}_y\delta T_w$.

Heated Free Jets (In the Z.N.H.T. Mode)

Reference to equation (61) will indicate that if

$$(\delta T_{Rsw} - \delta T_{sw}) = ({}_y\delta T_w - \delta T_w)$$

a balance will exist between ${}_yT_w$ and T_w.

If, at balance, ${}_y\delta T_w - \delta T_w \neq 0$ then a state of Z.N.H.T. will not exist between the wall jet and the surface since to maintain a balance $\delta T_{Rsw} - \delta T_{sw}$ would have to be finite, implying that heat transfer between the wall jet and S had taken place.

It is clear that, at balance, ${}_yT_w$ and T_w will be less than T_s (provided $T_s > {}_oT_F$). The departure from a Z.N.H.T. condition at balance will be proportional to $|{}_y\delta T_w| - |\delta T_w|$. It must be stressed that even if ${}_y\delta T_w = \delta T_w$, in which case a balance would correspond to a state of Z.N.H.T., the value of ${}_yT_w$ and T_w will only equal T_s if ${}_y\delta T_w$ and δT_w are both zero.

Entrainment Effects in the Wall Jet

It is helpful to examine these effects with the aid of a typical curve of wall jet temperature versus radial distance from the origin (see Fig. 30 and Fig. 31).

Suppose curve A in Fig.30 corresponds to the case of no wall jet entrainment. This curve will become asymptotic as R approaches ∞ with a value of $T_R = T_s$.

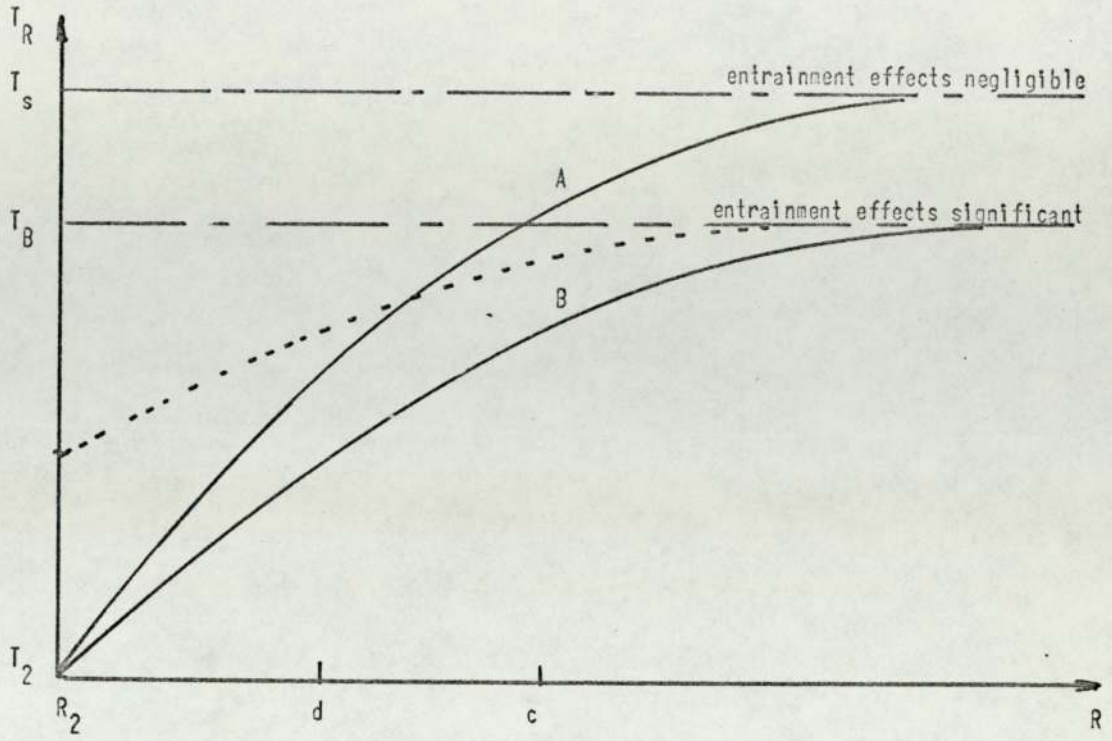

Fig. 30. Variation of T_R with R showing the effects of wall jet entrainment

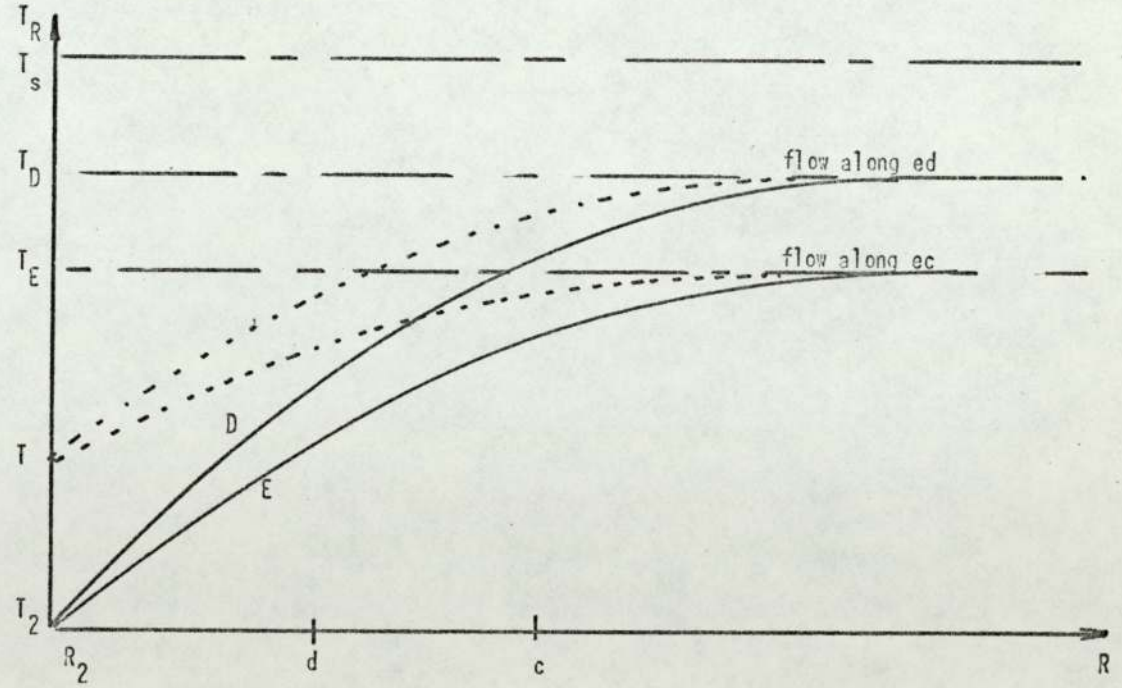

Fig. 31. The variation of T_R with R showing the possible influence of flow direction

If entrainment effects become evident then curve A will be suppressed to some curve B with T_R approaching some value T_B for large values of R where $T_B < T_s$.

It will be seen that the effect of entrainment is to reduce the differential between ${}_sT_w$ and ${}_{ys}T_w$. It can be seen that if T_2 is increased (see dotted curve) this differential is further reduced until when $T_2 = T_B$ a balance will exist between ${}_sT_w$ and ${}_{ys}T_w$ these temperatures being lower than T_s.

In the above it has been assumed that the rate of cooling due to entrainment of cold air into the wall jet is proportional to the local temperature of the wall jet (and hence proportional to R and T_s) and is independent of the flow direction of the wall jet.

If entrainment cooling depends on flow direction however, and if the rate of cooling were allowed to persist till R approached ∞, then for a given value of T_s there would result two curves each having a different asymptotic value (see Fig. 31). It is likely, for example, that flow along ec (see Fig. 29) will be subject to greater entrainment cooling than flow along ed because in the former case flow approaches the periphery of the orifice plate quicker than that along ed. In practice, of course, the asymptotic temperatures will never be reached, nevertheless, two independent curves could still exist, curve D corresponding to flow along ed and curve E corresponding to flow along ec.

It can be seen from Fig.31 that if T_2 is increased to some value T a balance can now be obtained at some temperature less than T_s and coinciding with neither of the asymptotic temperatures T_D and T_E.

Suppose ${}_{en}\delta T_{Rsw}$ represents the increase in wall jet temperature

along ec with wall jet entrainment and $_{en}\delta T_{sw}$ the increase in wall jet temperature along ed again with wall jet entrainment, then (61) becomes:

$$_{y}T_{w} - T_{w} = (_{en}\delta T_{Rsw} - _{en}\delta T_{sw}) + (\delta T_{w} - _{y}\delta T_{w}) \quad \ldots\ldots\ldots\ldots \quad (62)$$

let $\delta T_{Rsw} - _{en}\delta T_{Rsw} = _{en}\delta T_{R}$

also $\delta T_{sw} - _{en}\delta T_{sw} = _{en}\delta T$

thus $_{y}T_{w} - T_{w} = (\delta T_{Rsw} - _{en}\delta T_{R} - \delta T_{sw} + _{en}\delta T) + (\delta T_{w} - _{y}\delta T_{w})$

or $$_{y}T_{w} - T_{w} = (\delta T_{Rsw} - \delta T_{sw}) - (_{y}\delta T_{w} - \delta T_{w}) - (_{en}\delta T_{R} - _{en}\delta T) \ldots \quad (63)$$

which show that wall jet entrainment again serves to exaggerate the effect of WIS jet entrainment.

Thus taking both effects into account, i.e. wall jet and WIS jet entrainment it is found that a balance will occur between $_{y}T_{w}$ and T_{w} when:

$$(\delta T_{Rsw} - \delta T_{sw}) = (_{y}\delta T_{w} - \delta T_{w}) + (_{en}\delta T_{R} - _{en}\delta T) \quad \ldots\ldots\ldots\ldots \quad (64)$$

Note in equations (62) - (64) the values of δT_{w} and $_{y}\delta T_{w}$ will be slightly less than if wall jet entrainment effects had been neglected.

If temperature attenuation in the WIS jet away from the surface is the same along cb and da then the WIS jet term disappears from (64). Assuming, therefore, that $_{y}\delta T_{w} = \delta T_{w}$.

Then at balance $\delta T_{Rsw} - \delta T_{sw} = _{en}\delta T_{R} - _{en}\delta T$

and since $\delta T_{Rsw} - \delta T_{sw}$ increases with $T_{s} - T_{2}$ (or $_{s}T_{F}$)

then $T_{s} - T_{2}$ will increase with $_{en}\delta T_{R} - _{en}\delta T$.

Radiation Effects

It can be seen from Figs. 32 and 33 that both thermal sensors $T.C_{a}$ and $T.C_{b}$ lie close to the orifice plate away from either orifice,

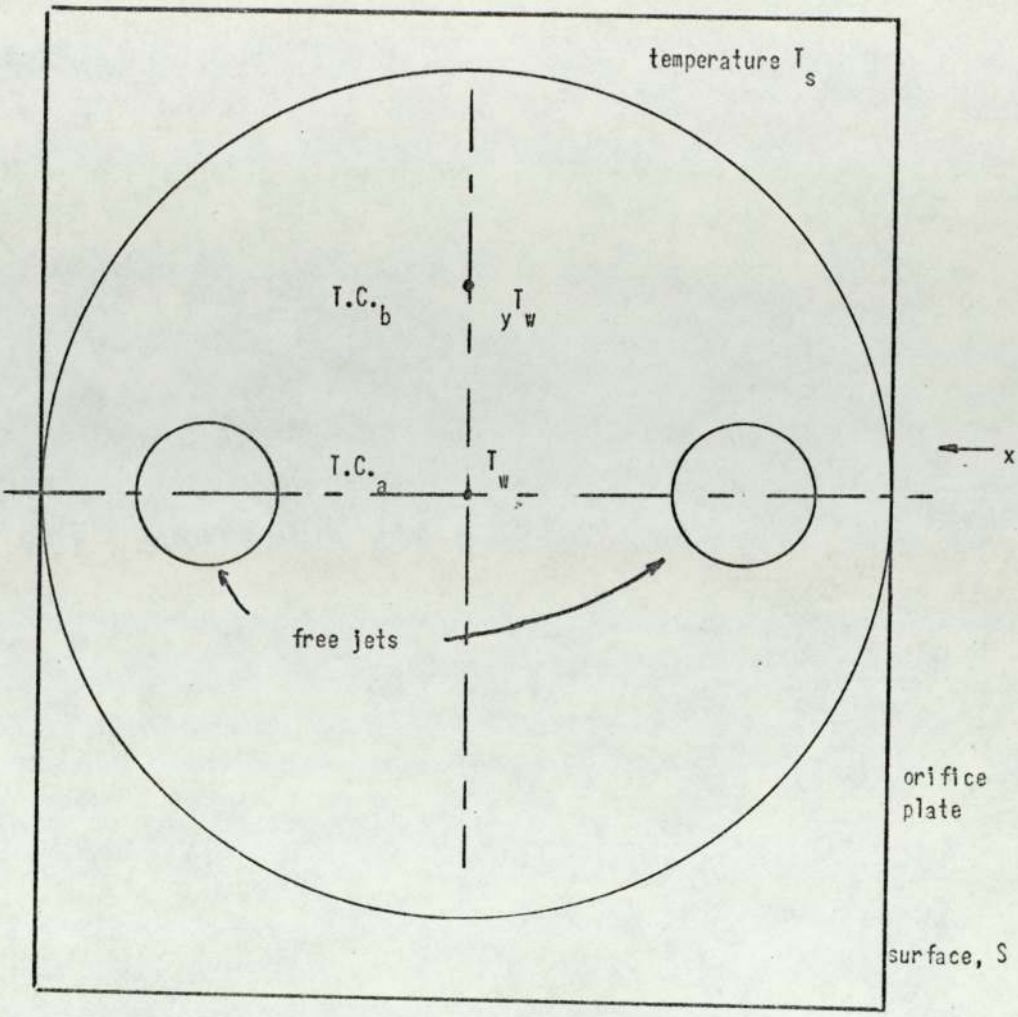

Fig. 32. Geometrical radiation effects in the two free jet method involving air temperature measurements in the vertical plane

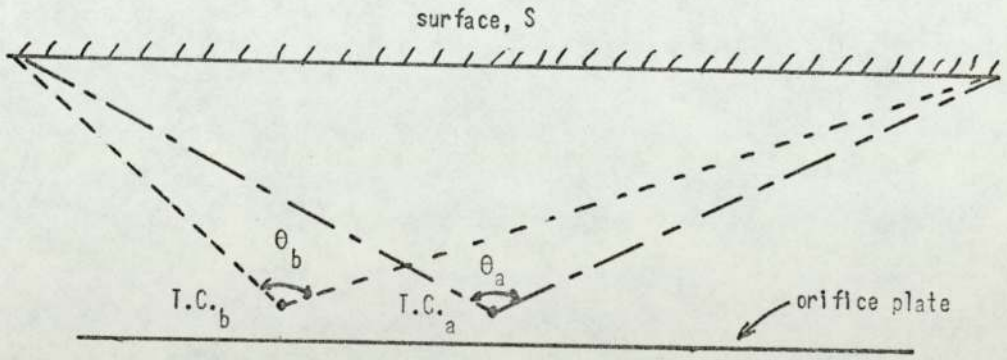

Fig. 33. Side elevation looking in direction x

thus the difference in contribution from reflected radiation from the orifice plate will be much smaller than for the measurements made in the horizontal plane, with $T.C_a$ receiving slightly more reflected radiation than $T.C_b$.

Unheated Free Jets

It can be seen from Fig. 33 that because $\theta_a > \theta_b$, $T.C_a$ will receive more direct and multiply reflected radiation than $T.C_b$. Only reflected radiation will emerge from the orifice plate and as has been seen above this will favour slightly $T.C_a$. The nett effect is therefore, that $T.C_a$ will receive a larger radiation contribution than $T.C_b$.

This would have the effect of reducing the differential between $T.C_b$ and $T.C_a$ as well as making the predictions of temperature dependent upon radiation and hence emissivity.

Heated Free Jets

The effects described for unheated free jets would also apply to heated ones. However, in this latter case the orifice plate will be hot and the space between this plate and S will represent a partial black body with an overall greater radiation flux density than for the unheated free jets. The direct radiation from the orifice plate will provide an almost equal contribution to $T.C_b$ and $T.C_a$, thus any difference between contributions to these thermo-couples will result from differences in direct and multiply reflected radiation from S with $T.C_a$ receiving the greater contribution.

Consider a balance between $T.C_b$ and $T.C_a$ under non-radiation conditions. Then the effect of radiation would be to upset this balance $T.C_a$ becoming greater than $T.C_b$.

In order to regain the balance a greater heat transfer due to convection from the surface would be required implying that ${}_{o}T_{F}$ must be reduced, i.e. the convective heat transfer is proportional to $T_{s} - {}_{o}T_{F}$.

Thus the effect of radiation would be the same as attenuation in the free WIS and wall jets, it would increase $T_{s} - {}_{o}T_{F}$ at balance.

THE PREDICTION OF SURFACE TEMPERATURE USING THREE FREE JETS WITH AIR TEMPERATURE MEASUREMENTS CONFINED TO THE HORIZONTAL PLANE

It is the purpose of this section to examine how the temperature of a surface may be predicted using three free jets and what factors influence the accuracy of such a prediction. See Figs. 34 and 35.

In the following analysis the nomenclature used will be as before except where otherwise indicated and with the following additions:

${}_{sX}T_{w}$ = temperature in large WIS jet (i.e. the one corresponding to the large free jet spacing) close to S.

${}_{X}T_{w}$ = temperature in large WIS jet close to the orifice plate.

${}_{sx}T_{w}$ = temperature in small WIS jet close to S.

${}_{x}T_{w}$ = temperature in small WIS jet close to the orifice plate.

${}_{X}\delta T_{w} = {}_{sX}T_{w} - {}_{X}T_{w}$; ${}_{X}\delta T_{sw} = {}_{sX}T_{w} - {}_{s}T_{F}$

${}_{x}\delta T_{w} = {}_{sx}T_{w} - {}_{x}T_{w}$; ${}_{x}\delta T_{sw} = {}_{sx}T_{w} - {}_{s}T_{F}$

Assumptions to be made in this analysis at this stage are:

(1) $T_{s} \geq {}_{s}T_{F} > T_{e}$

(2) All the free jets are identical.

(3) Transverse temperature gradients in the free jets at regions close to S and P_{o} are negligible.

(4) Radiation effects are negligible.

(5) Wall jet entrainment is negligible.

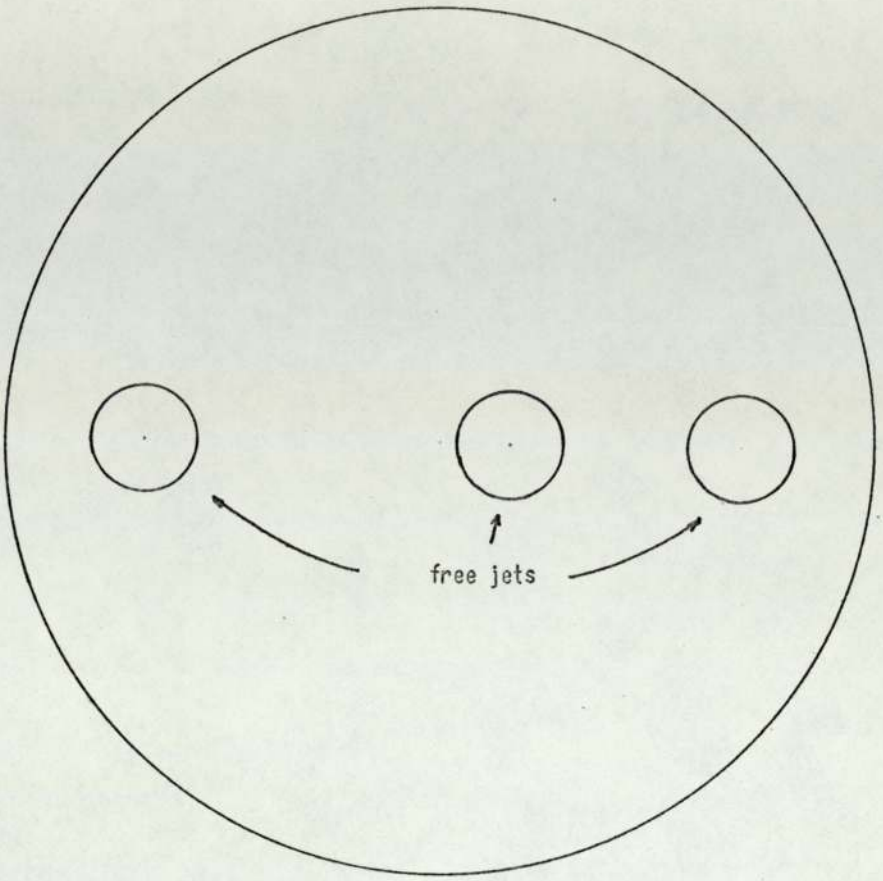

Fig. 34. Orifice plate

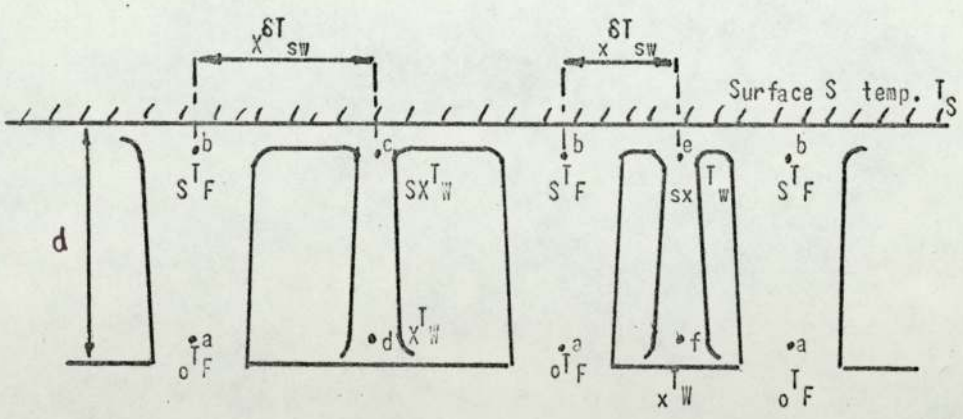

Fig. 35. Method employing three free jet and air temperature measurements in the horizontal plane

The significance of (4) and (5) will be discussed later.

The variation in temperature along the path abcd and abef in Fig. 35 will now be examined.

for path abcd:

$$ {}_{X}T_{w} = {}_{o}T_{F} - \delta T_{F} + {}_{X}\delta T_{sw} - {}_{X}\delta T_{w} \quad \ldots\ldots\ldots\ldots\ldots\ldots\ldots\ldots\ldots (65) $$

for path abef:

$$ {}_{x}T_{w} = {}_{o}T_{F} - \delta T_{F} + {}_{x}\delta T_{sw} - {}_{x}\delta T_{w} \quad \ldots\ldots\ldots\ldots\ldots\ldots\ldots\ldots\ldots\ldots (66) $$

Subtracting (66) from (65) gives:

$$ {}_{X}T_{w} - {}_{x}T_{w} = ({}_{X}\delta T_{sw} - {}_{x}\delta T_{sw}) - ({}_{X}\delta T_{w} - {}_{x}\delta T_{w}) \quad \ldots\ldots\ldots\ldots\ldots (67) $$

It can be seen from (67) that ${}_{o}T_{F}$ and δT_{F} are absent from this equation. However, ${}_{X}\delta T_{sw}$ and ${}_{x}\delta T_{sw}$ are both exponential functions of $T_{s} - ({}_{o}T_{F} - \delta T_{F})$ see equations (35) and (36), thus $({}_{X}\delta T_{sw} - {}_{x}\delta T_{sw})$ is a function of ${}_{o}T_{F}$ and δT_{F} resulting in ${}_{X}T_{w} - {}_{x}T_{w}$ being dependent upon ${}_{o}T_{F}$ and δT_{F}.

Although ${}_{X}\delta T_{w}$ and ${}_{x}\delta T_{w}$ will be finite their difference will be small thus the influence of $({}_{X}\delta T_{w} - {}_{x}\delta T_{w})$ on ${}_{X}T_{w} - {}_{x}T_{w}$ will be small.

If ${}_{X}\delta T_{w} = {}_{x}\delta T_{w}$ then the dependence of $({}_{X}T_{w} - {}_{x}T_{w})$ on WIS jet attenuation disappears and (67) becomes:

$$ {}_{X}T_{w} - {}_{x}T_{w} = ({}_{X}\delta T_{sw} - {}_{x}\delta T_{sw}) \quad \ldots\ldots\ldots\ldots\ldots\ldots\ldots\ldots\ldots\ldots (68) $$

Surface Temperature Predictions Using Unheated Free Jets

In this case the temperature differential between the two WIS jets is used as the parameter from which T_{s} is to be predicted. As in all unheated free jet modes of operation (i.e. 2 or 3 free jet methods) the method adopted is not absolute and requires a calibration of the appropriate parameter (i.e. the difference between two temperatures) against T_{s}.

Prediction Using Heated Free Jets (Z.N.H.T. Mode)

It has been mentioned above that ${}_XT_w - {}_xT_w$ was dependent upon ${}_oT_F$ and δT_F. Reference to (35) and (36) will show, however, that as T_2, i.e. $({}_oT_F - \delta T_F)$ approaches T_s the exponential term in these equations approaches zero. (This condition will, of course, be one of Z.N.H.T. between the wall jet and S.) At the same time if ${}_x\delta T_w = {}_X\delta T_w$ then ${}_XT_w - {}_xT_w$ will approach zero, i.e. a balance between the thermal sensors in the WIS jet will correspond to a state of Z.N.H.T. However, unless ${}_X\delta T_w = {}_x\delta T_w = 0$ the value of ${}_XT_w$ (or ${}_xT_w$) at balance will in general be less than T_s. If a finite differential WIS jet temperature attenuation existed then this balance would be upset. If, for example ${}_x\delta T_w < {}_X\delta T_w$ when Z.N.H.T. conditions existed then in order to regain a balance between ${}_XT_w$ and ${}_xT_w$ it would be necessary to reduce ${}_oT_F$ so making $({}_X\delta T_{sw} - {}_x\delta T_{sw}) > 0$. Thus under these conditions the air temperature ${}_XT_w$ or ${}_xT_w$ at balance would again be less than T_s.

If ${}_x\delta T_w > {}_X\delta T_w$ when Z.N.H.T. conditions existed then a balance could be regained by increasing ${}_oT_F$ so making $({}_X\delta T_{sw} - {}_x\delta T_{sw}) < 0$.

This could give a WIS jet temperature ${}_XT_w$ or ${}_xT_w$ at balance greater than T_s, depending on the magnitudes of ${}_x\delta T_w$ and ${}_X\delta T_w$.

The Effects of Wall Jet Entrainment

It will be assumed, for the moment, that the temperature gradients ${}_X\delta T_w$ and ${}_x\delta T_w$ along the two WIS jets are equal, in which case equation (68) may be used:

$$ {}_XT_w - {}_xT_w = {}_X\delta T_{sw} - {}_x\delta T_{sw} \quad \ldots\ldots\ldots\ldots\ldots\ldots\ldots\ldots\ldots\ldots (68) $$

Fig. 36 shows the variation of wall jet temperature with radial distance R, from the origin. x corresponds to R = be and X corresponds

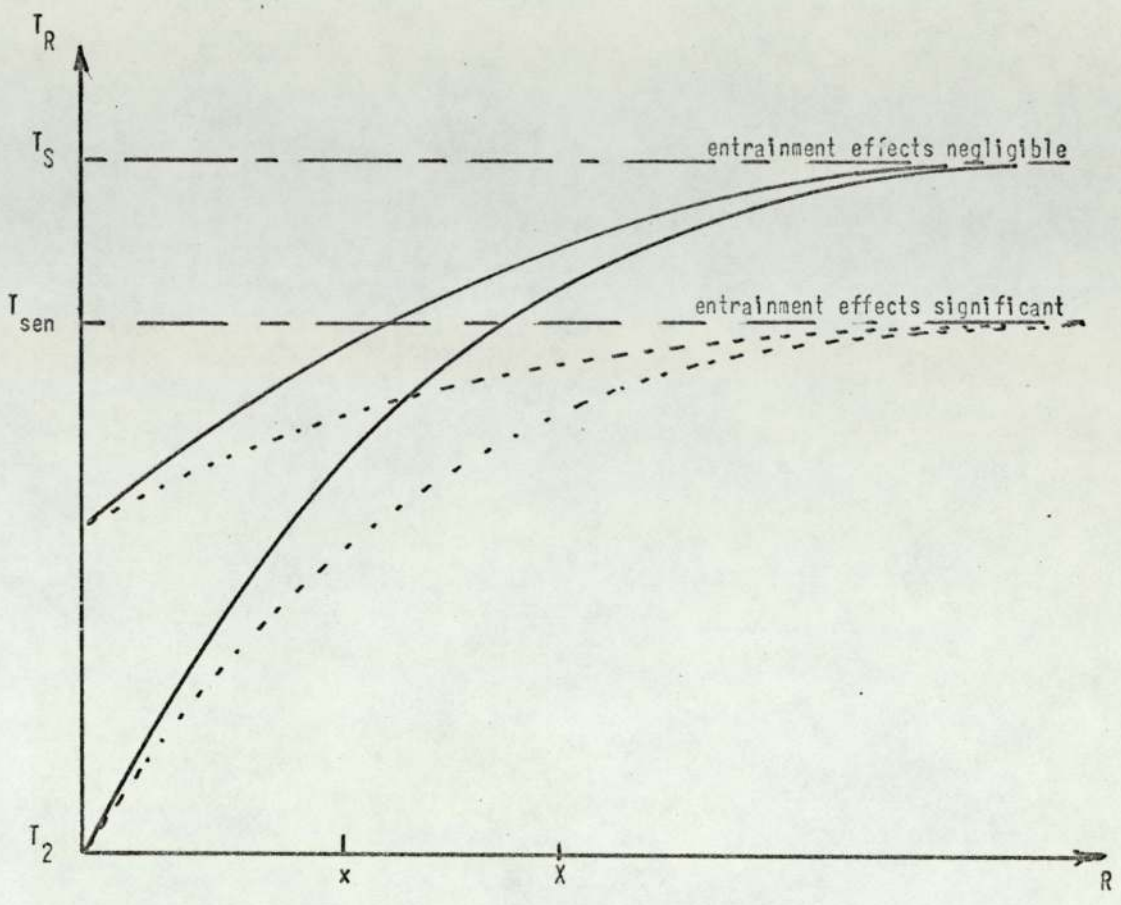

Fig. 36. Variation of T_R with R showing the effects of wall jet entrainment

to R = bc, see Fig. 35 .

In Fig. 36 the solid curves correspond to negligible cooling due to wall jet entrainment and the dotted curves correspond to finite cooling due to this entrainment. It is seen that in both cases the temperature differential corresponding to x and X decreases as T_2 increases (this differential also decreases with R). With entrainment effects the differential vanishes when $T_2 = T_{sen}$ but in the absence of such effects the differential becomes zero when $T_2 = T_s$, T_s being greater than T_{sen}.

It can be seen therefore, that the effect of cooling by entrainment is to reduce the WIS jet temperature, at balance, to a level less than T_s.

If a finite differential temperature existed between $_X\delta T_W$ and $_x\delta T_w$ then the balance indicated above would of course be modified.

Radiation Effects in the System Using Three Free Jets

Reference to Figs. 34, 35 and 37 will show that the thermo-couple at d,(T.C_d) is farther from the periphery of the orifice plate than the one at f,(T.C_f) making $\theta_d > \theta_f$.

For the unheated free jet mode, therefore T.C_d will receive slightly more direct and multiply reflected radiation from S than T.C_f. There will be no direct radiation from the orifice plate (or the amount will be negligible), but T.C_d will again receive slightly more reflected radiation from the orifice plate than T.C_f, (assuming the emissivity of the orifice plate to be constant across its width). The nett effect of the above will be to increase the temperature differential existing in the absence of radiation effects.

In the case of heated free jets operating under Z.N.H.T. conditions the effects described above will still exist but an

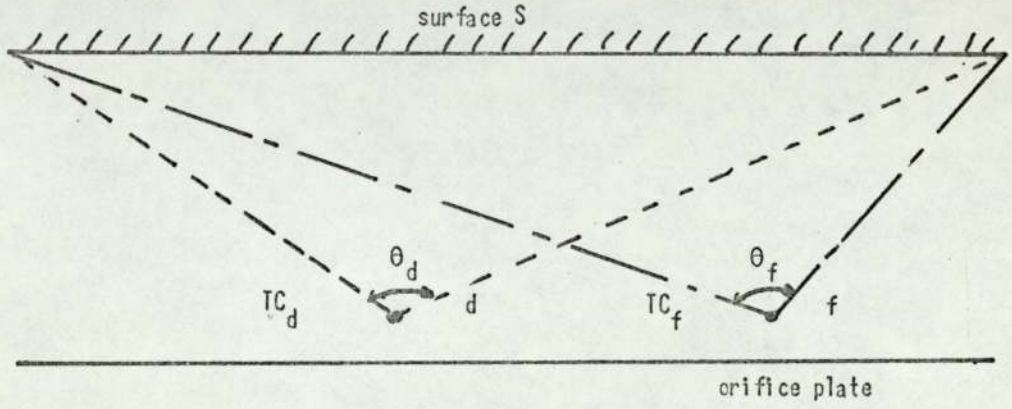

Fig. 37. Geometrical radiation effects in the three free jet method involving air temperature measurements in the horizontal plane

additional contribution due to direct radiation from the orifice plate will manifest itself. If there were no subsequent reflection of this orifice plate direct radiation, then $T.C_d$ would receive slightly more radiation from this source. Also, the effect of multiple reflections from S will again favour $T.C_d$.

The nett effect of radiation in the Z.N.H.T. mode, therefore, would be to make $T.C_d$ slightly greater than $T.C_f$ and in order to regain a balance (assuming one already existed), it would be necessary to increase ${}_oT_F$ slightly. This would have the effect of making $({}_X\delta T_{sw} - {}_x\delta T_{sw}) < 0$ and would compensate for the increased radiation contribution.

METHODS INVOLVING THREE FREE JETS AND MEASUREMENTS IN THE VERTICAL PLANE

It has been seen that the average temperature gradient in the y direction (i.e. normal to the horizontal plane) decreases as the corresponding free jet spacing increases. Thus for an asymmetrical free jet spacing the WIS jet corresponding to the free jets with the closest separation will have a larger average temperature gradient in the y direction than that corresponding to the free jets with the larger separation. The average gradient will also be a function of T_s, thus the difference in the large and small WIS jets average gradient will provide a parameter from which to predict T_s.

The theory of the method will not be given here but follows the same lines of reasoning involved in the other methods discussed above.

RADIATION EFFECTS RESULTING FROM DIFFERENTIAL CONVECTIVE HEAT TRANSFER COEFFICIENTS IN THE FLOW

These effects will be dealt with in greater depth in the results

section but it is appropriate to mention them at this stage.

The equilibrium temperature of the air temperature measuring thermo-couple is a function of both the radiative heat transfer coefficient h_R and the convective heat transfer coefficient h_c. It will be shown later that h_c increases with flow velocity thus the relative significance of h_R will decrease with flow velocity. Thus it can be seen that if the flow velocity at different thermo-couple locations differs then so also will the corresponding convective heat transfer coefficients, resulting in a variation in the significance of radiation at these locations, (inasmuch as this particular mechanism applies). Note, any geometrical radiation effects will still exist but may be modified by the above effect depending on the velocities involved.

It will be demonstrated in the results section that the WIS jets have, in general, a lower velocity than their constituent-free jets, hence for a given radiation flux the significance of the latter will be higher for the WIS jets than for the free jets.

CHAPTER 5

EXPERIMENTAL SECTION

This section will be divided into two parts, the first concerned with isothermal flow studies and the second with temperature studies.

PART 1

ISOTHERMAL FLOW STUDIES

The purpose of these studies was to identify the existence of the WIS jet and examine those flow characteristics appropriate to its subsequent exploitation in non-contact temperature measurement.

The flow characteristics of particular importance are:

(1) The variation of mean and turbulent velocity in the horizontal plane.

(2) The variation of mean and turbulent velocity in the vertical plane and planes parallel to the horizontal one but displaced in a vertical, y, direction.

It is also important to examine the influence of the orifice plate - impingement surface displacement, d, and free jet velocity on these characteristics.

A knowledge of (1) and (2) is necessary in defining the general structure of the WIS jet.

The Turbulence Characteristics of an Axially Symmetric Jet

When an axially symmetric jet is propagated, say from an orifice into a fluid of the same nature then turbulent mixing will take place in those regions adjacent to the jet.

If the jet is initially non-turbulent with a flat mean velocity

profile then on moving away from the orifice an annular turbulent zone will gradually manifest itself the width of the annulus increasing with axial distance from the orifice. At the same time the mean velocity profile will acquire rounded edges until when the turbulent zone reaches the axis of the jet the mean velocity will have assumed a 'normal' type profile with a general broadening of the jet[36,37,38,39].

It is this turbulent mixing which is responsible for the degredation of the initial flat mean velocity profile and if the jet is heated the subsequent thermal gradients in a direction parallel to the axis and across the jet, (assuming a temperature differential exists between the jet and the surrounding fluid).

The Turbulent Characteristics of a WIS Jet

Although of a different geometrical structure the WIS jet is still likely to be subject to the same type of turbulent mixing or entrainment effects discussed above. It is therefore important to examine the turbulent characteristics of the WIS jet since its breadth and integrity will be profoundly influenced by these characteristics.

A desirable characteristic of any non-contact temperature measuring system is that the particular temperature dependent parameter exploited should exhibit a low sensitivity to d within the limits selected.

Since the temperature characteristics of the WIS jet will be related to the mean and turbulent velocity characteristics it is appropriate to examine how the latter vary with d.

These characteristics will also depend upon the free jet velocity and it is therefore appropriate to examine its effect.

Apparatus for Flow Studies

The design of apparatus and the experimental procedure adopted

was based upon the requirements discussed in the last section. Since turbulent as well as mean velocities were involved a simple Pitot tube or similar device was found to be inadequate and it was necessary to employ a hot wire annemometry technique. Details of this technique have been given in some depth by Bradshaw[40,41]. It is convenient at this stage, however, to discuss briefly the general principles on which the hot wire annemometry technique is based together with its limitations. The design (by the author) of a piece of peripheral electronic equipment to measure the mean square value of the turbulent component of velocity (subsequently referred to as the turbulent mean square velocity device) together with the mean value of velocity (subsequently referred to as the mean velocity device) will be described in Appendix A1.

The Hot Wire Annemometer

When a current is passed through a wire it will heat up and since, in general, it will have a finite temperature coefficient of resistance (materials are chosen which give a large but consistent temperature coefficient of resistance) its resistance will change accordingly. If now the wire is placed in a fluid stream at a lower temperature (typically ambient) then the wire will cool, its resistance changing as a result. The efficiency of this cooling will be a function of the fluid velocity, the wire orientation with respect to the flow direction and the dimensions and thermal properties of the wire, together with the temperature differential between the wire and the fluid and the pressure, density and thermal properties of this latter.

The resistance of the wire sensor is usually measured by making

it one arm of a Wheatstone bridge. Two modes of operation may be employed:-

(1) The constant current mode.

(2) The constant temperature mode.

In the former case the wire sensor current is fixed and the effect of changing the fluid velocity and hence its cooling efficiency would be to alter the out of balance bridge current. Although this mode of operation has certain advantages its major disadvantage lies in the finite thermal inertia of the sensor in changing temperature and it is this which puts a limit on its ability to measure fast varying (turbulent) velocities accurately.

The alternative mode of operation is the constant temperature mode. As the name suggests the sensor temperature and hence its resistance is kept almost constant and it is the bridge voltage which becomes a function of heat transfer and hence fluid velocity.

The advantage of this method is that because of the small wire sensor temperature excursions the thermal inertia is correspondingly reduced and it is therefore capable of following faster time varying velocities. It is therefore, more suited to measurements of turbulent velocities than the constant current mode of operation.

Because of the complexity of the appropriate heat transfer equations a theoretical prediction of fluid velocity is not usually performed and in practice a calibration curve of annemometer output against fluid velocity is derived experimentally.

All the velocity studies performed in these investigations employed the constant temperature mode (C.T.M.) of operation.

A typical general purpose hot wire sensor (and one which was used in these experiments) would consist of a platinum coated

tungsten wire 5 μ diameter and 3 mm long and welded to two prongs as indicated in Fig. 38 .

The heat transfer and sensitivity will be a maximum when the wire is placed with its axis transverse to the direction of flow. However, due to its symmetry it is insensitive to direction of flow in a plane normal to its axis and this limitation must be borne in mind when interpreting the results of flow studies.

In the C.T.M. of operation the annemometer will provide a voltage proportional (not linearly) to flow velocity. If flow is in any way turbulent then there will be a varying component superimposed on a mean component U. (See Fig. 39)

The degree of turbulence in flow may be expressed in terms of the turbulence intensity which is defined as:- the root mean square (r.m.s.) value of the turbulent component of velocity.

When considering the turbulent velocity in relation to the corresponding mean velocity, $\bar{U}$, the percentage turbulence is an appropriate parameter to use and is defined as:-

$$\frac{\text{turbulence intensity}}{\bar{U}} \times 100$$

In order to obtain some quantitative measure of turbulence therefore it is necessary to process the signal such that the mean square or r.m.s. value of the fluctuating component may be measured together with the corresponding mean component $\bar{U}$ (for % turbulence). The equipment to perform these operations is described in Appendix A1.

Calibration of Turbulent Mean Square Velocity Device

Since no instrument was available to measure the mean square value of the turbulent velocity (from which the r.m.s. value may be obtained) and thus act as a standard against which the author's

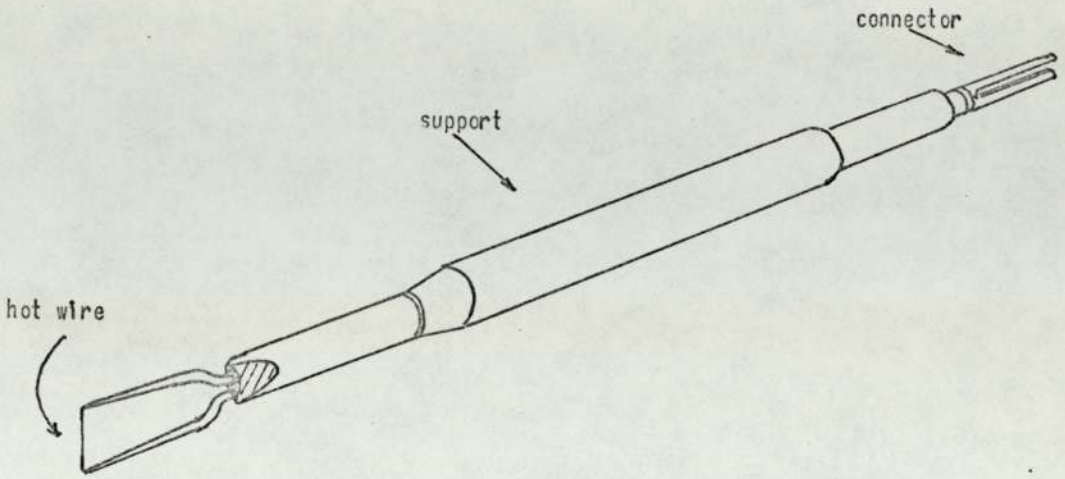

Fig. 38. Typical hot wire sensor

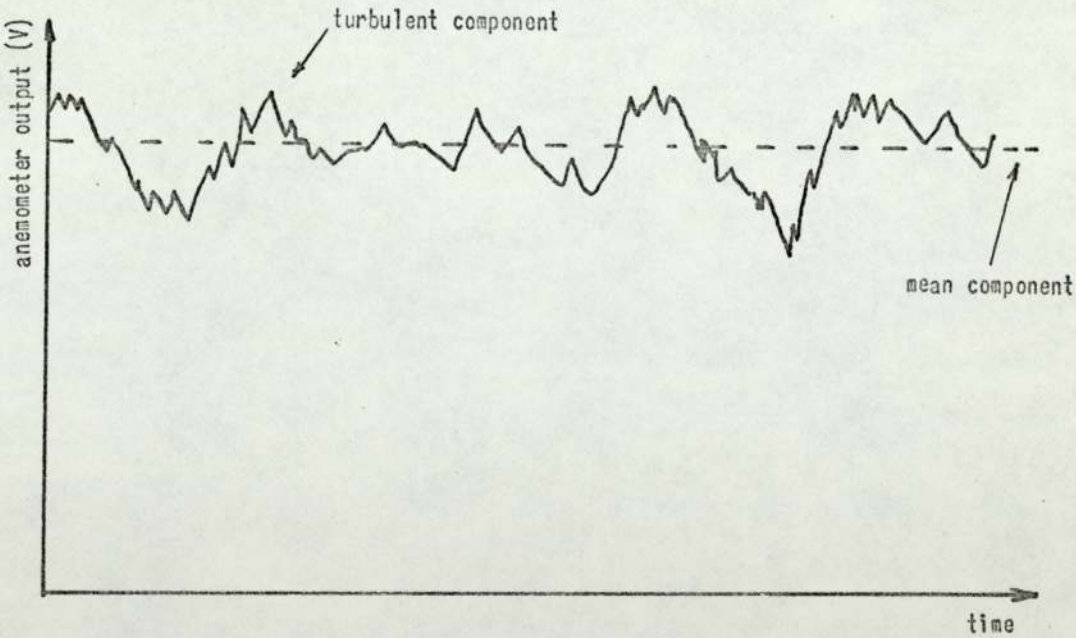

Fig. 39. Anemometer output corresponding to turbulent flow

device for this measurement could be calibrated, it was necessary to adopt a somewhat different calibration approach.

Now it would be be very difficult, if not impossible to predict, analytically, the mean square voltage of a randomly varying voltage of the type discussed above. On the other hand it is fairly simple to predict the mean square voltage of a sine wave and hence its r.m.s. value from a knowledge of the peak voltage. The calibration procedure adopted was therefore as follows:

A sine wave signal was injected into the input of the device and the output, which was proportional to the mean square value of the input, fed into a Honeywell chart recorder. Various peak input voltages (to cover the turbulence range encountered in the flow studies) were applied. To estimate the frequency response of the device frequencies ranging from 15 Hz to 50 kHz were employed. The results of this calibration are given in Chapter 6.

Mean Velocity Calibration

The mean velocity calibration was performed with the aid of a Pitot tube, an 'Air Flow Developments' manometer and a wind tunnel capable of producing controlled flow rates with low turbulence levels. (See Fig. 40)

The hot wire sensor, which was mounted vertically on a support was located close to the opening of the Pitot tube. The tube was orientated so that the cross section of the opening lay in a plane normal to the direction of flow.

During the course of these studies two different anemometers were employed thus two different calibration curves were necessary. Fig. 48 shows the calibration curve for one of these anemometers,

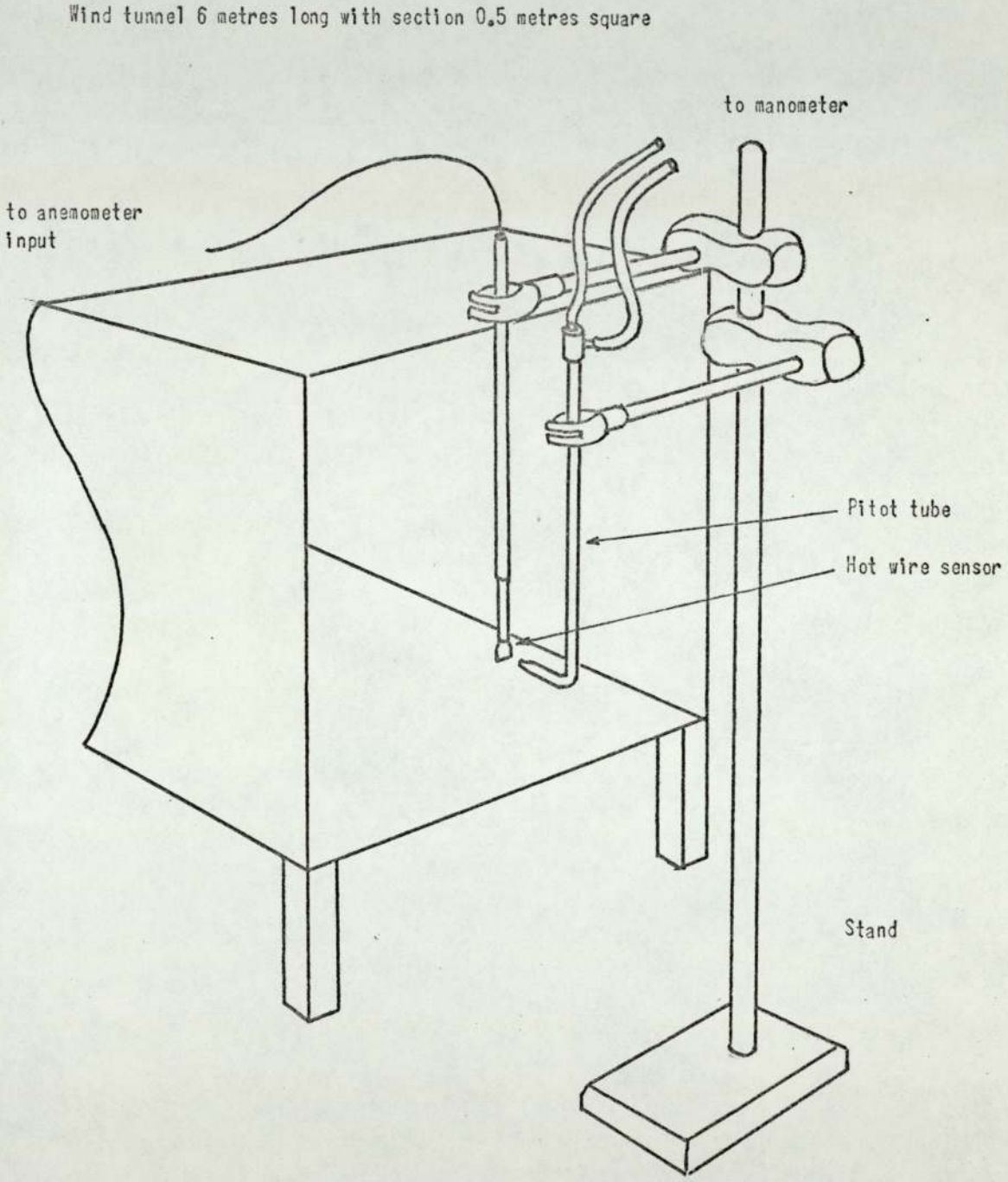

Fig. 40. Schematic diagram of calibration rig.

a DISA type 55D01CTA and Fig.49 the curve for the other a DISA type 55D05CTA. (See Pages 117 and 118)

DESCRIPTION OF THE TEMPERATURE MEASURING DEVICE AND THE ASSOCIATED FLOW MEASURING RIG

The general principles on which the operation of the device is based have been given in the 'Theory' section. Some of the practical details of the device itself will now be given together with the experimental method adopted to measure the appropriate flow characteristics.

The Device

This was built around an aluminium dish of the dimensions shown in Fig.41 .

Air from a blower was introduced into the device (see Fig. 42) through a 5-cm diameter tube and was baffled by a 17.7-cm diameter plate finally emerging through three 2.2-cm diameter holes asymmetrically displaced along a diameter in the orifice plate. The line joining the axes of the free jets was horizontal.

Apart from a series of preliminary scans employing a symmetrical hole distribution, the diameter again being 2.2 cm, all the flow studies and subsequent temperature studies employed the asymmetrical distribution shown in Fig. 41.

Since all flow studies were performed under isothermal conditions it would appear that the heater in Fig. 42 was superfluous. However, it was often convenient to express free jet velocities in terms of the corresponding blower motor voltages thus if the heater had been omitted during the flow studies then, because

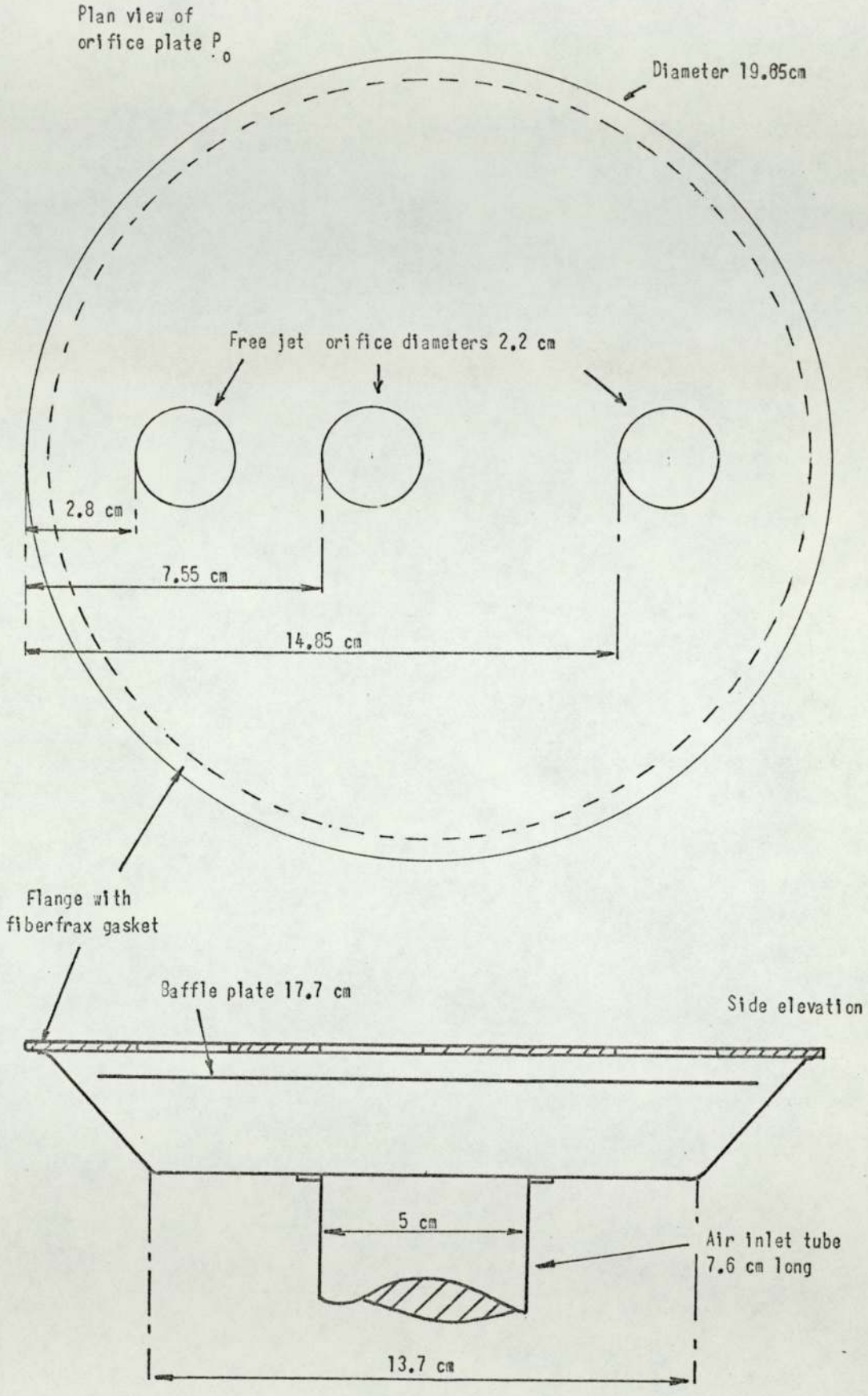

Fig. 41. Dimensioned drawing of sensing head.

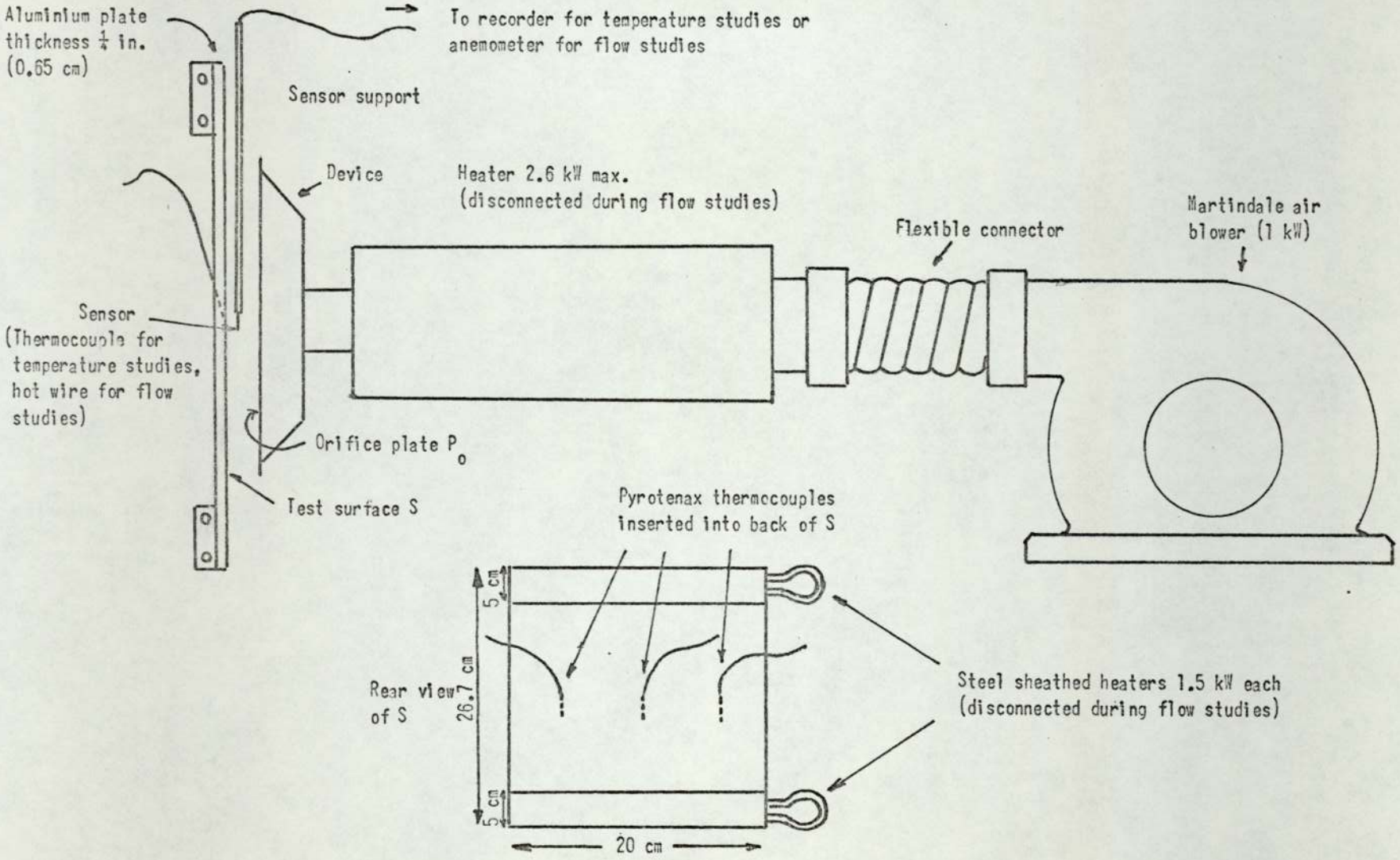

Fig. 42. Schematic diagram of experimental arrangement (excluding scanning rig).

it presented a finite resistance to flow, the free jet velocities would have been slightly higher for a given blower motor voltage than if the heater were present.

The Measurement of Flow Characteristics

In order to obtain an adequate knowledge of the flow characteristics within the region bounded by the orifice plate P_o and the test surface S it was necessary to scan the hot wire sensor within this region.

Plate 3 shows the rig constructed for this purpose. The probe support was mounted vertically on a carriage and facilities were provided to allow for sensor movement in three mutually perpendicular directions, x, y, and z. The processed signals, one corresponding to the mean velocity and the other the mean square of the turbulent velocity components of flow, were fed into a Honeywell two-channel chart recorder, the mean velocity signal on one channel and the mean square of the turbulent velocity signal on the other.

Horizontal Scans

The scanning procedure adopted in this set of experiments was as follows: The sensor was scanned in a horizontal, x, direction parallel to the planes of P_o and S which were, themselves, parallel.

The scan range was 20 cm and corresponded to a complete traverse, in the horizontal direction, of the region bounded by P_o and S. Scans were performed at different normal displacements, y, from the horizontal plane, (i.e. the plane through the axes of the free jets) as well as at different normal displacements, z, from S.

In order to assess the influence of d on the flow characteristics between P_o and S, sets of horizontal, x, scans described above were

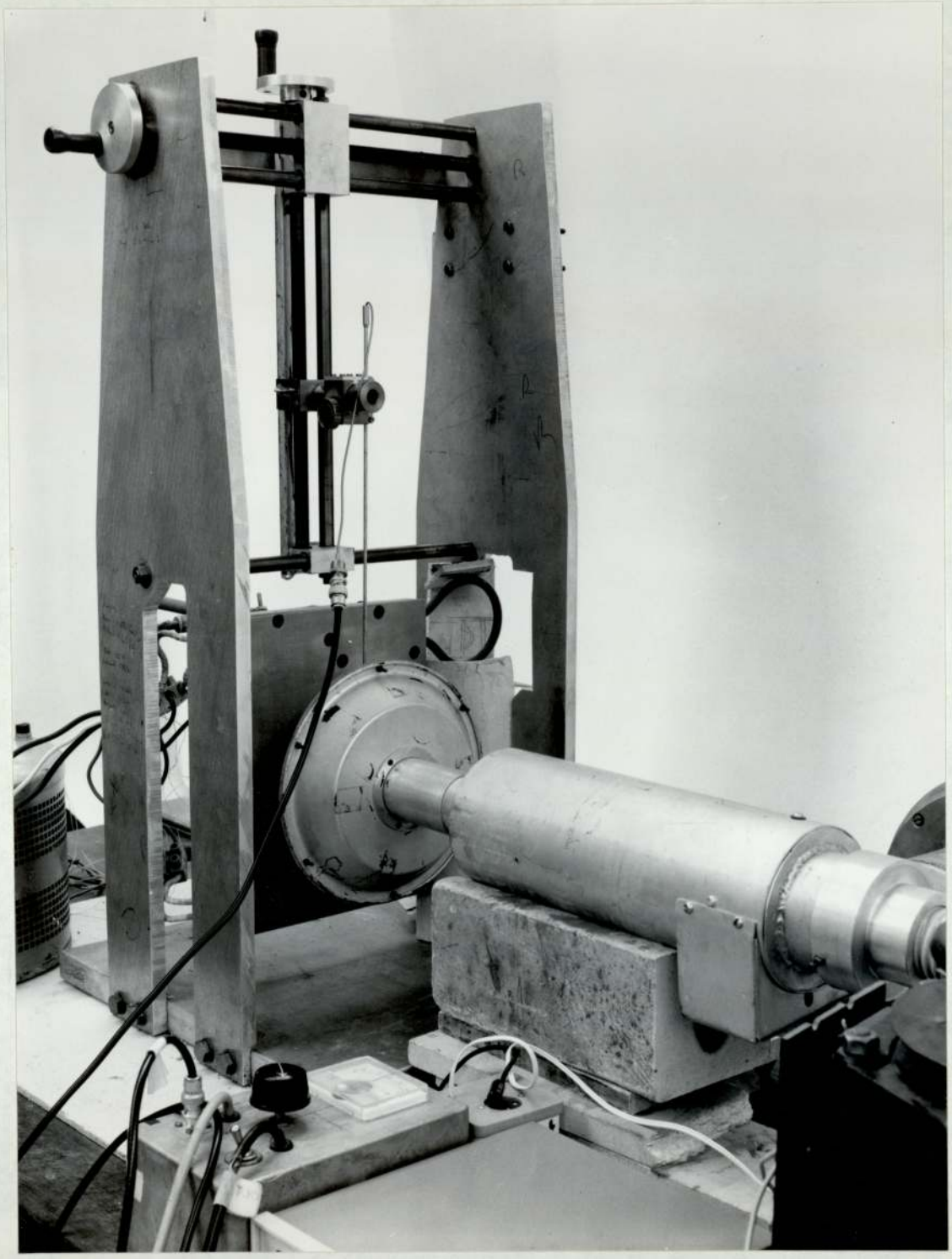

Plate 3. Scanning rig set up for flow studies.

performed for different values of d and appropriate values of y and z.

Each of these sets of scans was repeated for three different free jet mean velocities in order to determine the influence of these velocities on the general flow characteristics.

All the scans discussed so far were performed using two different sensor wire orientations, one with its axis transverse to the axis of the free jets and the other with its axis parallel to the free jet axis.

Scanning Speed and the Effects of Finite Time Constants Associated with the Turbulent Mean Square Velocity and Mean Velocity Devices

The sensor was displaced manually, in 2 mm steps, and 10 seconds was allowed to elapse between consecutive positions. The time for a single scan was approximately 17 minutes.

The frequency response of the annemometer (a type DISA55D01 for these horizontal scans) and hot wire sensor was such as to follow fairly accurately any turbulent velocity changes to which the sensor was subject, a corresponding voltage change appearing at the annemometer output. However, the signal processing equipment, i.e. the turbulent mean square and mean velocity devices had time constants somewhat longer than the annemometer and sensor and a certain amount of signal amplitude degredation resulted.

This effect could have been minimized had a slow enough scanning speed been employed. However, this would have involved a very lengthy research programme. A method was therefore developed to correct for these time-constant errors. (see Appendix 1)

Scans in the y anx z Directions

As well as the horizontal, x, scans described above, a number

of y and z scans were performed in order to assess the degree of mean velocity attenuation in these directions.

In these scans the sensor element was again parallel to the horizontal plane but transverse to the free jet axes. The sensor was displaced in small steps as for the horizontal scans, but since the total number of y and z scans was considerably less than the number of horizontal scans, as well as the scanning range of the former being smaller than that of the latter, it was found possible to allow the mean velocity measuring device output to reach equilibrium between consecutive steps in the scans. This avoided the signal amplitude degredation to which the horizontal scans were subject.

These y and z scans employed the same hot wire sensor as was used in the horizontal scans but a different type of annemometer - a DISA55D05, was used though it still operated in the constant temperature mode. A different calibration curve was necessary however.

PART 2

TEMPERATURE STUDIES

Having identified the existence and general characteristics of the WIS jet (see results of flow studies) it was necessary to examine the temperature characteristics of flow between P_o and S in order to assess whether they may be successfully exploited in non-contact temperature measurement.

The variables involved in these studies were as follows:

(1) Surface temperature T_s.

(2) Free jet temperature.

(3) Location of thermal sensor within the region bounded by S and P_o.

(4) The displacement, d, of S from P_o.

(5) The free jet velocity expressed in terms of blower motor voltage V_B.

All temperatures were measured with respect to ambient ($23 \pm 3^{\circ}C$) by zeroing the recorder at ambient.

All air temperatures were measured with a 36 s.w.g. chromel alumel thermo-couple since, within the limits which were to apply, i.e. $23^{\circ}C \rightarrow 270^{\circ}C$ approximately, this had a nearly linear thermal e.m.f. vs temperature characteristic. The small thermo-couple bead size (0.8 mm average diameter) was chosen in order to keep the thermal inertia and radiation effects down to a minimum.

The thermo-couple was mounted in a ceramic tube which acted as a support, the bead protruding about 1 cm. The same scanning rig as that used for the flow measurements was employed and the thermo-couple support dimensions were as close as could be obtained to those of the hot wire sensor support. The thermo-couple was mounted vertically on the carriage in the same manner as the hot wire support.

The above precautions were taken to ensure that there would be no significant modification of the flow characteristics by the thermo-couple support within the region bounded by P_o and S.

S was heated by means of two steel sheathed 1.5 kW heaters embedded in aluminium bars and bolted to the back of the plate. (See Fig. 42)

The temperature of S was measured by means of three Pyrotenax chromel-alumel thermo-couples inserted into closely fitting holes drilled at an oblique angle into the back of S and extending to within

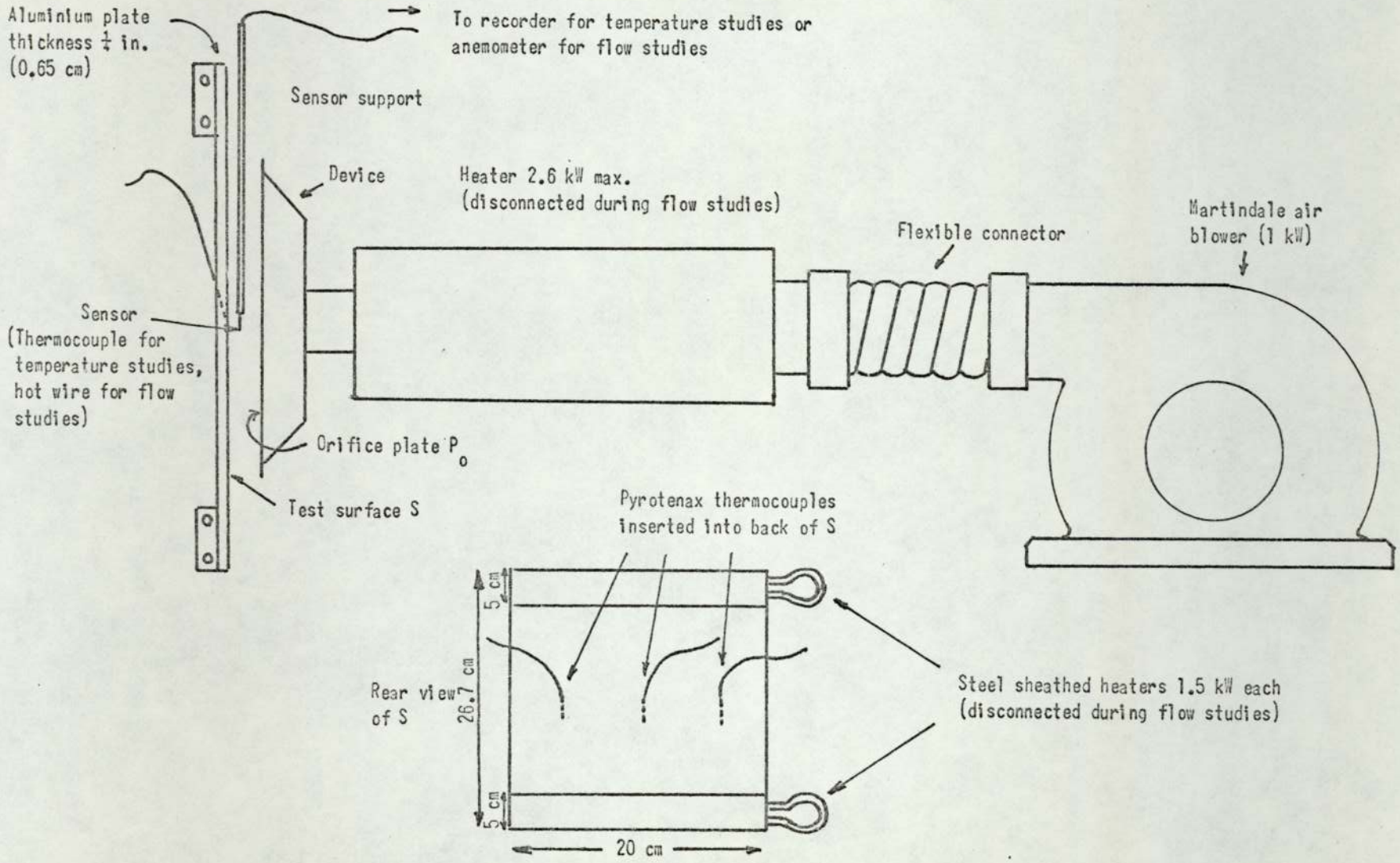

Fig. 42. Schematic diagram of experimental arrangement (excluding scanning rig).

1 mm of the front (test) surface of S. This was to minimize conduction losses down the sheathing from the thermo-couple junction.

The temperature difference between the three thermo-couples under equilibrium conditions was found to be sufficiently small (max. difference approx. 2%) to permit the recording of the thermal e.m.f. from just one of them, this being the centre thermo-couple.

Fig. 42 and Plate 4 show the general experimental arrangement.

The air was heated by a 2.6 kW heater. Air temperatures ranging from ambient to greater than 300°C could be obtained with the appropriate adjustment of heater voltage even under conditions of highest flow rate.

Temperature Scanning Procedure

In view of the long time constants associated with the turbulent mean square and mean velocity processing equipment it was necessary to employ a fairly slow scanning speed which resulted in a single horizontal scan time of approximately 17 minutes.

In the temperature studies, however, because of the much shorter response time of the thermo-couple faster scan speeds could be employed without too much signal amplitude degredation. Scans were still performed manually in the x, y, and z, directions. Those in the x and y, directions were continuous but in the z direction the thermo-couple was displaced in small steps.

For the horizontal, x, scans, speeds of 0.5 mm/second were used giving a scan time of approximately 7 minutes. The y scans employed a speed of 2 mm per second which for the 10 cm y scan range represented a scan time of 50 seconds. The z scans employed an average speed of approximately 0.5 mm per second.

Plate 4. Experimental arrangement.

A series of exploratory horizontal, x, and vertical, y, scans were first performed to derive a general picture of the appropriate temperature characteristics between P_o and S and to discover whether any WIS jet characteristics would be particularly suitable for thermo-couple location in the x direction in subsequent y and z scans employing heated free jets. Such a characteristic might be the consistent occurrence of a broad temperature peak under conditions of varying P_o - S separation, d, and blower motor voltage V_B.

All these exploratory scans were performed with S hot but the free jets unheated. Three different blower motor voltages, V_B, were used and for each value of V_B different temperatures of S ranging from approximately 270°C down to 30°C were employed with the thermo-couple always 0.5 cm from P_o. The scans were performed for values of d ranging from 1 cm to 4 cm.

Although a WIS jet temperature peak did occur its size, shape and definition varied, the peak being most pronounced for small values of d. In some cases a small dimple occurred in the middle of the 'peak'.

Any practical temperature measuring device would require that the thermo-couple in a WIS jet be located in a region of low temperature gradient and furthermore that this location be fixed with respect to P_o.

The x locations of those regions in the WIS jets with low temperature gradients were, therefore, noted and the most frequently recurring values used as the thermo-couple x locations in all subsequent WIS jet scans in the y and z directions. Note there are two WIS jets involved, one corresponding to the large hole separation and the other to the small hole separation. These will be referred to

as the large and small WIS jets respectively.

Temperature Scans Using Heated Free Jets

Having selected the optimum x locations of the air thermo-couple in the two WIS jets a series of scans was performed using free jets with temperatures ranging from ambient (approx.) to 270°C (approx.).

This series involved scans in the y direction (y scans) and scans in the z direction (z scans). The purpose of the y scans was to examine the variation of WIS jet temperature in this direction with a view to exploiting the average temperature gradient (or temperature difference between two selected vertical locations) in temperature measurement. The purpose of the z scans was to assess the degree of temperature attenuation in the free and WIS jets.

In the case of the y scans the variables involved were V_B, d, T_s and free jet temperature, the thermo-couple bead always lying in a plane parallel to S and P_o, and displaced from P_o by 0.6 cm. The y scan range was 10 cm.

The z scans employed a relatively high surface temperature, T_s, of approximately 270°C throughout but varying values of free jet temperature were used and both d and V_B were allowed to vary independently.

Let x_L and x_S denote the selected x locations of the large and small WIS jet peaks respectively. The y scans were confined to these two x locations. The z scans were performed at x_L and x_S with y locations of y = 0 cm and y = 5 cm. They were also performed at x locations close to the axes of the free jets.

The overall temperature scanning schedule is included in Appendix A5.

Included, also, in this Appendix is a catalogue of the velocity scans performed in the horizontal, x direction.

CHAPTER 6

RESULTS OF FLOW STUDIES

Before presenting the results of the flow studies it is important to examine some of the characteristics of the hot wire sensor and annemometer, since these will affect the interpretation of the recorded signals.

Sensor Calibration

L.V. King and others[42] have verified that a linear relationship exists between the electrical power input to the sensor and the square root of the flow velocity. King's law states:

$$\frac{V^2}{R} = \alpha + \beta U^{0.5}$$

where V = bridge voltage

U = mean flow velocity

R = hot wire operating resistance

α and β are two constants.

Collis and Williams[43] have derived a similar type of expression to King's but with a velocity exponent of 0.45 instead of 0.5. This appears to produce a better correlation than King's law within the normal annemometer operating range of Reynolds numbers - $0.02 < Re < 44$.

Even with the above type of expressions available uncertainties in fluid and flow properties usually necessitate an experimental calibration of annemometer output vs flow velocity, a typical example of which is shown in Fig. 43 overleaf.

It can be seen from Fig. 43 that as U increases the slope becomes progressively smaller, i.e. the sensitivity of the

annemometer and sensor decreases. The effect of this non-linearity is two-fold.

(1) The recorded mean velocity signals are under-emphasised for high flow velocities.

(2) A certain amount of amplitude distortion will occur for fluctuating velocities (i.e. turbulent velocities), the extent of which will increase with the magnitude of the velocity excursions about the mean.

A figure of 5% turbulence intensity is often quoted as a limit beyond which the above amplitude distortion becomes significant, i.e. below this value the effect of non-linearity of the curve may be neglected.

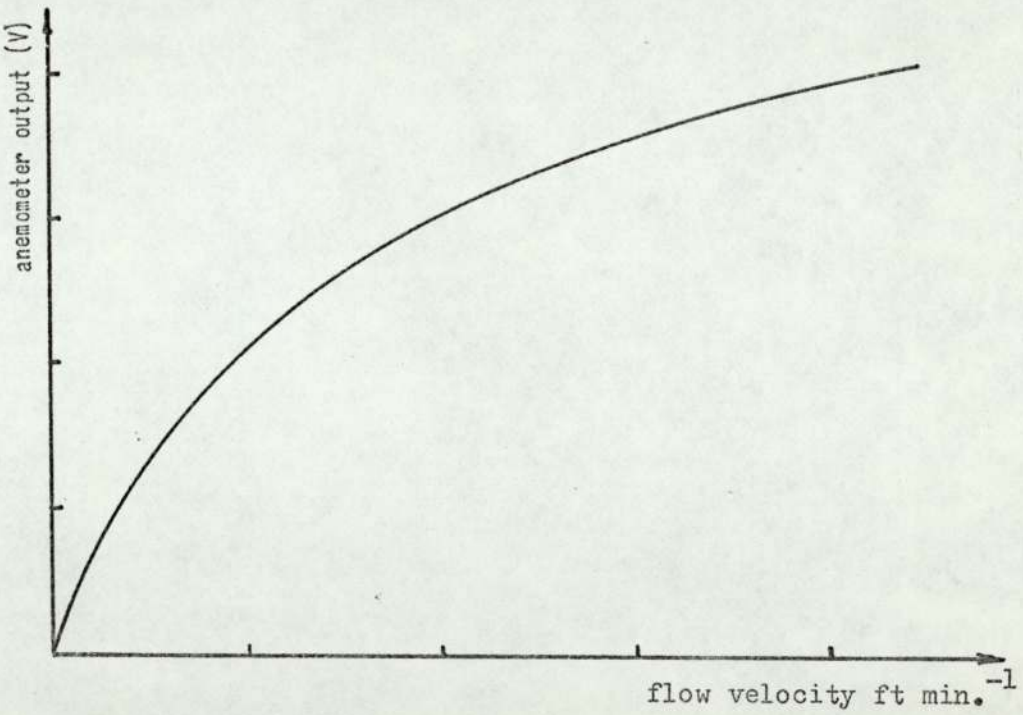

Fig. 43. Typical anemometer calibration curve

R.M.S. Turbulence Calibration

Ideally any turbulence measuring device (whether it measures the

r.m.s. or mean square value) should have a constant gain over the range of frequencies associated with the randomly varying voltages corresponding to the turbulent velocity fluctuations.

It is appropriate, therefore, to examine the frequency response of the turbulent mean square velocity device developed for these experiments.

Fig. 44 shows the variation of the output from this device with input sine wave peak to peak voltage amplitude for a number of input frequencies within the range 15 Hz to 50 kHz.

Fig. 45 shows the variation of output with sine wave input frequency for a number of input peak voltages.

It can be seen from these characteristics that the low frequency 3 db point lies at a frequency of about 50 Hz and above about 1 kHz the gain is almost independent of frequency.

Figs. 44 and 45 involve input sine wave voltages expressed in terms of peak to peak values. The equivalent r.m.s. voltage may be derived directly by multiplying the input voltage by 0.353 or by consulting Fig. 46 .

Fig. 47 indicates the turbulent fluctuations in the small WIS jet with the hot wire sensor transverse to the free jet axes, lying on a line joining these axes and at a position 3 cm from S. The value of d was 4 cm. These figures are in fact copies of polaroid photographs of waveforms displaced on a storage oscilloscope.

Although a frequency analysis of these signals has not been made it is clear that a large proportion of the frequency components associated with these waveforms lies above 50 Hz, the 3 db point. Nevertheless there will still be some frequency components lying below 50 Hz and these will undergo amplitude degredation the extent

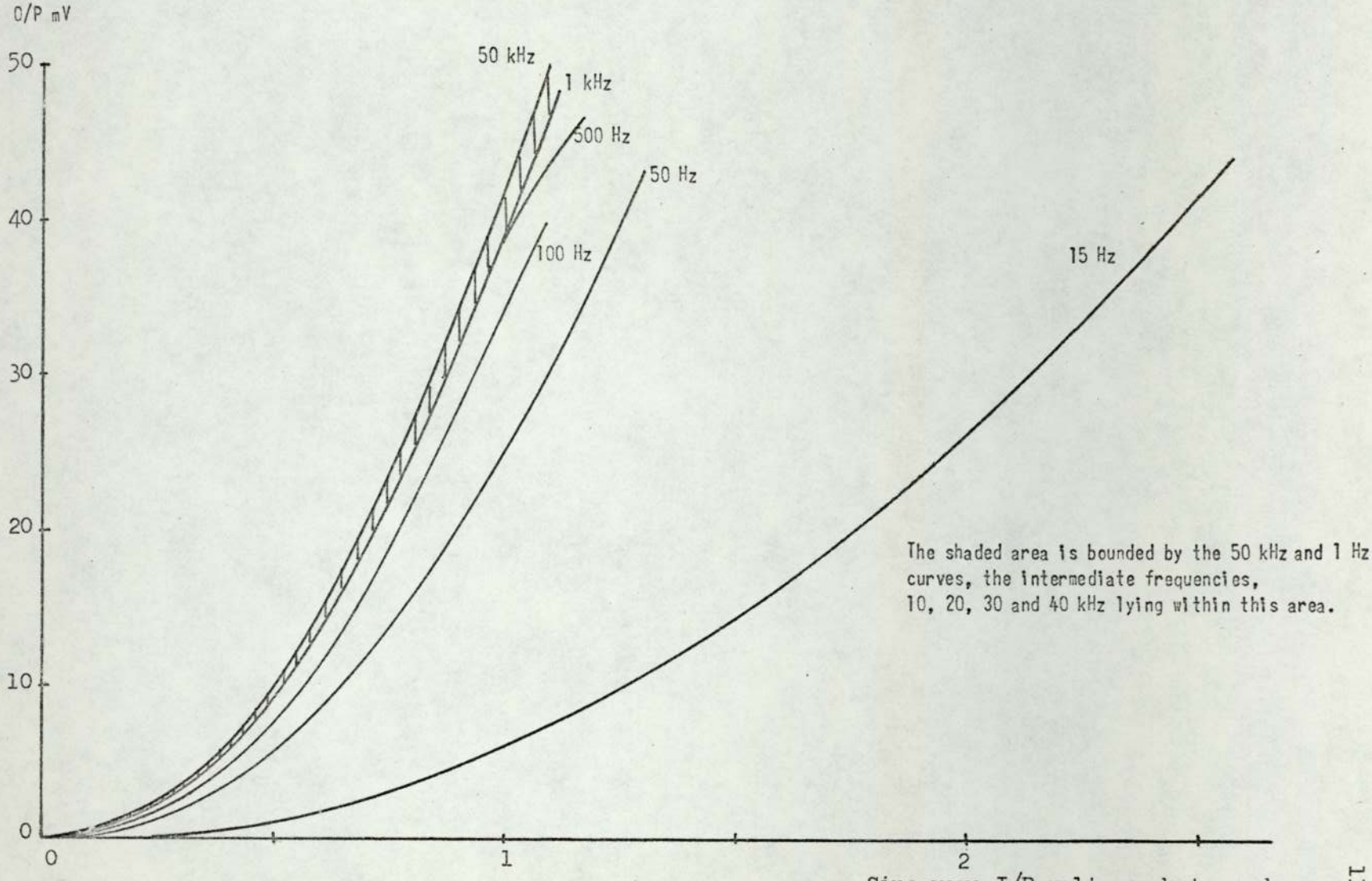

Fig. 44. Turbulent mean square velocity measuring device output vs sine wave peak to peak voltage input for a range of input frequencies.

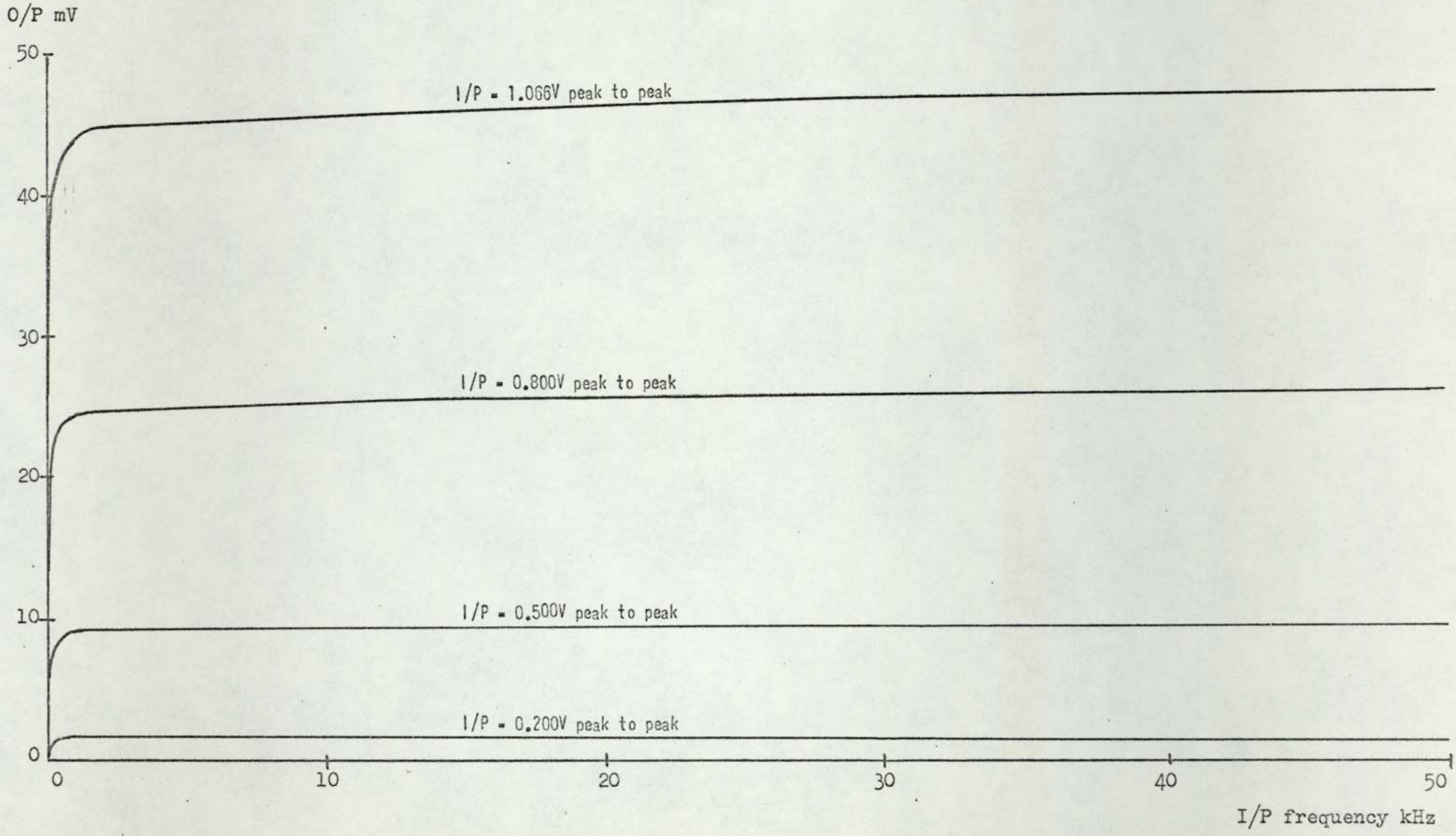

Fig. 45. Variation of turbulent mean square velocity device output with input sine wave frequency for different input voltage levels

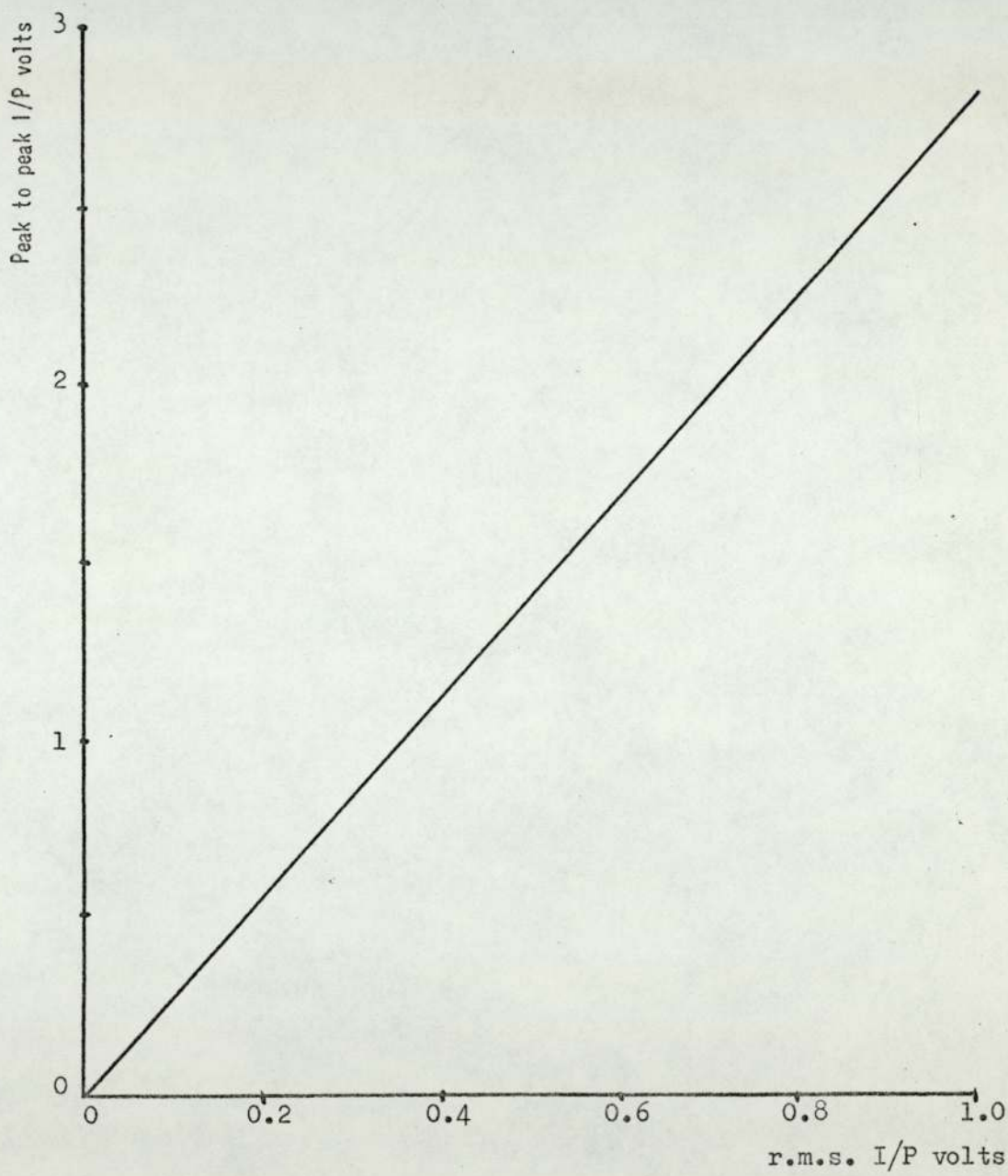

Fig. 46. Sine wave peak to peak voltage versus corresponding r.m.s. voltage.

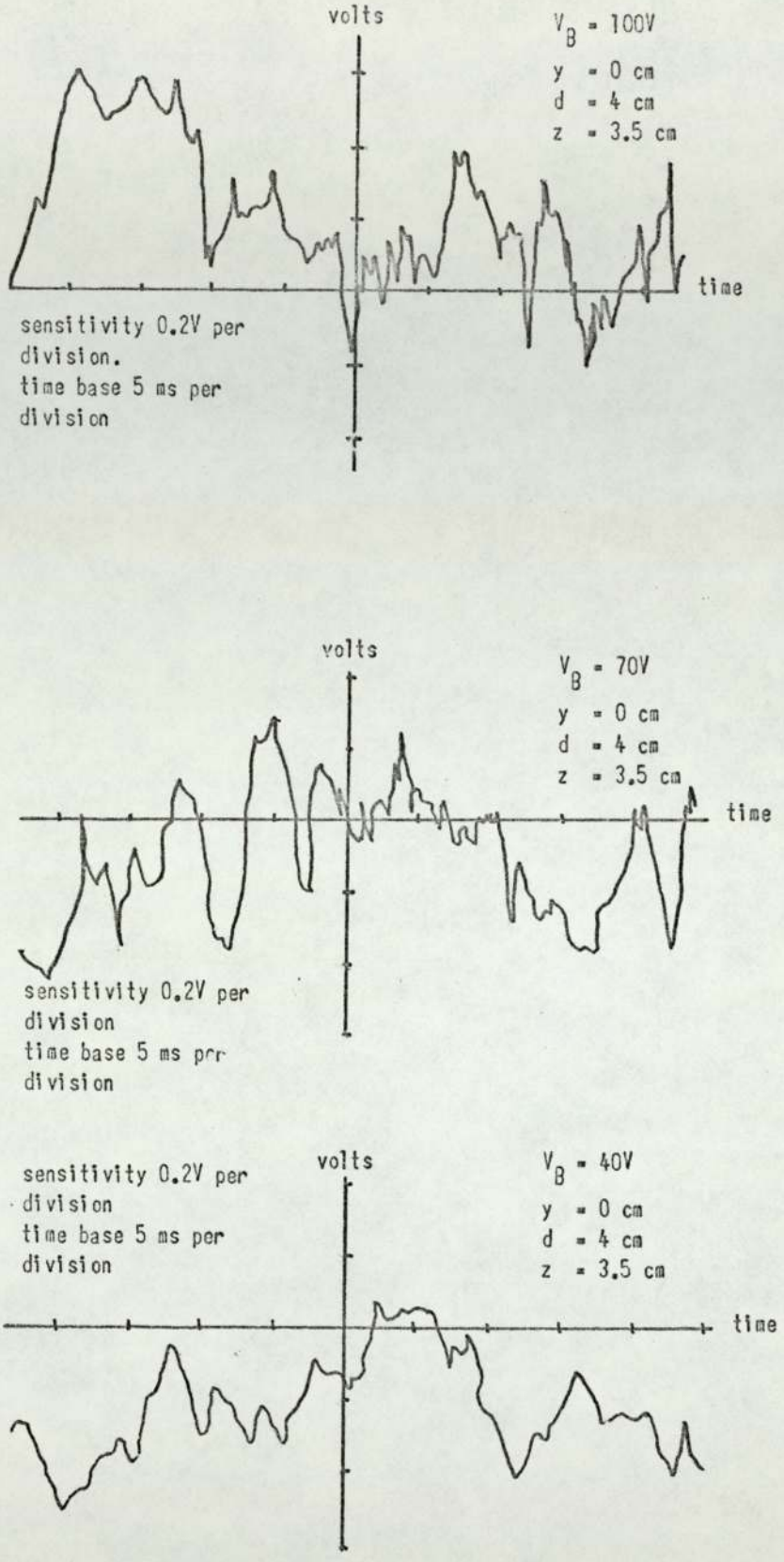

Fig. 47. Turbulent velocity in small WIS jet midway between the constituent free jet with the sensor wire transverse to the free jet axes

of which will depend upon the actual frequencies involved.

An inspection of Figs. 44 and 45 will indicate that no such amplitude degredation will occur for the higher frequencies.

Thus it can be seen that the chart recordings of mean square signals will have experienced a certain amount of frequency discrimination against very low frequency components and will, in fact, be a little lower than they would have been had the true mean square value been measured.

ANALYSIS OF THE RESULTS OF FLOW STUDIES

Having examined the characteristics and limitations of the equipment employed for deriving mean velocity and the mean square value of the turbulent component of velocity some of the results of the flow studies will now be examined.

As a preliminary to the velocity scans employing an asymmetrical orifice distribution a number of scans using a symmetrical orifice distribution were performed. This was to determine first, whether the WIS jet was of the form predicted in the theory and second the degree of interaction of the WIS jet with the corresponding free jets. A knowledge of this latter would assist in choosing an appropriate orifice separation in the final asymmetrical distribution, i.e. if the interaction is such that the WIS jet loses its identity then it would be desirable to increase the orifice separation until the WIS jet's identity is regained.

Scans Performed using the Asymmetrical Free Jet Orifice Distribution

The horizontal x scans

A catalogue of these scans is included in Appendix A5.

The following parameters are appropriate to all scans in this set:

Scan range = 20 cm (which covers completely the three free jets and two WIS jets);

Scan speed = 2 mm/10 seconds (in 2 mm steps), and

Chart speed = 1 inch per minute.

For each location scans were performed with the hot wire sensor axis both transverse and parallel to the free jet axis. In the latter case the y and z values were measured from the middle of the sensor element.

y values indicate the displacement of the sensor in this direction from the horizontal plane.

z values indicate the displacement of the sensor in this direction from S.

All scans are presented in terms of the processing equipment output voltages. The reason for this procedure is as follows. For a given turbulence intensity the output from the turbulent mean square velocity device will depend upon the corresponding mean velocity $\bar{U}$. Most of the velocity scans in the x direction involve a considerable variation of mean velocity with x. For example, for small values of d and z, $\frac{d\bar{U}}{dx}$ is very high at the 'edge' of the free jets but almost zero at axial positions in these jets. Since any estimate of turbulence intensity requires a knowledge of $\bar{U}$ (see later) considerable errors would be incurred in transforming the turbulent mean square velocity device recorded output into absolute turbulence intensity. Thus it was considered appropriate to present these velocity turbulence levels in terms of the device output voltage and in order to maintain dimensionally consistent scales the mean

velocity was also presented in terms of the the mean velocity device output voltage.

These device output voltage profiles will still reveal the same general trends as the corresponding mean and turbulent mean square velocities and in particular the locations of the WIS jets with respect to their free jets will remain unaltered. A direct conversion into mean velocity (continuous line) may be made with the aid of the appropriate calibration curves. (See Figs. 48 and 49) A method of determining the turbulence intensity and percentage turbulence will be given in the next section. Since a turbulent frequency spectrum is not available for the flow under study the choice of curve in Fig. 44 is to a certain extent arbitrary. The 500 Hz curve was finally chosen on the assumption that it represented an approximate weighted average.

The Determination of Turbulence Intensity and Percentage Turbulence

During these investigations two of the flow characteristics which have been considered are (a) the mean velocity and (b) the turbulent velocity. It has been shown that this latter may be expressed in terms of (1) the turbulence intensity which is defined as:

r.m.s. value of the turbulent component of velocity

or (2) the percentage turbulence intensity:

$$\frac{\text{turbulence intensity} \times 100}{\text{mean velocity}}$$

Before presenting some of the flow study results it is helpful to discuss a method of obtaining the turbulent intensity.

Fig. 50 shows a typical calibration curve. Any voltage amplitude distortion caused by non-linearity of the curve will be neglected for the moment. Suppose δU represents the r.m.s. value of the

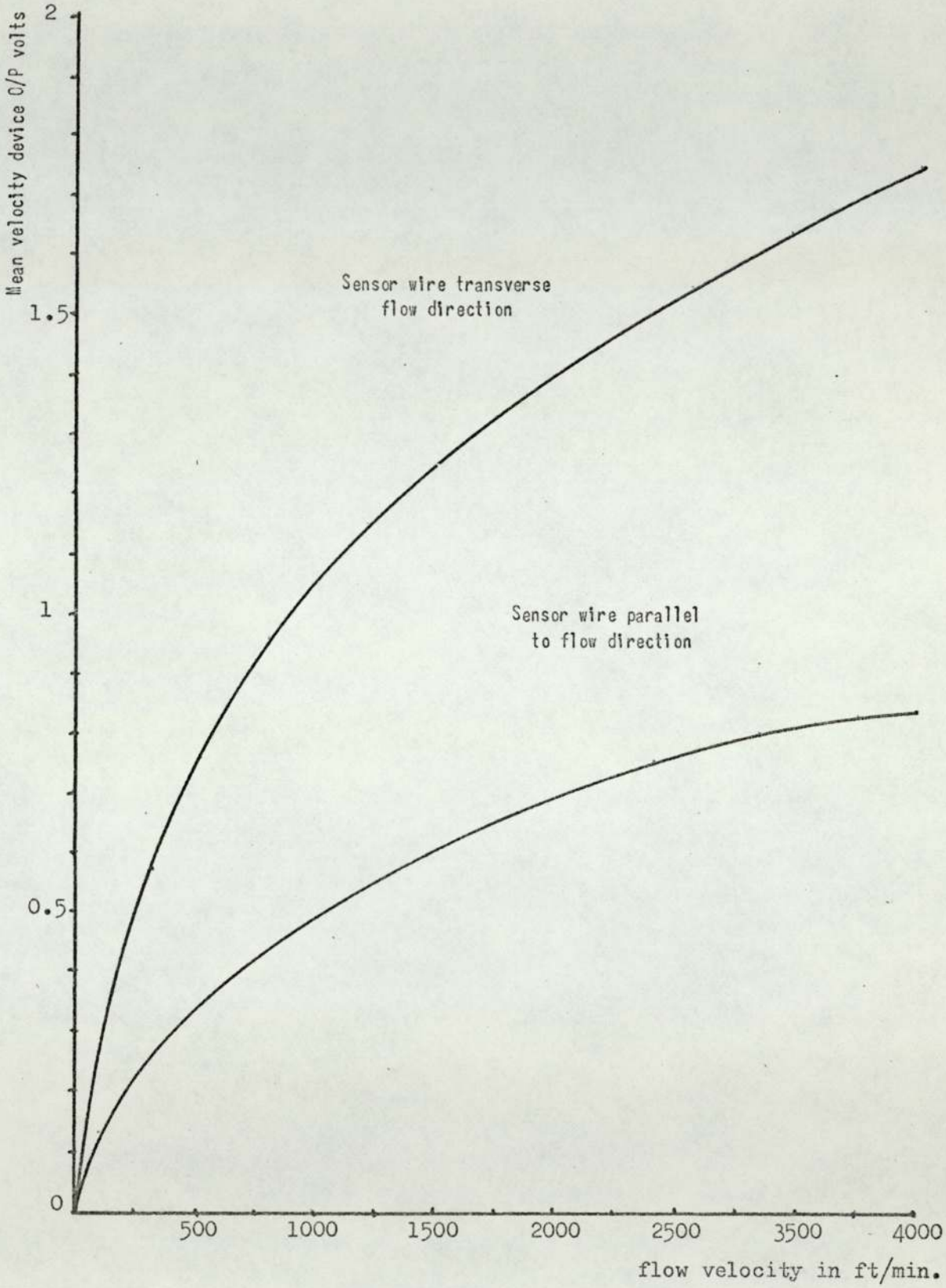

Fig. 48. Mean velocity calibration for type 55001 anemometer

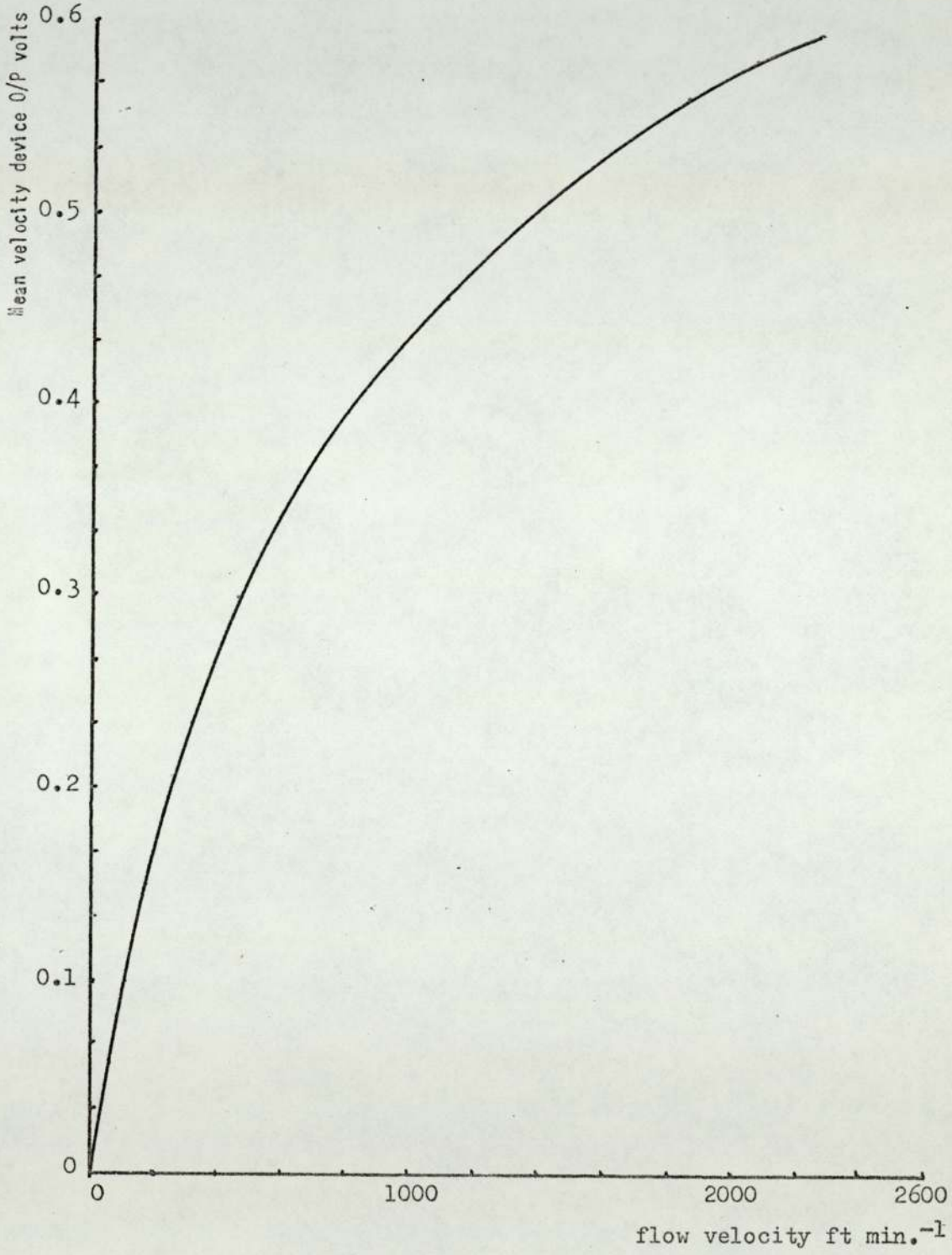

Fig. 49. Mean velocity calibration for type 55005 anemometer with sensor element transverse to flow direction.

turbulent component of velocity (i.e. the turbulence intensity) corresponding to a mean velocity $\bar{U}$ and δV represents the corresponding r.m.s. voltage from the annemometer.

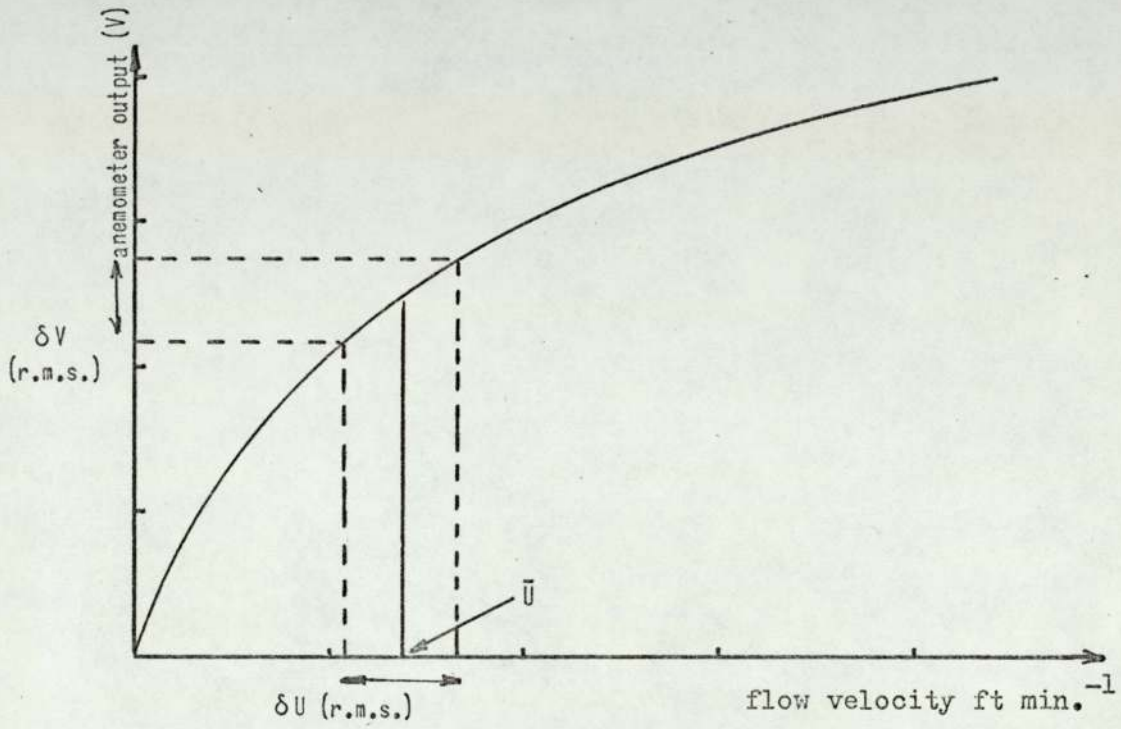

Fig. 50. Calculation of turbulence intensity

The average slope of the curve at $\bar{U}$ is $\frac{dV}{dU}$

thus the turbulence intensity $\delta U = \delta V \div \frac{dV}{dU}$

and the % turbulence intensity $= \frac{\delta U}{\bar{U}} \times 100$

$$\% \text{ turbulence intensity} = \frac{\delta V \times 100}{\frac{dV}{dU} \times \bar{U}}$$

Now δV may be derived from the recorded turbulence traces (shown dotted in the figures to be presented) together with Figs 44 & 46 $\frac{dV}{dU}$ may be measured directly from the appropriate calibration curve

and % turbulence intensity calculated directly.

An example of this calculation procedure follows.

One of the highest WIS jet mean square turbulent velocity levels is shown for the small WIS jet in scan 4, Fig. 52.

The measured voltage (broken line) = 9.8 mV

Reference to the 500 Hz curve in Fig. 44 will show that the equivalent peak to peak sine wave amplitude is approximately 0.53 volts. Using Fig. 46 the corresponding r.m.s. voltage is found to be 0.19 V.

From scan 4 the voltage corresponding to the mean velocity is 0.86 V and from Fig. 48 the corresponding mean velocity is found to be 675 ft/min.

At this velocity the slope $\frac{dV}{dU}$ is approximately:

$$\frac{0.1}{150} \quad \text{V min.ft}^{-1}$$

$$\therefore \text{ \% turbulence intensity} = \frac{0.19 \times 100}{(\frac{0.1}{150}) \times 675} \simeq 42\%$$

This represents a high level of turbulence intensity and since no linearizing network was employed in these studies the value will certainly be in error due to amplitude distortion resulting from the curves non-linearity, nevertheless it will be of the correct order of magnitude.

In order to achieve some qualitative idea of the turbulence intensities encountered in the subsequent scans without actually calculating the values, reference to the appropriate calibration curve, e.g. Fig. 48, will show that for a given r.m.s. voltage the turbulence intensity will increase with $\bar{U}$ although the % turbulence intensity will in fact decrease.

These points are illustrated in Table 4 for an r.m.s. voltage

of 0.2 V and values of $\bar{U}$ of 500, 1000 and 2000 ft/min. The calibration curve is that for the sensor wire transverse to the flow direction in Fig. 48.

TABLE 4

ft/min.	turbulence intensity	% turbulence intensity
500	250 ft/min.	50
1000	420 ft/min.	42
2000	700 ft/min.	35

Before examining these scans in detail a few points relating to their interpretation are appropriate.

It has been stated that the hot wire sensor is insensitive to direction of flow in a plane normal to its axis. Assuming free convective and radiative heat transfer from the sensor to be negligible, so long as there is flow at all, be it turbulent or steady or a combination of the two, there will be forced convective heat transfer from the hot wire irrespective of the flow direction. Thus in order to deduce flow directions it is necessary to accompany the annemometer processed data with a certain amount of physical reasoning.

It must also be noted that even if there exists a condition of complete isotropic turbulence (so that the true time and space means are zero) because the hot wire is sensitive only to $\sqrt{u^2}$ a finite 'mean' value will be indicated.

The calibration curve Fig.48 for the sensor axis parallel to the flow shows that, although not as sensitive as if it were transverse to this flow, it still responds quite significantly. Thus it must not be concluded that the sensor is completely insensitive to flow along its axis.

Examination of Scans Performed in the Horizontal Plane

Although velocity scans were performed using a number of different values of d examples of flow characteristics will only be drawn from those for which d = 4 cm.

Scans 1, 4 and 7 (see Figs.51,52 and 53) correspond to a blower motor voltage V_B of 100 V with respective z values 3.5 cm, 2 cm and 1 cm and the sensor element transverse to the free jet axes.

As has been stated the continuous lines correspond to the mean velocity and the broken lines the turbulent velocity.

For z = 3.5 cm in Fig. 51 the mean velocity free jet characteristics are well defined and the turbulence intensity and % turbulence intensity is small at the centre of the jets. However, both these parameters increase as the periphery of the jet is approached. The two outside jets have a fairly narrow but high amplitude turbulent peak on the side away from the centre free jet.

Both the small and large WIS jets can be identified though their amplitude is fairly low and their definition poor.

Unlike the free jet characteristics which have a minimum turbulence near the centre of the jet the WIS jets mean and turbulent velocity profiles have their maxima lying in the middle of the jet approximately mid-way between the constituent-free jets.

As z decreases, see scans 4 and 7 in Figs.52 and 53, the free jet mean velocity peak amplitudes decrease the jet itself broadening with a more rounded profile. At the same time the average turbulence intensity increases and the narrow peaks at the outside of the jets broaden. This degredation of the mean velocity profiles is most pronounced in the outer jets for which the turbulence is in general higher thus reflecting the fact that turbulent mixing with surrounding

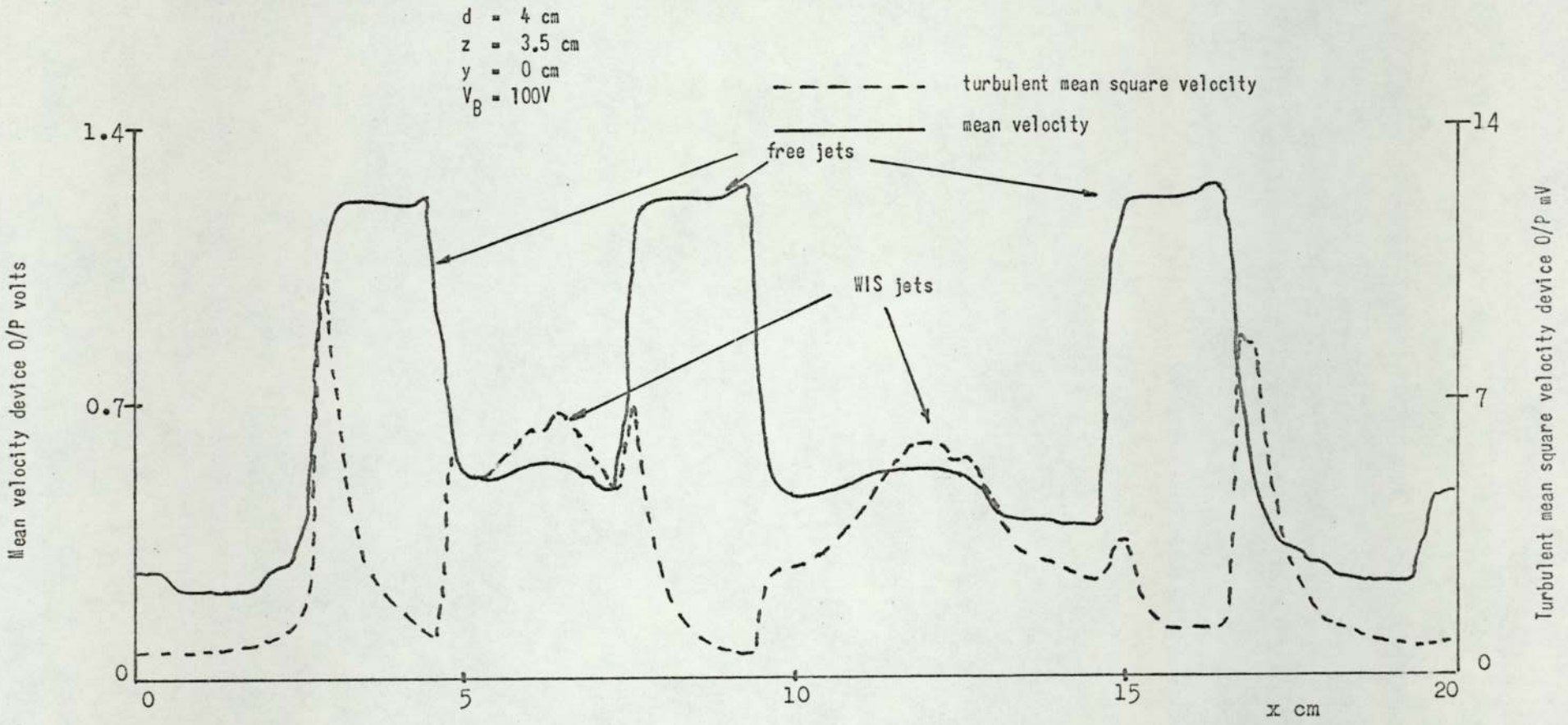

Fig. 51. Horizontal velocity scan 1 with sensor element transverse to free jet axes.

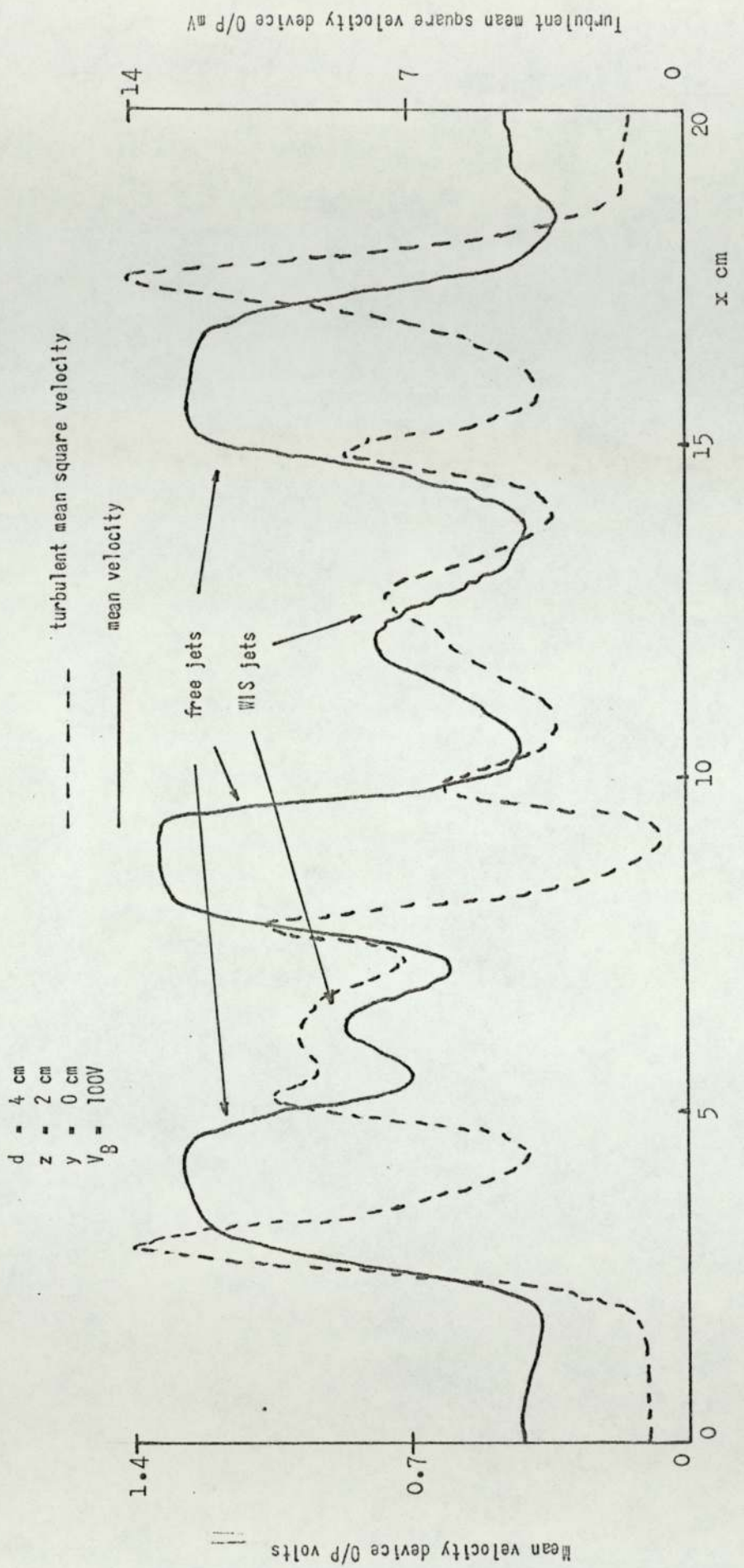

Fig. 52. Horizontal velocity scan 4 with sensor element transverse to free jet axes.

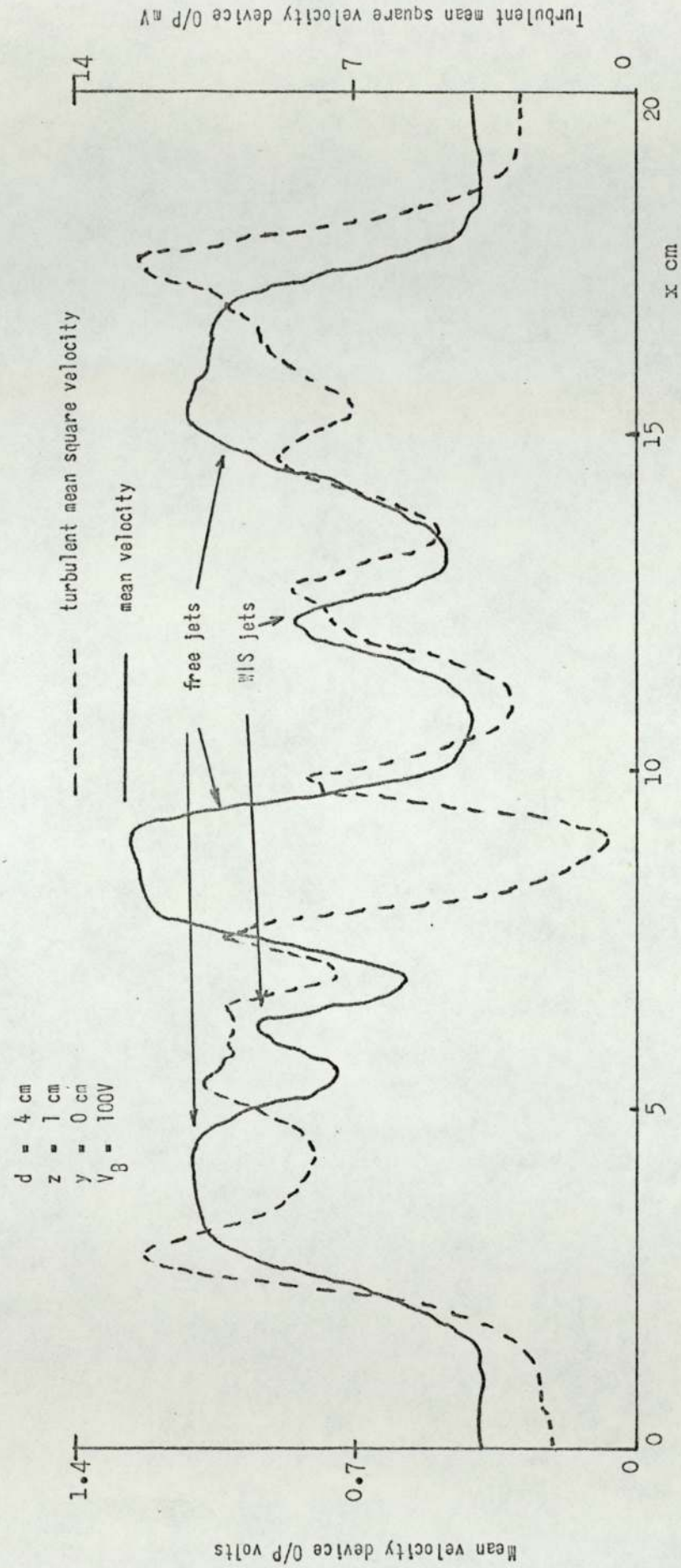

Fig. 53. Horizontal velocity scan 7 with sensor element transverse to free jet axes.

air is mainly responsible for mean velocity attenuation (and, as will be seen later, temperature attenuation of the jets if these are hotter than the surrounding air).

Despite these high turbulence levels the free jets never become fully turbulent within the spatial limits investigated.

The WIS jets, themselves, become narrower and the mean velocity amplitudes and turbulent intensities increase as z decreases. The high turbulence levels in these WIS jets will give rise to a considerable amount of interaction with their adjacent free jets. This will have a profound effect on the temperature characteristics of the WIS jets.

The flow characteristics appropriate to the scans 11, 17 and 20 in Figs.54,55 and 56 with V_B = 70 V and scans 21, 27 and 30 in Figs.57, 58 & 59 with V_B = 40 V are similar in shape to those of 1, 4 and 7 but in general have reduced mean and turbulent velocity amplitudes as would be expected. The turbulent velocity peaks, are not as pronounced as for the V_B = 100 V scans this being particularly clear for the V_B = 40 V scans.

The mean velocity calibration curve for all the horizontal scans is in Fig. 48 (curve with sensor wire transverse to the flow direction).

Fig. 60 shows the variation, for y = 0 cm and d = 4 cm, of mean velocity (expressed in terms of mean velocity device output volts) with z at a point in the large WIS jet mid-way between the two constituent free jets. These scans were peformed with the sensor again transverse to the free jet axis. Since a different annemometer (a DISA type 55D05 CTA) was used it was necessary to derive a different calibration curve for these Z scans and this is shown in Fig. 49.

One interesting characteristic of these Z scans is that for all

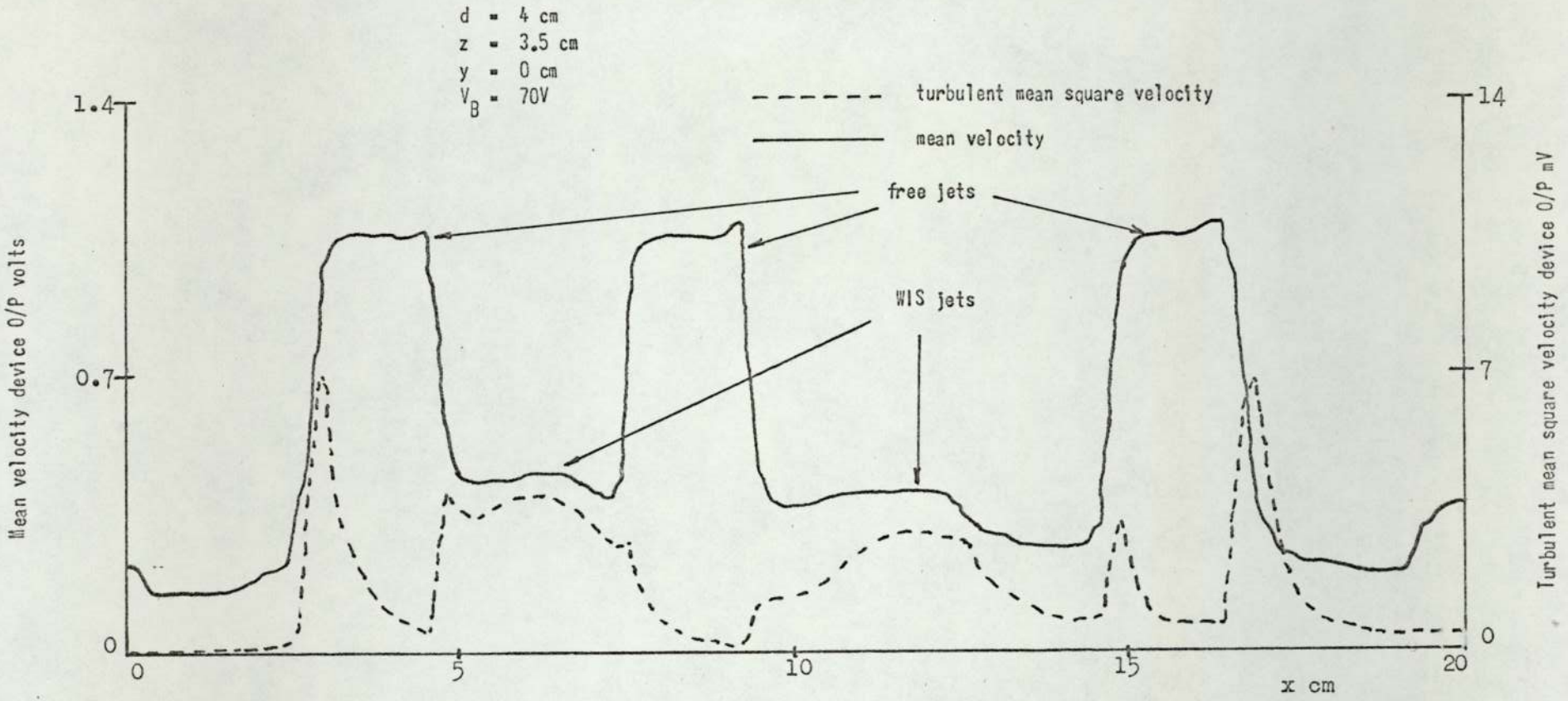

Fig. 54. Horizontal velocity scan 11 with sensor element transverse to free jet axes.

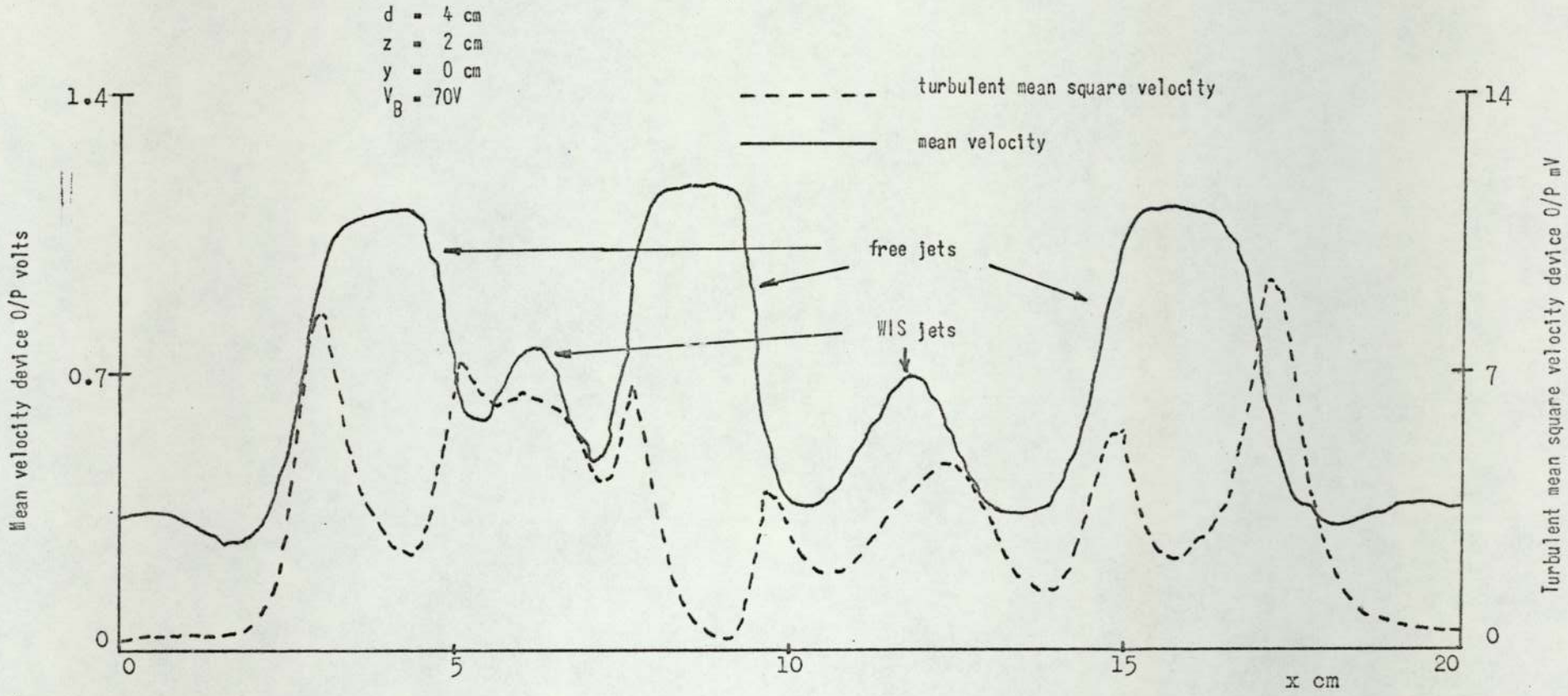

Fig. 55. Horizontal velocity scan 17 with sensor element transverse to free jet axes.

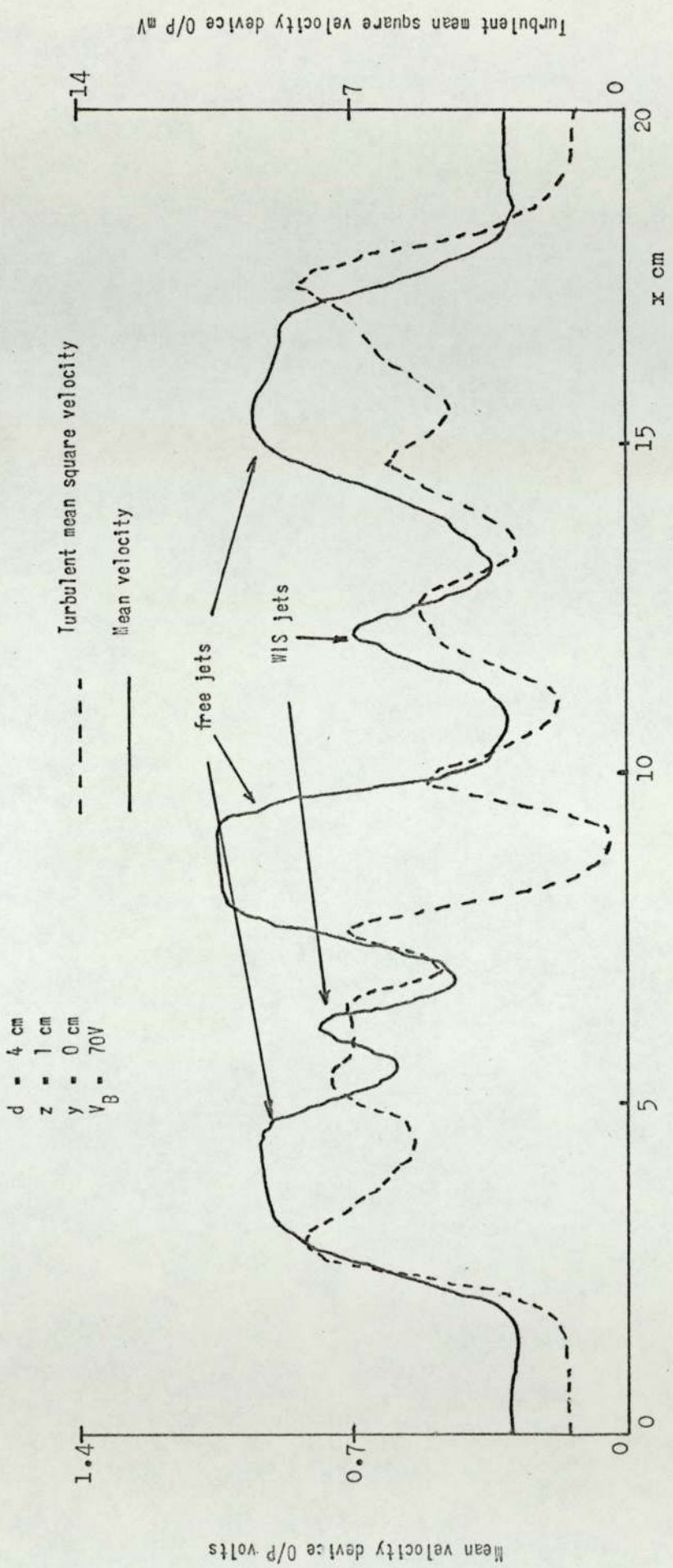

Fig. 56. Horizontal velocity scan 20 with sensor element transverse to free jet axes.

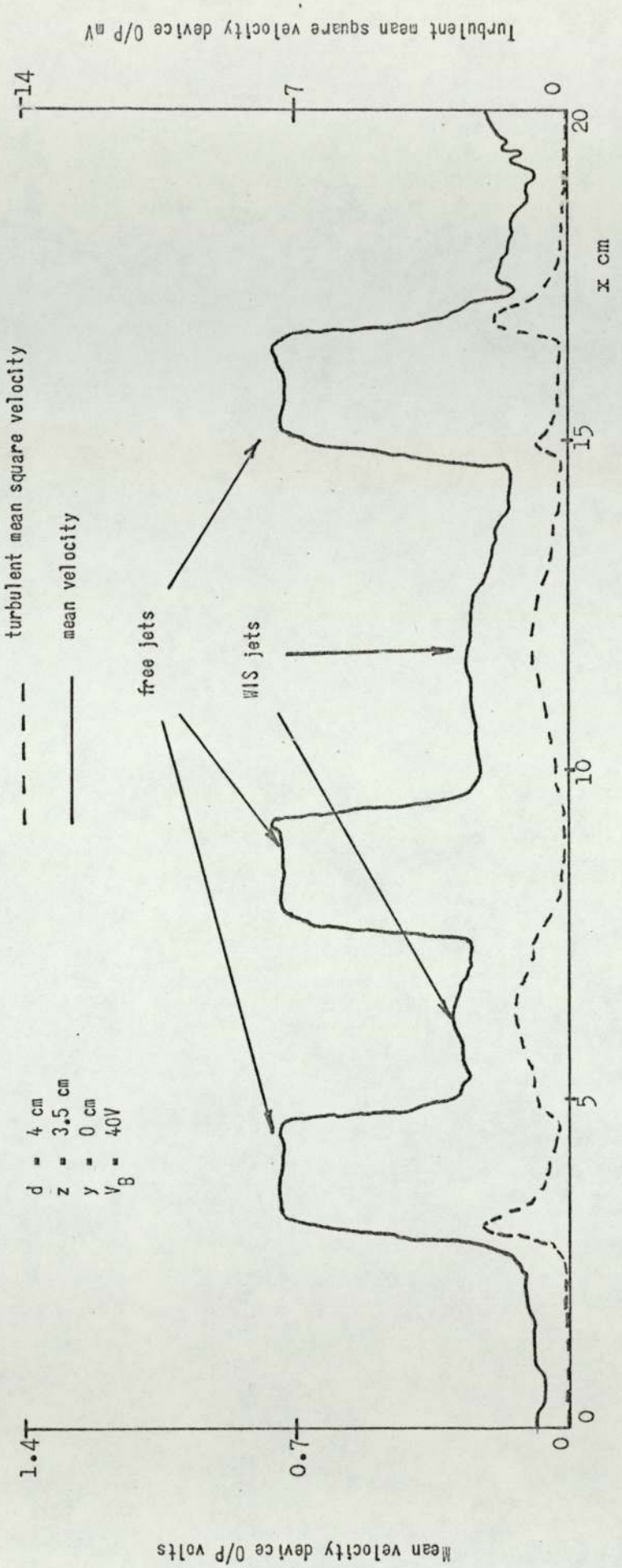

Fig. 57. Horizontal velocity scan 21 with sensor element transverse to free jet axes.

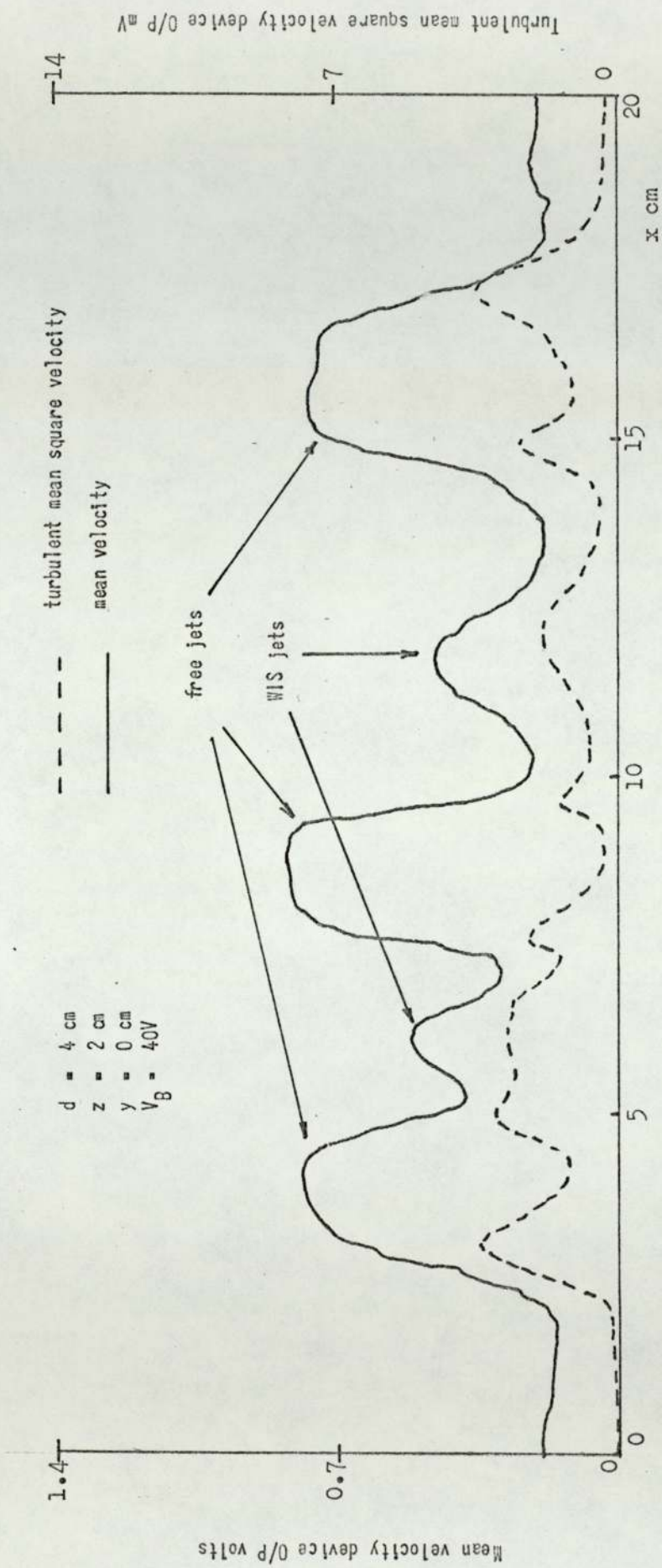

Fig. 58. Horizontal velocity scan 27 with sensor element transverse to free jet axes.

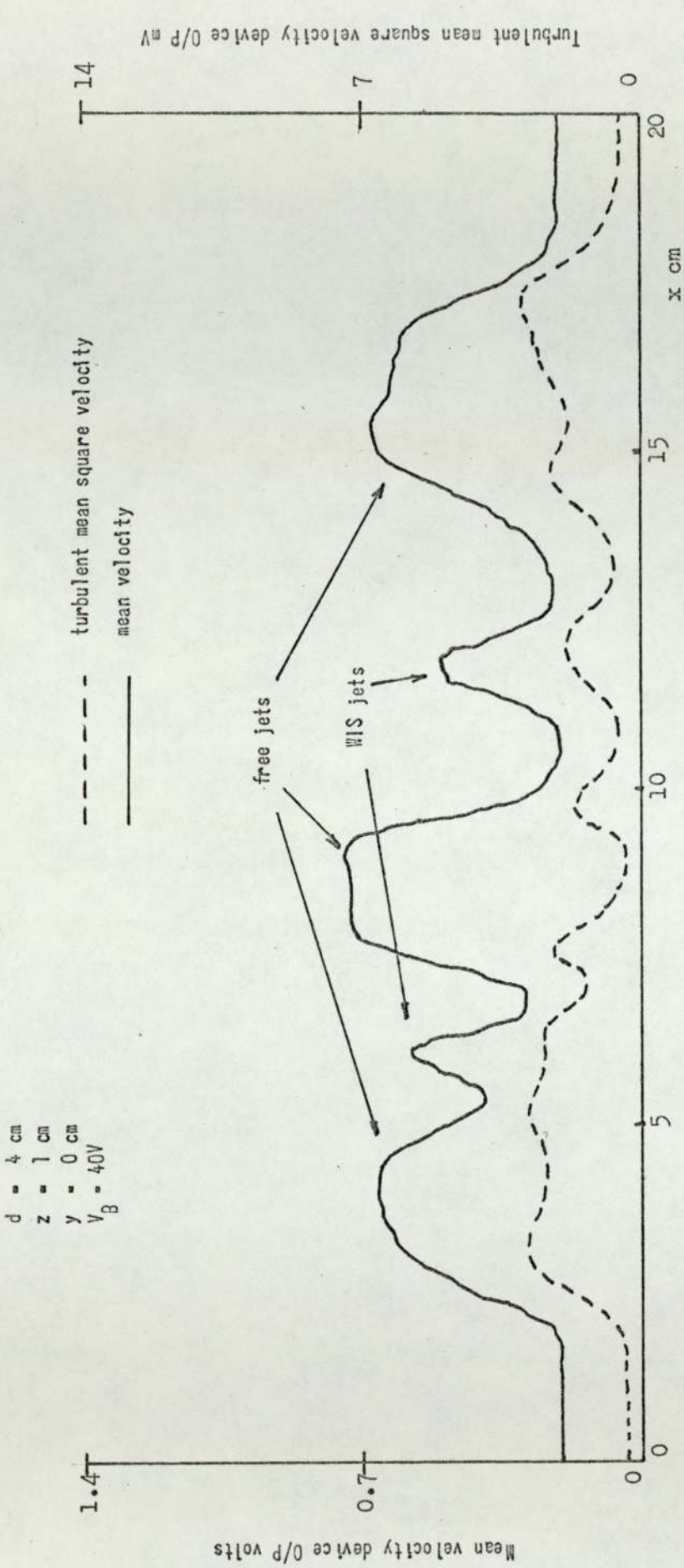

Fig. 59. Horizontal velocity scan 30 with sensor element transverse to free jet axes.

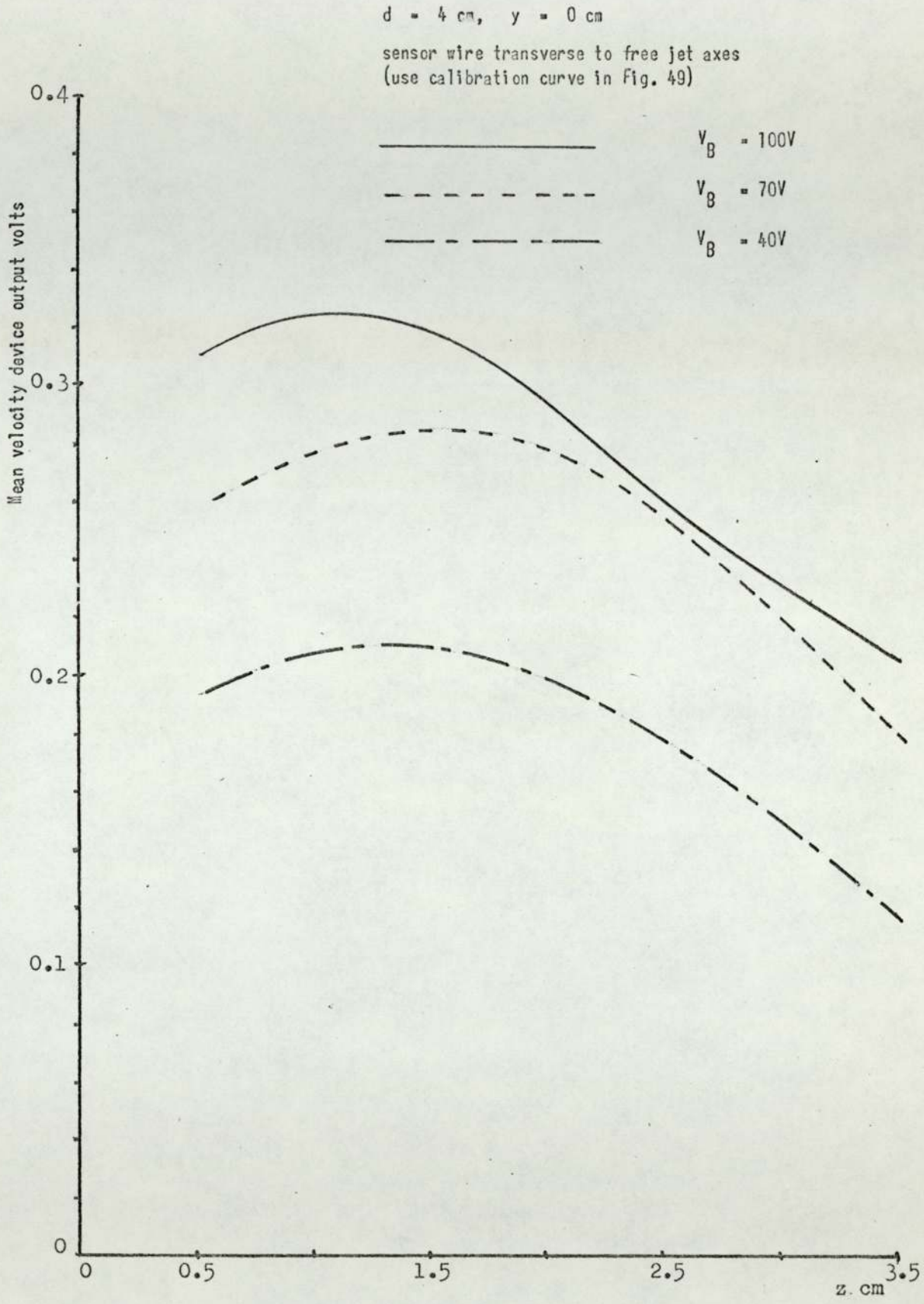

Fig. 60. Variation of mean velocity (expressed in mean velocity device output voltage) with z at a point in the large WIS jet midway between the two constituent free jets.

three values of V_B, 100 V, 70 V and 40 V the peak does not lie at the smallest value of Z, i.e. Z = 0.5 cm.

This could be due to the fact that this point probably lies within the wall jet impingement zone where the flow is in the process of changing direction but is not yet normal to the surface. Thus there would exist a velocity component parallel to the axis of the wire sensor resulting in a reduced sensitivity (see Fig. 48 - calibration curve for 55D01 annemometer with sensor wire parallel to flow direction).

The progressive reduction in velocity with Z for points to the right of the peak will be due to mean velocity attenuation in the jet due to turbulent mixing with the surrounding air - a phenomenon consistent with the horizontal scans.

Scans 37, 47, and 57 (Figs. 61, 62, and 63) correspond to values of V_B = 100 V, 70 V and 40 V respectively with the sensor axis parallel to the free jet axis, and d again 4 cm with y = 0 cm and Z = 2 cm.

A comparison between these 'parallel' scans and the corresponding 'transverse' scans yields a certain similarity particularly between the turbulent components. For example the free jet axial turbulent minima is still present in the parallel scans though their amplitudes are higher than those of corresponding transverse scans. The WIS jets turbulent maxima are still evident but somewhat ill-defined.

The amplitudes of the free jet mean velocity profiles are such that it may be assumed that radial flow is small compared to axial flow. Any radial flow would be lowest at the centre of the jet due to symmetry. Since a small dimple tends to appear close to the centre of each free jet in these 'parallel' scans it would imply that radial flow will probably not be zero at locations in the jet away from the axis.

This observation is not unexpected on physical grounds since it

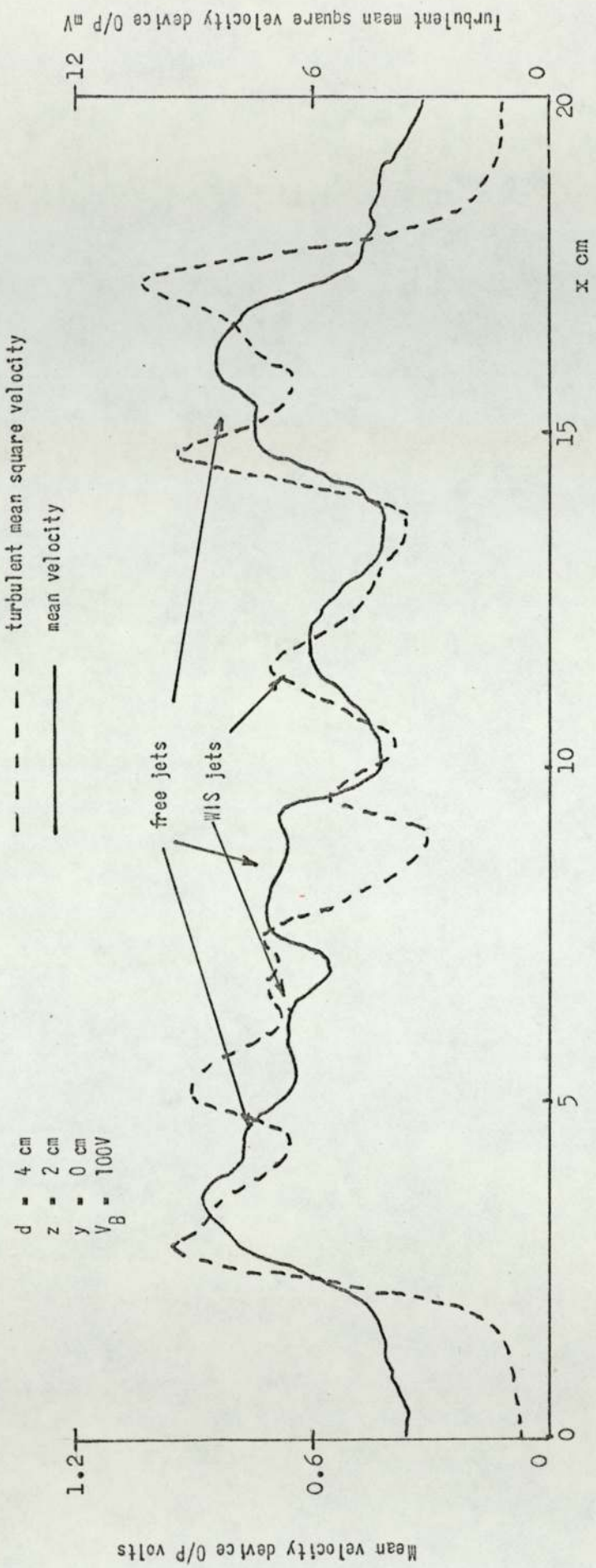

Fig. 61. Horizontal velocity scan 37 with sensor element parallel to free jet axes.

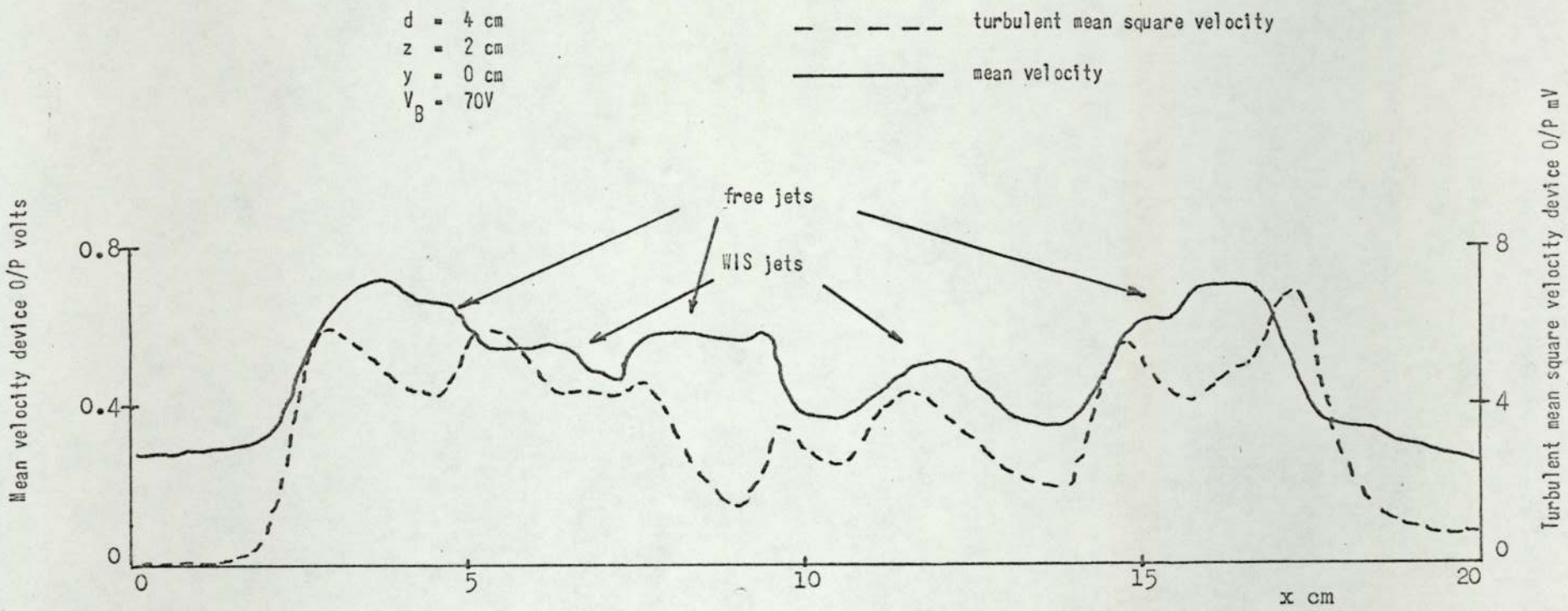

Fig. 62. Horizontal velocity scan 47 with sensor element parallel to free jet axes.

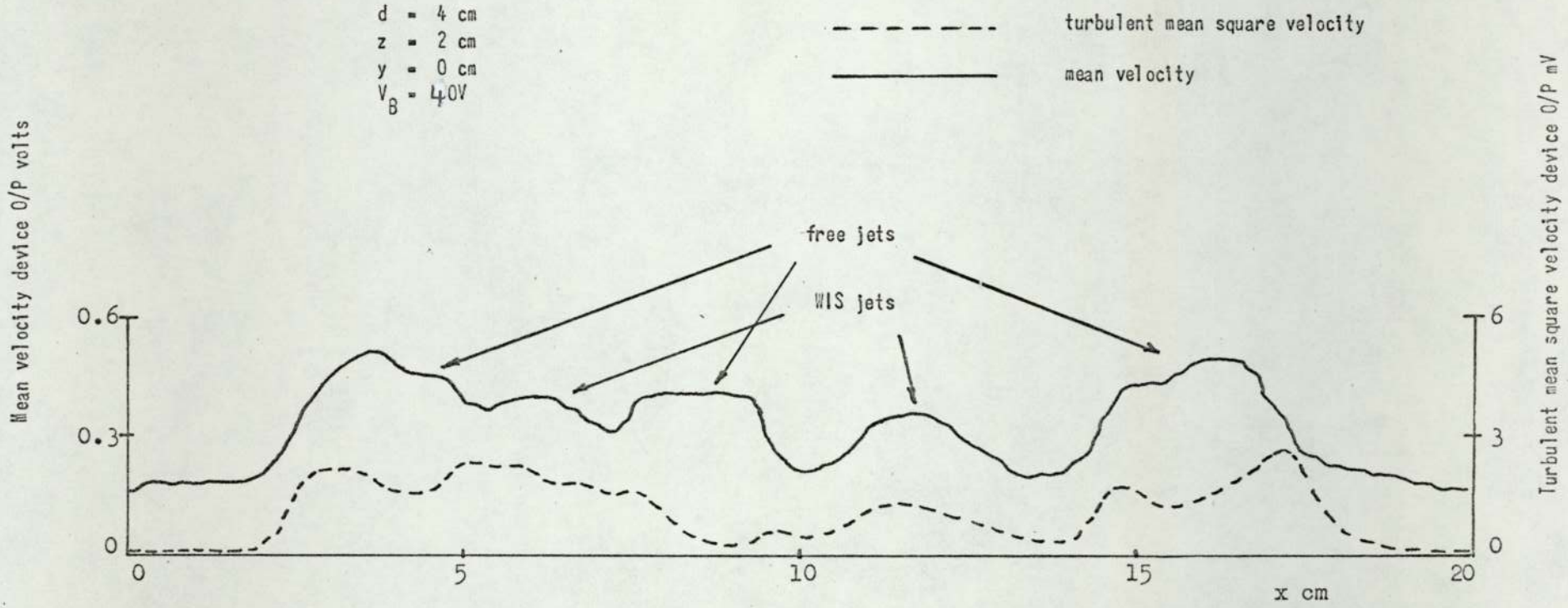

Fig. 63. Horizontal velocity scan 57 with sensor element parallel to free jet axes.

is clear that the jet will broaden as it moves away from the orifice from which it originated.

Although only scans for d = 4 cm in the horizontal plane have been examined the scans for smaller values of d exhibit similar flow characteristics with the two WIS jets always present.

Examination of x Scans with Non Zero Values of y

All the scans to be considered in this section will involve a sensor wire orientation transverse to the axes of the free jets. Scans will only be presented with y values of 10 cm, d = 4 cm and z = 2 cm and 3.5 cm.

Scans 3 and 6 (Fig. 64) with V_B = 100 V have respective z values of 3.5 and 2 cm. As would be expected, there is no evidence of free jet flow in either trace, the two peaks corresponding to the two WIS jets. The turbulent and mean velocity maxima again tend to lie close together but decrease in amplitude with increasing z. As for the y = 0 scans the WIS jet widths increase with z as a result of turbulent mixing with the air surrounding the jets.

An examination of scans 13 and 19 (Fig. 65) with V_B = 70 V and respective z values of 3.5 cm and 2 cm, and scans 23 and 29 (Fig. 66) with V_B = 40 V and respective z values of 3.5 cm and 2 cm, will show that the general flow characteristics are similar to those for V_B = 100 V. The mean velocities, turbulence intensities and % turbulence intensities, however, are smaller, and for V_B = 40 V the turbulence intensity and % turbulence intensity are very small.

Figs. 67 and 68 show the variation of mean velocity with y with respective z values of 3.5 cm and 2 cm at a point in the large WIS jet approximately mid-way between the two constituent-free jets.

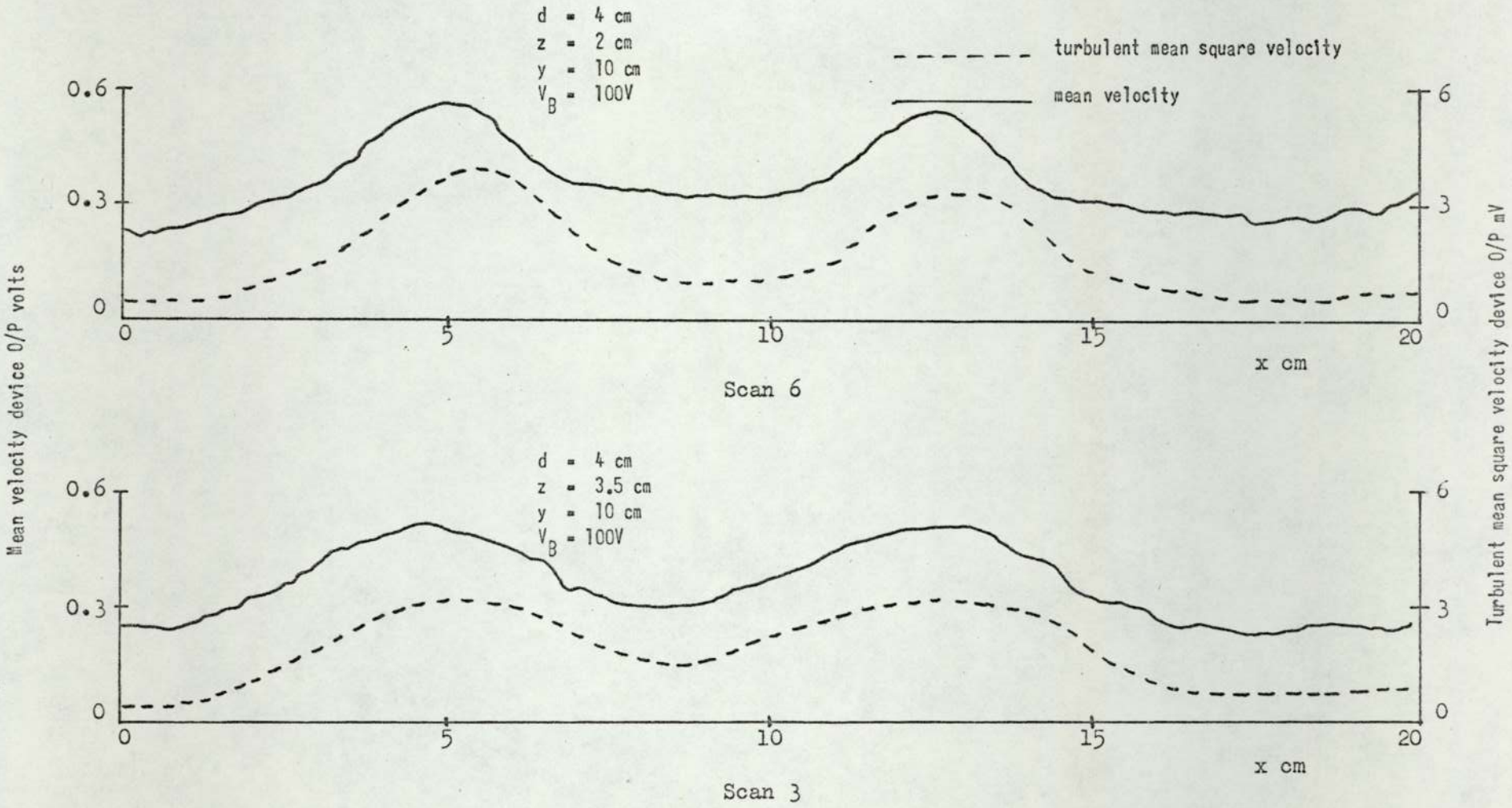

Fig. 64. Horizontal velocity scans with sensor element transverse to free jet axes.

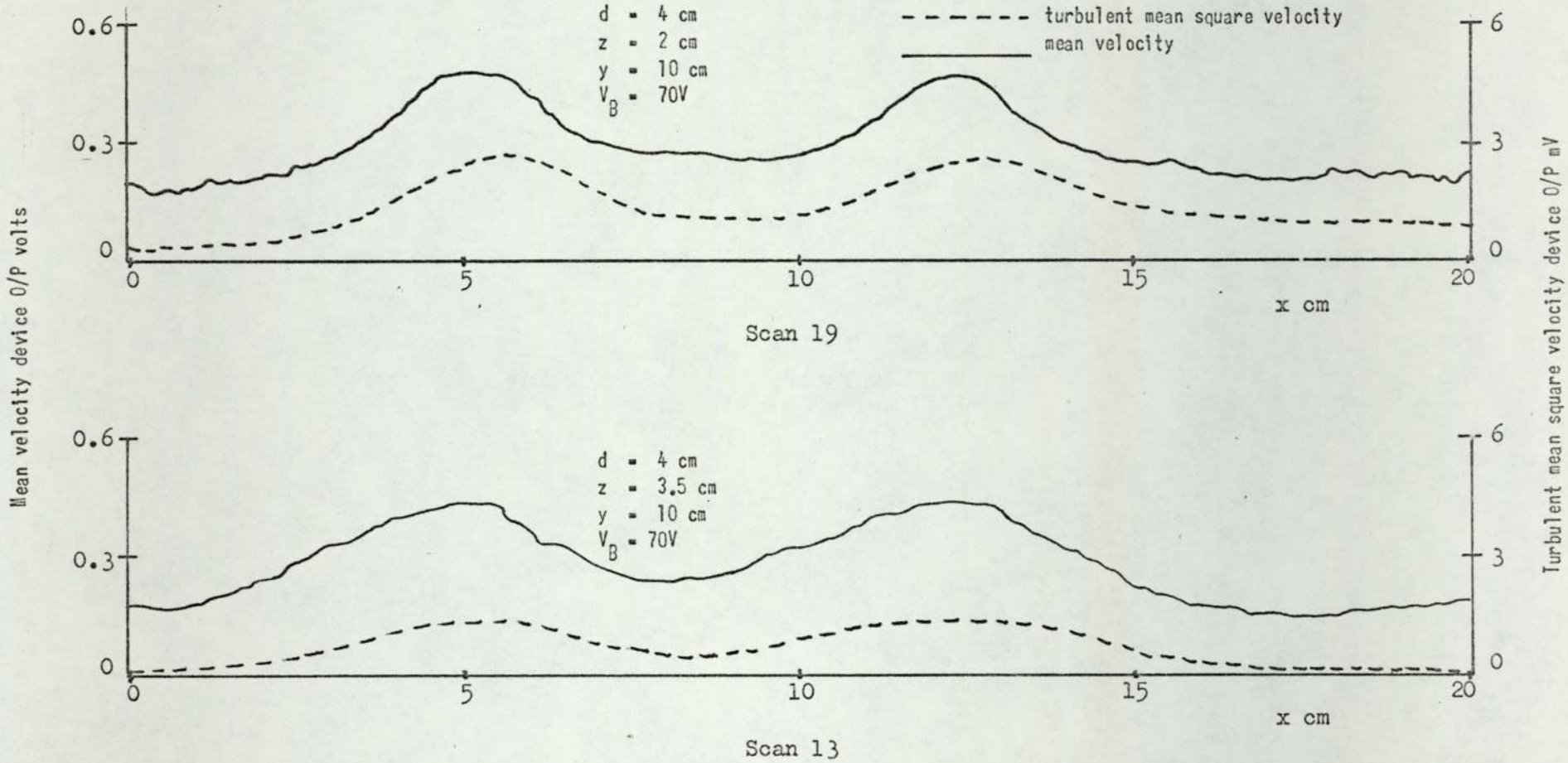

Fig. 65. Horizontal velocity scans with sensor element transverse to free jet axes.

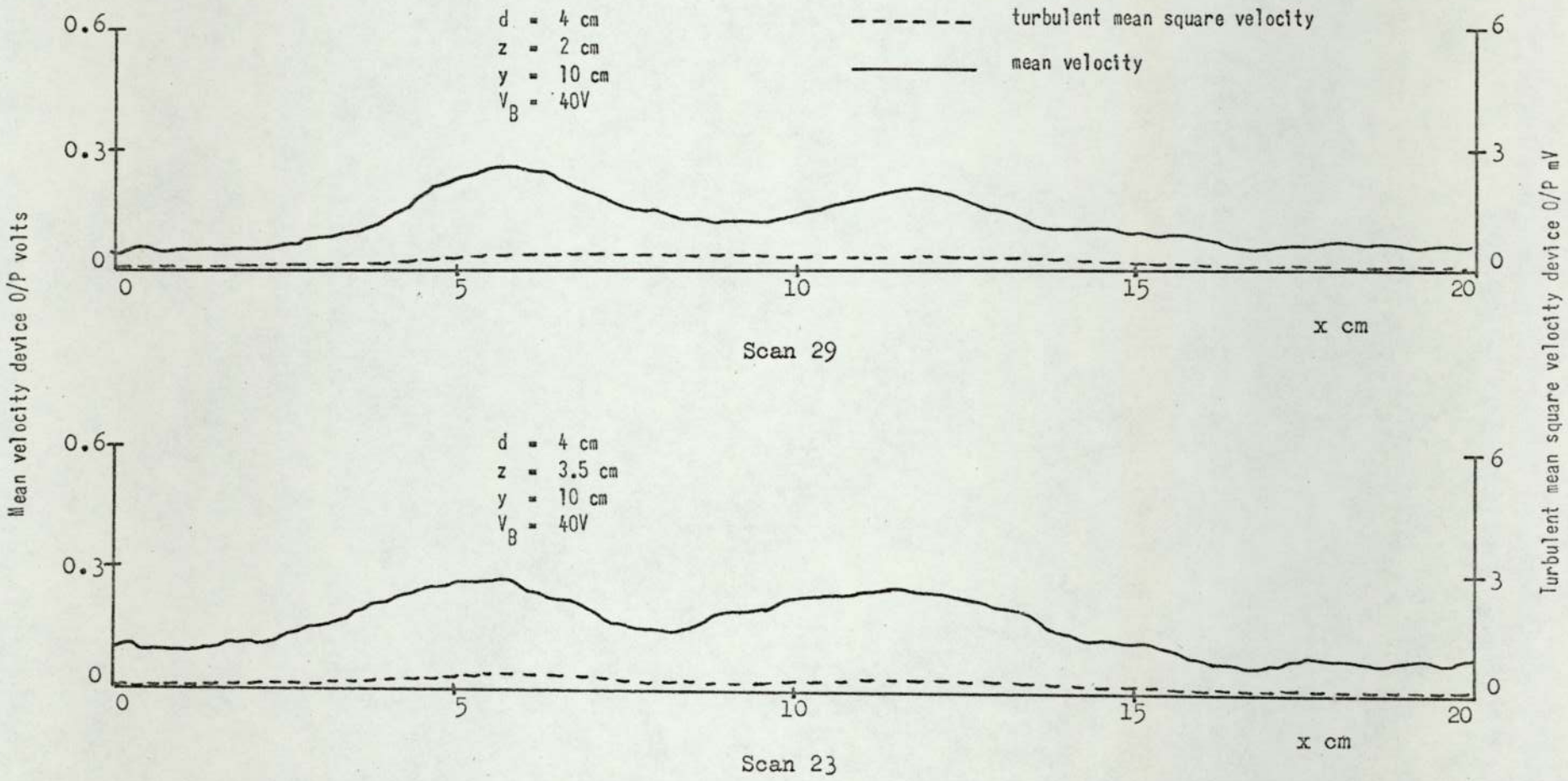

Fig. 66. Horizontal velocity scans with sensor element transverse to free jet axes.

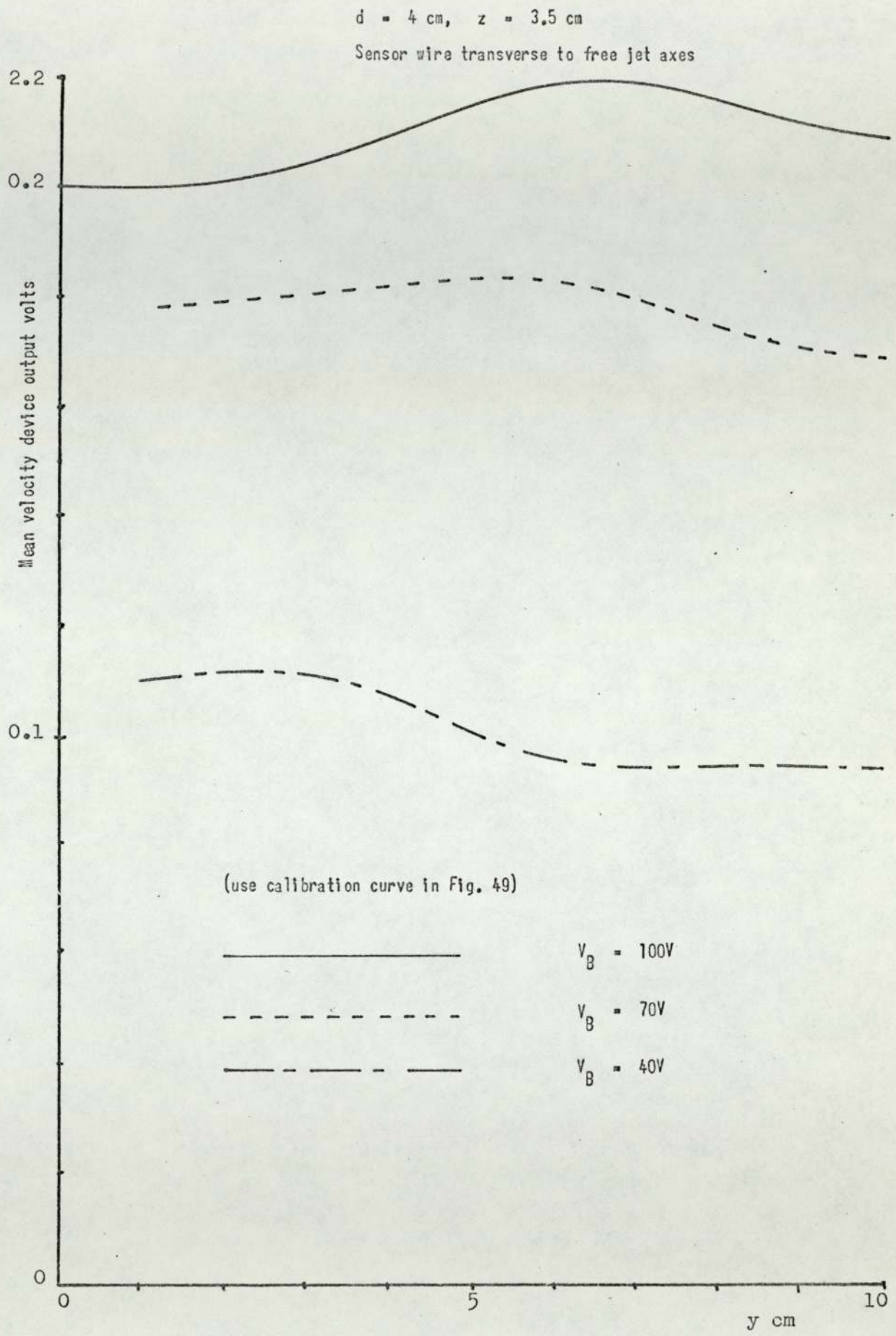

Fig. 67. Variation of mean velocity (expressed in mean velocity device output voltage) with y at a point in the large WIS jet midway between the two constituent free jets.

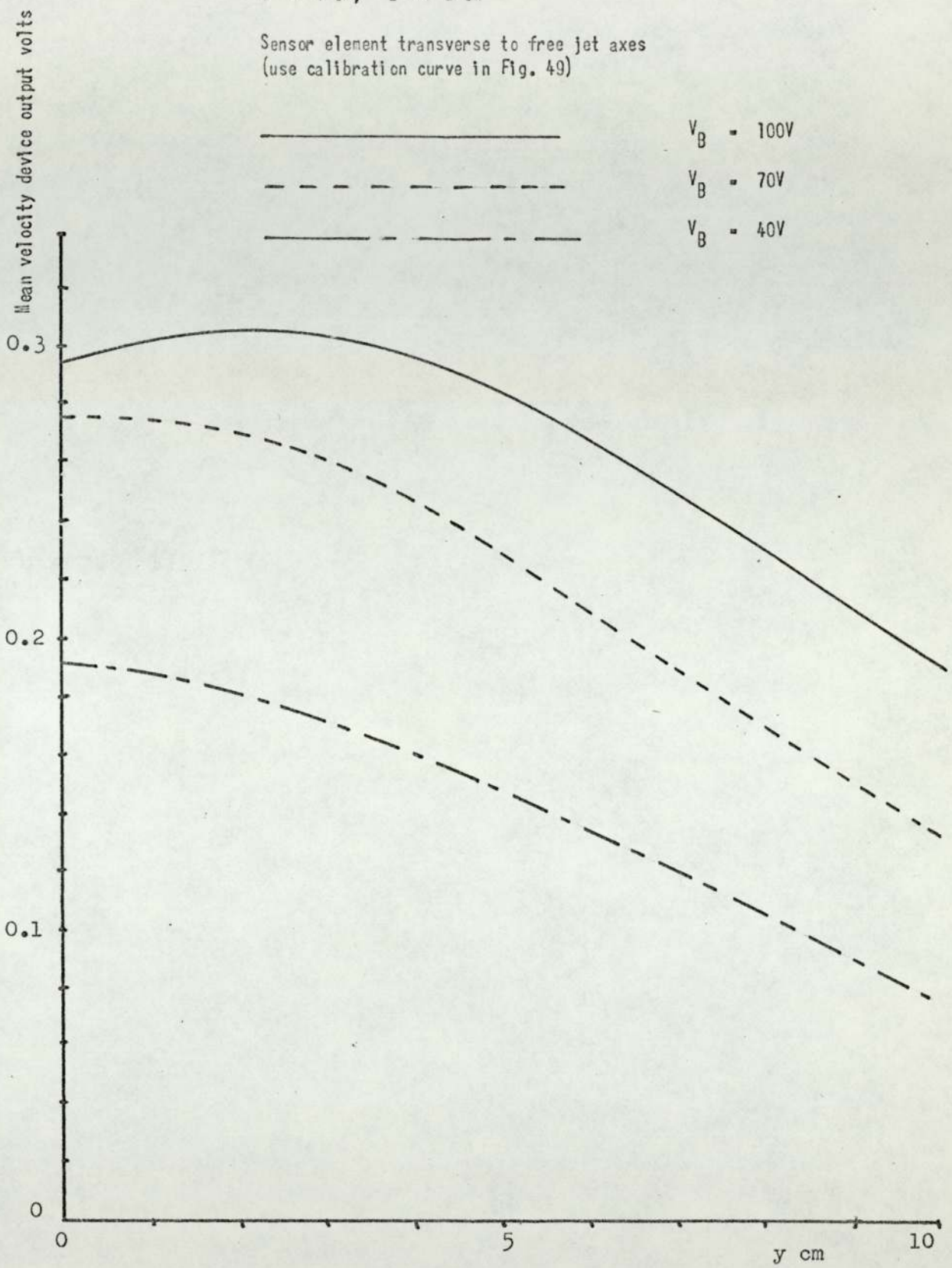

Fig. 68. Variation of mean velocity (expressed in mean velocity device output voltage) with y at a point in the large WIS jet midway between the two constituent free jets.

Plots for V_B = 100 V, 70 V and 40 V have been made with the sensor always transverse to the free jet axes.

For z = 2 cm the maxima occur close to or at y = 0 cm, however, for z = 3.5 cm which corresponds to a sensor displacement of 0.5 cm from P_o, the maxima occur at y values away from the zero. For example, the maximum for V_B = 100 V has a y displacement of almost 7 cm.

The exact cause of this shift in maxima is not certain, but is probably related to the fact that the sensor is close enough to P_o to experience the effect of WIS jet impingement on this surface.

One possible explanation for this phenomenon is as follows. Just prior to impingement on P_o the flow is in the process of changing direction and in so doing acquires an x component of velocity. This component lies parallel to the sensor axis resulting in a reduced sensitivity and hence output. Note reasoning similar to that used in the theory of the WIS jet will indicate that for y = 0 cm the y component of velocity, Uy, is zero. As y increases so also will Uy and since Uy is normal to the axis of the sensor a greater sensitivity to flow will be experienced, resulting in the observed shift away from y = 0 cm of the mean velocity maxima.

Scans with the Sensor Parallel to the Free Jet Axis

These scans again employed a value of d = 4 cm and z = 2 cm, see Figs.69-71. Scans 38 and 39 with V_B = 100 V had y displacements of 5 and 10 cm respectively. Scans 48 and 49 with V_B = 70 V again had respective y displacements of 5 and 10 cm as did scans 58 and 59 with V_B = 40 V.

For all three values of V_B the mean velocities and turbulence intensities decrease with y the turbulence intensity for scan 59

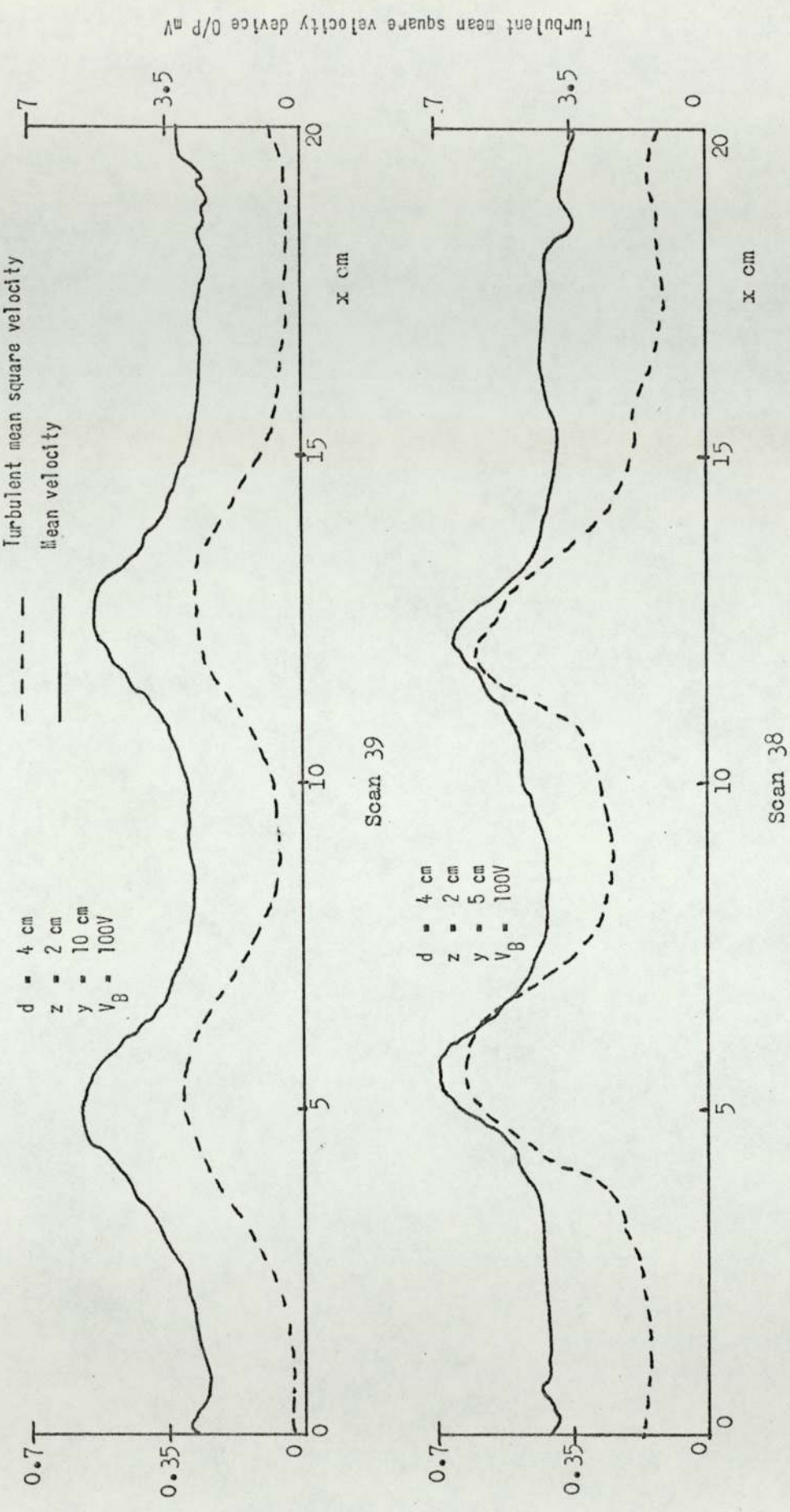

Fig. 69. Horizontal velocity scans with sensor element parallel to free jet axes.

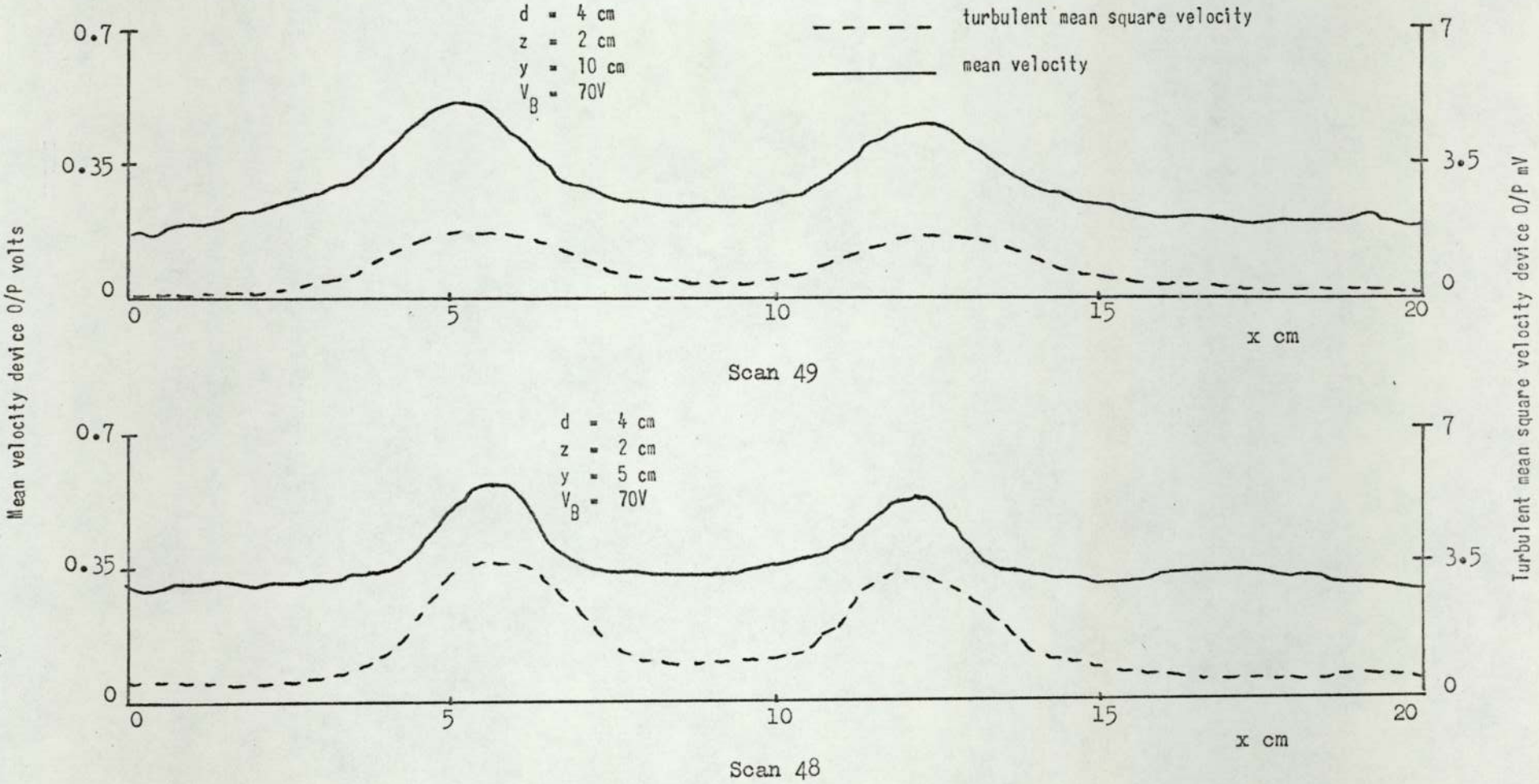

Fig. 70. Horizontal velocity scans with sensor element parallel to free jet axes.

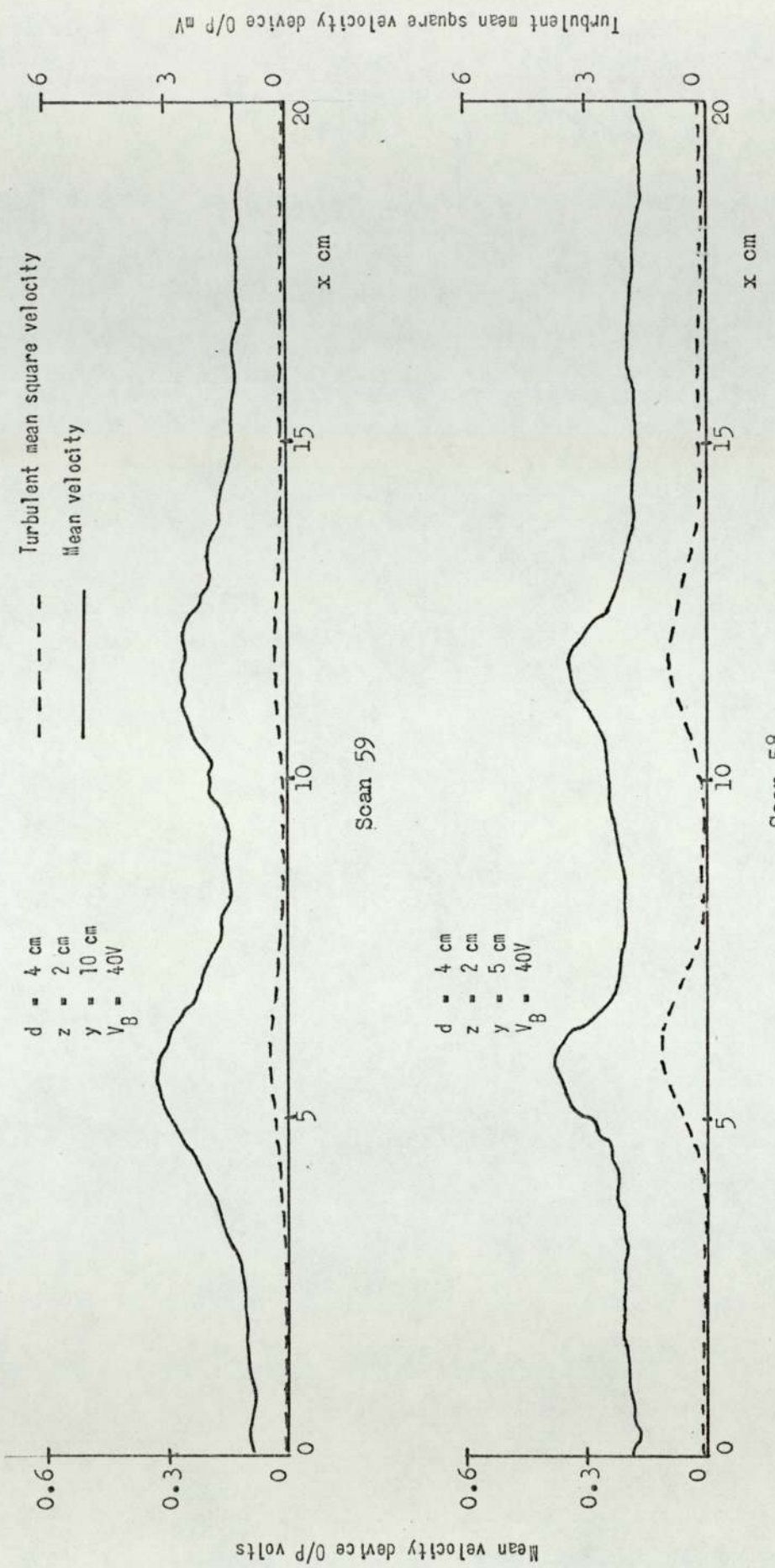

Fig. 71. Horizontal velocity scans with sensor element parallel to free jet axes.

being very low. Also as y increases the mean and turbulent velocity peaks broaden. This is another example of jet degredation resulting from turbulent mixing.

It must be remembered that for non-zero values of y according to the theory presented earlier there will be a finite y component of velocity Uy and this fact is reflected in the mean velocity peak amplitudes corresponding to V_B = 100 V, 70 V and 40 V, which are in fact not very different from those for which the sensor element lay transverse to the free jet axes.

CHAPTER 7

RESULTS AND ANALYSIS OF THE TEMPERATURE SCANS

Introduction

The purpose of these scans was to derive those temperature characteristics existing between the orifice plate, P_o, and test surface S which could conceivably be exploited in non-contact temperature measurement.

Several different temperature dependent parameters will be examined and their accuracy in surface temperature prediction together with their sensitivity to changes in this temperature will be assessed. The influence of free jet temperature, velocity and P_o - S displacement, d, on these parameters will also be investigated.

As well as being fairly readily exploitable practically, the temperature dependent parameter finally chosen must ideally exhibit a low sensitivity to the following variables:

(1) P_o - S displacement, d

(2) Radiation

(3) Surface roughness

(4) Surface velocity.

Low sensitivity to radiation is important since it also implies a low sensitivity to surface emissivity.

The influence of radiation has been dealt with in the theory section but a few further comments will emerge from this section. However, no experiments were designed specifically to investigate this effect.

The effect of surface roughness and velocity together with the

extent of any perturbation of the surface temperature by the impinging jets will be discussed in Appendices 2, 3 and 4.

RESULTS OF TEMPERATURE STUDIES

Horizontal Scans

The purpose of these scans was to measure the variation of temperature in the x direction. All scans in this set were performed in the horizontal plane, (i.e. y = 0 cm) but the following parameters were allowed to vary: V_B, d, z and T_s.

The upper scale in these scans represents thermo-couple displacement in the x direction measured from the start of the scan and the lower scale represents time.

All temperatures have been measured with respect to ambient and have been expressed in terms of thermal e.m.f. generated by the thermo-couple. They may be transformed directly into temperatures, however,with the aid of the thermal e.m.f. vs temperature calibration curve (see Fig. 72).

Scans 1, 7 and 12 in Figs. 73,74 & 75 have d = 1 cm and z = 0.5 cm with V_B's of 100 V, 70 V and 40 V respectively. J_A, J_B and J_C represent the unheated free jets and W_D and W_E the small and large WIS jets respectively. It can be seen that these latter are fairly well defined for all three values of V_B. For the 40 V and 70 V values a dip appears in the large WIS jet, a possible explanation for which is described below.

The temperature of the thermo-couple bead is a function of both the radiative and convective heat transfer coefficients. It has been shown that the latter increases with gas velocity, U, by some power

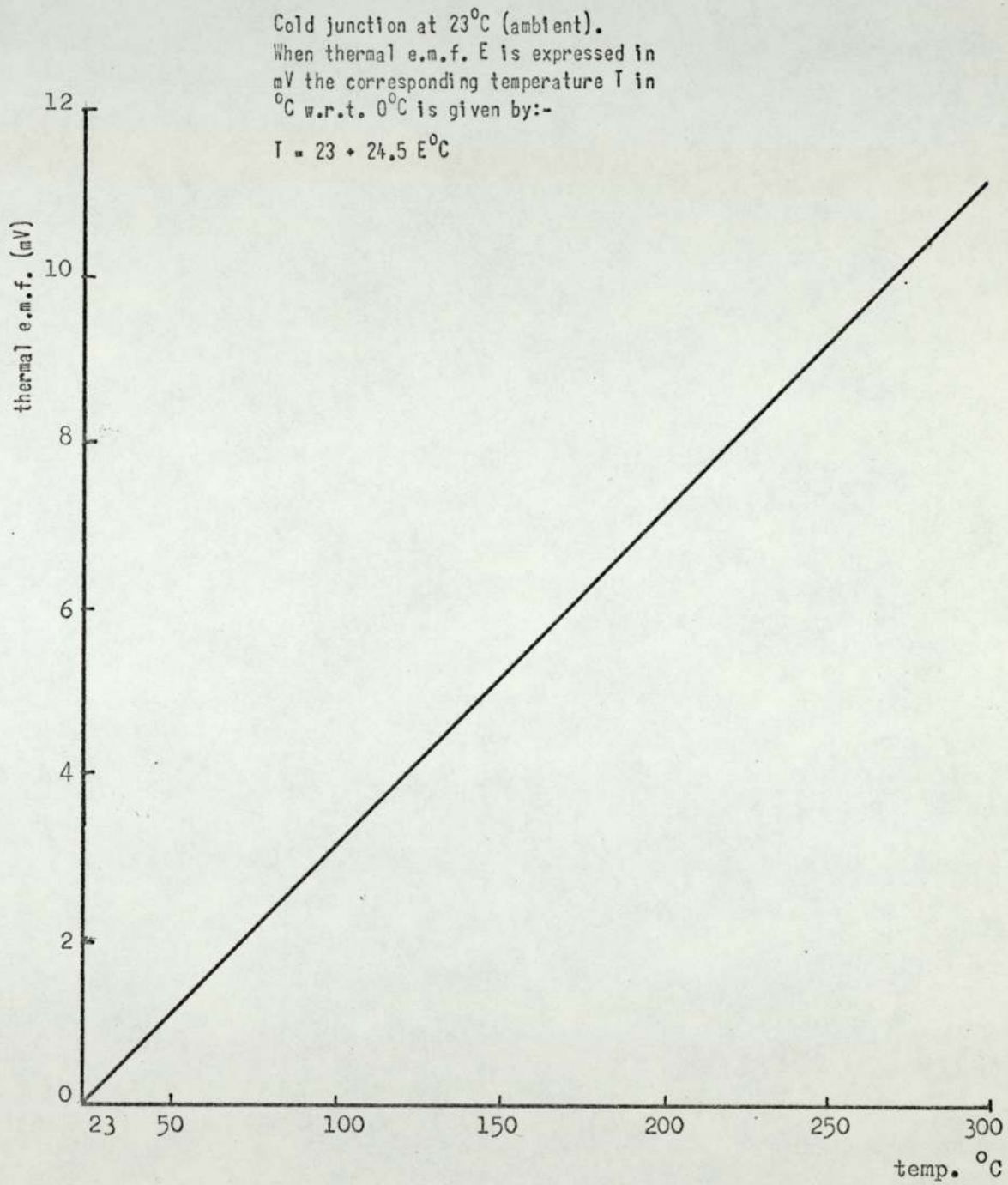

Fig. 72. Calibration curve for the Cr-Al thermocouple used in the temperature scans

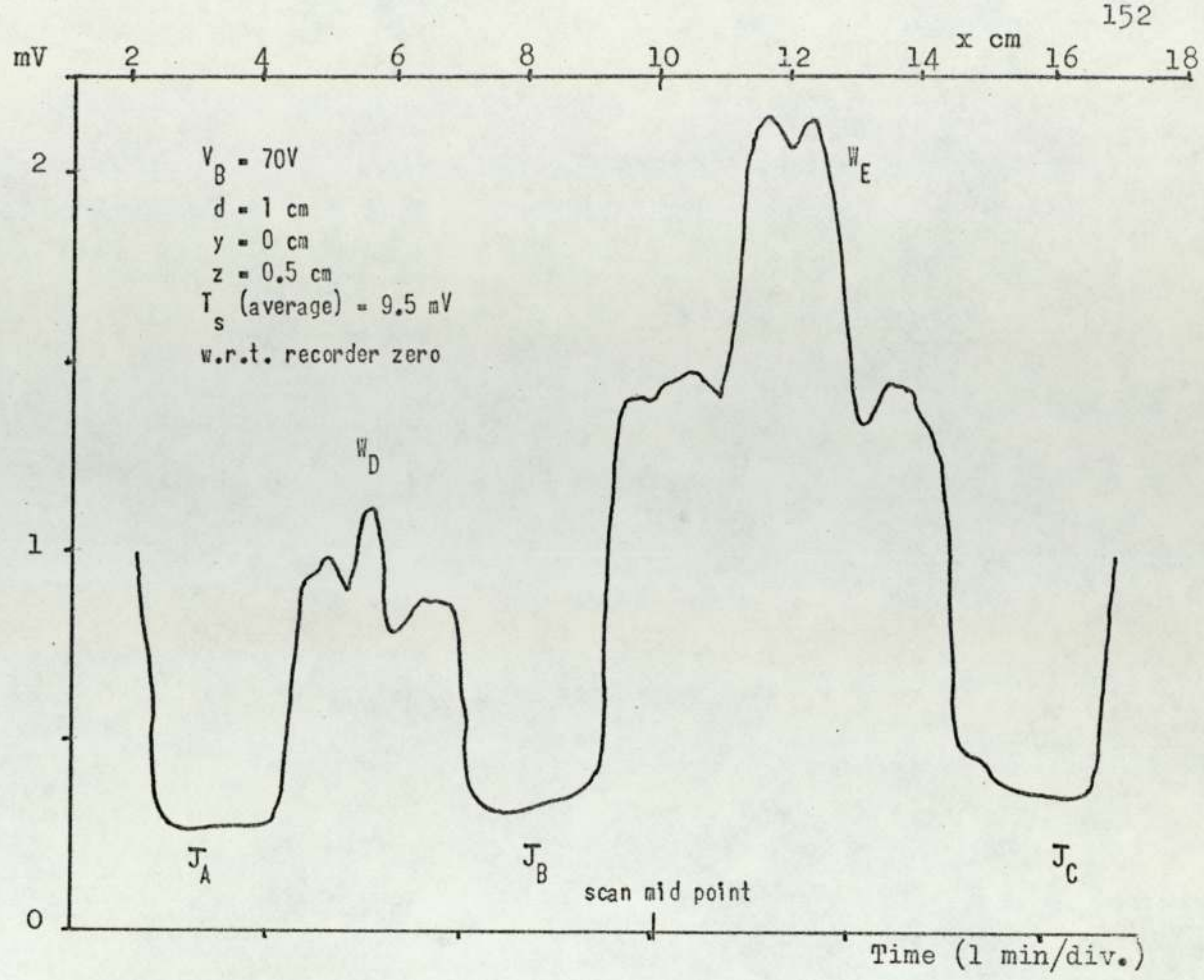

Fig. 74. Horizontal temperature scan 7

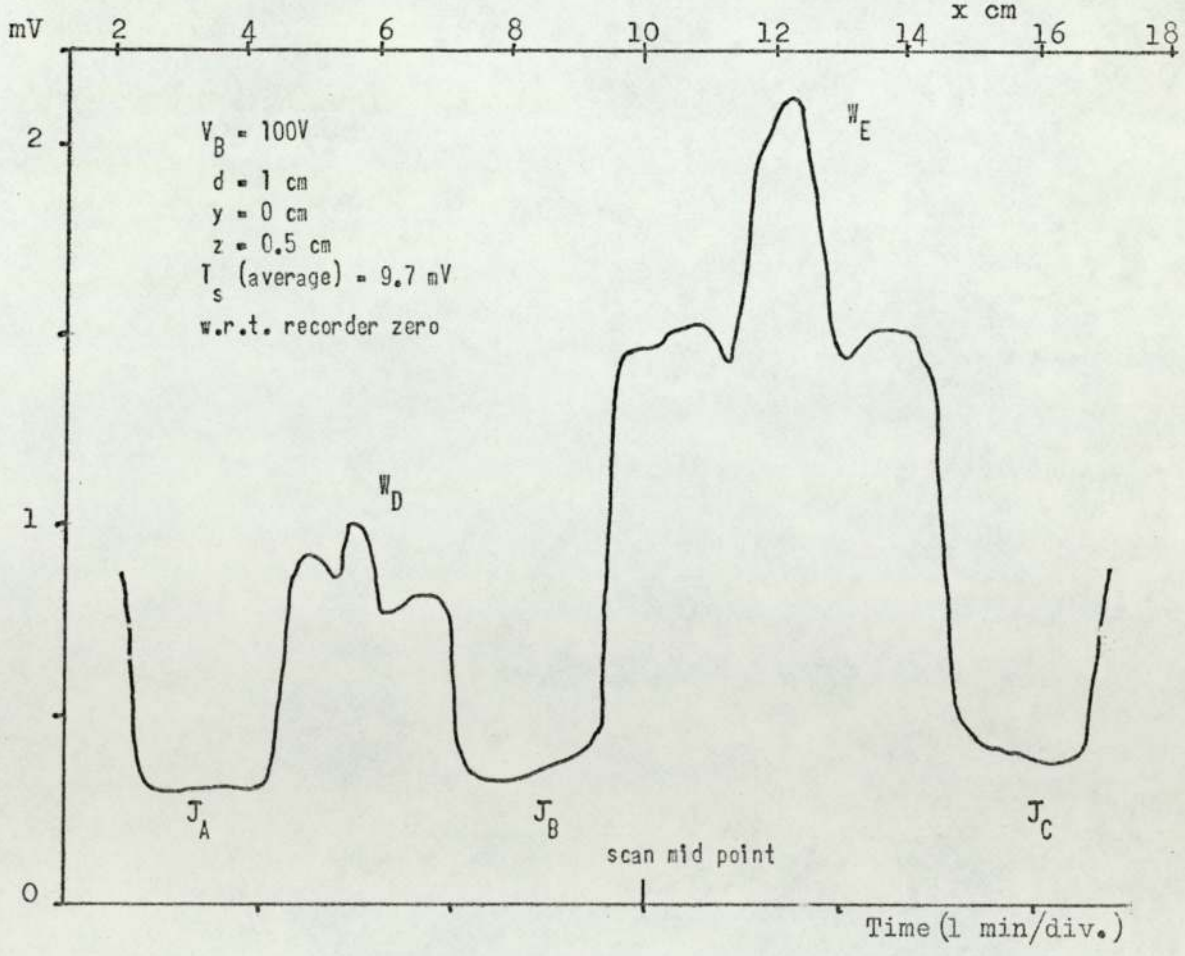

Fig. 73. Horizontal temperature scan 1

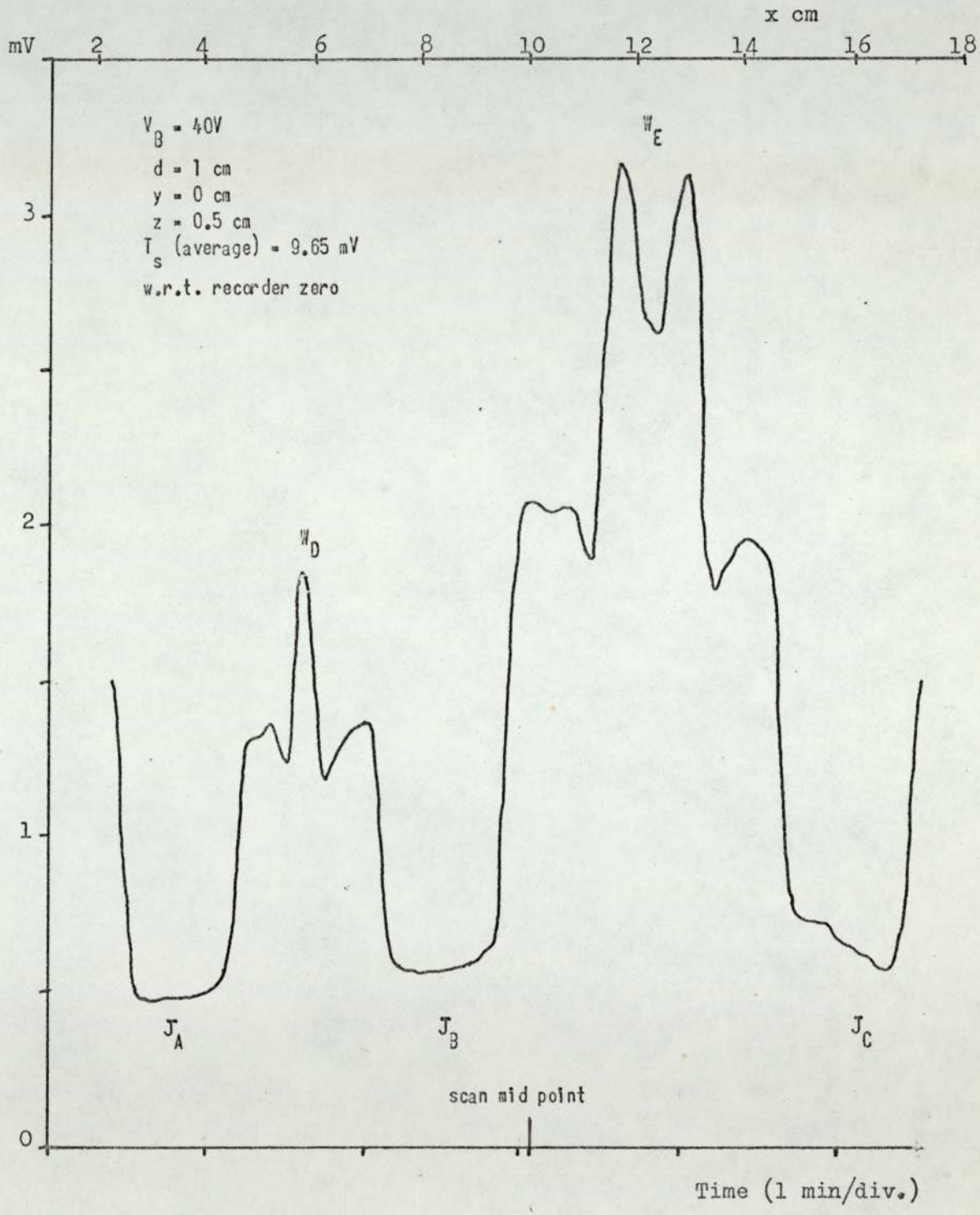

Fig. 75. Horizontal temperature scan 12

of U less than unity[44], as well as with the degree of turbulence in the flow. Although the wall jet impingement zone is not very well defined (see horizontal velocity scans) it can be seen that the flow velocity increases as the line of symmetry between the constituent-free jets is approached and at the same time the flow will be changing direction*. This increase in velocity (mean and turbulent) will manifest itself as an increase in convective heat transfer coefficient.

Consider now the 40 V scan for which this dip is most pronounced. If it is assumed that radiative heat transfer is significant compared to convective heat transfer in those regions away from the line of symmetry in the impingement zone then the actual thermo-couple temperature will be higher than the temperature of the gas flowing over it. As this line of symmetry is approached the temperature of the thermo-couple will decrease due to the increase in convective heat transfer coefficient (note the air temperature is less than the thermo-couple temperature). For the 70 V scan the convective heat transfer coefficient will be greater in those regions away from the impingement zone, therefore radiation effects will not be as significant as for the 40 V scan and an increase in the convective heat transfer coefficient for the 70 V scan will not show as pronounced a dip in the WIS jet.

For the 100 V scans the dip has completely disappeared implying that the convective heat transfer coefficient is very much higher than the radiative heat transfer coefficient for regions on and away from the line of symmetry in the impingement zone.

---

* Note in some cases it is seen from the horizontal scans that there is a slight displacement of turbulent and mean velocity maxima in the WIS jets. This is probably due to the differential time constants associated with the mean velocity and turbulent mean square velocity devices.

There is no evidence of the dip in the middle of the small WIS jet. This is probably due to the fact that there is less variation in convective heat transfer coefficient between those regions in and away from the impingement zone. Also the velocity of the small WIS jet is a little higher than the corresponding large WIS jet.

A further examination of scans 1, 7 and 12 will reveal a reducing sensitivity with increasing free jet velocity (expressed in terms of V_B). The reason for this is twofold.

(1) If the convective heat transfer coefficient, h_c, were independent of velocity then the air temperature would vary inversely with velocity. However, h_c does vary with velocity in the opposite sense to the above but at a lower rate thus the net effect will be that the air temperature will increase with decreasing velocity.

(2) The radiative heat transfer coefficient will be more significant for the lower free jet velocities than the higher ones. Thus since the air temperatures will, in general, be less than the thermo-couple temperatures for these unheated free jets the thermo-couple temperatures will increase with decreasing V_B.

An examination of the unheated free jet temperatures will indicate that for the lowest velocity (V_B = 40 V) these free jets have temperatures higher than those of the 70 V and 100 V ones. Experiments to assess the significance of adiabatic cooling of the free jets as they emerged from their respective orifice showed that no such cooling existed. This increased free jet temperature for V_B = 40 V must be due to one or both of the following: (a) interaction of the WIS jets with the orifice plate, (b) radiation from S increasing the temperatures of both the orifice plate and free jet thermo-couples.

The magnitude of these effects should diminish with increasing z. An inspection of the free jet temperatures corresponding to d = 2.5 cm and d = 4 cm with respective z values of 2 cm and 3.5 cm (see Figs. 76 to 81) show that the free jet temperatures

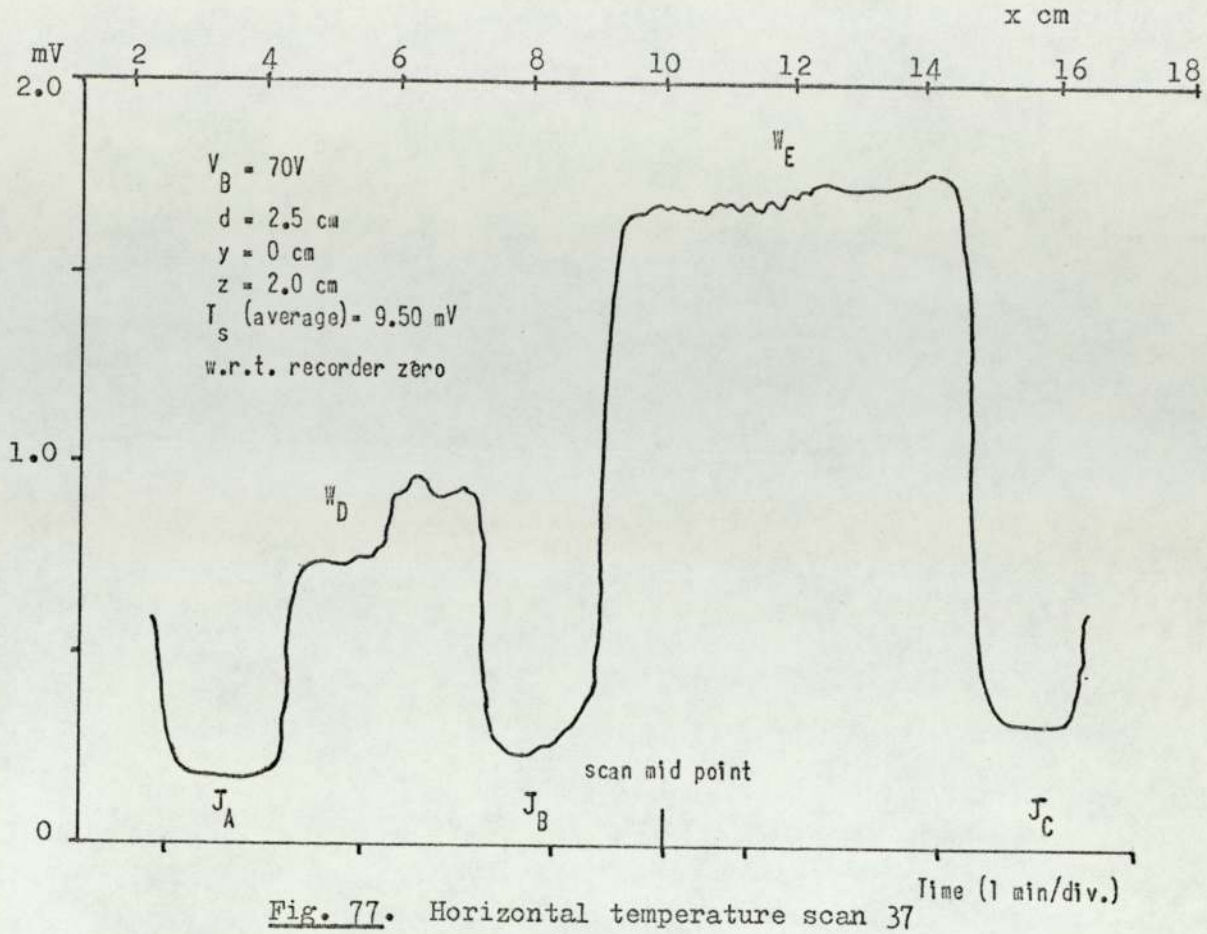

Fig. 77. Horizontal temperature scan 37

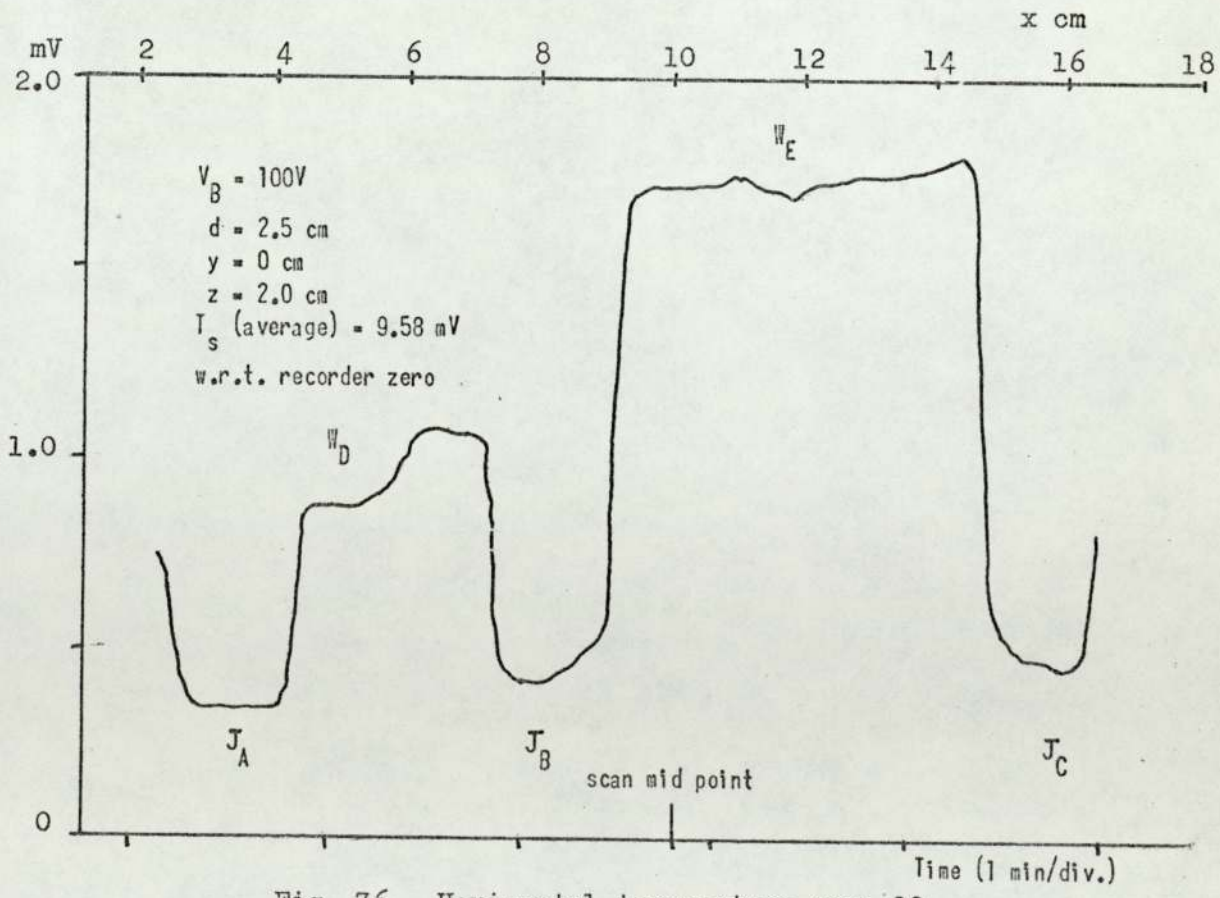

Fig. 76. Horizontal temperature scan 32

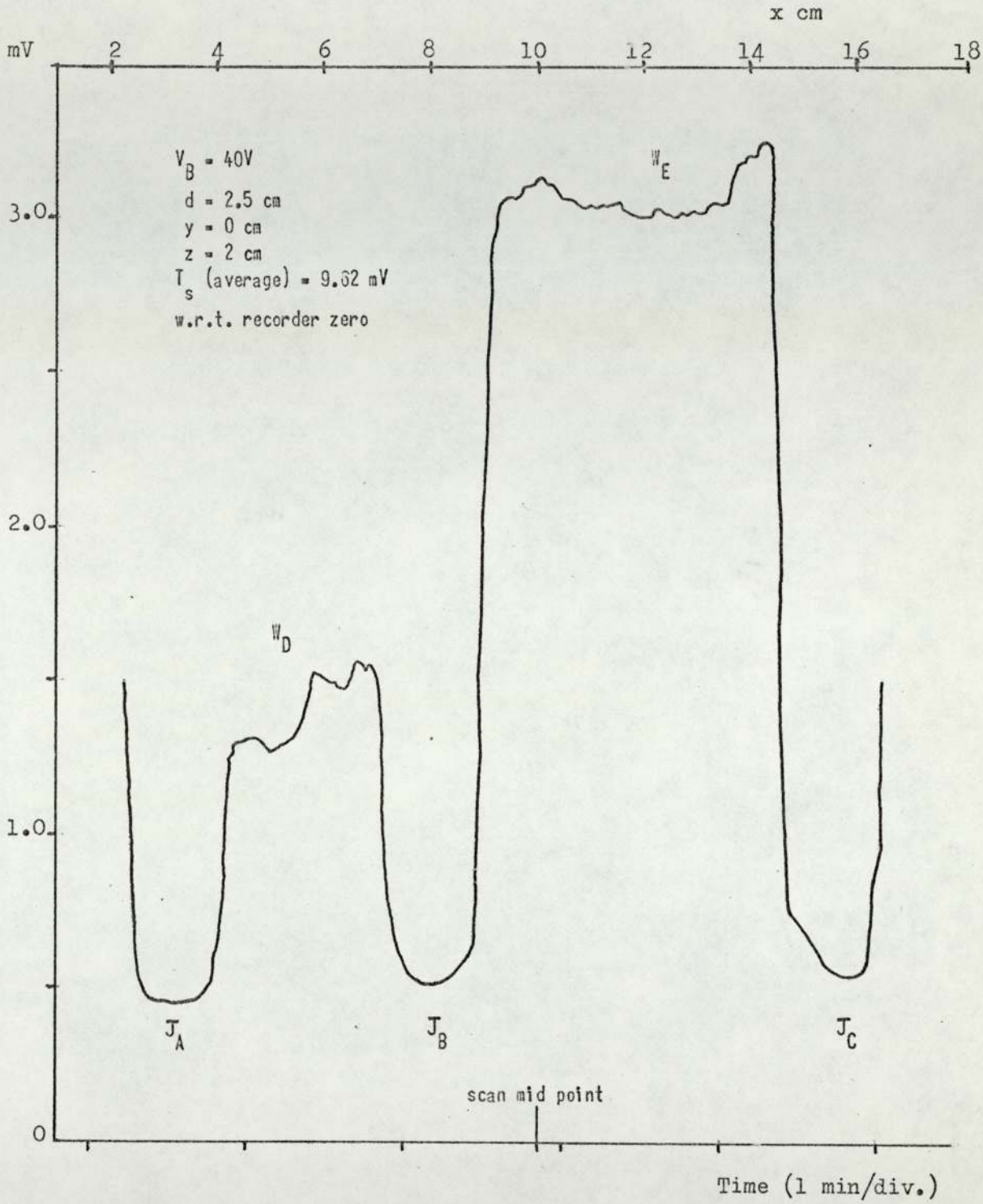

Fig. 78. Horizontal temperature scan 42

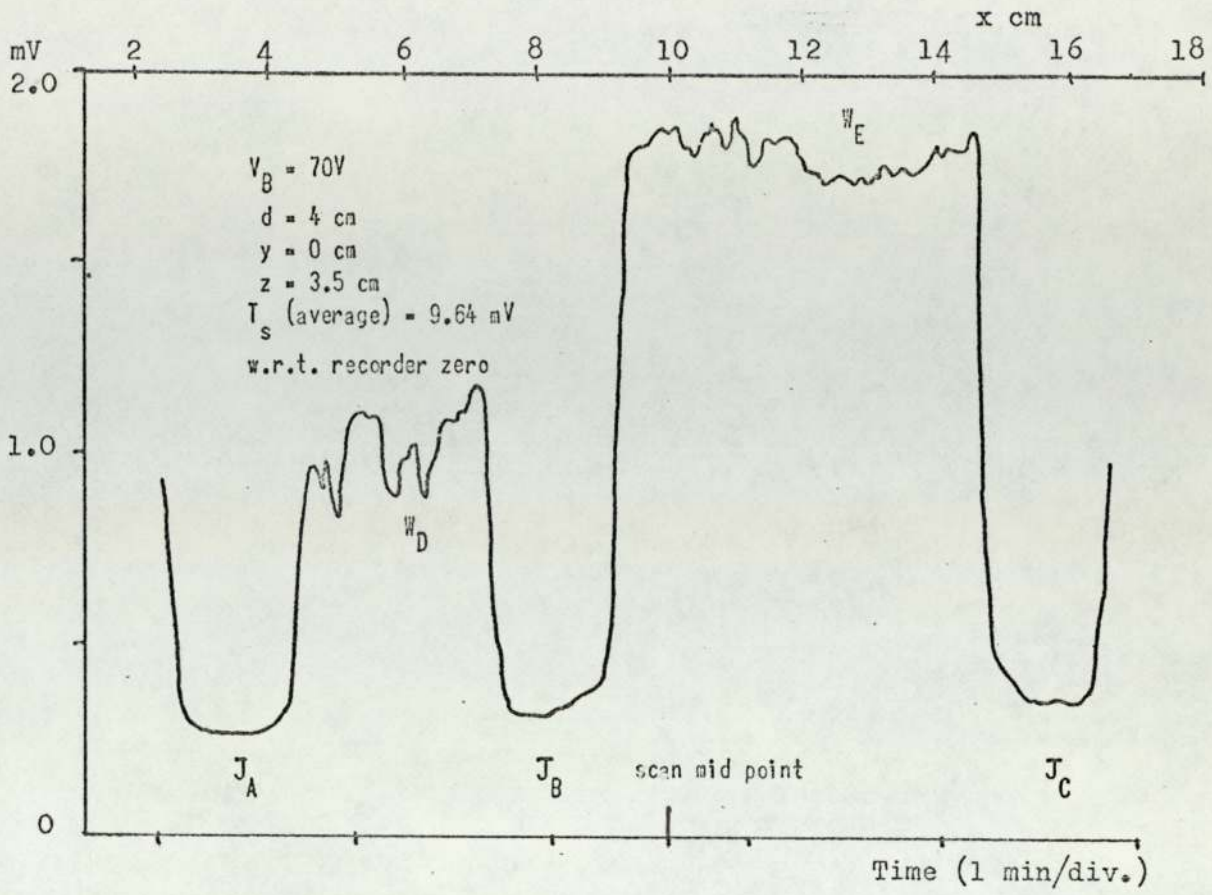

Fig. 80. Horizontal temperature scan 67

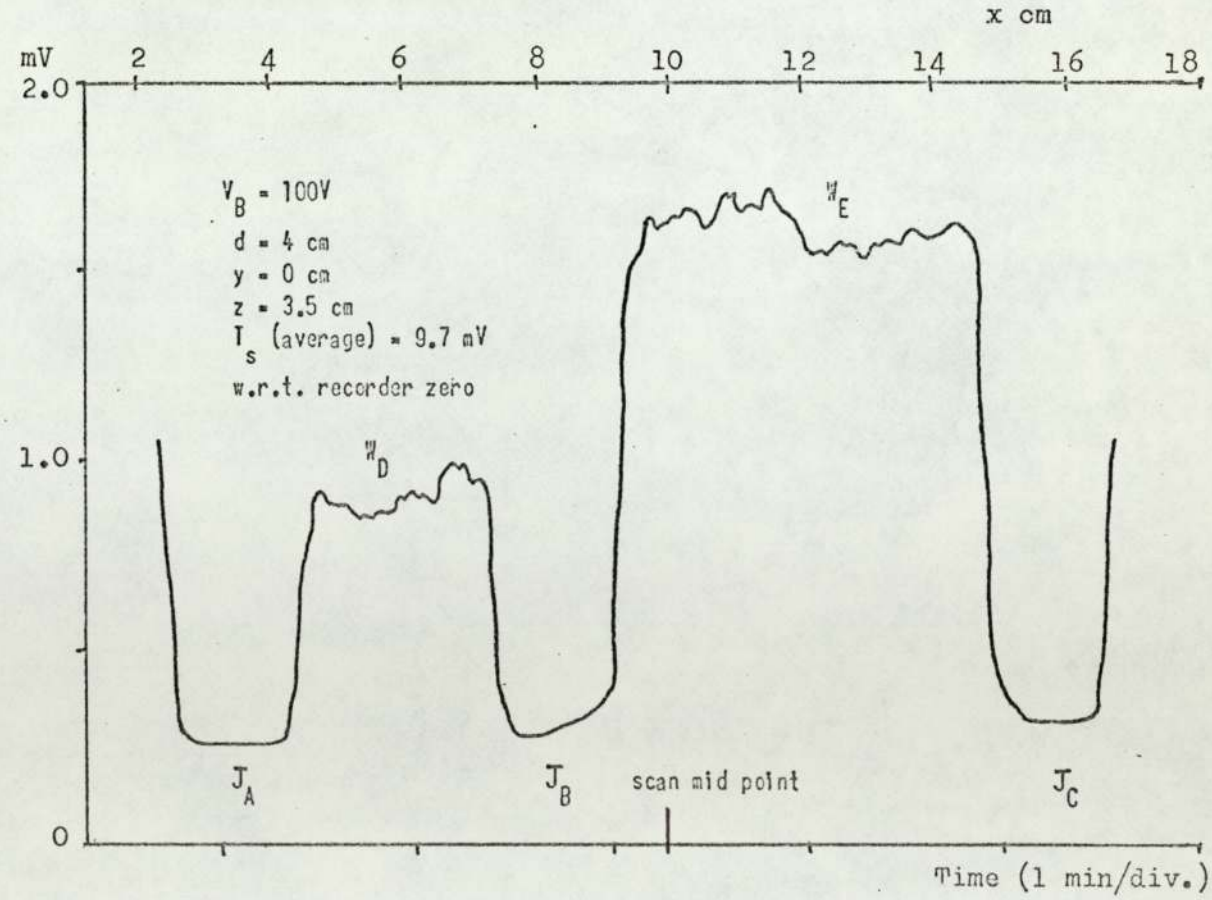

Fig. 79. Horizontal temperature scan 62

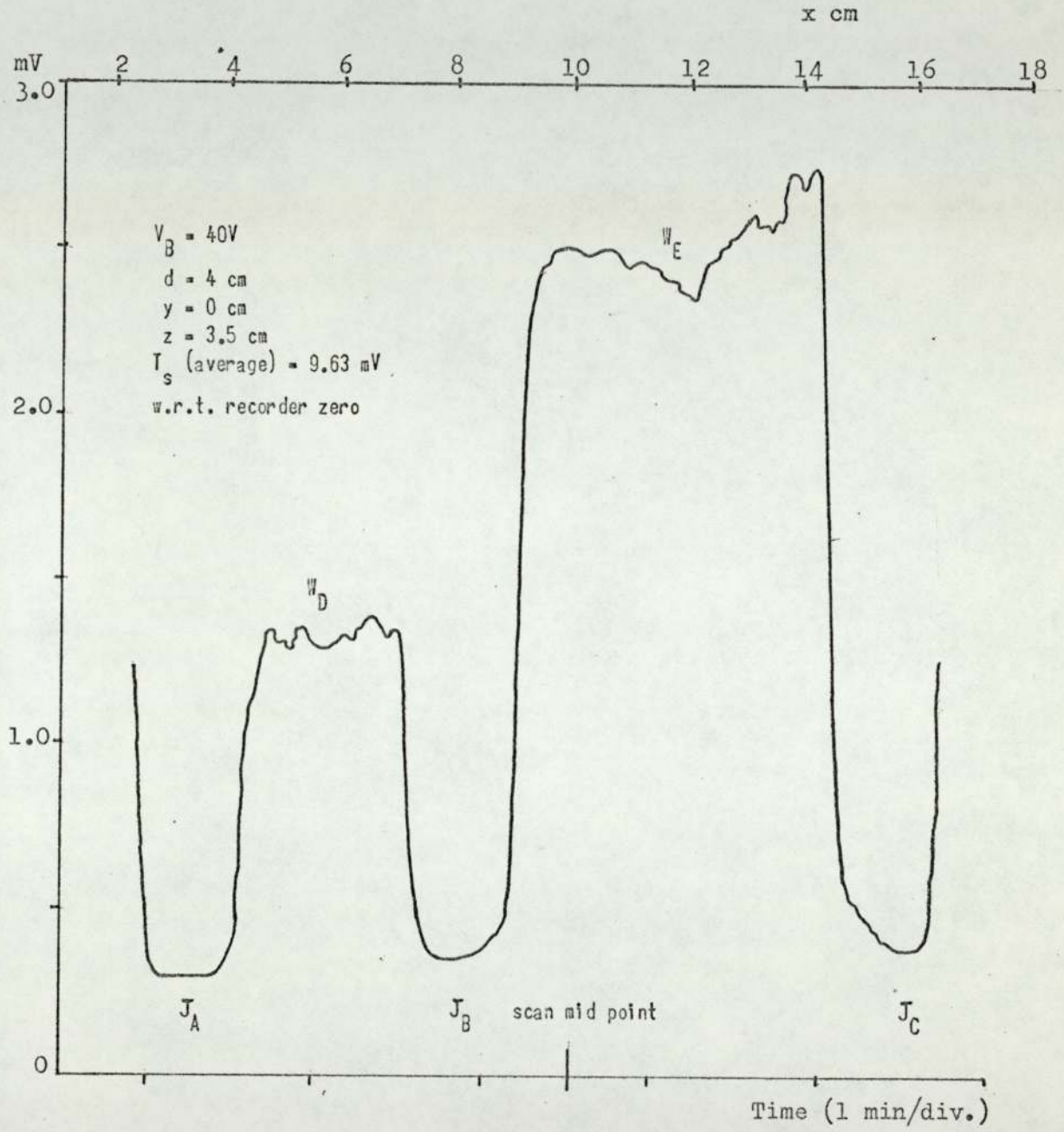

Fig. 81. Horizontal temperature scan 72

do in fact decrease with z when V_B = 40 V and V_B = 100 V.

However, the trend is not the same for V_B = 70 V and the minimum indicated free jet temperature corresponds to a value of z = 2 cm with d = 2.5 cm and not z = 3.5 cm with d = 4 cm as might be expected. It can be seen that there are 4 competing effects, the relative significance of which are not known.

(1) Radiative heat transfer to the free jet thermo-couples.

(2) Convective heat transfer from the free jets to their thermo-couples.

(3) Radiative heat transfer to the orifice plate.

(4) WIS jet convective heat transfer to the orifice plate.

The effect of (3) and (4) would be to pre-heat the free jet air since it must pass over the orifice plate before emerging.

An examination of scans 32, 37 and 42 in Figs. 76, 77 and 78 with V_B = 100 V, 70 V and 40 V respectively and d = 2.5 cm shows that the well defined WIS jet peaks have disappeared and given way to a flatter temperature profile extending throughout the regions between the free jets. Note a significant temperature differential still exists between the small and large WIS jets. The variation in temperature across the region correspondong to the large WIS jets is very small. This disappearance of the WIS jet peak is probably a result of efficient mixing due to high turbulence in the WIS jet and its surrounds. The same effect is observed in scans 62, 67 and 72 (see Figs.79, 80, 81) with respective V_B values of 100 V, 70 V, and 40 V but with d = 4 cm. In this latter case, however, temperature turbulence is somewhat higher.

It has been indicated that the temperature of the thermo-couple bead is a function of both radiative and convective heat transfer

coefficients. This latter, it has been seen, increases with flow velocity, as well as the degree of turbulence. Now both of these vary with z and thus so also will the convective heat transfer coefficient. It is possible, therefore, that the highest value of thermo-couple temperature need not necessarily correspond to the smallest value of z. Since the convective heat transfer coefficient is generally lower for the VB = 40 V scans the significance of radiative heat transfer for these low velocities will be most pronounced.

An inspection of the scans 12 and 42 in Figs. 75 and 78 with V_B = 40 V shows that the average thermo-couple temperature between J_B and J_C (including the large WIS jet) is considerably higher for the d = 2.5 cm scan than for the d = 1 cm scan although the maximum, WIS jet, temperatures differ very little. This may be due to a fall off with z of average convective heat transfer coefficient resulting in an enhanced radiation significance for the larger value of z. The average temperature of the thermo-couple between J_B and J_C decreases as d increases further. This is probably due to the fact that the significance of entrainment cooling increases with d resulting in a reduced WIS jet temperature and hence thermo-couple temperature.

Apart from acquiring a flatter temperature profile the average temperature in the small WIS jet (i.e. between J_A and J_B) for V_B = 40 V varies little with d (and hence z). (See scans in the z direction later.) This may be due to the fact that the average turbulence intensity and mean velocity are a little higher between J_A and J_B than between J_B and J_C, thus the significance of radiation for a given d and z will be slightly lower for the former case than the latter. As d (and hence z) increases the relative average radiative contribution will probably increase. There is, of course,

an opposing mechanism resulting from entrainment cooling which could conceivably balance this radiation effect.

An examination of scans 7, 37 and 67 with V_B = 70 V and scans 1, 32 and 62 with V_B = 100 V (in Figs. 74, 77 and 80) show similar variations with d as the 40 V scans with the suppression of the well defined peaks for values of d > 1 cm. The radiative contribution will of course be less significant with these higher velocities, particularly, for the V_B = 100 V scans. This is partly reflected in the overall reduced levels in these higher velocity scans.

The Temperature Gradients in the WIS Jets

It is clear that in order to successfully exploit any of the above characteristics in temperature measurement, certain criteria must be met. An examination of scans for which d = 1 cm (z = 0.5 cm) indicate very large temperature gradients in the vicinity of the peaks. This would make thermo-couple location very critical. For this reason therefore, it would be appropriate when exploiting these characteristics in temperature measurement to employ values of d greater than about 2 cm.

On the other hand, for values of d approaching 4 cm a certain amount of temperature turbulence appears. This latter may be removed with an appropriate smoothing circuit at the expense of response time.

VERTICAL SCANS

Introduction

These scans were performed in the vertical plane, i.e. the plane normal to the horizontal plane and parallel to the free jet axes. Regions with small values of temperature gradient in the x direction, were desirable for the WIS jet thermo-couple locations.

It was found from the set of exploratory horizontal scans that x locations of 11.4 cm and 5.6 cm represented regions of low temperature gradient in the large and small WIS jets respectively. Unfortunately exceptions to these low temperature gradient x locations were found for scans with d = 1 cm for which the WIS jet peaks were relatively narrow.

For a given value of d and V_B three pairs of scans are presented in the vertical scan diagrams. The left-hand scans correspond to the small WIS jet and the right-hand scans to the large WIS jet. Three scans with progressively higher free jet temperatures are indicated for each WIS jet, the scans at the foot of the page corresponding to 'unheated' free jets and those at the top the highest free jet temperatures (≙ surface temp.) Those in the middle had free jet temperatures lying between these two extremes. In a later section a number of temperature dependent parameters will be generated the data for which will be drawn from the vertical scans (a few examples of which will be shown in this section).

Relationships between these parameters and surface temperature will be derived and it will be appropriate, in these cases, to distinguish between the surface temperature corresponding to scans in the small WIS jet and that corresponding to scans in the large WIS jet. To be consistent, therefore, with the nomenclature to be used in these later sections the following definitions of surface temperature will be adopted in this section*:-

P_S = time mean surface temperature corresponding to vertical scans in the small WIS jet.

---

* Certain other definitions of surface temperature will emerge in the later sections but it would be inappropriate to introduce them at this stage.

P_L = time mean surface temperature corresponding to vertical scans in the large WIS jet.

These new definitions will replace 'T_s' used in the horizontal scans.

Each scan was performed in an upward direction, from y = 0 cm to y = 10 cm and a downward direction, from y = 10 cm to y = 0 cm, giving a scan range of 10 cm in each direction. This range is defined by the vertical broken lines. The scan speed was 2 mm per sec. so the time to perform a unidirectional scan was 50 sec.

Consider first the scans for which d = 1.1 cm shown in Figs. 82, 83 and 84 with respective V_B values of 40, 70, and 100 V.

For the unheated free jets corresponding to scans 954 and 579 for V_B = 40 V, 729 and 354 for V_B = 70 V and 604 and 229 for V_B = 100 V there exists a positive value of temperature gradient $\frac{dT}{dy}$. As was predicted in the theory this 'gradient' is steeper for the small WIS jets. However, for both the small and large WIS jets $\frac{dT}{dy}$ increases with V_B implying that if a temperature dependent parameter based upon $\frac{dT}{dy}$ were exploited V_B = 100 V would be the most sensitive. This is due to the higher temperature differential between the WIS jet and surface at the start of the scan when these higher free jet velocities are used.

As the free jet temperatures are increased, this gradient diminishes as a result of the reduced temperature differential between the surface and the free jets. When the free jet temperature is close to that of the surface then the average value of $\frac{dT}{dy}$ becomes negative. It is seen that an interpolation between the middle and highest free jet temperatures would reveal a $\frac{dT}{dy} = 0$ at a free jet temperature less than the surface temperature, i.e. a 'premature balance' exists, the causes of which have been dealt with in the theory section.

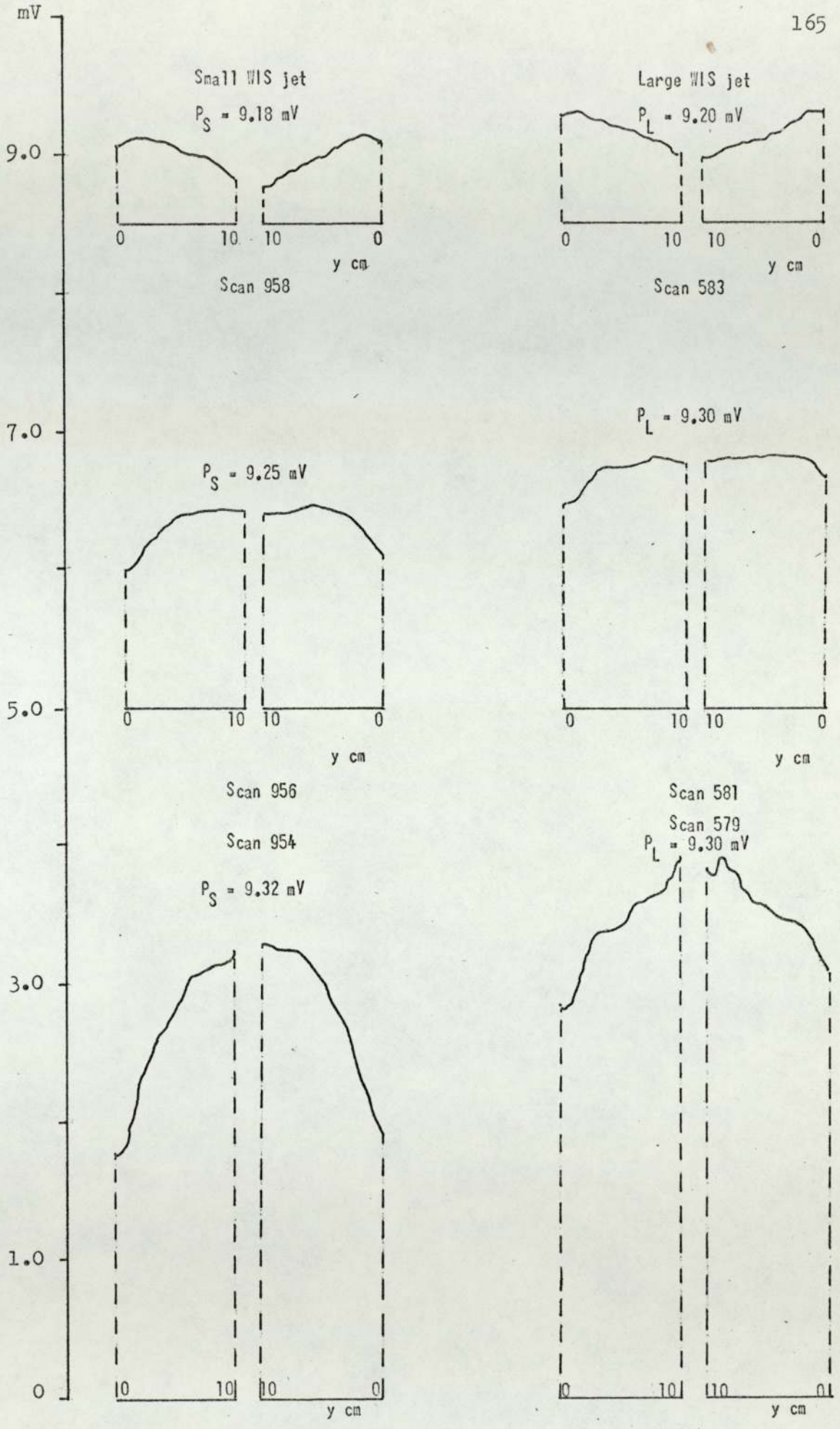

Fig. 82. Vertical temperature scans in WIS jets, d = 1.1 cm, z = 0.5 cm, V_B = 40V

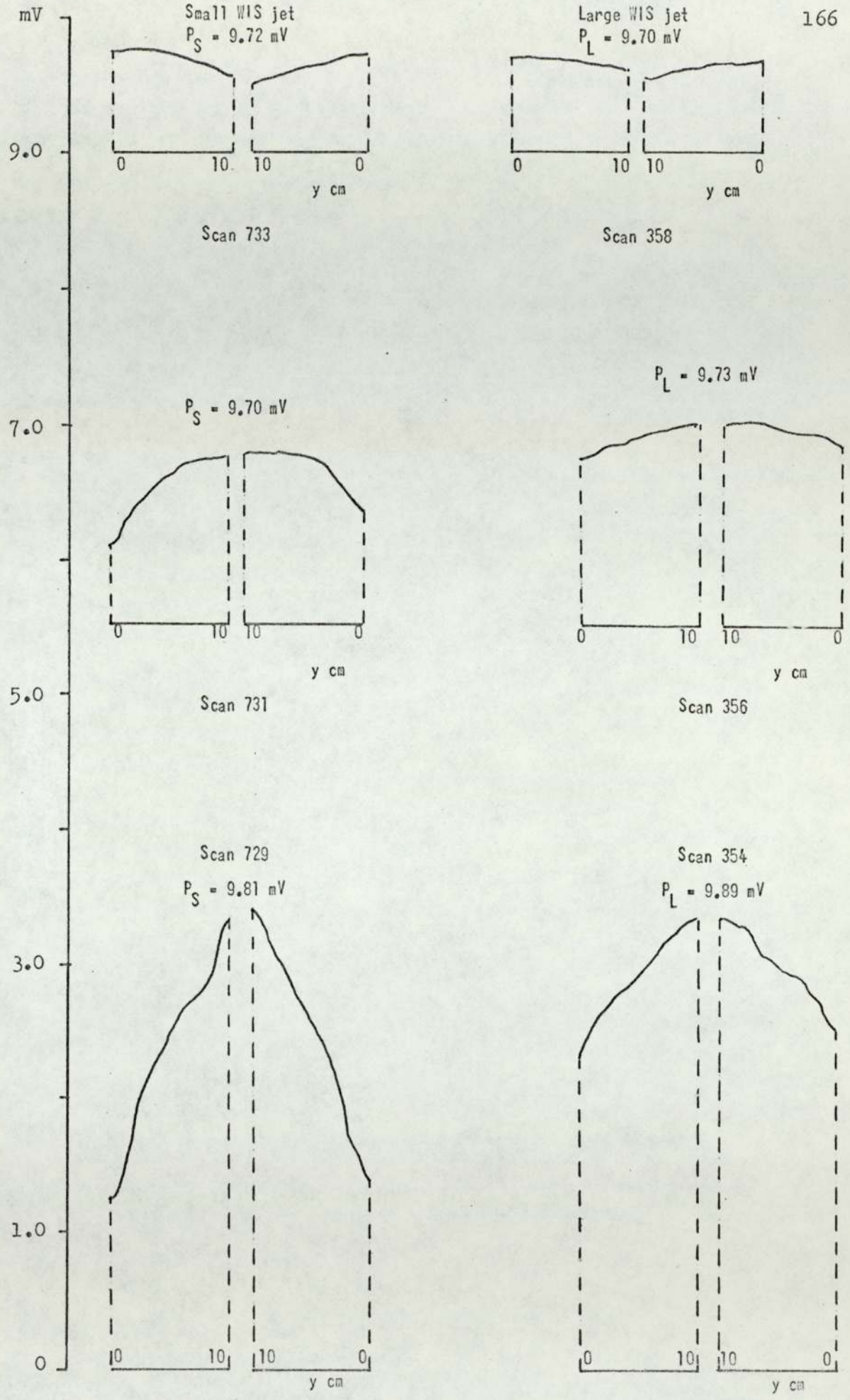

Fig. 83. Vertical temperature scans in WIS jets, d = 1.1 cm, z = 0.5 cm, V_B = 70V

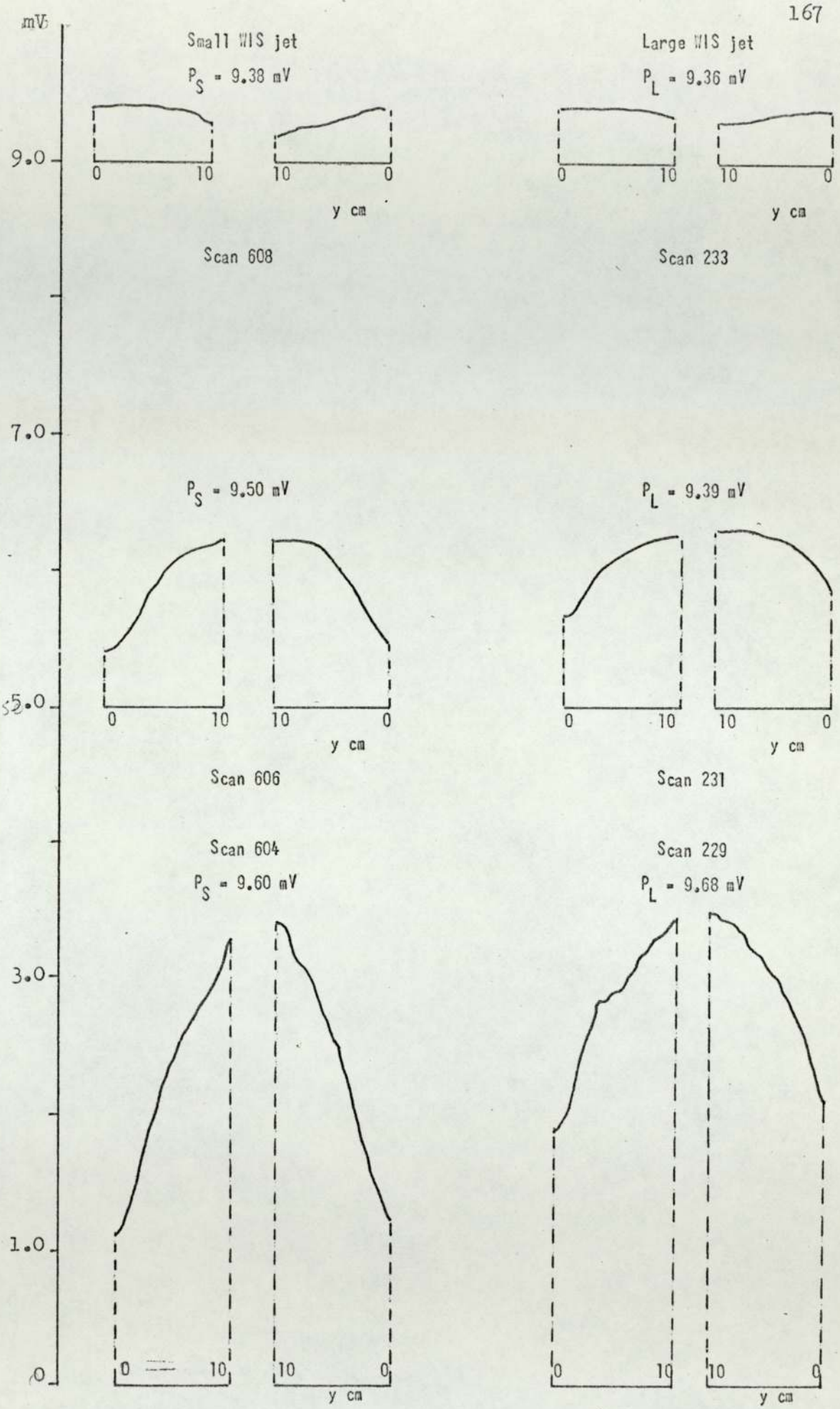

Fig. 84. Vertical temperature scans in WIS jets, d = 1.1 cm, z = 0.5 cm, V_B = 100V

It is interesting to note that the error in balance, i.e. the difference between the free jet temperature when $\frac{dT}{dy} = 0$ and the surface temperature diminishes as V_B increases.

An examination of scans for which d = 2.6 cm in Figs. 85, 86 and 87 shows a similar trend to those for which d = 1.1 cm except that corresponding average values of $\frac{dT}{dy}$ are a little lower and the error in balance greater. In scan 533, however, $\frac{dT}{dy}$ seems unexpectedly high.

The above trends persist for the d = 4.1 cm scans in Figs. 88 to 90 but with corresponding values of $\frac{dT}{dy}$ further reduced and errors in balance larger.

In general for the unheated free jets $\frac{dT}{dy}$ remains positive but decreases with d, with the exception of the large WIS jet (scan 479) with d = 4.1 cm and V_B = 40 V where $\frac{dT}{dy}$ becomes slightly negative.

As the free jet temperatures and d increase the significance of turbulent mixing with cooler air in the immediate environment, increases resulting in the erratic temperature profiles associated with the heated free jets for large values of d. The small WIS jets appear to be more susceptible to turbulent mixing effects. This is probably due to the fact that they have a higher turbulence intensity than the corresponding large WIS jet.

An examination of the large WIS jet scans (404, 454, 529 in Figs. 86, 89 and 85 respectively shows that as y increases from 0 to 10 cm the temperature profile passes through a minimum before it starts to climb. The temperature of the thermo-couple in the WIS jet is a function of a number of competing mechanisms including:

(1) The convective heat transfer coefficient.

(2) The temperature differential between the WIS jet and the surrounding air.

(3) Radiative heat transfer coefficient.

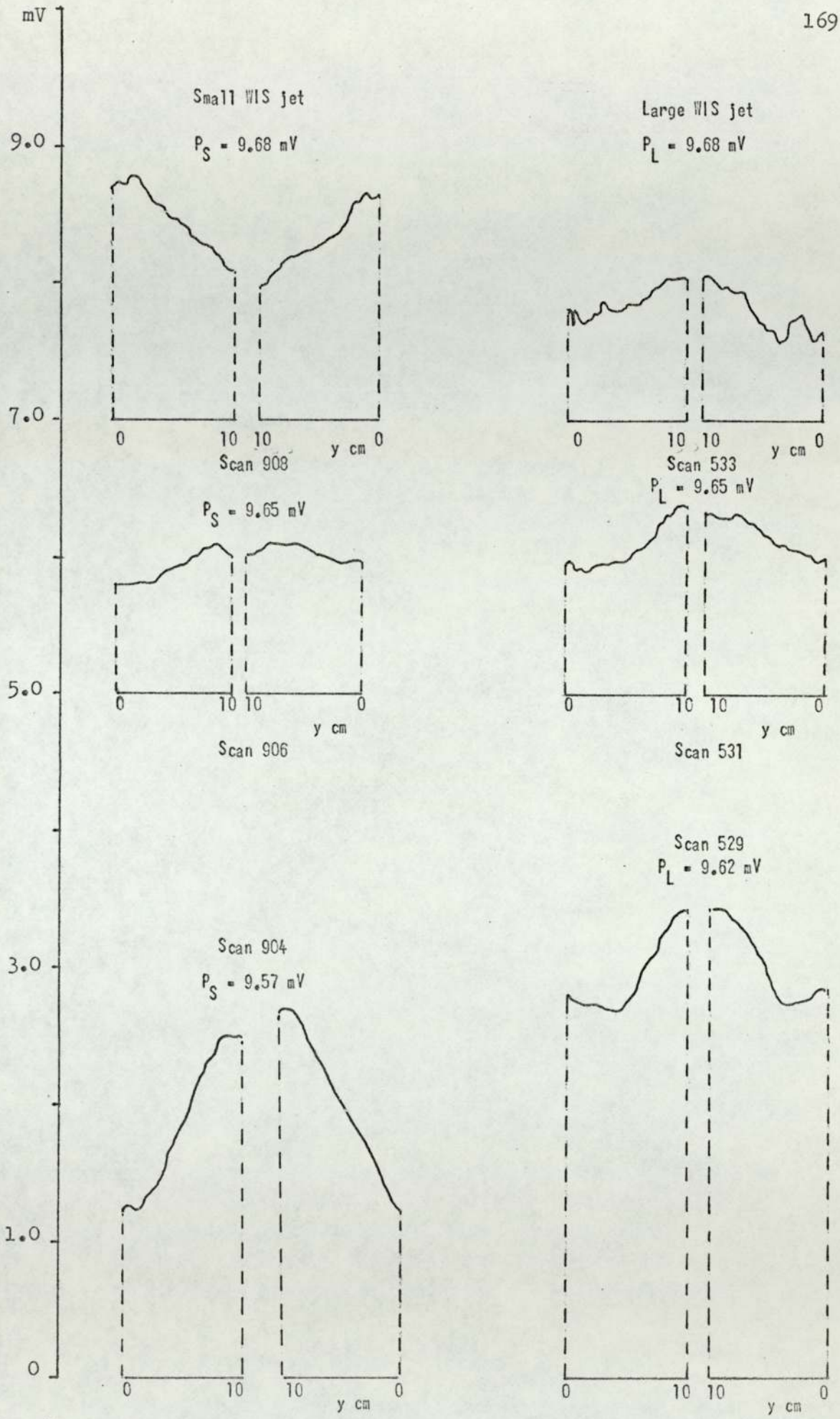

Fig. 85. Vertical temperature scans in WIS jets, d = 2.6 cm, z = 2.0 cm, V_B = 40V

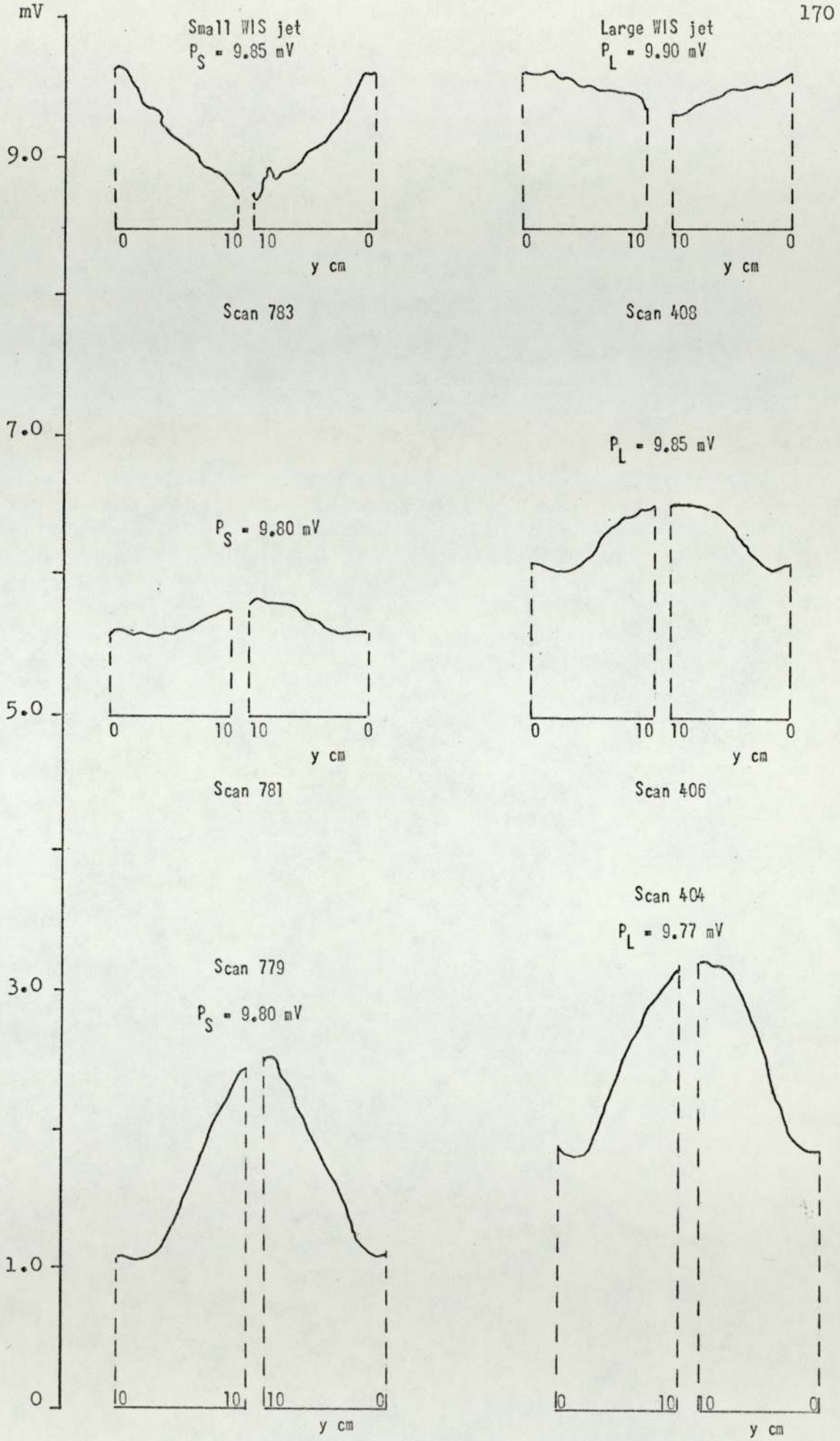

Fig. 86. Vertical temperature scans in WIS jets, d = 2.6 cm, z = 2.0 cm, V_B = 70V

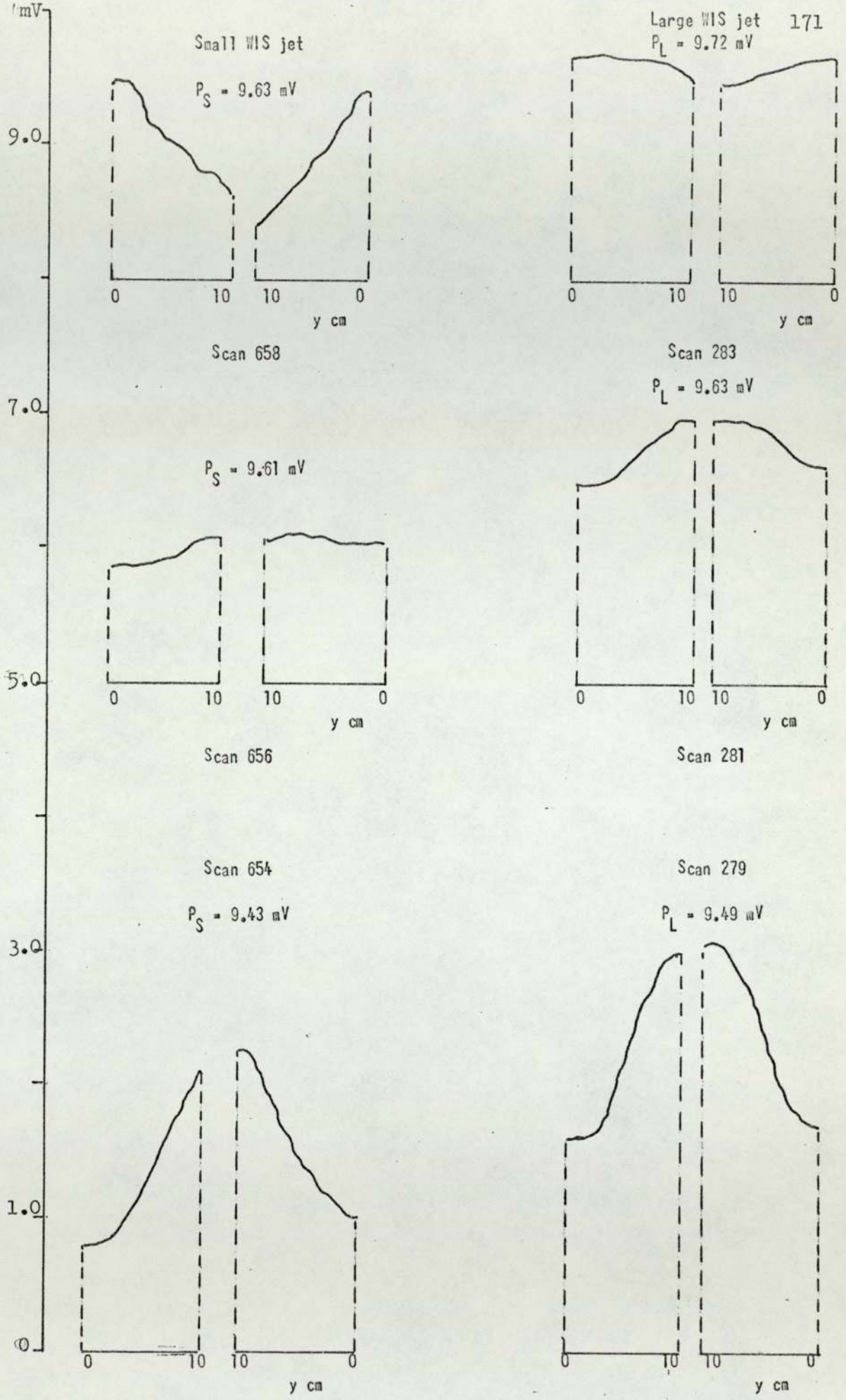

Fig. 87. Vertical temperature scans in WIS jets, d = 2.6 cm, z = 2.0 cm, V_B = 100V

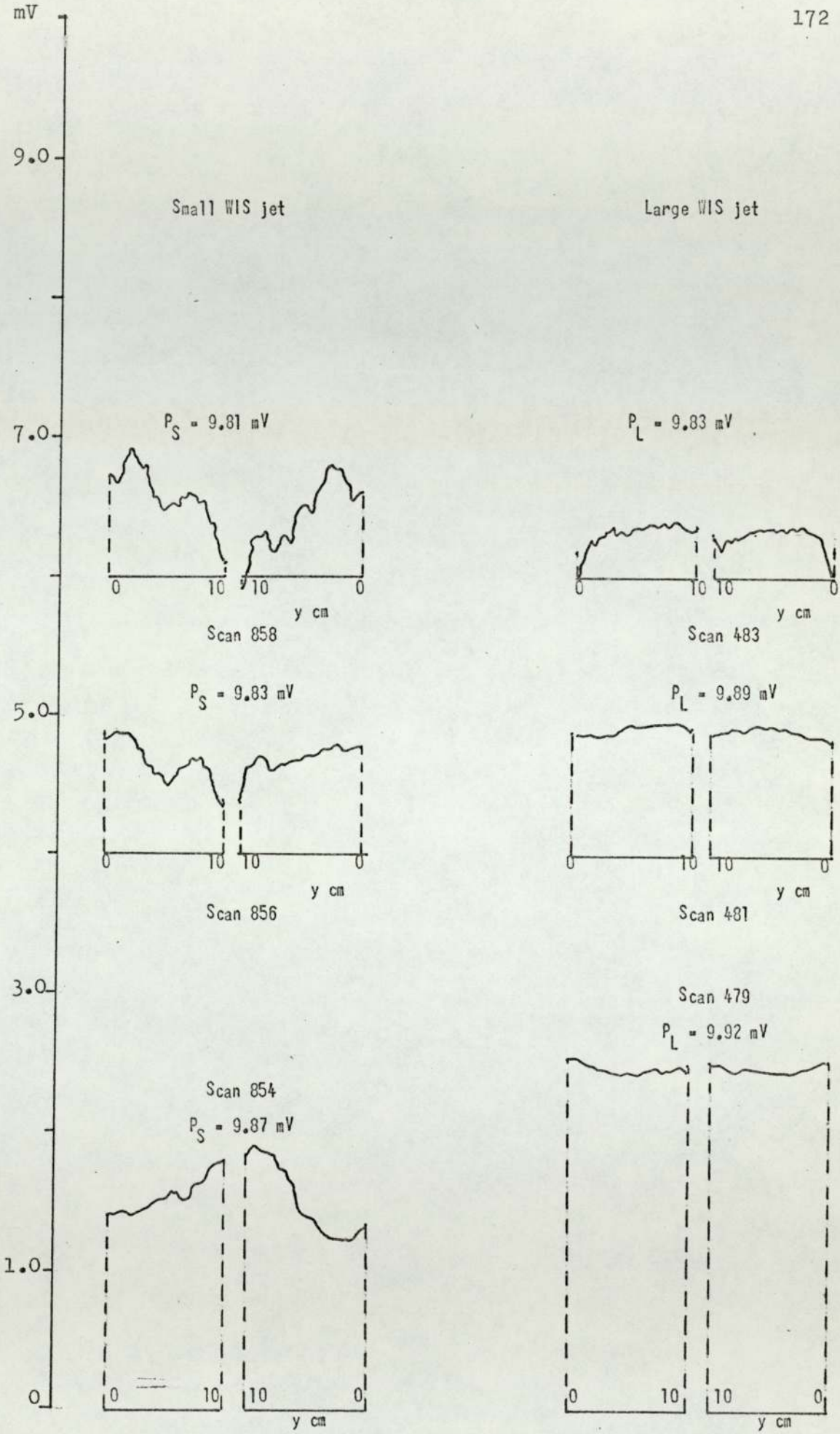

Fig. 88. Vertical temperature scans in WIS jets, d = 4.1 cm, z = 3.5 cm, V_B = 40V

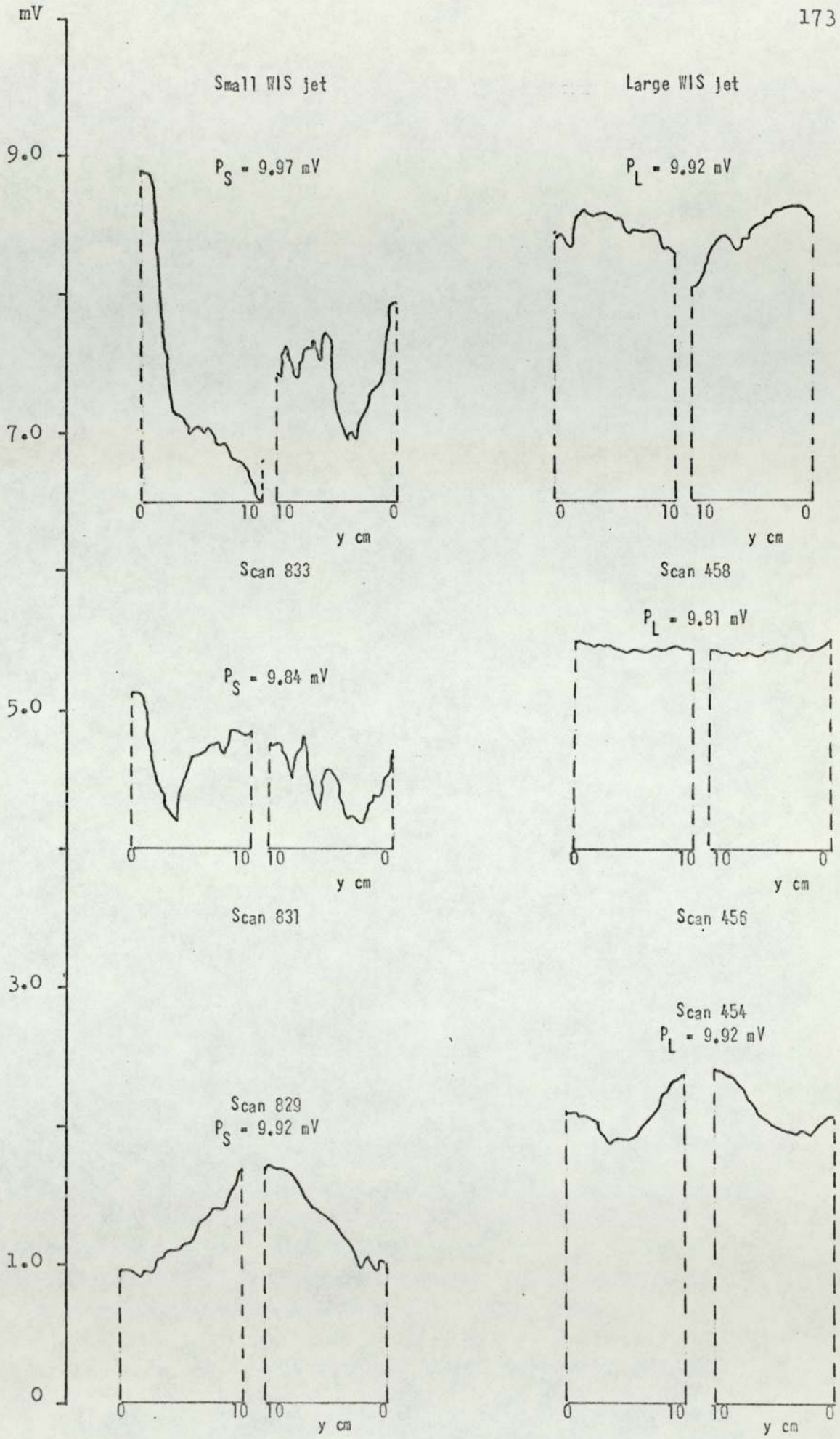

Fig. 89. Vertical temperature scans in WIS jets, d = 4.1 cm, z = 3.5 cm, V_B = 70V

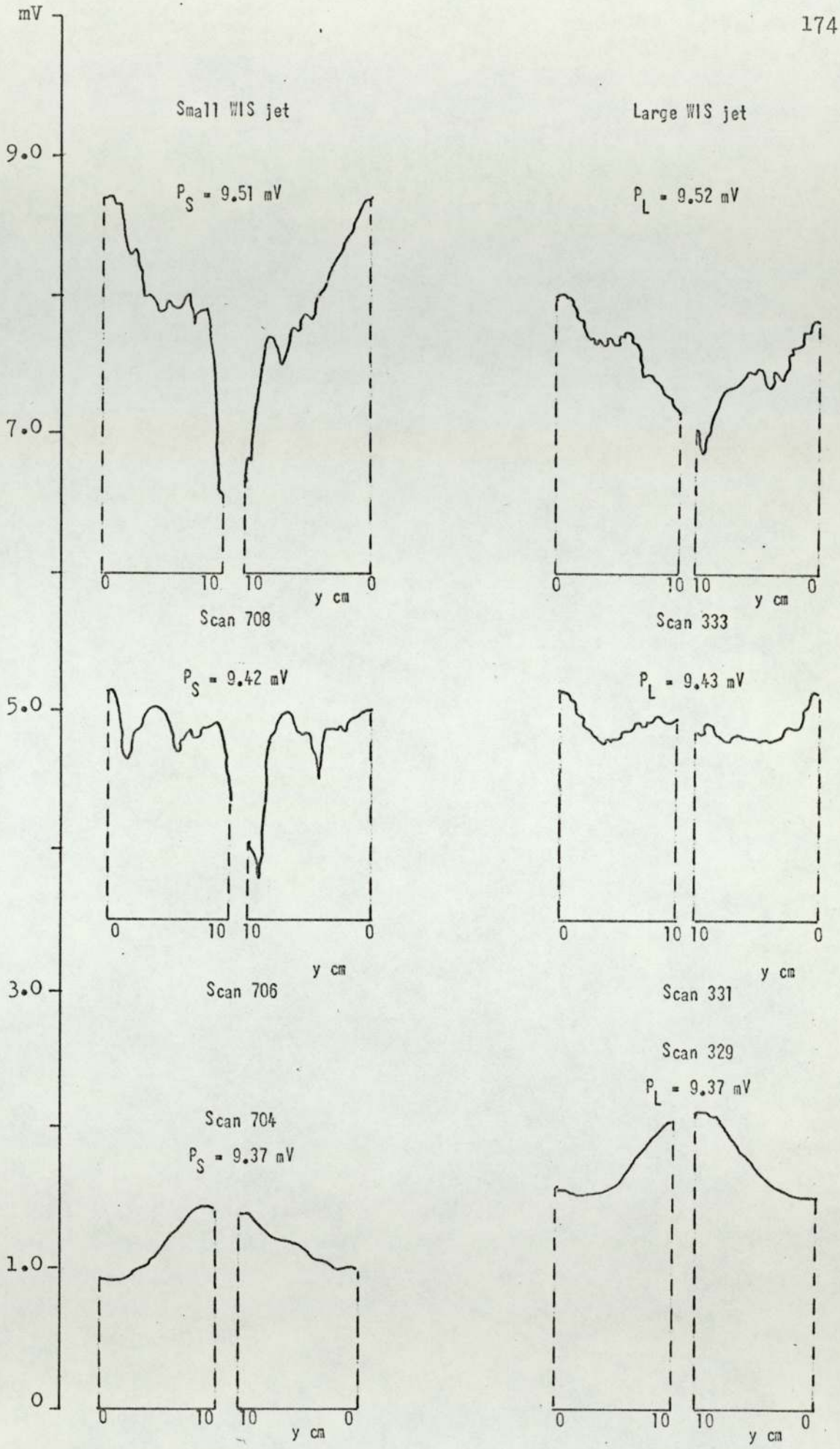

Fig. 90. Vertical temperature scans in WIS jets, d = 4.1 cm, z = 3.5 cm, V_B = 100V

This temperature minimum is most pronounced for the lowest free jet velocity for which any variation in convective heat transfer coefficient is likely to have the greatest effect. As y increases the WIS jet velocity decreases and the jet becomes more susceptible to cooling by turbulent mixing with the surrounding air. At the same time the convective heat transfer coefficient will decrease giving rise to increased radiation effects which will tend to oppose the above turbulent cooling effects. There will of course be heat transfer from the surface to the WIS jet which will augment any radiative heat transfer from the surface. It is conceivable that the relative significance of the above mechanisms will vary in such a way as to give rise to the observed temperature minimum.

Note the small WIS jets seem less vulnerable to this effect as do the large WIS jets for which V_B = 100 V. This may be partly due to the lower overall temperatures associated with the small WIS jets and the large ones, for which V_B = 100 V, which could reduce the significance of entrainment cooling.

SCANS TO SHOW THE VARIATION OF TEMPERATURE WITH z IN THE FREE JETS AND WIS JETS

Introduction

Although these scans were performed for values of d = 4.1 cm, 2.6 cm and 1.6 cm only those for which d = 4.1 cm will be presented here, since for this value the effects of jet cooling due to turbulent mixing with the surrounding air will be most pronounced. Since none of the temperature dependent parameters to be examined in later sections drew data from these z scans the original definition of surface temperature, T_s, will be used throughout this section.

The thermo-couple bead was displaced from z = 5 mm to z = 35 mm giving a range of 30 mm, the scan time being 65 sec. (Scans were performed in both directions, i.e. z = 5 mm → 35 mm and z = 35 mm → 5 mm but only the latter have been presented.)

Heated Free Jets

Figs. 91 and 92 show variations of temperature with z along the axes of the free jets. Note since z is measured from S (the hot surface) z = 5 mm lies on the right-hand end of the abscissa and z = 35 mm on the left-hand end.

It can be seen that the attenuation along the free jets as z decreases (i.e. as S is approached) is highest for scans 15z, 17z and 19z in Fig. 91 for which V_B = 40 V and becomes progressively lower for increasing free jet velocities, the minimum attenuations corresponding to V_B = 100 V, see Fig. 92.

It may also be seen that the centre free jet corresponding to scans 3z (V_B = 100 V) 10z (V_B = 70 V) and 17z (V_B = 40 V) undergoes less attenuation than the corresponding outer free jets. This is due to the fact that they are furthest from the periphery of the orifice plate and also have a lower turbulence intensity than the outer jets. The effect of the above is that the turbulent mixing efficiency is lower and in any event any mixing which does occur will be from regions of generally higher temperature. In contrast the higher turbulence intensity, particularly on the outer edge of the outer free jets together with the cooler air temperatures in these regions, result in higher attenuations of these latter. This turbulence intensity increases as z decreases (for a given d). This is reflected in the increased temperature gradient, $\frac{dT}{dz}$, for small values of z.

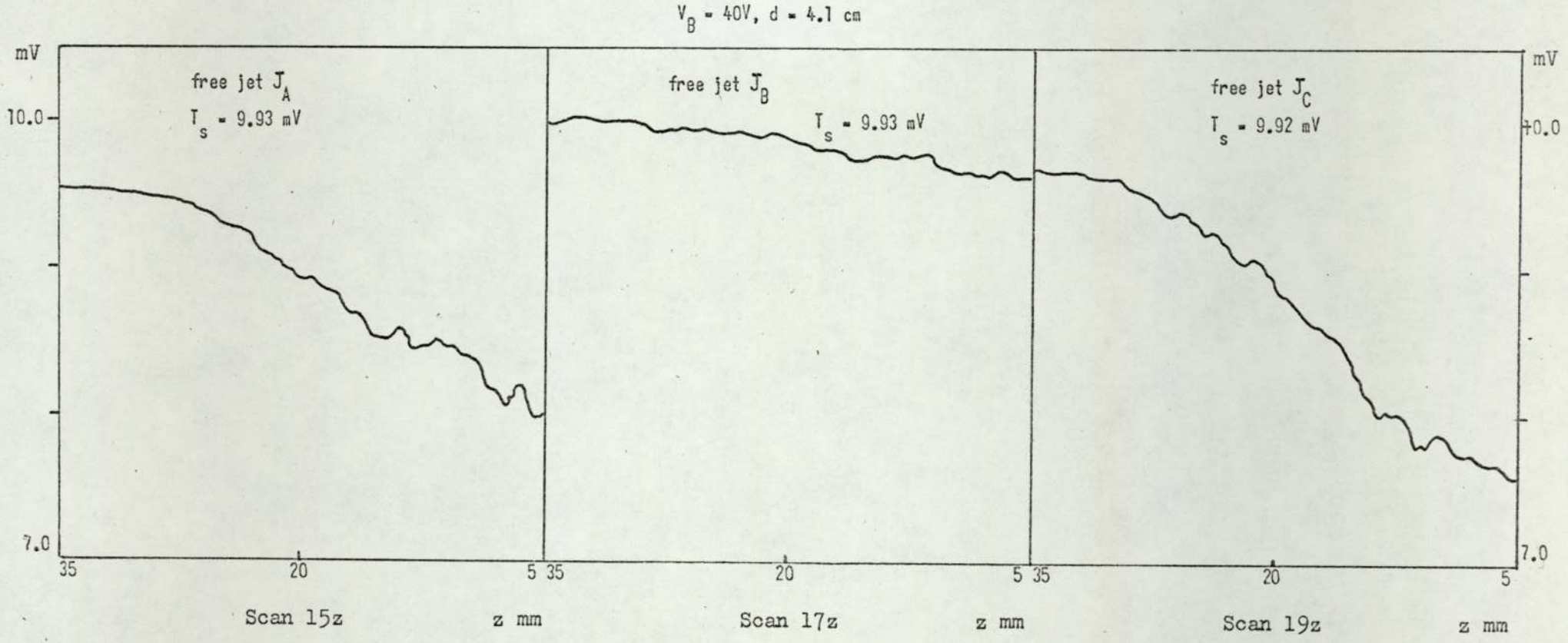

Fig. 91. Heated free jet temperature scans in the z direction

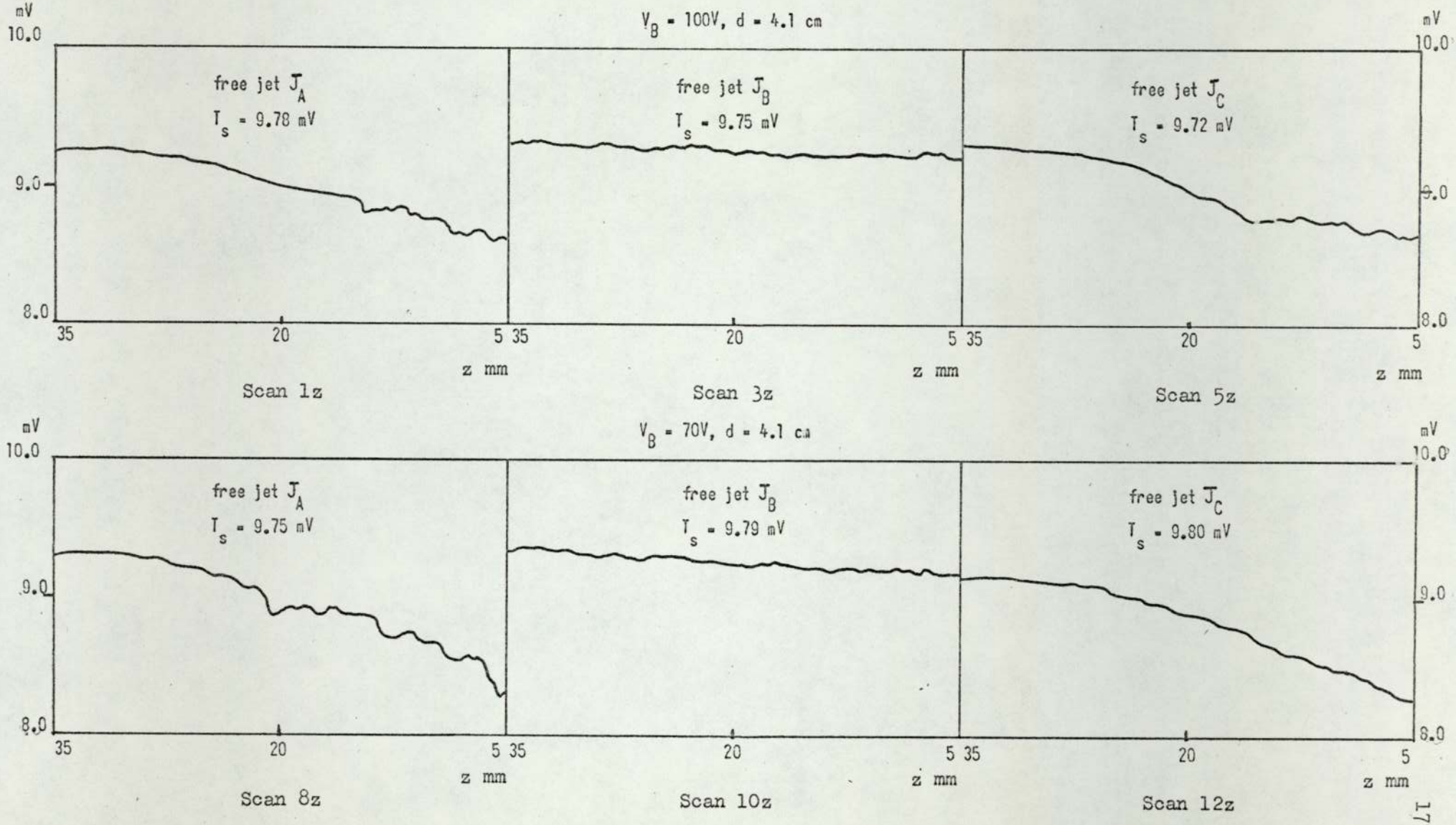

Fig. 92. Heated free jet temperature scans in z direction

WIS Jets (with heated free jets at temperatures close to T_s)

The horizontal, x, locations were the same as those used for the vertical scans. Two values of y were selected one with y=0 cm lying in the horizontal plane and the other with y = 5 cm. As with the free jets, scans were performed in both directions, i.e. z = 5 mm → 35 mm and z = 35 mm → 5 mm but only the latter have been indicated here since they are representative of either direction. Figs. 93 and 94 show the variation of temperature with z in the small WIS jet for the V_B = 100 V, 70 V and 40 V scans and y = 0 cm and 5 cm. In these WIS jet scans the slope of course is in the opposite direction to that of the free jets since the WIS jets originate at S whereas the free jets originate at the orifice plate.

The Small WIS Jet

Scans 2z (V_B = 100 V), 9z (V_B = 70 V) and 16z (V_B = 40 V) in Figs. 93 and 94 for which y = 0 cm show that the attenuation is inversely proportional to V_B. Note, because the WIS jets lie away from the periphery of the orifice plate, although they are characterized by high turbulence intensities because the air in the immediate surrounds is considerably higher than ambient, the cooling of these jets is not as high as may be expected (these surrounds of course include the heated free jets themselves for y = 0 cm).

The general trend appropriate to the y = 0 cm scans also applies to the y = 5 cm scans. In this latter case the jet has become broader, and its turbulence intensity decreased. As a result, although the heated free jets no longer lie in the immediate environment the turbulent mixing efficiency of the WIS jets will be lower. It can be seen that scan 16z (V_B = 40 V, y = 0 cm) undergoes a little more attenuation than scan 21z (V_B = 40 V, y = 5 cm).

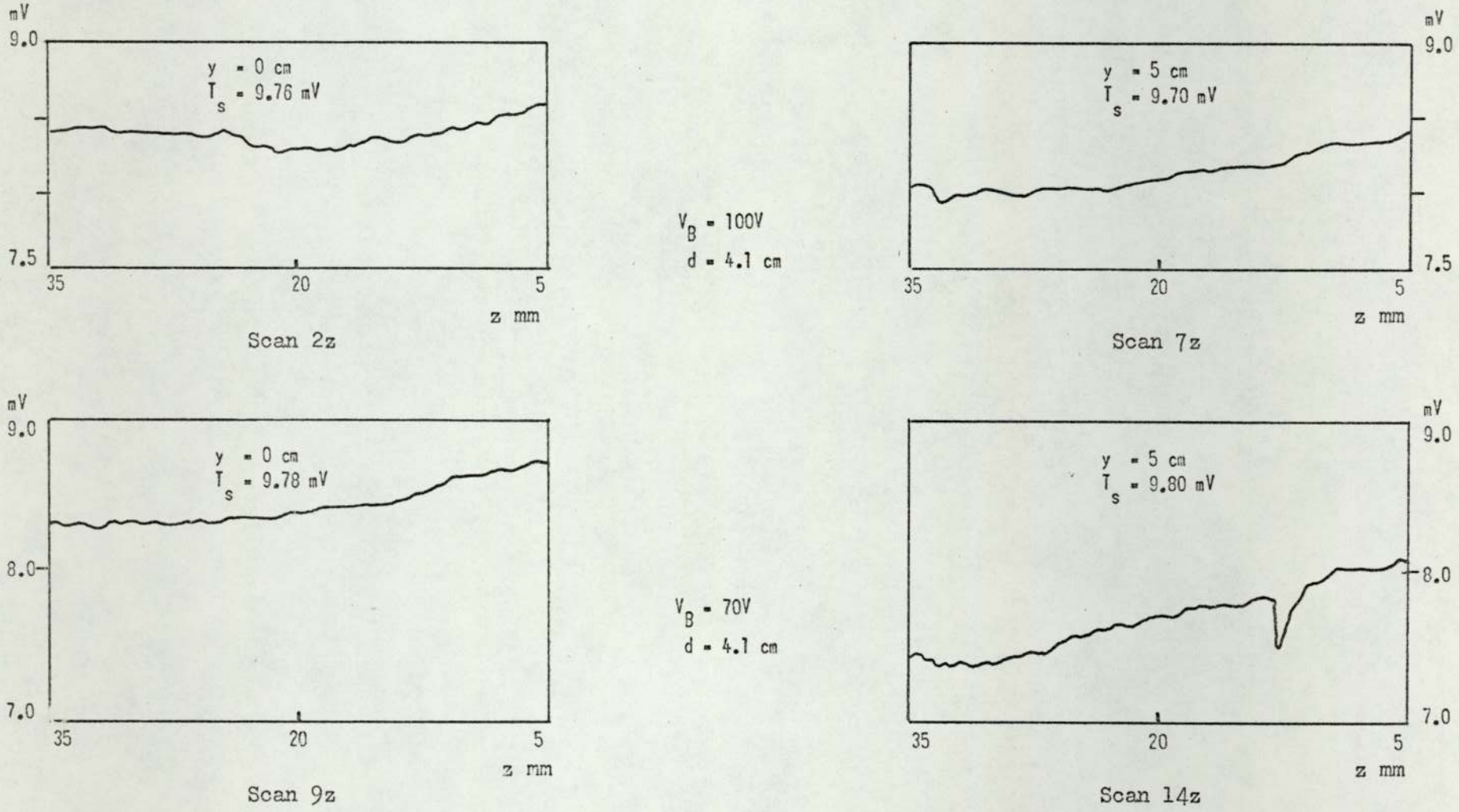

Fig. 93. Small WIS jet temperature scans in the z direction for heated free jets

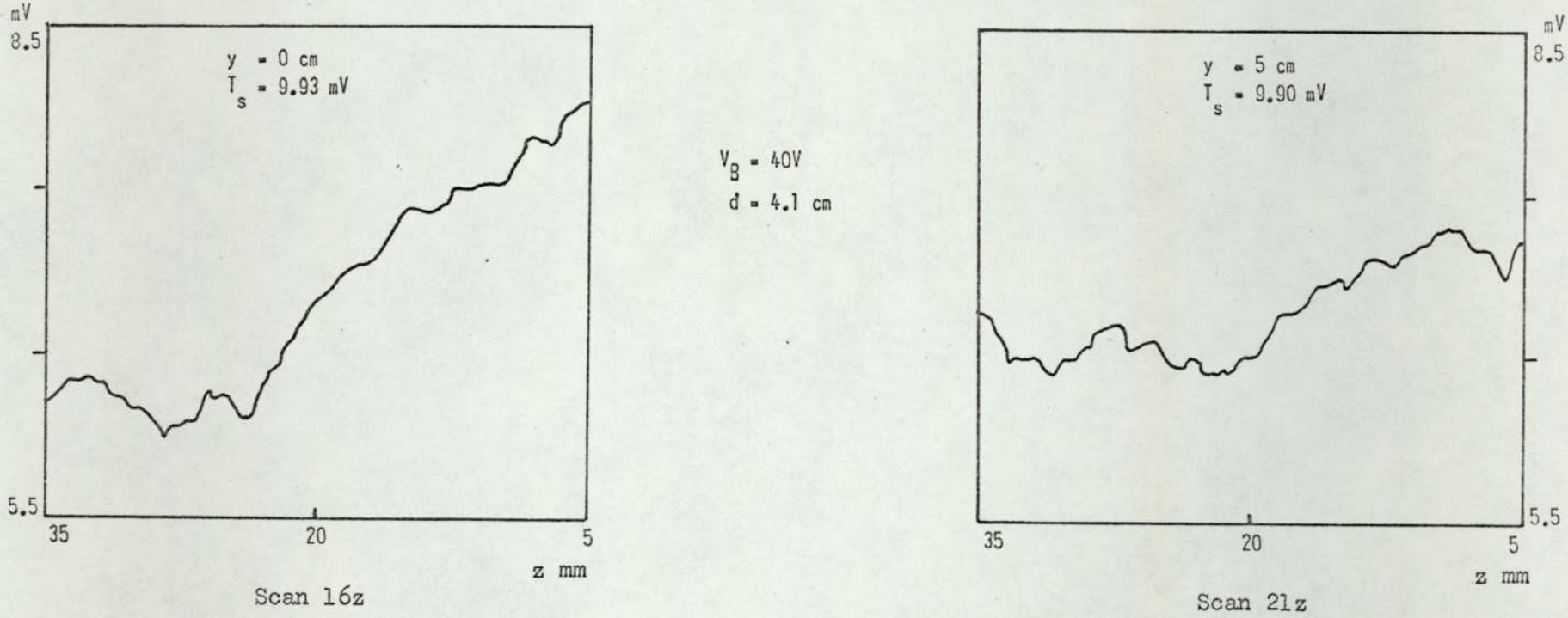

Fig. 94. Small WIS jet temperature scans in the z direction for heated free jets

The Large WIS Jet

The behaviour of these jets is similar to that of the small WIS jet with temperature attenuation decreasing as V_B increases for both y = 0 cm and y = 5 cm (see Figs. 95 and 96). There appears to be a slightly higher temperature turbulence associated with the large WIS jet however.

For these heated free jet scans where the free jet temperature is close to T_s there is little heat transfer from S to the wall jets. However, because the wall jets corresponding to the large WIS jet move further before impingement than those corresponding to the small WIS jet, the cooling effect of turbulent mixing in the outer layers of the wall jet becomes more significant for the large WIS jet than the small one. The effect is hardly noticable for the V_B = 70 V and 100 V scans but is easily detectable for the V_B = 40 V scans.

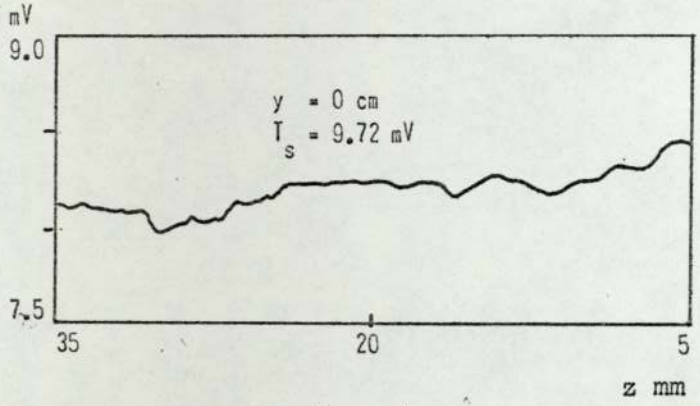

Scan 4z

V_B = 100V
d = 4.1 cm

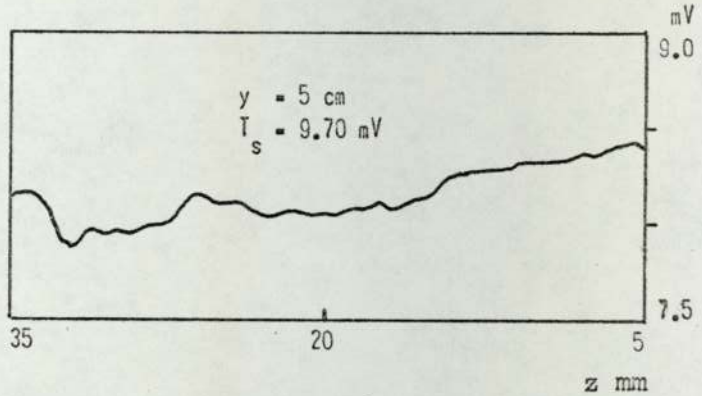

Scan 6z

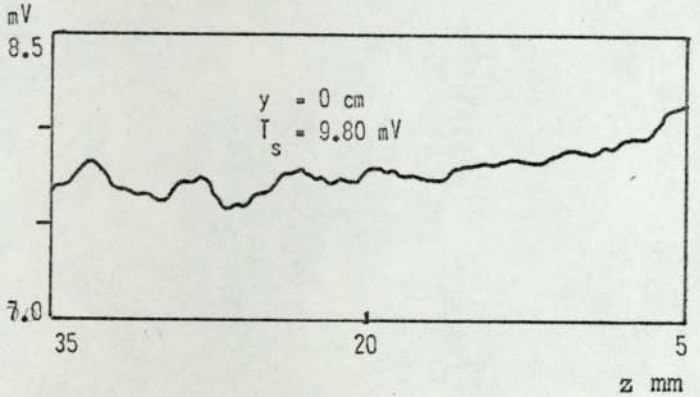

Scan 11z

V_B = 70V
d = 4.1 cm

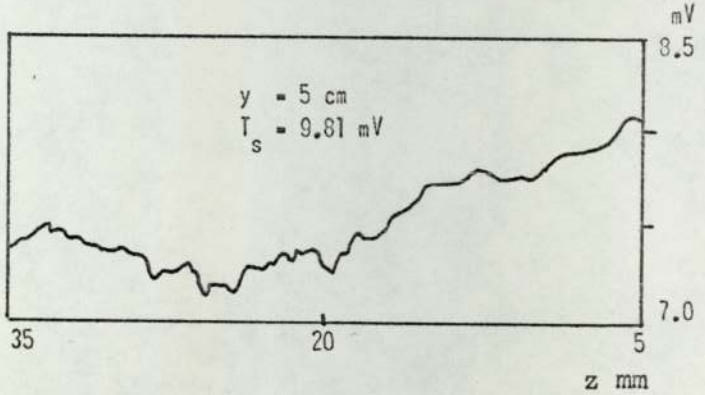

Scan 13z

Fig. 95. Large WIS jet temperature scans in the z direction for heated free jets

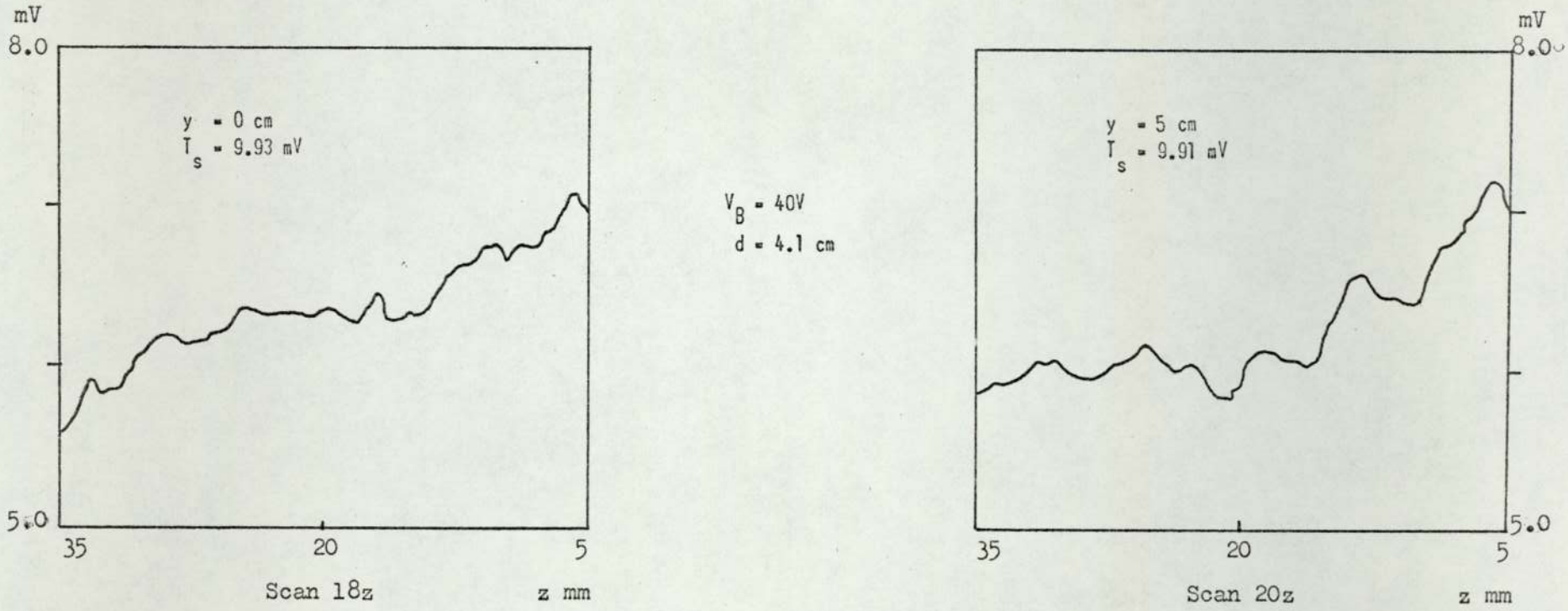

Fig. 96. Large WIS jet temperature scans in the z direction for heated free jets.

CHAPTER 8

THE TEMPERATURE DEPENDENT PARAMETERS

It has been shown in the theory that a device may employ 2 or 3 free jets, which may be either heated or unheated and air temperature measurements may be made in either the vertical or horizontal planes, or in some cases both. It is the purpose of this section to derive temperature dependent parameters appropriate to each of the above modes of operation.

Fig. 97 shows the general form of temperature scan in the horizontal plane parallel to the surface S. A, B and C represent the free jet temperatures corresponding to free jets J_A, J_B and J_C respectively, measured close to their respective axes and orifices. D and E represent the small and large WIS jet temperatures respectively measured at the x locations employed for scans in the y and z directions.

Figs. 98 and 99 represent typical vertical, y, scans (i.e. scans for fixed values of x and z but variable y), for the small and large WIS jets respectively.

In Figs. 98 and 99 the upward scan involves moving the thermocouple bead from y = 0 cm to y = 10 cm (the vertical range) and the downward scan moving the bead from y = 10 cm back to y = 0 cm. The various symbols in these Figures represent temperatures or temperature differences at/or between the locations indicated.

Definitions of these symbols will now be given.

Small WIS Jet

D_1 = WIS jet temperature at y = 0 cm at start of upward scan.

D_2 = WIS jet temperature at y = 0 cm at end of downward scan.

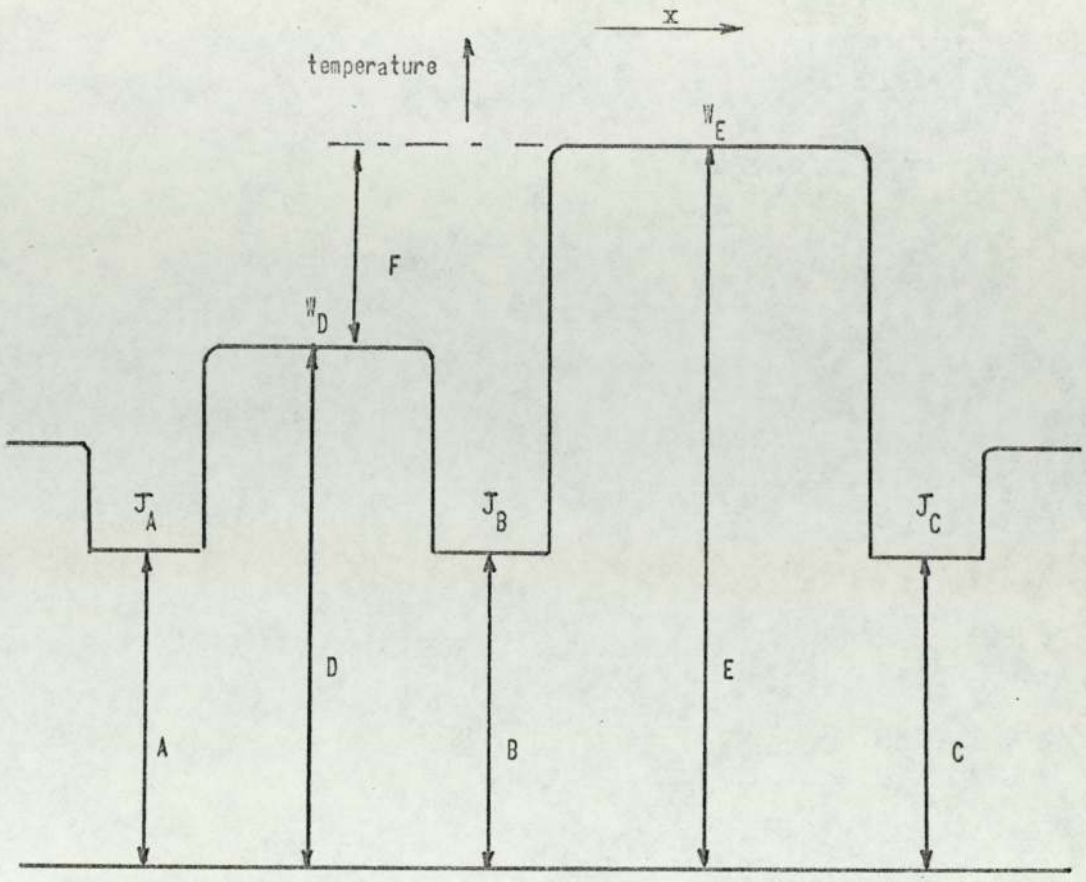

Fig. 97. Typical horizontal, x, scan

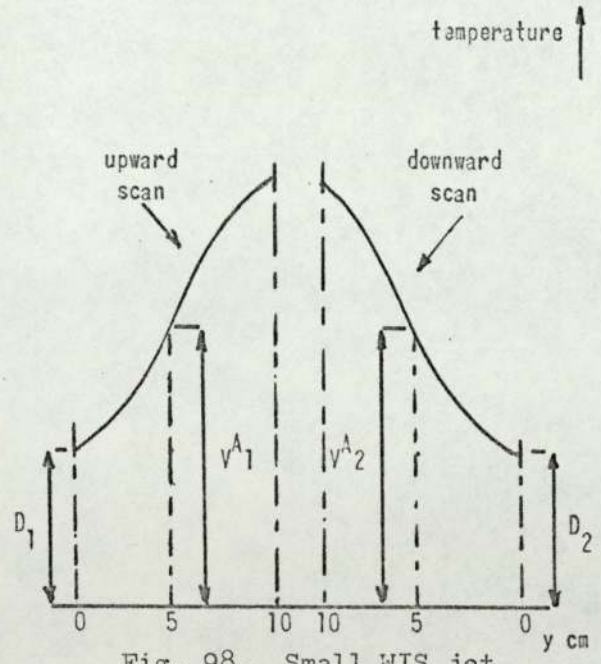

Fig. 98. Small WIS jet

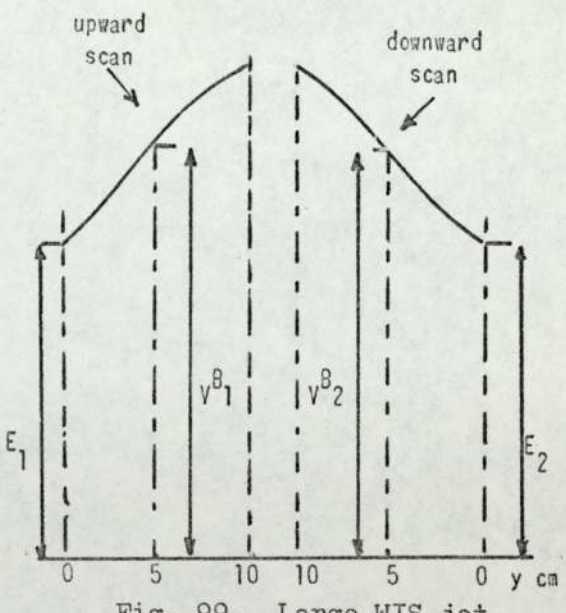

Fig. 99. Large WIS jet

Typical vertical, y, scans

V^{A}_{1} = WIS jet temperature at y = 5 cm at the midpoint of the upward scan.

V^{A}_{2} = WIS jet temperature at y = 5 cm at the midpoint of the downward scan.

Large WIS Jet

E_1 = WIS jet temperature at y = 0 cm at start of upward scan.

E_2 = WIS jet temperature at y = 0 cm at end of downward scan.

V^{B}_{1} = WIS jet temperature at y = 5 cm at the midpoint of the upward scan.

V^{B}_{2} = WIS jet temperature at y = 5 cm at the midpoint of the downward scan.

It can be seen from Figs. 97-99 that D_1 and D_2 correspond to D and E_1 and E_2 correspond to E. Thus any temperature dependent parameters generated from the horizontal scans and using the above temperatures (i.e. E or D or both) could equally well have been generated from the vertical scans (with E replaced by $\frac{E_1+E_2}{2}$ and D replaced by $\frac{D_1+D_2}{2}$) together with the corresponding values of free jet temperature where appropriate.

To avoid repetition, therefore, although temperature dependent parameters were generated using data from the horizontal scans they will not be presented in this thesis. It is helpful however, to derive the general form of these parameters in order to demonstrate the similarities between these and the equivalent ones generated from the vertical scans.

The last two Chapters indicated the origin of the variables from which the temperature dependent parameters will be derived. Since the temperature of a WIS jet is a function of both the temperature of the surface over which the constituent wall jets flow, and the corresponding free jet temperatures, it is appropriate to take these

latter into consideration when deriving the temperature dependent parameters.

PARAMETERS ASSOCIATED WITH SCANS IN THE HORIZONTAL PLANE

Using the nomenclature in Fig. 97 the parameter associated with the small WIS jet is:

$$D - \frac{A+B}{2} = {}_{H}\theta_{S} \quad \ldots\ldots (69)$$

and that associated with the large WIS jet is:

$$E - \frac{B+C}{2} = {}_{H}\theta_{L} \quad \ldots\ldots (70)$$

combining (69) and (70)

$$H^{\theta}L - {}_{H}\theta_{S} = H^{\theta}(L-S) \quad \ldots\ldots (71)$$

or $$E - D = {}_{H}\theta_{(L-S)} + \frac{C-A}{2} = F \quad \ldots\ldots (72)$$

note, if C-A approaches zero, i.e. J_C and J_A have the same temperature then:

F approaches ${}_{H}\theta_{(L-S)}$

Thus any difference between (71) and (72) will arise from a differential outer free jet temperature.

PARAMETERS ASSOCIATED WITH SCANS IN THE VERTICAL PLANE

Using the nomenclature in Figs. 98 and 99 the following parameter definitions follow:

For the Small WIS Jet:

$$\frac{({}_{V}A_1 - D_1) + ({}_{V}A_2 - D_2)}{2} = {}_{V}T_S \quad \ldots\ldots (73)$$

and $$\frac{(D_1 + D_2) - (A + B)}{2} = V^{\theta}S \quad \cdots\cdots (74)$$

For the Large WIS Jet:

$$\frac{({}_{V}B_1 - E_1) + ({}_{V}B_2 - E_2)}{2} = V^{\tau}L \quad \cdots\cdots (75)$$

$$\frac{(E_1 + E_2) - (B + C)}{2} = V^{\theta}L \quad \cdots\cdots (76)$$

For Both WIS Jets:

$$V^{\tau}S - V^{\tau}L = V^{\tau}(S-L) \quad \cdots\cdots (77)$$

$$V^{\theta}L - V^{\theta}S = V^{\theta}(L-S) \quad \cdots\cdots (78)$$

$$\frac{(E_1 + E_2) - (D_1 + D_2)}{2} = F_{(1+2)} \quad \cdots\cdots (79)$$

Note if $A = C$

then $$V^{\theta}(L-S) = F_{(1+2)} \quad \cdots\cdots (80)$$

Parameters Associated with the Test Surface Temperature

Although the temperature of S has been measured with respect to ambient temperature, it is appropriate when deriving relationships between WIS jet temperature dependent parameters involving unheated free jets and surface temperature to relate the surface temperature to the corresponding free jet temperatures. (Note: for the zero net heat transfer studies using heated free jets the surface temperatures will be related to ambient, i.e. recorder zero.) The general form of this modified surface temperature will be denoted by T_{mod}. The specific forms of T_{mod} will be indicated below.

Surface Temperature Measurement Corresponding to Small WIS Jet Scans

P_S = measured time mean temperature of S w.r.t. ambient thus the surface temperature w.r.t. that of the corresponding free jets J_A and J_B

is defined by:

$$P_{SAB} = P_S - \frac{A_C + B_C}{2} \quad \ldots\ldots\ldots\ldots\ldots\ldots\ldots\ldots\ldots\ldots (81)$$

where A_C and B_C are the temperatures of the free jets when the latter are unheated. (Note: in the case of scans in the horizontal plane which employ unheated free jets throughout $A_C = A$ and $B_C = B$.)

Surface Temperature Measurement Corresponding to the Large WIS Jet Scans

P_L = measured time mean temperature of S w.r.t. ambient thus the surface temperature w.r.t. that of the corresponding free jets J_B and J_C is defined by:

$$P_{LBC} = P_L - \frac{B_C + C_C}{2} \quad \ldots\ldots\ldots\ldots\ldots\ldots\ldots\ldots\ldots\ldots (82)$$

where the subscript C has the same significance as above.

For relationships between temperature dependent parameters involving both WIS jets and surface temperature it is appropriate to use the following definition of surface temperature:

$$P_{ABC} = P_{SL} - \frac{A_C + B_C + C_C}{3} \quad \ldots\ldots\ldots\ldots\ldots\ldots\ldots\ldots (83)$$

where $P_{SL} = \frac{P_S + P_L}{2}$ $\ldots\ldots\ldots\ldots\ldots\ldots\ldots\ldots\ldots\ldots (84)$

In practice the values of A, B and C, corresponding to unheated free jets, i.e. A_C, B_C and C_C are only a little higher than ambient temperature, so the new definitions of surface temperature will be a little lower than those for which ambient temperature is used as a reference.

NORMALIZATION OF TEMPERATURE DEPENDENT PARAMETERS

In this section the surface temperature w.r.t. ambient will be denoted by P but will be representative of P_L, P_S and P_{SL}.

In deriving a relationship between the temperature dependent parameters and free jet temperature, it was desirable to keep V_B, d and P constant throughout the range of free jet temperatures selected. This latter consisted of five levels ranging from a little above ambient to approx. P. No difficulty was encountered in fixing V_B and d, but it was found that P was influenced a little by the free jets, particularly for the lowest temperatures of these latter. This perturbation of P by the free jets could be eliminated by an appropriate adjustment of the heaters in S, but due to the high thermal capacity (and hence thermal inertia) of S this was found to be a very time consuming and tedious procedure. It was therefore decided to accept these small variations in P and normalize the temperature dependent parameter to the maximum within each set of five.

Normalization Procedure for Plots of Temperature Dependent Parameter vs Corresponding Free Jet Temperature

Let all temperature dependent parameters be normalized to the maximum surface temperature P_m in each set of five.

Since the size of each temperature dependent parameter is proportional to the temperature difference between the corresponding free jets and the surface temperature it is appropriate to adopt the following procedure.

Let the temperature dependent parameter be X units corresponding to the small WIS jet with free jets J_A and J_B.

Then the value of X when normalized from P to P_m will be given by:

$$\frac{P_m - \left(\frac{A+B}{2}\right)}{P - \left(\frac{A+B}{2}\right)} X \qquad \text{.......................................} (85)$$

(85) becomes $\frac{P_m - (\frac{A+B}{2})}{P_{SAB}}$ X ..... (86)

The normalized temperature dependent parameter corresponding to the large WIS jet with free jets J_B and J_C is:

$$\frac{P_m - (\frac{B+C}{2})}{P_{LBC}} \text{ X} \quad \text{.....} \quad (87)$$

and for both WIS jets with free jets J_A, J_B and J_C the normalized temperature dependent parameter is:

$$\frac{P_m - \frac{A+B+C}{3}}{P_{ABC}} \text{ X} \quad \text{.....} \quad (88)$$

Note: (86) is appropriate to $V^{\tau}S$ and $V^{\theta}S$

(87) is appropriate to $V^{\tau}L$ and $V^{\theta}L$

(88) is appropriate to $V^{\tau}(S-L)$ $V^{\theta}(L-S)$ and $F_{(1+2)}$

CHAPTER 9

THE RELATIONSHIPS BETWEEN TEMPERATURE DEPENDENT PARAMETERS X AND THE MODIFIED SURFACE TEMPERATURE T_{mod} USING UNHEATED FREE JETS

Having derived the different forms of X and T_{mod}, the variations of X with T_{mod} for different values of V_B and d will now be examined. Linear best fit plots involving these parameters and employing data derived from the temperature scans in the vertical, y, direction will be examined in the following sections.

LINEAR BEST FIT PLOTS OF $V^{\theta}{}_L$ AND $V^{\theta}{}_S$ vs T_{mod}

Before dealing with the individual curves in detail it is helpful to discuss a few relevant characteristics common to many of them. This will assist in assessing the significance of certain variables relating to these curves. Some of the comments emerging from this section will apply in later sections where other temperature dependent parameters are involved.

An inspection of Figs.100 to 102 will indicate that there are two characteristics common to all plots in this set.

(1) There is a variation of $\frac{dX}{dT_{mod}}$ with d.

(2) The interception of all lines on the T_{mod} axis corresponds to a $T_{mod} > 0$.

The following section will suggest mechanisms which may be responsible for these effects. Fig.103 shows a typical plot of X vs T_{mod}.

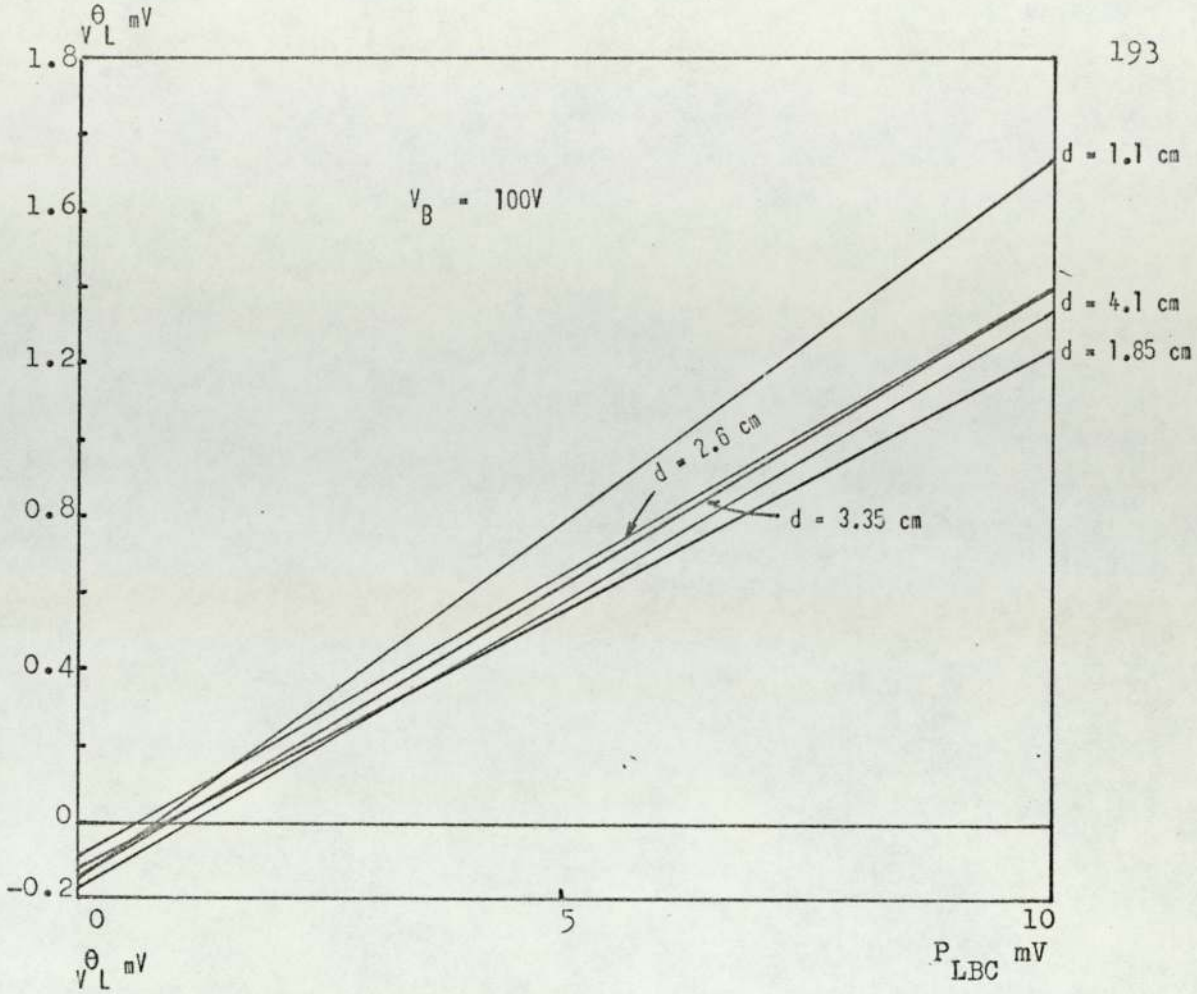

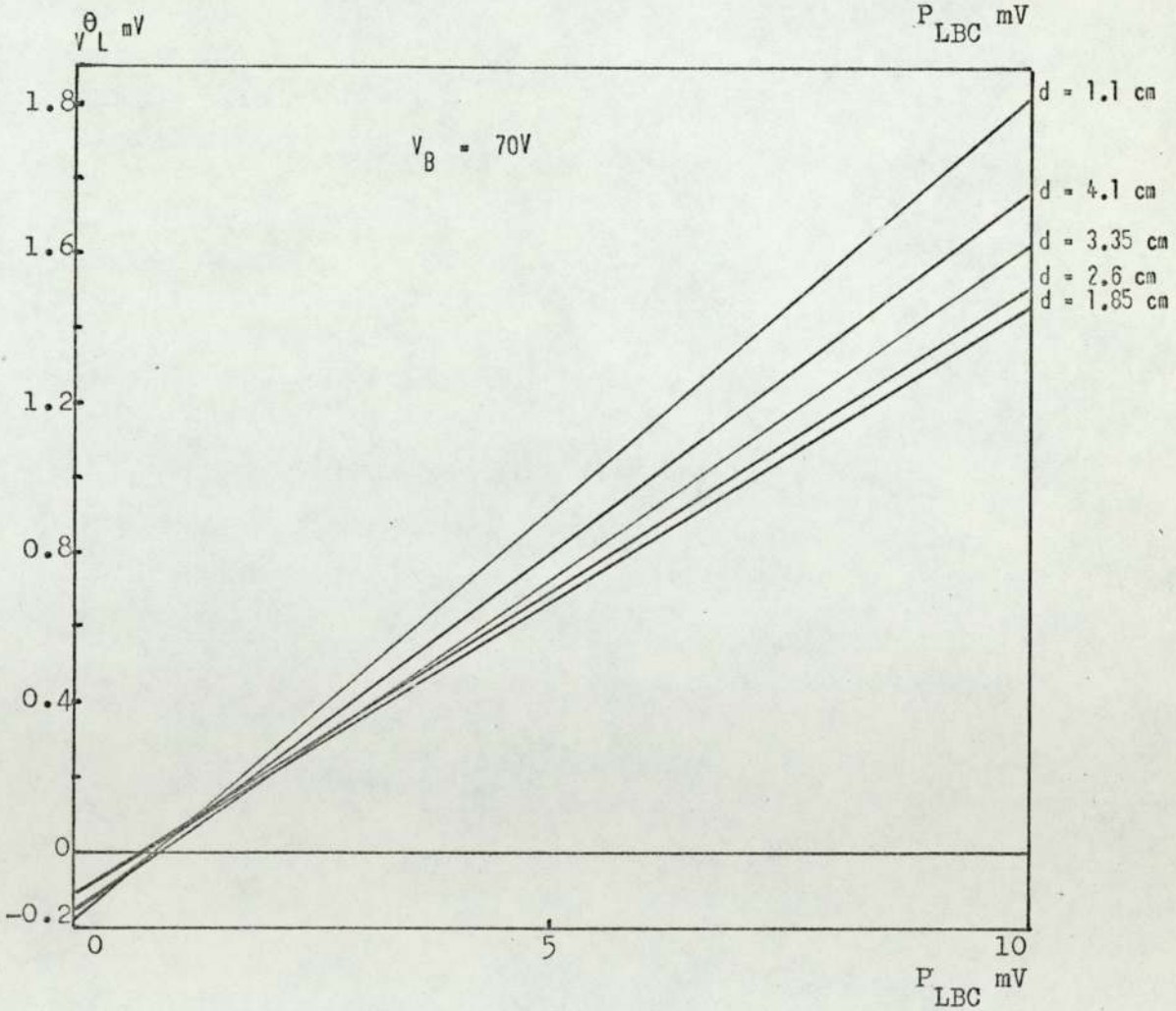

Fig. 100. Linear best fit for $_{V}\theta_{L}$ vs P_{LBC}

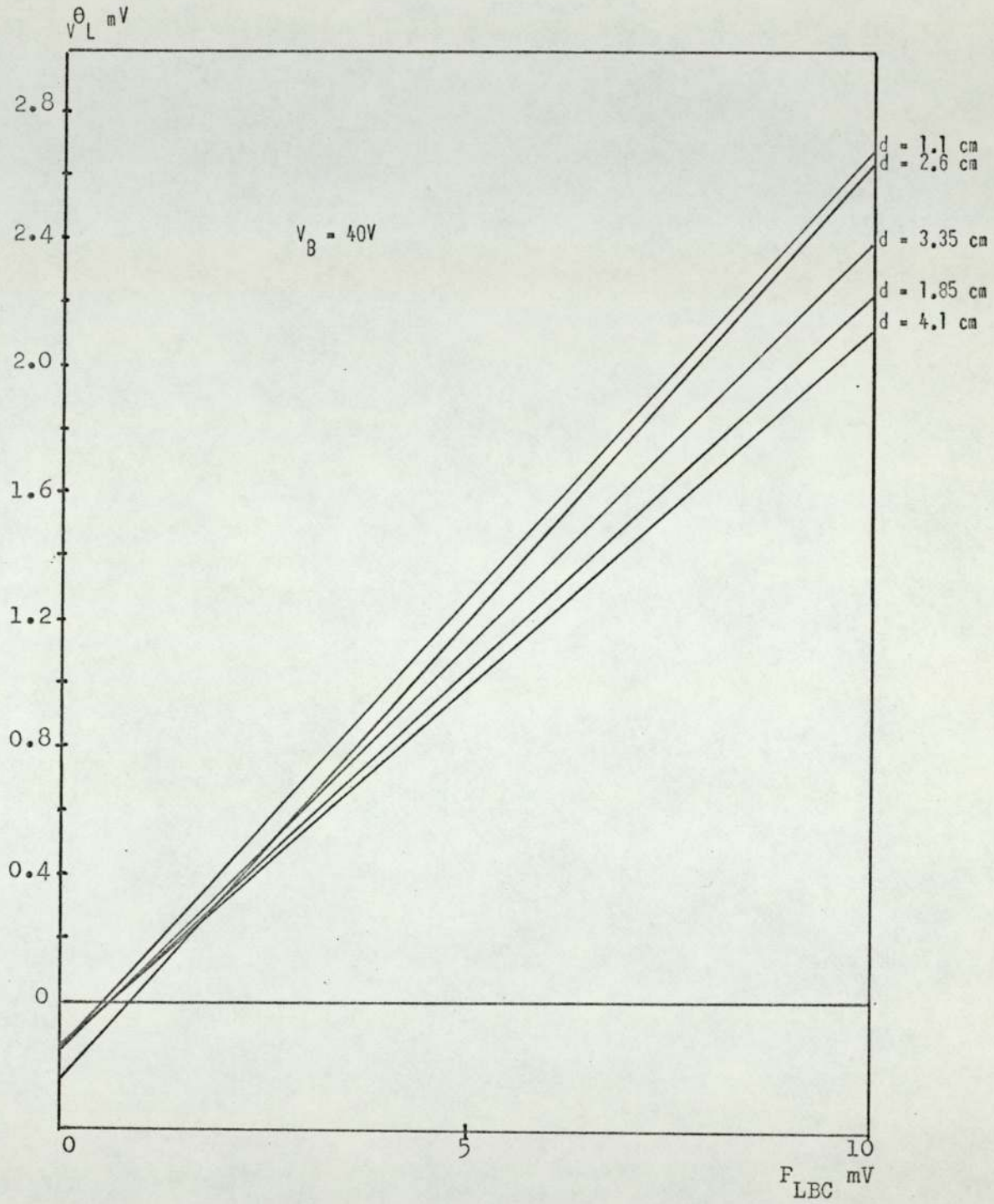

Fig. 101. Linear best fit for $_V\theta_L$ vs P_{LBC}

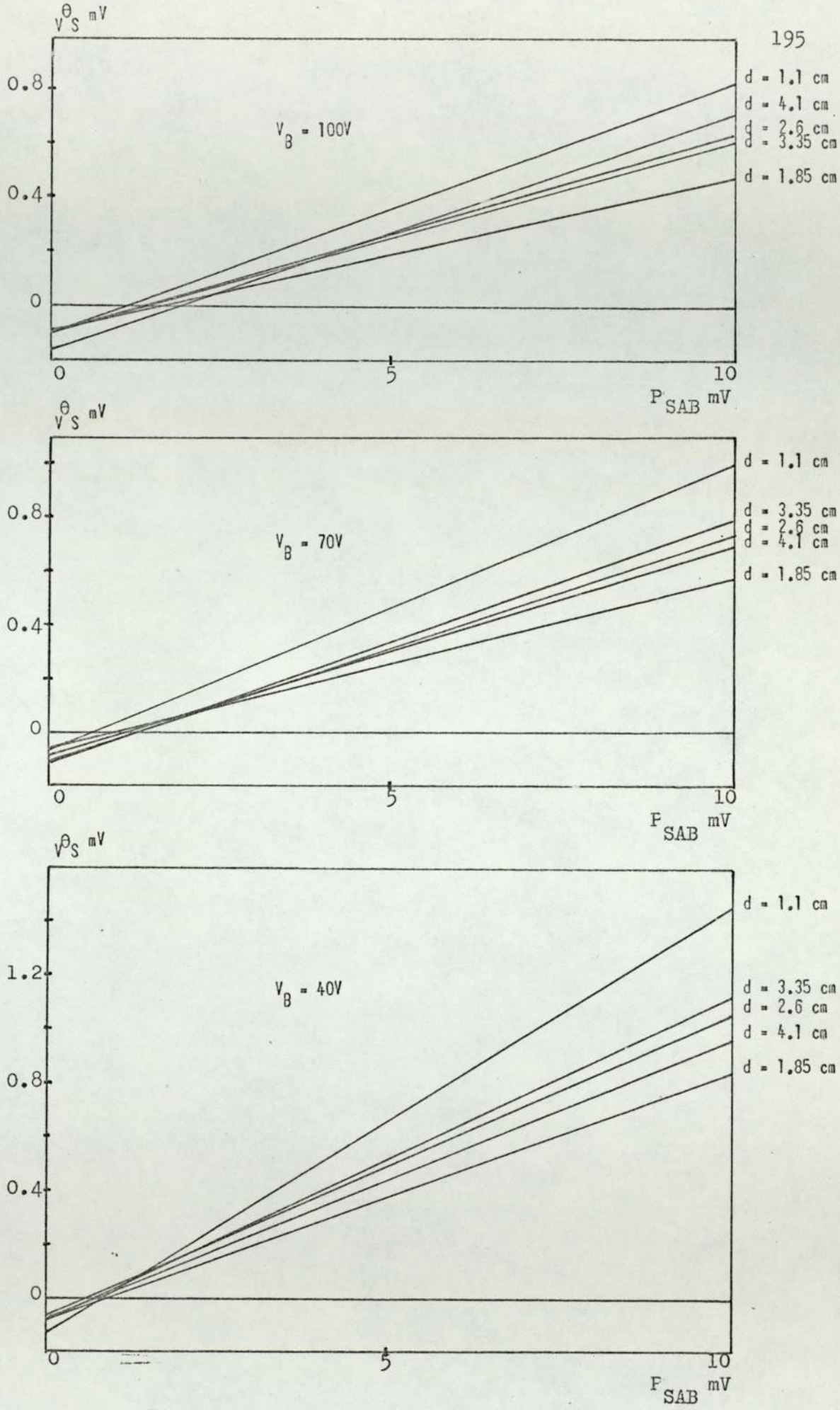

Fig. 102. Linear best fit for V^{θ}_S vs P_{SAB}

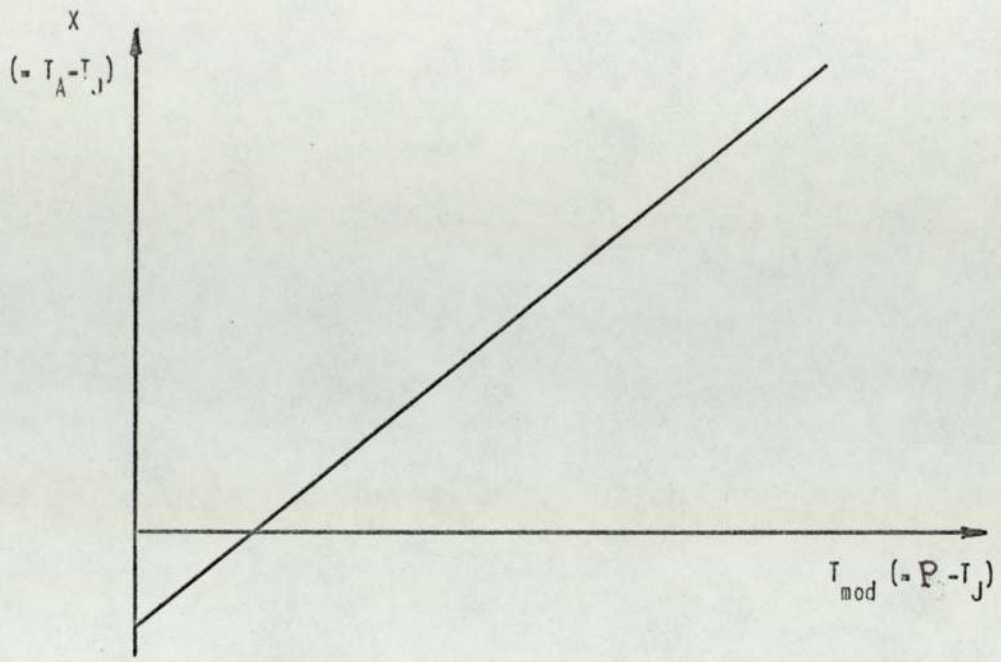

Fig. 103. Typical plot of X vs T_{mod}

Let T_A represent the WIS jet temperature and T_J represent some appropriate average free jet temperature, both measured w.r.t. ambient. For example, consider the large WIS jet temperature dependent parameter appropriate to measurements in the horizontal plane, i.e. $X = {}_V\theta_L$ then:

$$T_A = \frac{E_1+E_2}{2} \quad \text{and} \quad T_J = \frac{B_C+C_C}{2}$$

thus in this case $X = T_A - T_J = \frac{E_1+E_2}{2} - \frac{B_C+C_C}{2}$

and $$T_{mod} = P - T_J$$
$$= P_L - \frac{B_C+C_C}{2}$$
$$= P_{LBC}$$

Radiation Effects

If $T_A \geq T_J$ then P will be greater than T_J and $P > T_A$. This latter statement is true because for T_A to be $> T_J$ heat must have been transferred from S to the wall jets before the latter impinge.

In general, for finite surface dimensions the wall jet will never reach P and on leaving S, in the form of a WIS jet, it is likely to undergo attenuation as has been indicated earlier.

Now in general the convective heat transfer coefficients associated with the thermo-couple in the free jets will be greater than if it were in the WIS jets because the velocity of the former is greater than that of the latter. Thus any radiation effects will be more pronounced in the WIS jet than the free jet.

If it is assumed that T_A has a greater radiation contribution than T_J then X will be greater than it would have been had radiation effects been absent, thus $\frac{dX}{dT}_{mod}$ will be correspondingly larger.

It has been seen that the significance of radiation depends on the convective heat transfer coefficient which is a function of flow velocity and turbulence intensity.

As d increases the convective heat transfer coefficient associated with the thermo-couple in the WIS jet will probably decrease, (see velocity scans earlier) for a given (d - z), i.e. thermo-couple displacement from the orifice plate. This radiation effect will be greater for this reason. However, a competing effect exists. As d is increased the radiation leakage from between the plates is increased. Note, the convective heat transfer coefficient associated with the thermo-couple in the free jets will remain constant except maybe for very small values of d where the thermo-couple could possibly lie in a partial stagnation region, giving rise to increased radiation effects in the free jets. However, for small values of d the WIS jet thermo-couple may also lie in a region of partial stagnation, so the enhanced free jet radiation contribution would conceivably be

compensated for to a certain extent in the temperature dependent parameter (X). It would still exist, however, in T_{mod} and its effects here would be to reduce $P - T_J$ due to an increase in T_J. This again would result in an increased value of $\frac{dX}{dT_{mod}}$.

It can be seen, therefore, that there are two competing radiation effects, both of which vary with d in an opposite sense.

Another effect of radiation is to make the plot of X versus T_{mod} non-linear the value of $\frac{dX}{dT_{mod}}$ increasing with X. A linear best fit line would, under these circumstances, intercept the T_{mod} axis at some point to the right of the origin where T_{mod} is positive.

It is seen from the above comments therefore, that as far as radiation effects are concerned, no simple trend is likely to exist between both the slope and point of interception on the T_{mod} axis and d.

The Significance of Attenuation Along the WIS Jets

Consider the situation when X = 0 (i.e. $T_A = T_J$ for $_V\theta_L$ and $_V\theta_S$), then P will be greater than T_J (see the +ve intercept on the T_{mod} axis). As well as the above radiation effects this may be explained as follows:

It has been observed that the free jet temperature is a little above ambient and this is probably due to the interaction of the heated WIS jet with the orifice plate together with radiation from S. Thus since $T_J < P$ the WIS jet close to S will be hotter than T_J but will cool as it moves away from S. It is conceivable, therefore, that the WIS jet will have cooled to a temperature equal to T_J by the time it reaches the measuring thermo-couple.

Note if the free jet were at ambient and P was greater than

ambient then the equality between the free and WIS jet temperatures could not have arisen from the WIS jet attenuation effect described above since the WIS jet could not have cooled to ambient within the spatial limits involved in these experiments.

It was noted above that preheating of the free jets could have arisen partly from radiative heat transfer from S to P_o. Since the area of the latter is very much greater than that of the thermo-couple beads and the relative significance of radiative heat transfer increases with area it is possible that this preheating could have taken place in the absence of any significant radiative heat transfer to the thermo-couples.

For higher values of P the WIS jet temperature will be higher and will undergo correspondingly greater attenuation. The net effect of this is to make X lower than it would have been had attenuation not been present. Thus the effect of attenuation is to oppose that of radiation (which itself will be more significant for these higher values of P) and tend to reduce $\frac{dX}{dT_{mod}}$.

The effect of increasing d will be to increase the WIS jet attenuation for a given P, and hence reduce $\frac{dX}{dT_{mod}}$ still further.

Having discussed the possible causes of variations of $\frac{dX}{dT_{mod}}$ with d and T_{mod} (for X = 0) with d, a closer examination of the individual curves involving $_V\theta_L$ and $_V\theta_S$ in Figs.100 to 102 will now be made.

In all cases the best fit line has the highest value of $\frac{dX}{dT_{mod}}$ when d = 1.1 cm. It has been seen that a number of radiation effects exist and the relative significance of each is not known. However, it can be said that as d increases the significance of WIS jet cooling due to entrainment of cooler surrounding air will

increase the effect of which will be to reduce the value of $\frac{dX}{dT_{mod}}$. Thus the high value of $\frac{dX}{dT_{mod}}$ is probably due to the fact that these entrainment effects will be least significant for these small values of d. Radiation, although increasing $\frac{dX}{dT_{mod}}$ is likely to have a different significance for different values of d, and V_B, and will be partially responsible for the somewhat unpredictable variation of $\frac{dX}{dT_{mod}}$ with d for values of d greater than 1.1 cm.

The Influence of Free Jet Velocity on $\frac{dX}{dT_{mod}}$

In general the best fit lines are steepest for V_B = 40 V for a given temperature dependent parameter.

Perry has shown[45] for flow velocities up to 250 ft/sec. that for flow parallel to the surface (i.e. a free jet impingement angle of 0°) $Nu \propto U^{0.8}$ and for flow perpendicular to the surface (i.e. a free jet impingement angle of 90°) $Nu \propto U^{0.7}$ where Nu is the Nusselt number - a dimensionless convective heat transfer coefficient.

Now the temperature of the air will be proportional to the time it has been exposed to the surface and this time will vary inversely as the flow velocity but at a greater rate than the convective heat transfer coefficient. Thus, as has been indicated earlier, the net effect of the above is to cause the air temperature to increase with decreasing velocity resulting in the steepest value of $\frac{dX}{dT_{mod}}$ for the lowest free jet velocity, V_B = 40 V.

It has been seen that the lower velocities are most vulnerable to radiation, thus assuming the radiation to be more significant for the WIS jet than the free jet, the curves for V_B = 40 V will have a greater radiation contribution than the higher velocity ones, the effect of which will be to increase $\frac{dX}{dT_{mod}}$.

It is seen that those curves involving the small WIS jet are in general not as steep as those involving the large WIS jet. This follows directly from the fact that the wall jets corresponding to the large WIS jet move a greater distance from their origins (free jet axes) than the wall jets corresponding to the small WIS jet, thus the temperature of the former will in general be higher for a given surface temperature P.

LINEAR BEST FIT PLOTS OF $V^{\theta}_{(L-S)}$ AND $F_{(1+2)}$ VERSUS T_{mod}

Both these temperature dependent parameters involve three free jets and WIS jet temperature measurements in the horizontal plane. Fig. 104 corresponds to $V^{\theta}_{(L-S)}$ and Fig. 105 corresponds to $F_{(1+2)}$.

If the free jet temperatures A and C are equal then the two parameters should be identical, but any difference between A and C will be manifest in a difference between $V^{\theta}_{(L-S)}$ and $F_{(1+2)}$ for a given V_B and d.

Comparison between the V_B = 100 V plots show them to be very similar. However, the similarity is less for the 70 V and 40 V plots. This is probably due to a small difference in convective heat transfer coefficient between J_A and J_C resulting from a small difference between both mean and turbulent components of velocity in these free jets. Note, these effects will increase in significance as the jet velocities decreases due to the corresponding increased significance of radiative heat transfer coefficient.

Radiation Effects

One of the radiation effects in scans involving two free jets

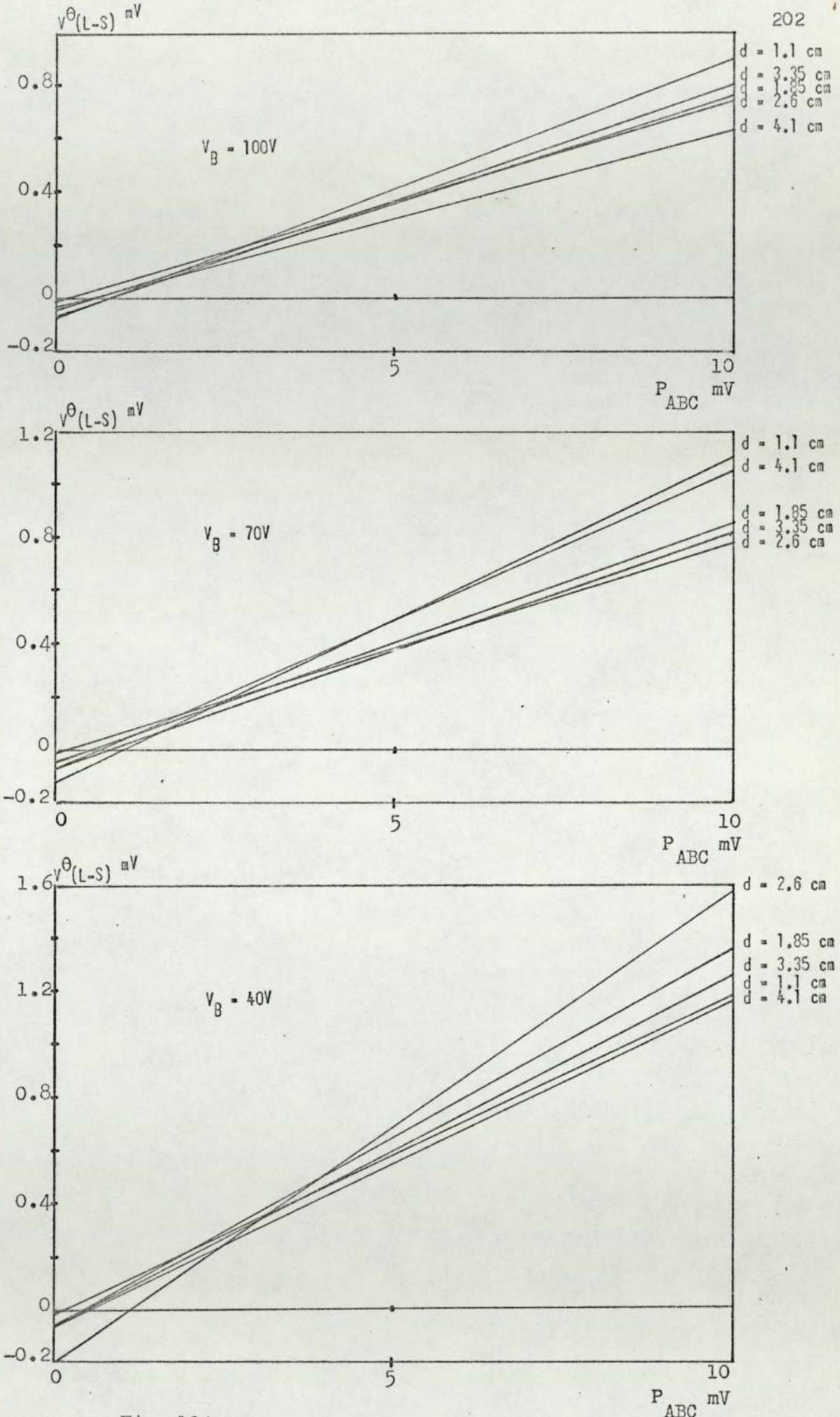

Fig. 104. Linear best fit for $V^{\theta}(L-S)$ vs P_{ABC}

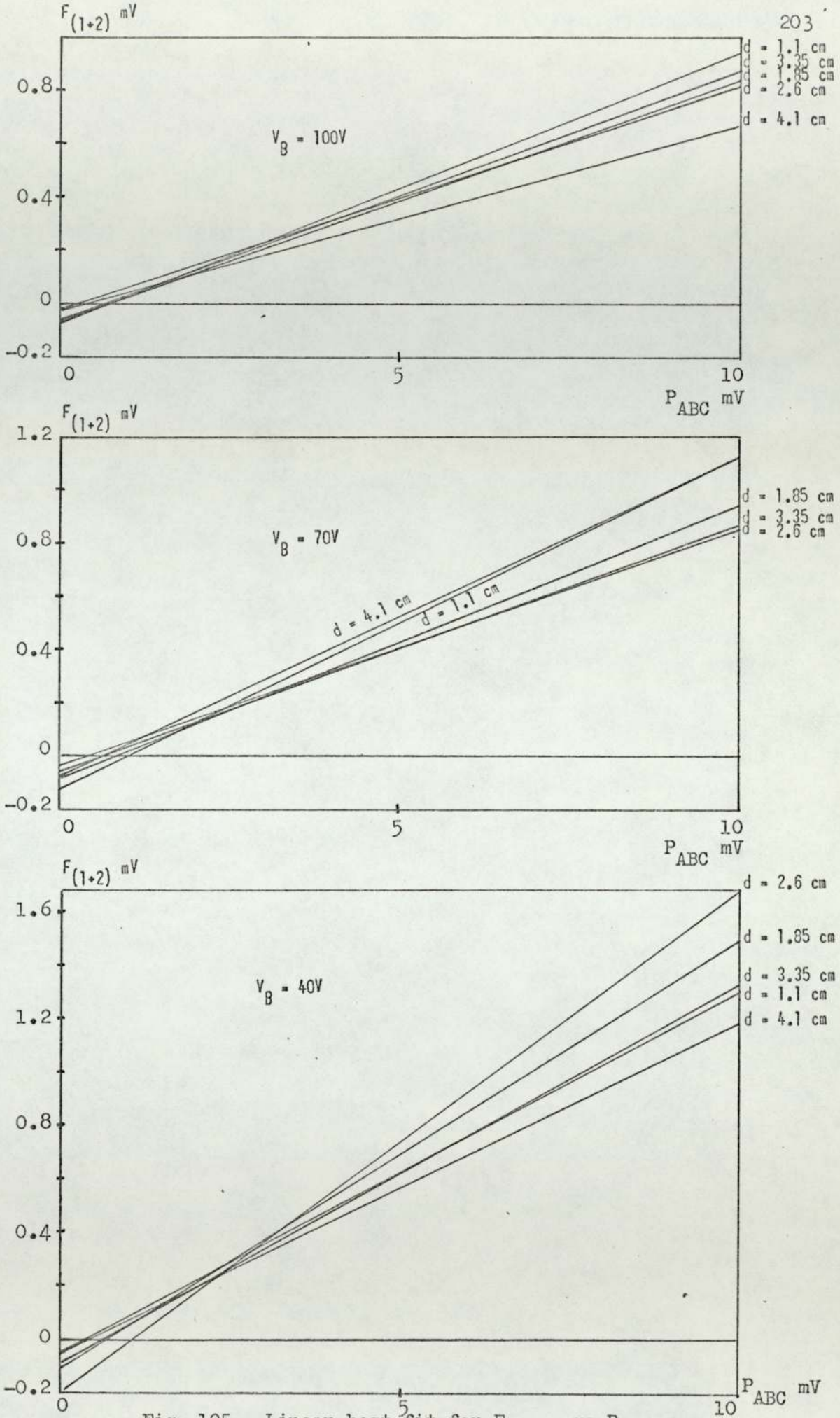

Fig. 105. Linear best fit for $F_{(1+2)}$ vs P_{ABC}

resulted from different relative contributions to the free and WIS jets however these effects should be very much smaller for the three free jet systems.

It is seen in the velocity studies that in general the small WIS jet has a slightly higher velocity and turbulence intensity than the corresponding large one. Thus the convective heat transfer coefficient for the small WIS jet will be slightly higher. The effect of this will be to make the relative radiation contribution to the thermocouple in the large WIS jet slightly higher than that in the small WIS jet, resulting in a slight radiation contribution to $\frac{dX}{dT_{mod}}$ the effect being to increase this gradient.

Attenuation Effects in the Three Free Jet Systems

As for radiation, the effect of attenuation should be lower than when two free jets are used since the temperature dependent parameter involves the difference between the attenuations in the large and small WIS jets. This should be reflected in an intercept on the T_{mod} axis closer to the origin which is indeed the case for most of the lines. The spread in $\frac{dX}{dT_{mod}}$ for the three free jet parameters is less than for the two free jet ones, as would be expected. However, the relative spread in each set of 5 (i.e. the spread divided by the corresponding mean of each set) does not vary much between $_{V}\theta_{(L-S)}$, $F_{(1+2)}$ and $_{V}\theta_{L}$. However, $_{V}\theta_{S}$, indicates a slightly higher relative spread than the others.

Table 4a shows the residual standard deviation RSD on T_{mod} for the linear best fit plots discussed so far. In this Table, all values of d are expressed in terms of cm. The values of RSD are expressed in thermal e.m.f. in units of 10^{-3} mV.

TABLE 4a

RESIDUAL STANDARD DEVIATIONS ON T_{mod} FOR MEASUREMENTS MADE IN THE HORIZONTAL PLANE

V_B = 100 V	d=1.1	d=1.85	d=2.6	d=3.35	d=4.1
V^{θ}_L	247	87	161	394	323
V^{θ}_S	295	753	639	702	679
$V^{\theta}(L-S)$	468	450	454	383	519
$F_{(1+2)}$	374	287	337	431	569

V_B = 70 V	d=1.1	d=1.85	d=2.6	d=3.35	d=4.1
V^{θ}_L	439	264	360	444	308
V^{θ}_S	397	402	890	899	776
$V^{\theta}(L-S)$	594	261	284	630	505
$F_{(1+2)}$	674	135	336	515	439

V_B = 40 V	d=1.1	d=1.85	d=2.6	d=3.35	d=4.1
V^{θ}_L	234	254	205	249	300
V^{θ}_S	277	490	367	113	526
$V^{\theta}(L-S)$	284	134	340	519	227
$F_{(1+2)}$	555	236	280	653	244

All values of d are in cm.

All R.S.D's are in units of 10^{-3} mV.

There seems to be no strong correlation between residual standard deviation and any of the related parameters such as X, V_B and d. Fig.106 shows the experimental points only for $_V\theta_L$ vs P_L. Note in this Figure the surface temperature has been related to ambient and not the unheated free jets as for the other plots discussed so far in this section. Nevertheless it will be representative of a plot of $_V\theta_L$ vs P_{LBC}. A comparison between Fig.106 and Table 4a will give some idea of the degree of scatter of the experimental points about the corresponding linear best fit plots. The cause of the above scatter is not certain but may be related to the 'temperature turbulence' associated with the temperature scans, see Figs.107 to 112. These Figures show the temperature turbulence in the large WIS jet with d = 4.1 cm, z = 3.5 cm and y = 0 cm. Two plots are indicated for each value of V_B. The upper corresponds to the unintegrated signal from the thermo-couple and the lower to the corresponding integrated signal with a T.C. of 25 sec. It can be seen that the lowest free jet velocity V_B = 40 V is most vulnerable to this temperature turbulence and the integrated signal shows that it is fairly long term in this case.

These random temperature variations could be partly responsible for creating the somewhat unpredictable variations of $\frac{dX}{dT_{mod}}$ with d in some of the scans discussed.

LINEAR BEST FIT PLOTS OF $_V\tau_L$ AND $_V\tau_S$ VERSUS T_{mod}

An examination of Figs.113 to 115 indicates a much greater spread in $\frac{dX}{dT_{mod}}$ than existed in any of the best fit plots involving measurements in the horizontal plane.

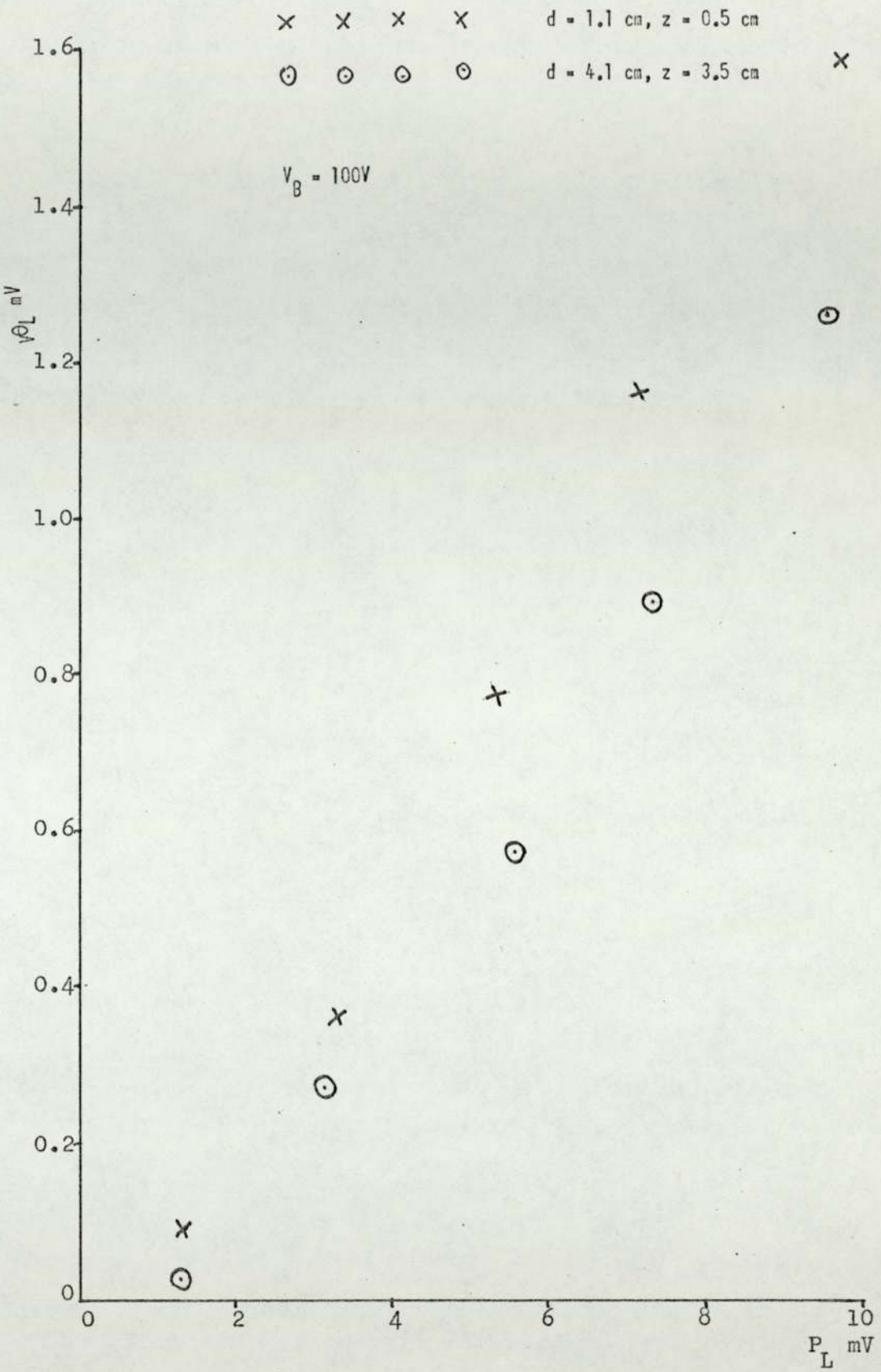

Fig. 106. $V\theta_L$ vs P_L for unheated free jets

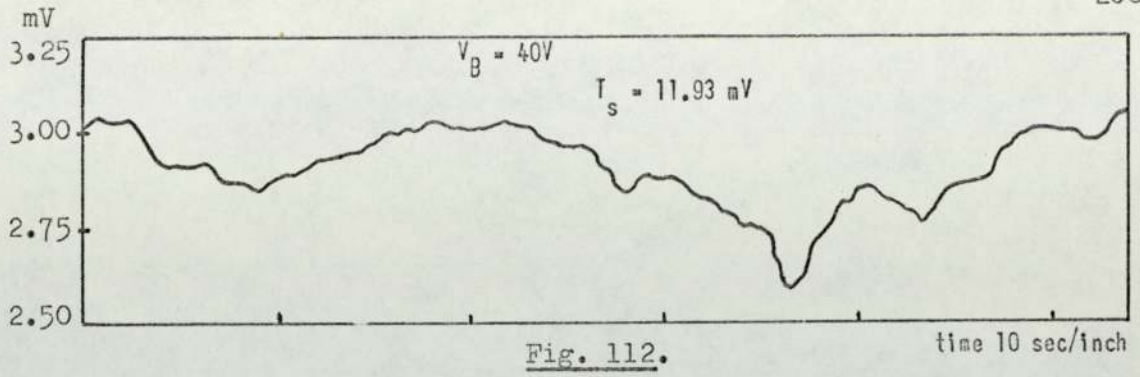

Fig. 112.

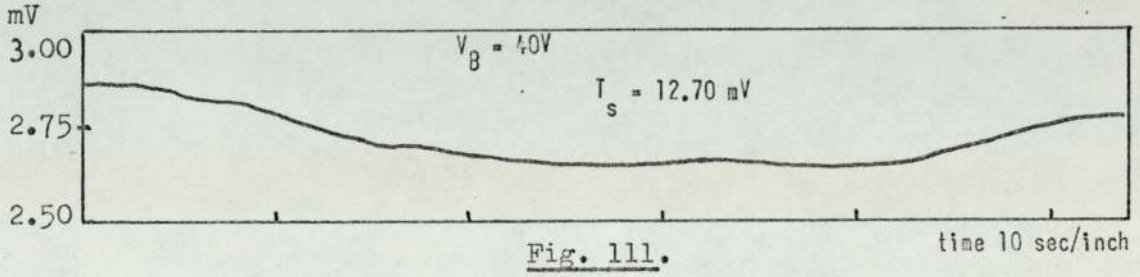

Fig. 111.

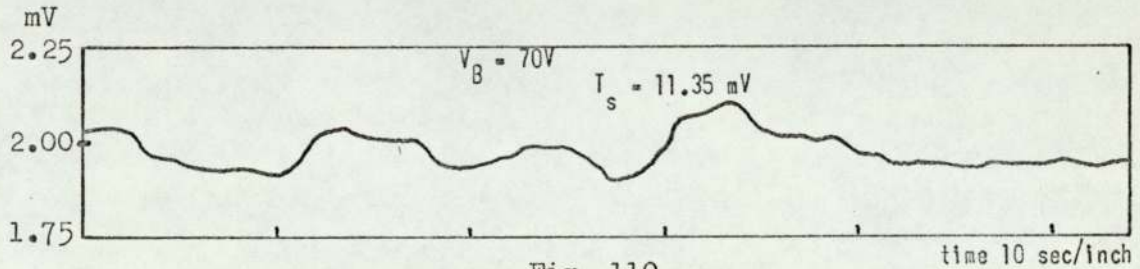

Fig. 110.

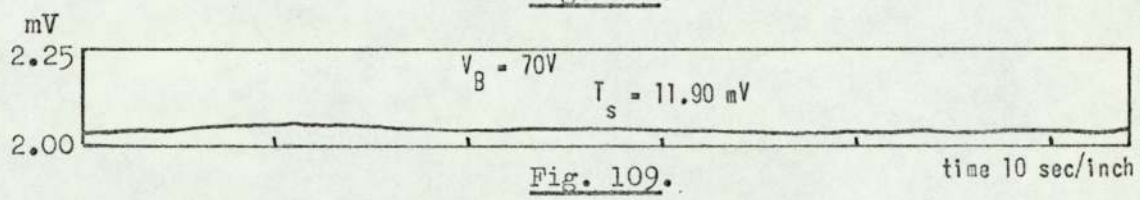

Fig. 109.

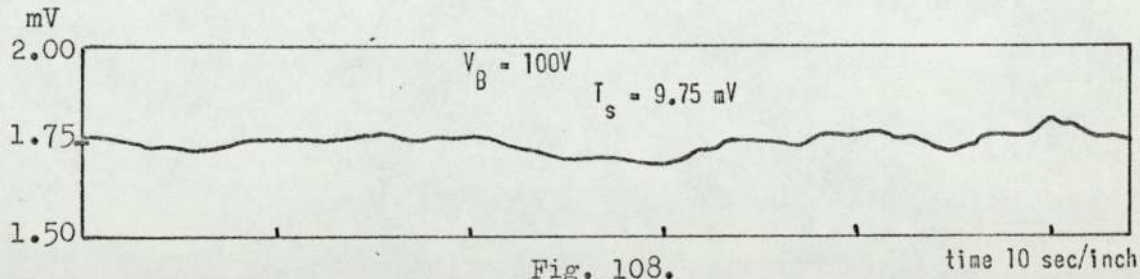

Fig. 108.

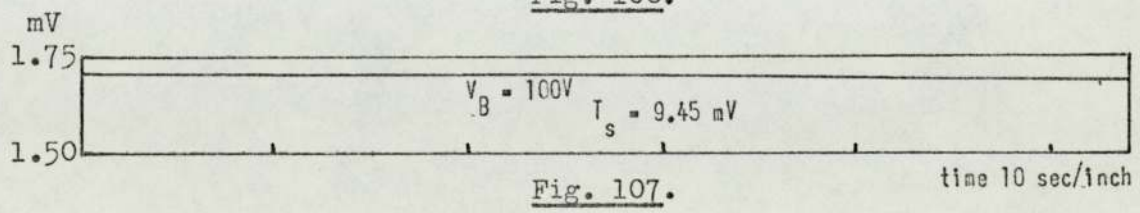

Fig. 107.

Temperature turbulence measurements in large WIS jet with thermocouple midway between J_B and J_C (unheated)
d = 4.1 cm, z = 3.5 cm, y = 0 cm

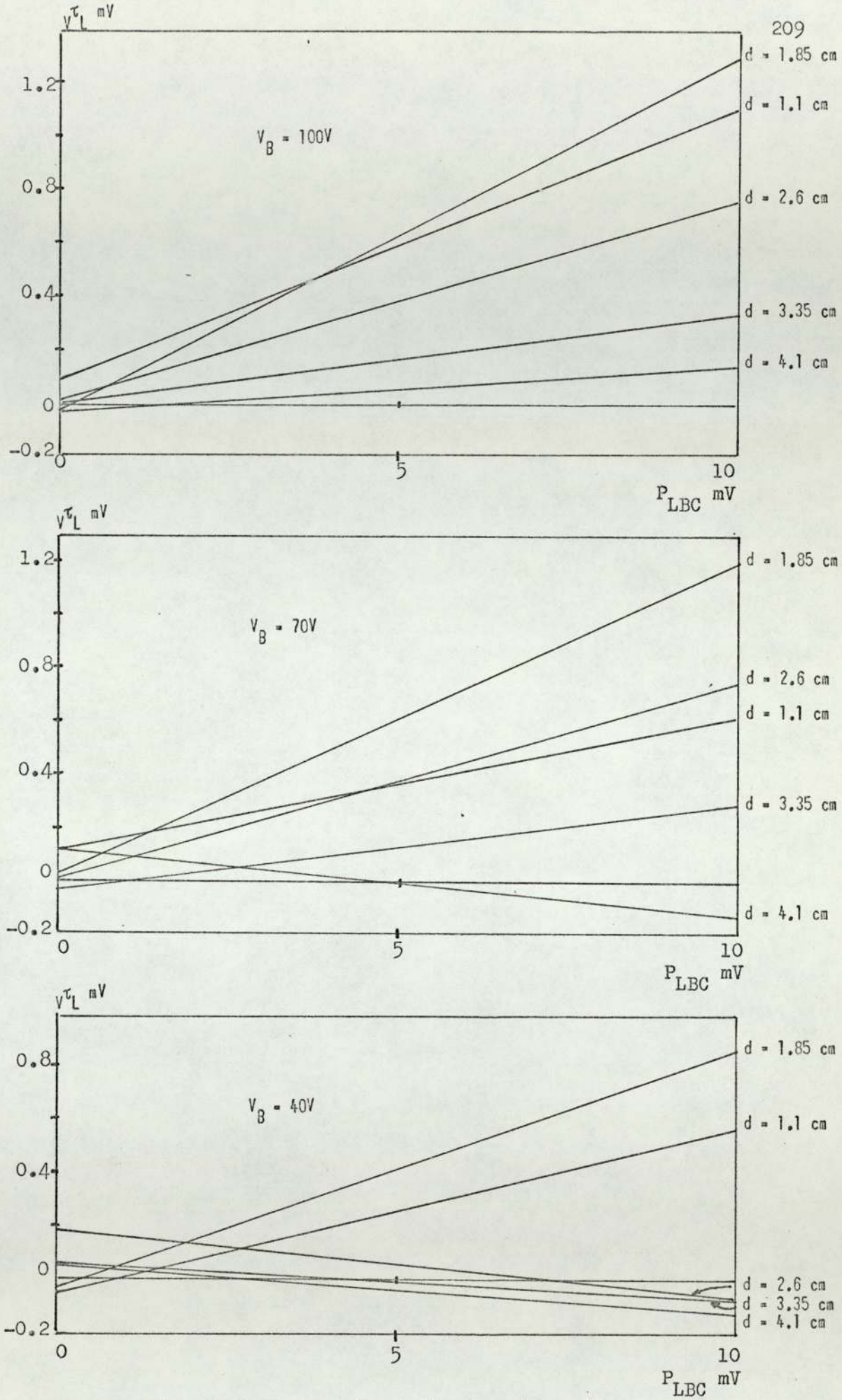

Fig. 113. Linear best fit for $V\tau_L$ vs P_{LBC}

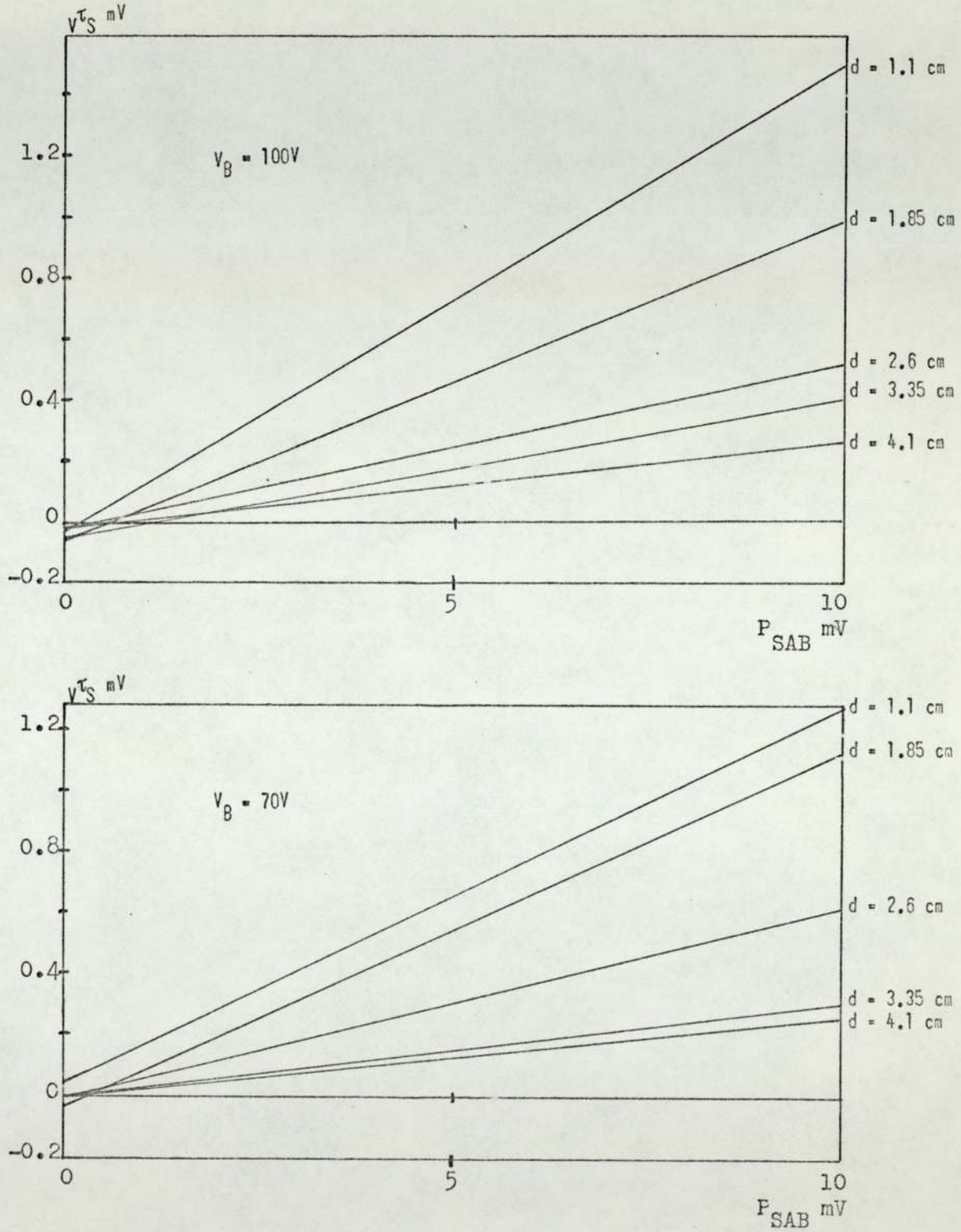

Fig. 114. Linear best fit for $V\tau_S$ vs P_{SAB}

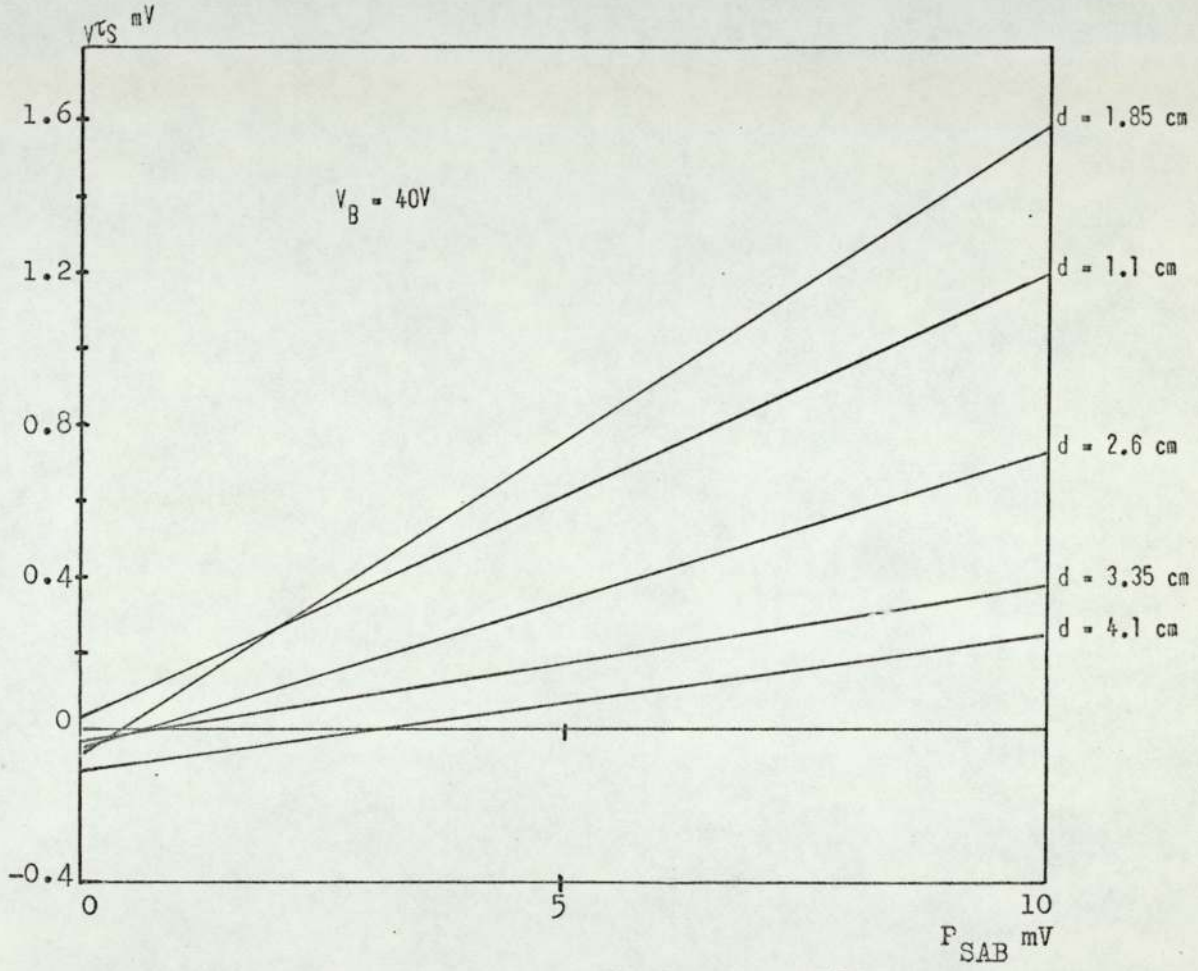

Fig. 115. Linear best fit for $_V\tau_S$ vs P_{SAB}

These plots give a slightly more predictable variation of $\frac{dX}{dT}_{mod}$ with d with the d = 4.1 cm plot having the smallest slope (which in fact is negative in some cases). The largest value of $\frac{dX}{dT}_{mod}$ corresponds to either d = 1.1 cm or d = 1.85 cm. For $_{V}\tau_{L}$ with V_B = 70 V the trend is not quite as would be expected since here the d = 1.1 cm plot has a smaller gradient than both the d = 1.85 cm and d = 2.6 cm plots.

An attempt to explain these observations will now be made.

Radiation Effects

The velocity scans for which d = 4.0 cm and z = 3.5 cm in Fig. 67 (V_B = 100 V, 70 V and 40 V), Figs. 51 and 64 (V_B = 100 V), Figs. 54 and 65 (V_B = 70 V) and Figs. 57 and 66 (V_B = 40 V) are indicative of a reduction in convective heat transfer coefficient with increasing y for a given free jet velocity V_B. Although the above curves relate to d = 4 cm the trend persists for smaller values of d.

The net effect of these velocity characteristics is to make the thermo-couple at y = 5 cm more vulnerable to radiation incident upon it than when it is at y = 0 cm. However, the actual radiation flux intercepted by the thermo-couple at y = 5 cm will be less than that at y = 0 cm, due to the geometry of the system, thus this geometrical radiation effect will oppose the former. The geometrical effect will of course be highest for d = 4.1 cm and will diminish with decreasing d (i.e. the radiation leakage will increase with d).

The convective heat transfer coefficient will be smallest for the largest values of d (for a given value of y) since the mean velocity and turbulence intensity are smallest for this value. This

will result in an increased radiation significance for a given radiation flux density. Any radiation effects will increase as V_B decreases since the mean velocity and turbulence intensities decrease with V_B resulting in a decreased convective heat transfer coefficient.

It is seen, therefore, that as far as the temperature dependent parameter is concerned, its size will depend upon the relative significance of the convective and geometrical radiation effects. Radiation effects associated with the thermo-couple in the free jets will only exist in the modified surface temperatures T_{mod}, their result being to steepen the curves $\frac{dX}{dT_{mod}}$, since they will reduce the size of T_{mod}.

The Results of Turbulent Mixing in the WIS Jet

The fairly high turbulence intensities associated with the WIS jet will have two effects. (Note this is reflected in a broadening of the jet as y and d increase.)

(1) It will tend to reduce any temperature gradients especially along the y direction.

(2) Because the jet extends to the periphery of the orifice plate where the surrounding air is cooler, the effect of turbulent mixing and entrainment from these regions will be to cool the jet.

Both the above effects will increase with d. An inspection of the vertical, y, scans corresponding to unheated free jets in Chapter 7 shows that for a given free jet velocity and surface temperature the average WIS jet temperature decreases with d as does the temperature gradient in the y direction.

An examination of the $_V\tau_L$ and $_V\tau_S$ best fit plots shows that the slope of the d = 4.1 cm plot is the lowest and indeed becomes negative in the large WIS jet for V_B = 70 V and 40 V, implying that

in these cases the turbulent mixing effect swamps the effect of increasing WIS jet temperature with y due to heat transfer from S. The radiation effects discussed earlier may or may not influence the value of $\frac{dX}{dT_{mod}}$.

LINEAR BEST FIT PLOTS OF $_{V}\tau_{(S-L)}$ VERSUS T_{mod}

The temperature dependent parameter $_{V}\tau_{(S-L)}$ in these plots, Fig. 116 corresponds to the difference between $_{V}\tau_{S}$ and $_{V}\tau_{L}$, where the latter may be considered as the average, y, temperature gradients in the small and large WIS jets respectively within the limits y = 0 cm and y = 5 cm.

It has been shown that $_{V}\tau_{S}$ should be greater than $_{V}\tau_{L}$, the values of each increasing with T_{mod}. Thus $_{V}\tau_{(S-L)}$ should increase with T_{mod}. However, the variation of $\frac{dX}{dT_{mod}}$ with d is somewhat unpredictable and even becomes negative in some cases. The smaller values of d do tend to have the steepest slopes however.

Table 5 shows the residual standard deviation on T_{mod} for the vertical scans.

As in Table 4a there are no strong correlations between residual standard deviations and V_B, d or X apart from the fact that the largest values of d tend to have high residual standard deviations. And for $_{V}\tau_{S}$ the residual standard deviation tends to increase with d. For given values of d and V_B the R.S.D's in Table 5 tend to be higher than those in Table 4a (with a few exceptions) particularly for V_B = 40 V and d = 4.1 cm. Fig. 117 shows the experimental points for $_{V}\tau_{L}$ vs P_L. In this case the spread in $\frac{dX}{dT_{mod}}$ for d = 1.1 cm and d = 4.1 cm is much too large to have arisen from temperature turbulence and it is

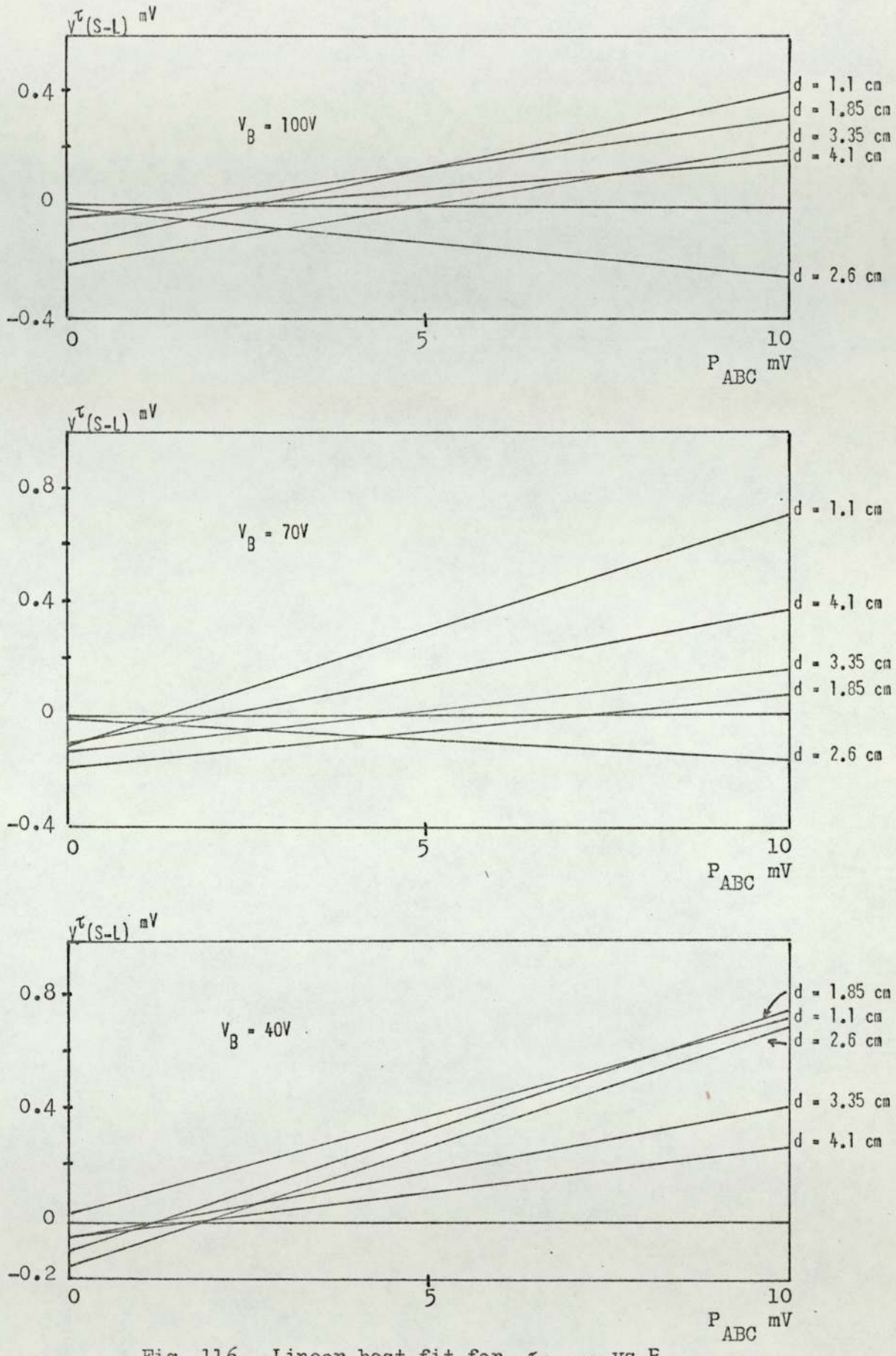

Fig. 116. Linear best fit for $V^{\tau}(S-L)$ vs P_{ABC}

TABLE 5

RESIDUAL STANDARD DEVIATIONS ON T_{mod} FOR MEASUREMENT MADE IN THE VERTICAL PLANE

V_B = 100 V	d=1.1	d=1.85	d=2.6	d=3.35	d=4.1
V^{τ}_L	507	82	403	1366	2965
V^{τ}_S	202	105	741	911	1330
$V^{\tau}(S-L)$	843	914	826	3176	1721

V_B = 70 V	d=1.1	d=1.85	d=2.6	d=3.35	d=4.1
V^{τ}_L	1486	371	425	3118	2258
V^{τ}_S	214	151	858	664	683
$V^{\tau}(S-L)$	607	3557	2086	2662	1268

V_B = 40 V	d=1.1	d=1.85	d=2.6	d=3.35	d=4.1
V^{τ}_L	1173	248	3192	3163	2134
V^{τ}_S	158	211	706	868	3390
$V^{\tau}(S-L)$	1009	281	463	270	2197

All values of d are in cm.

All R.S.D's are in units of 10^{-3} mV.

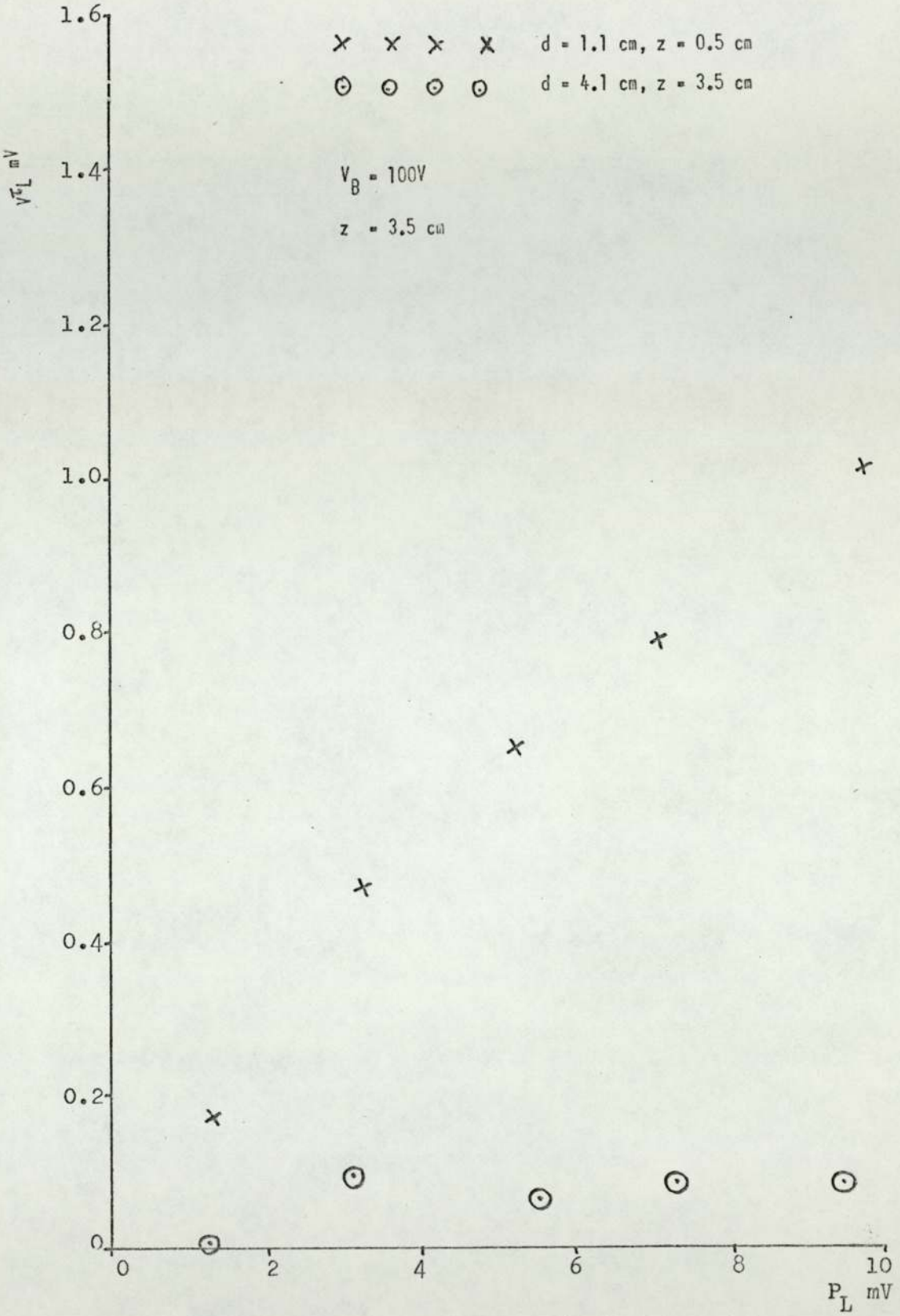

Fig. 117. $V\tau_L$ vs P_L for unheated free jets

probable that the cooling of the WIS jet due to turbulent mixing has a major influence on the very large spreads of $\frac{dX}{dT}_{mod}$ in these plots and others examined in this section.

CHAPTER 10

ANALYSIS OF LINEAR BEST FIT PLOTS OF SURFACE TEMPERATURE, P, VERSUS HEATED FREE JET TEMPERATURE T_J WHEN X = 0

Introduction

Before examining the individual curves in this set in detail it is helpful, in assisting in their interpretation, to discuss a few general characteristics and to examine the way in which the curves were derived.

The primary purpose of this mode of operation was to predict surface temperature P by identifying a state of zero nett heat transfer between the surface, S, and the air flowing over it in the form of a wall jet.

Figs. 118 and 119 show the variation of normalized temperature dependent parameters $_V\theta_L$ and $_V\tau_L$ with free jet temperature for two values of d. It is seen that $\frac{dX}{dT_J}$ is negative, a result which is to be expected on physical grounds, since the heat transfer from S to the wall jets will be proportional to the temperature differential between the two. It is seen that for d = 1.1 cm in Fig. 118 both $_V\theta_L$ and $_V\tau_L$ intercept on the free jet temperature axis T_J at a point close to P. On the other hand for d = 4.1 cm in Fig. 119 the point of interception has a value of free jet temperature considerably lower than P, as well as there being a much greater differential between $\frac{dX}{dT_J}$ for $_V\theta_L$ and for $_V\tau_L$. The value of T_J corresponding to this intercept will subsequently be denoted by T_o.

The reasons for these characteristics will be discussed later.

A small, but important, distinction must be made at this point when considering plots relating to $_V\theta_L$ and $_V\theta_S$, and those relating to

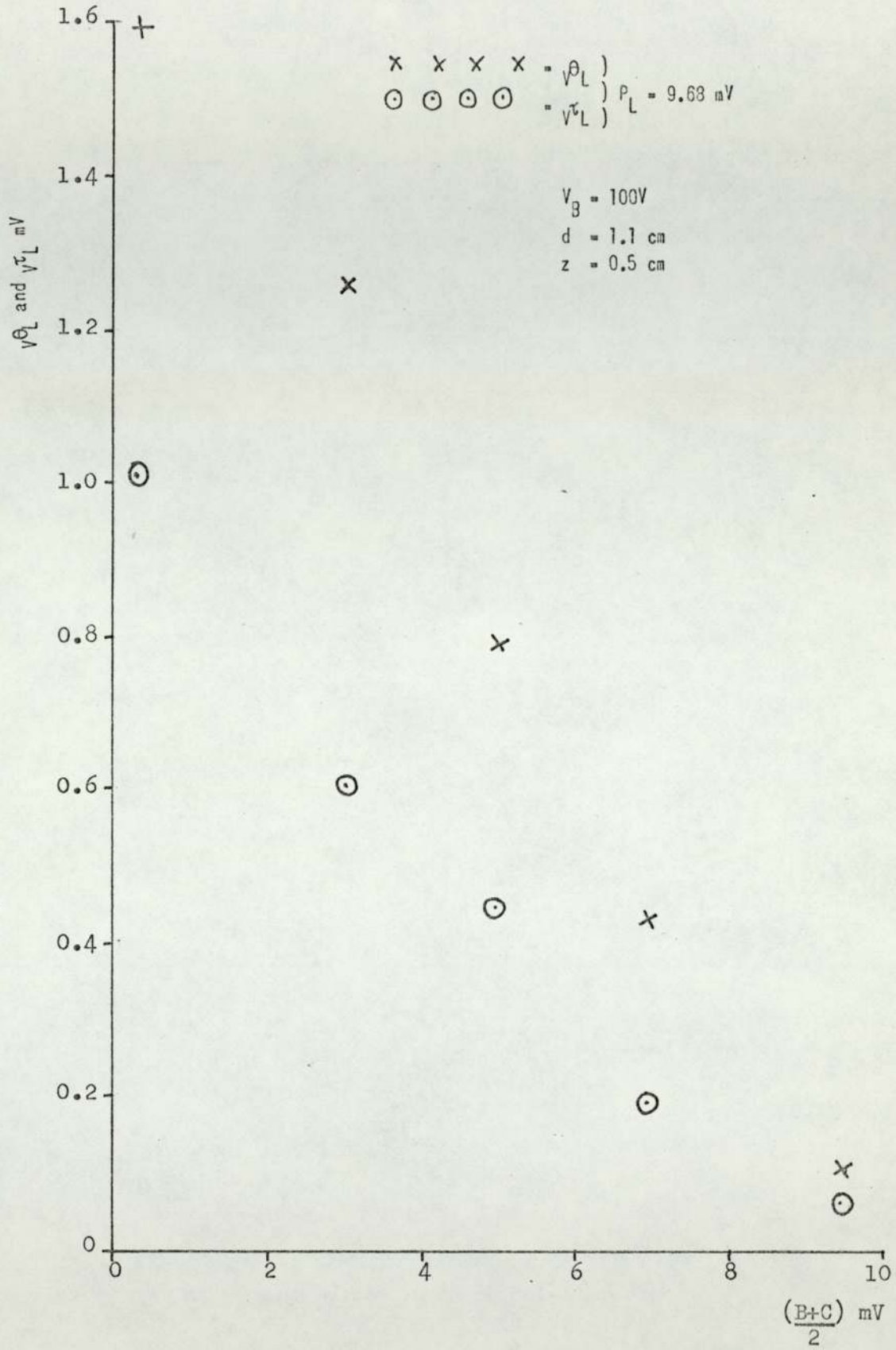

Fig. 118. V^{θ}_L and V^{τ}_L vs $\frac{(B+C)}{2}$

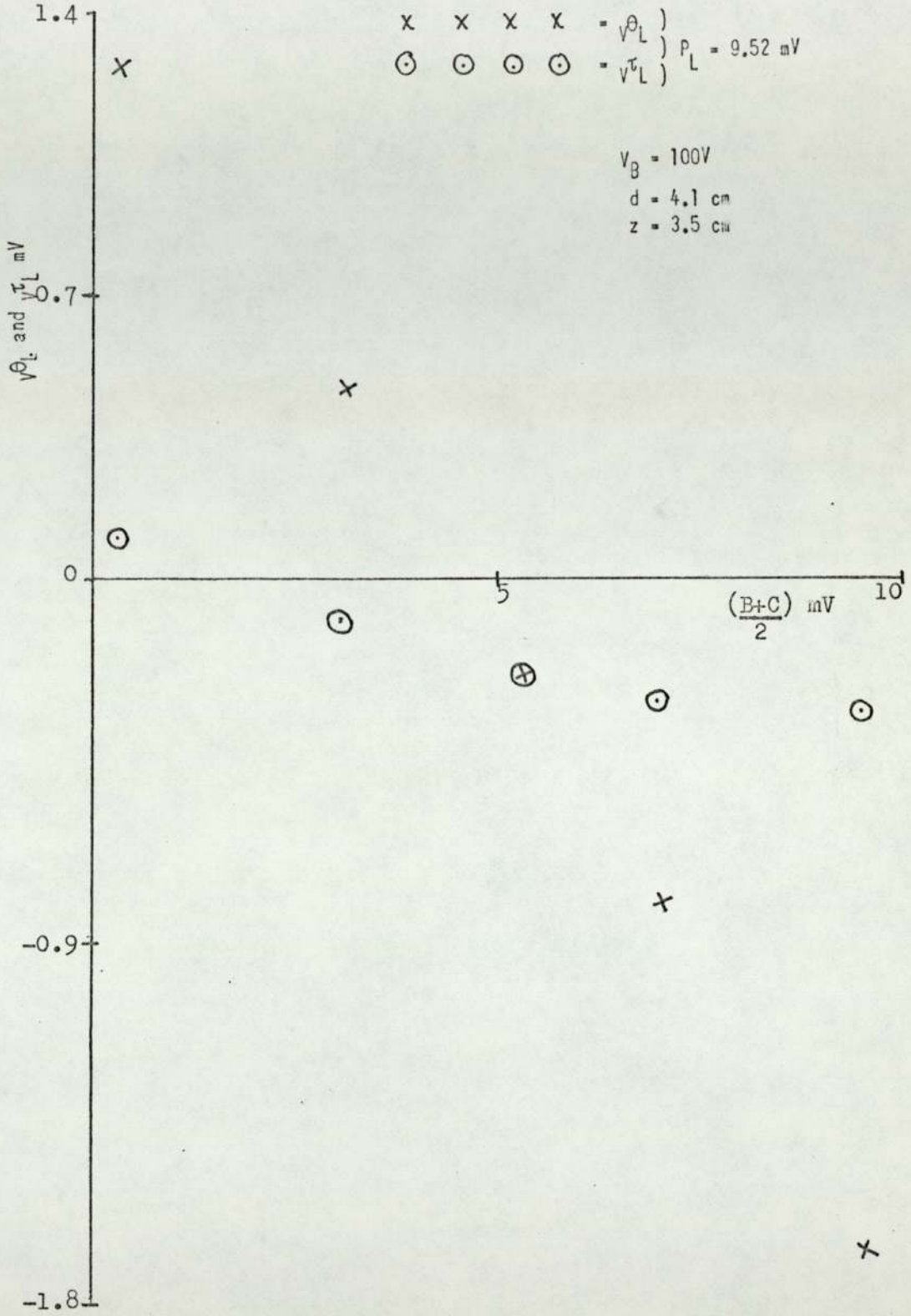

Fig. 119. $V\theta_L$ and $V\tau_L$ vs $\frac{(B+C)}{2}$

the remaining temperature dependent parameters. In the former case the reference temperature involved in the temperature dependent parameters is the free jet temperature measured close to the orifice. The difference between T_o and P in this case will be equal to the difference between the WIS jet temperature T_A and P since when X = 0 $T_A = T_J$ thus $T_A = T_o$.

For the other temperature dependent parameters, however, the free jet does not form the reference temperature and a value of X = 0 (giving an intercept on the free jet axes at T_o) will not necessarily imply that T_o = the WIS jet temperature, and in fact, due to attenuation in the free and WIS jets, T_o will usually be greater than the WIS jet temperature T_A.

In this section a 'balance' will imply a zero value of X and the 'error in balance' will represent the difference between an appropriate average free jet temperature, T_J, and the surface, P, under balance conditions.

In order to compare the errors in balance for different forms of X and with different values of d and V_B a series of linear best fit plots of P vs T_o were generated.

Only those plots with a slope of unity, i.e. $\frac{dP}{dT_o} = 1$ will have a zero error in balance. A value of $\frac{dP}{dT_o} > 1$ will be indicative of a free jet temperature less than the surface temperature at balance.

Linear Best Fit Plots of P vs T_o for $_V\theta_L$ and $_V\theta_S$

An examination of the above best fit plots shown in Figs. 120 and 121 will indicate that in all cases the error in balance increases with d. For small values of d this error is very small since $\frac{dP}{dT_o}$ is close to unity but increases quite significantly for values of d

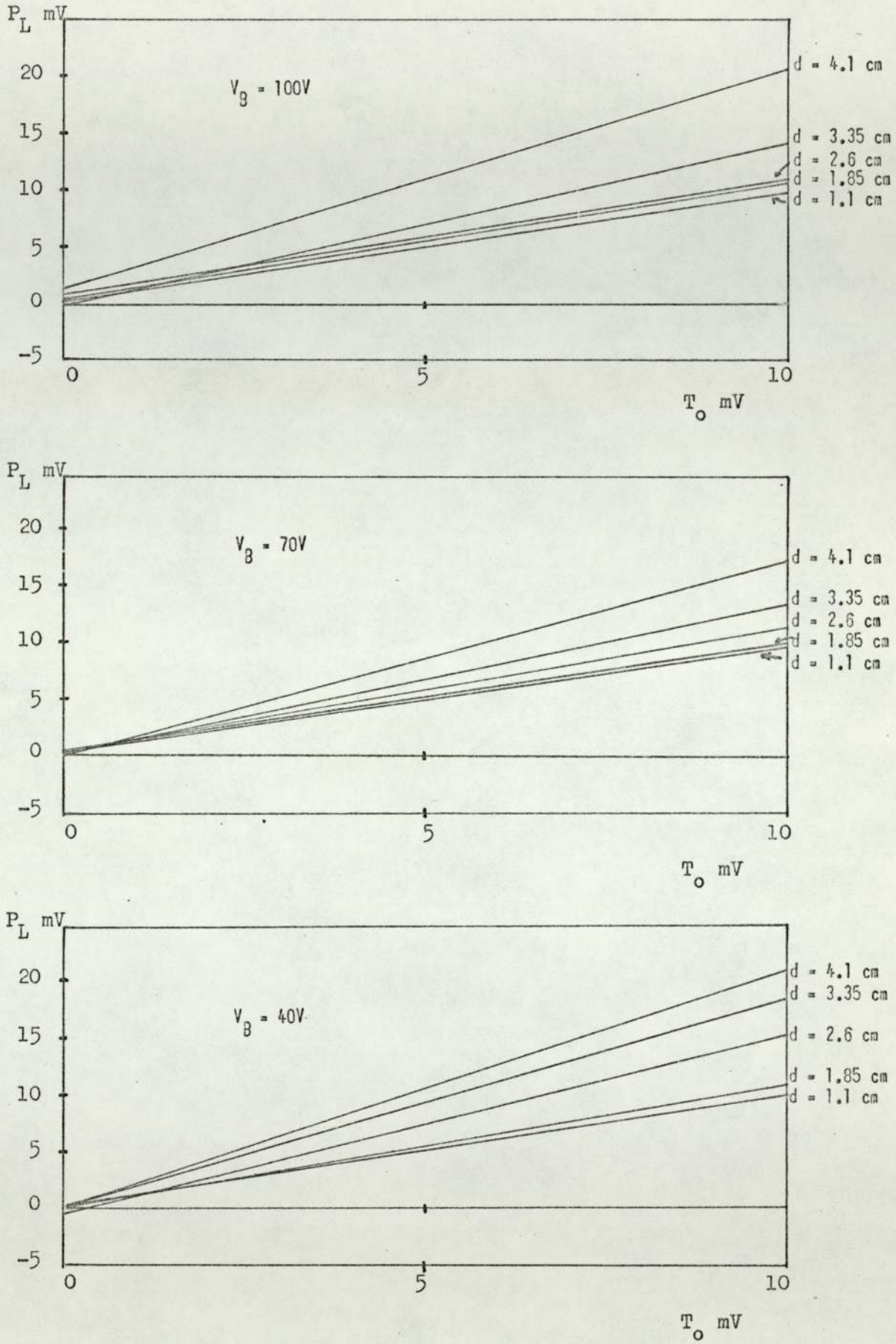

Fig. 120. Linear best fit for P_L vs T_o for $X = {}_V\theta_L$

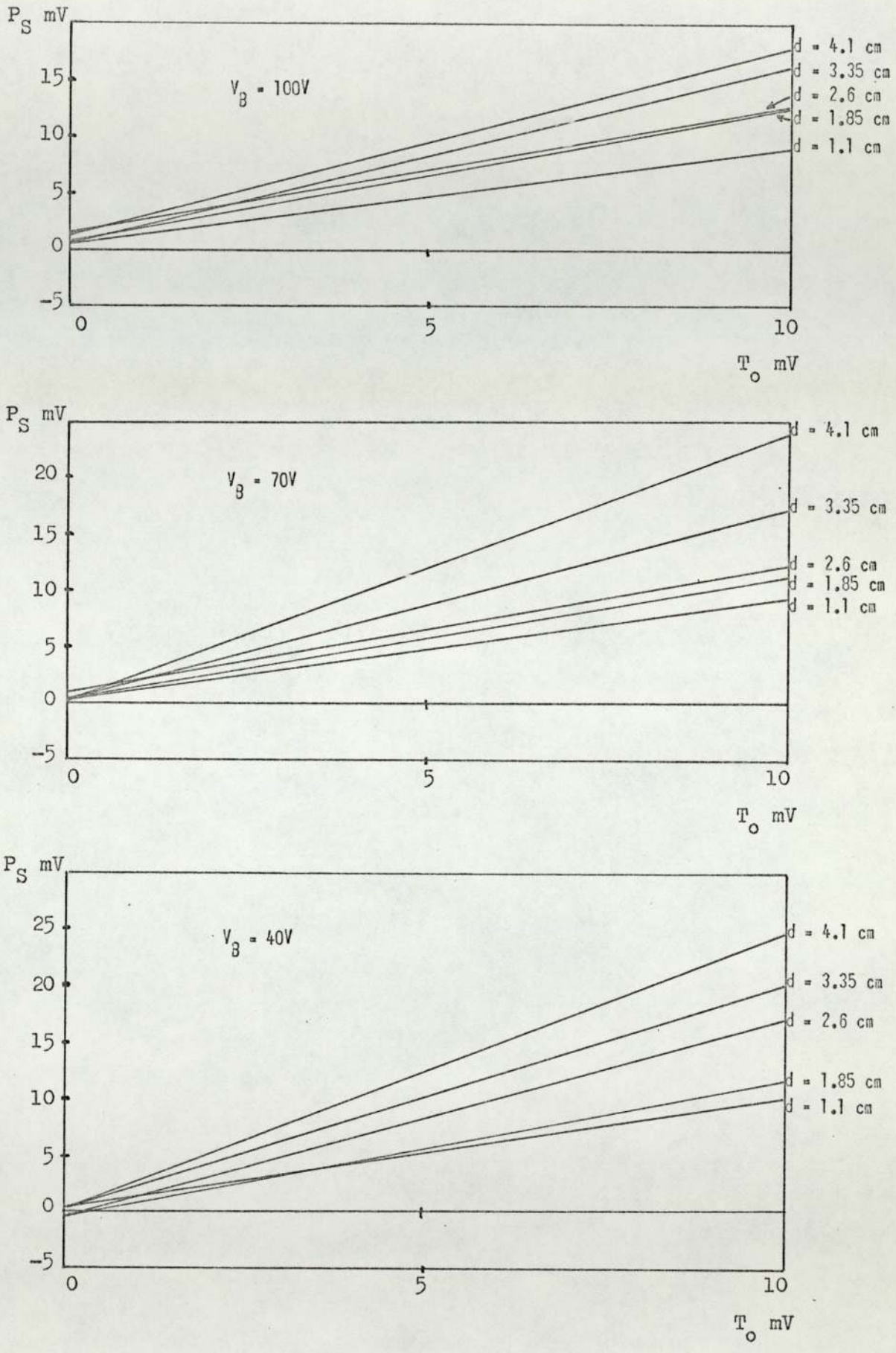

Fig. 121. Linear best fit for P_S vs T_o for X = $_V\theta_S$

appraching 4.1 cm. For ${}_V\theta_L$ the overall spread in $\frac{dP}{dT_o}$ with d is least for V_B = 70 V.

For ${}_V\theta_S$ this spread increases as V_B decreases.

Linear Best Fit Plots of P vs T_o for ${}_V\theta_{(L-S)}$ and $F_{(1+2)}$

These plots are shown in Figs. 122 and 123.

As for the above parameters the error in balance is smallest for d = 1.1 cm and apart from the V_B = 40 V plots is greatest for d = 4.1 cm. However, for these plots the value of $\frac{dP}{dT_o}$ is not so simply related to d as for ${}_V\theta_L$ and ${}_V\theta_S$ where it increases with d. It is interesting to note the very small spread in slope for V_B = 70 V. Note both these parameters give rise to very similar best fit plots.

This is not surprising since any variation only arises from a difference in free jet temperatures A and C and in general this difference is small.

The mechanisms responsible for the variations of $\frac{dP}{dT_o}$ in all these horizontal plots are probably similar to those in the unheated free jet plots. Thus it can be seen that a correlation exists between the error in balance and d. Since turbulent mixing resulting in jet cooling becomes more significant with d, it is likely that this has a strong influence on the errors in balance.

Under true Z.N.H.T. conditions as d decreases perfect black body conditions are approached and radiation effects become less significant, this is partly reflected in the small error associated with the d = 1.1 cm plots. As d increases the departure from perfect black body conditions increases and the significance of radiation effects similar to those discussed for the unheated free jets increases, i.e. geometrical and convective heat transfer effects. (The latter,

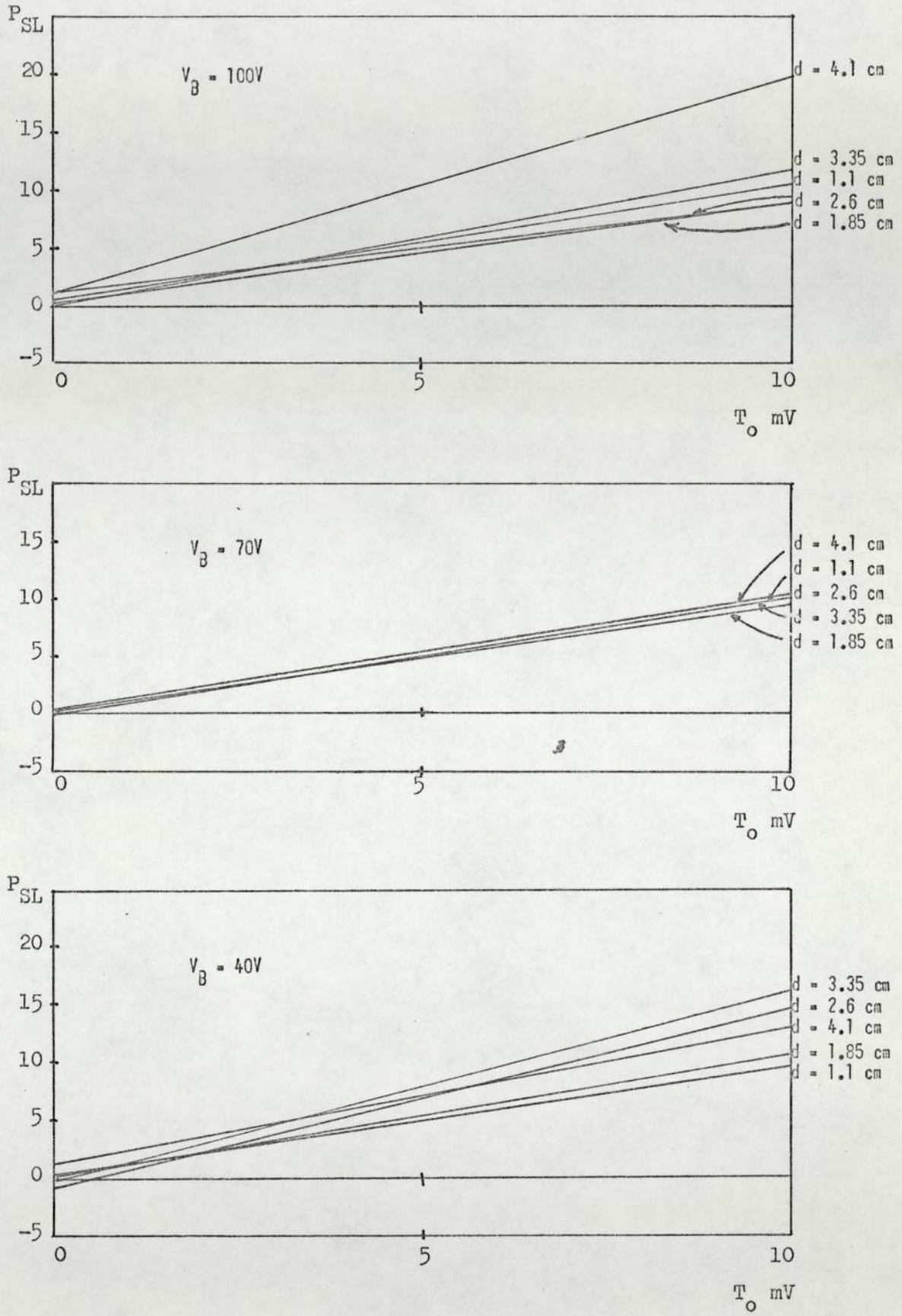

Fig. 122. Linear best fit for P_{SL} vs T_o for $X = V^{\theta}(L-S)$

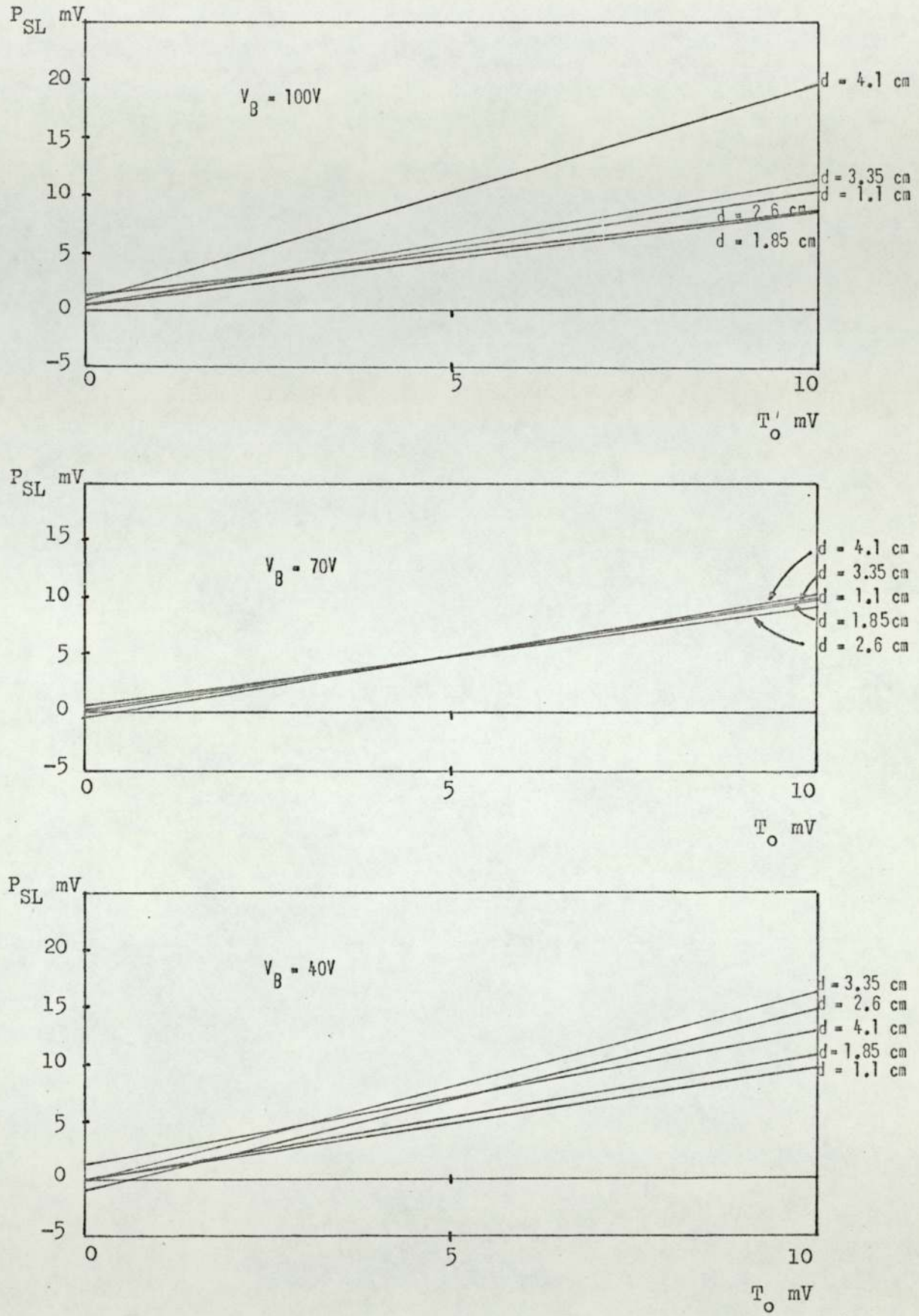

Fig. 123. Linear best fit for P_{SL} vs T_o for $X = F_{(1+2)}$

however, will not be as pronounced for the heated free jets.) These radiation effects are likely to be greatest in the temperature dependent parameters which involve the WIS jet and the free jets ($_{V}\theta_{L}$ and $_{V}\theta_{S}$), since higher differential convective heat transfer coefficients will exist between these jets. For $_{V}\theta_{(L-S)}$ and $F_{(1+?)}$ the reference temperature is effectively the small WIS jet temperature (apart from the slight influence on $_{V}\theta_{(L-S)}$ of free jet temperatures if a difference exists between A and C). The result of this is that the convective heat transfer coefficients will be closer thus any differential radiation effects will be smaller.

In one or two cases for small values of d, particularly for $_{V}\theta_{(L-S)}$ and $F_{(1+2)}$ in which V_B = 100 V a value of $\frac{dP}{dT_o}$ slightly less than unity exists. This implies that T_o > P at balance. Because the effect does not persist for the larger values of d (i.e. 3.5 cm and 4.1 cm) the likelihood of its being due solely to differential cooling in the large and small WIS jets, is small.

Table 6 shows the R.S.D. on T_o associated with these linear best fit plots. It must be noted that as well as absorbing any experimental scatter they also absorb any non-linearity which may exist in the relationship between P and T_o. It is seen that the largest values of d tend to have relatively large values of R.S.D. (with one or two exceptions) this being particularly evident for the case of V_B = 40 V.

Linear Best Fit Plots of P vs T_o Employing Temperature Dependent Parameters Derived From Measurements in the Vertical Plane, i.e. $_{V}\tau_{L}$, $_{V}\tau_{S}$ and $_{V}\tau_{(S-L)}$

The above plots are shown in Figs. 124, 125 and 126.

As for the parameters corresponding to measurements in the

TABLE 6

RESIDUAL STANDARD DEVIATIONS ON T FOR MEASUREMENTS MADE IN THE HORIZONTAL PLANE

V_B=100 V	d=1.1 cm	d=1.85 cm	d=2.6 cm	d=3.35 cm	d=4.1 cm
V^{θ}_L	203	57	180	443	606
V^{θ}_S	309	499	1077	420	865
$V^{\theta}_{(L-S)}$	104	235	957	996	846
$F_{(1+2)}$	115	345	1095	611	583

V_B=70 V	d=1.1 cm	d=1.85 cm	d=2.6 cm	d=3.35 cm	d=4.1 cm
V^{θ}_L	334	99	329	857	223
V^{θ}_S	122	207	621	520	1335
$V^{\theta}_{(L-S)}$	693	192	330	417	229
$F_{(1+2)}$	201	219	493	593	612

V_B=40 V	d=1.1 cm	d=1.85 cm	d=2.6 cm	d=3.35 cm	d=4.1 cm
V^{θ}_L	114	564	685	723	557
V^{θ}_S	305	808	733	635	1522
$V^{\theta}_{(L-S)}$	129	476	576	1021	1338
$F_{(1+2)}$	171	433	676	912	1414

All R.S.D's are expressed in terms of mV x 10^{-3}

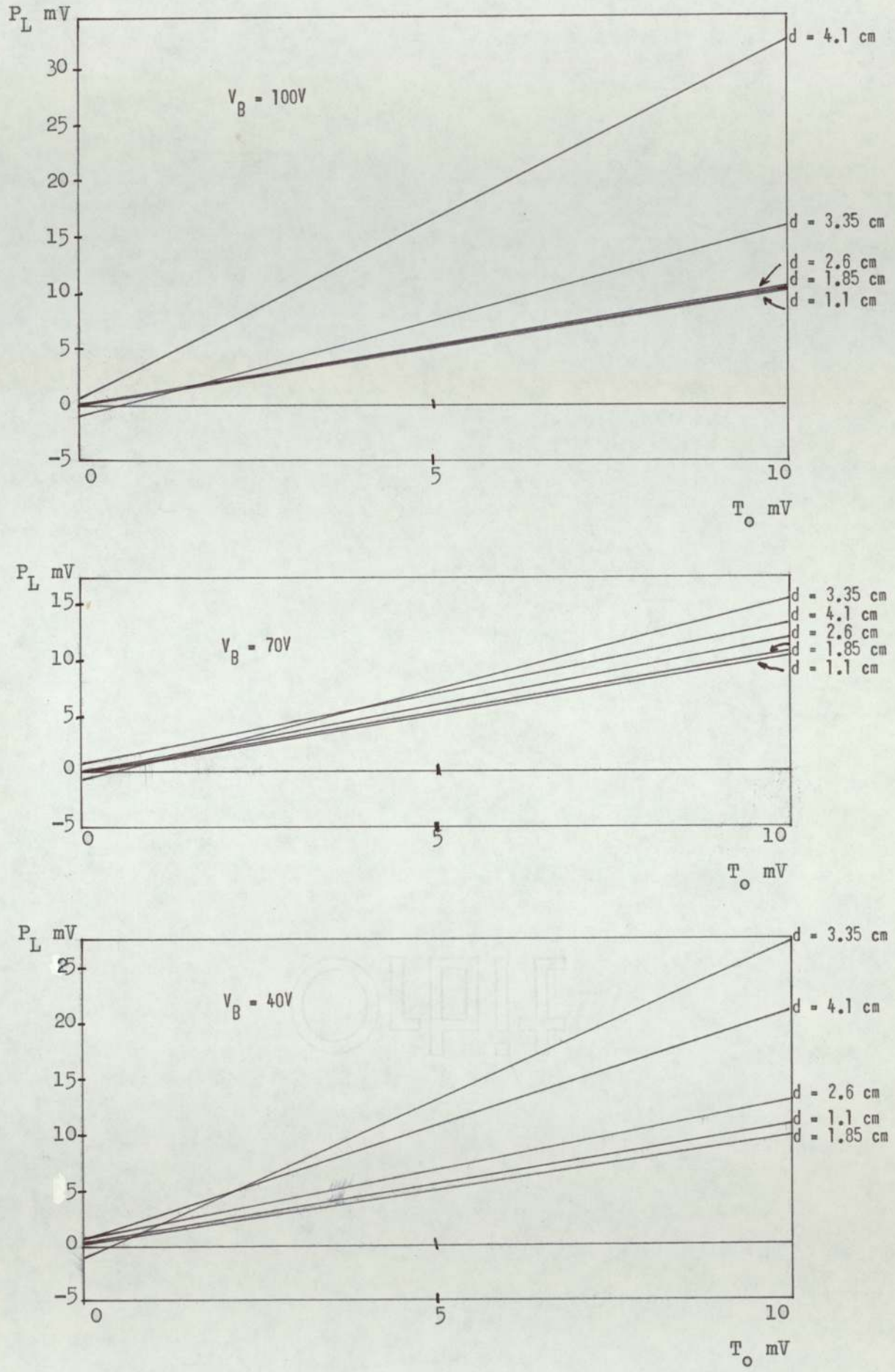

Fig. 124. Linear best fit for P_L vs T_o for $X = V^{\tau}_L$

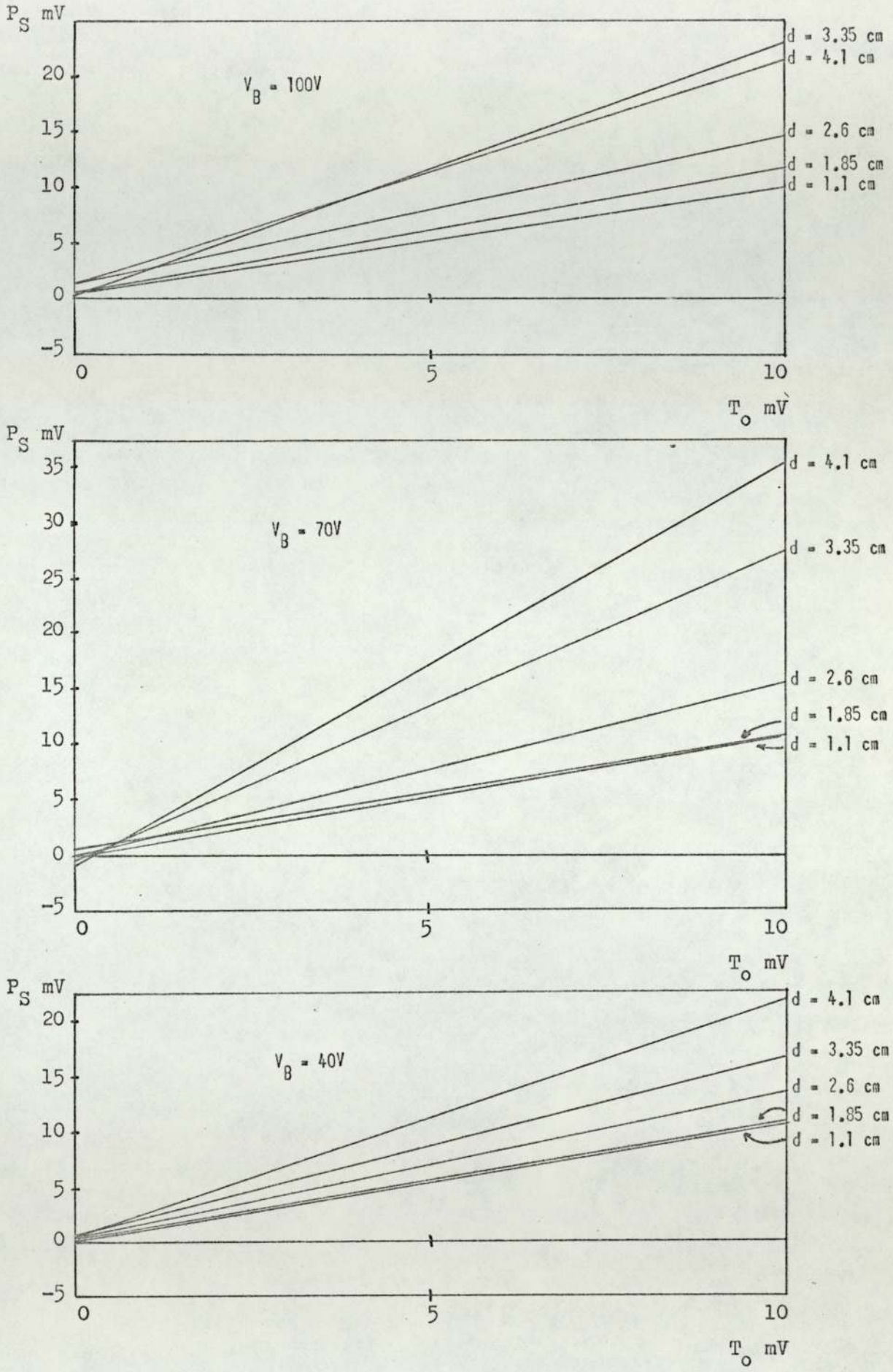

Fig. 125. Linear best fit for P_S vs T_o for $X = {}_V\tau_S$

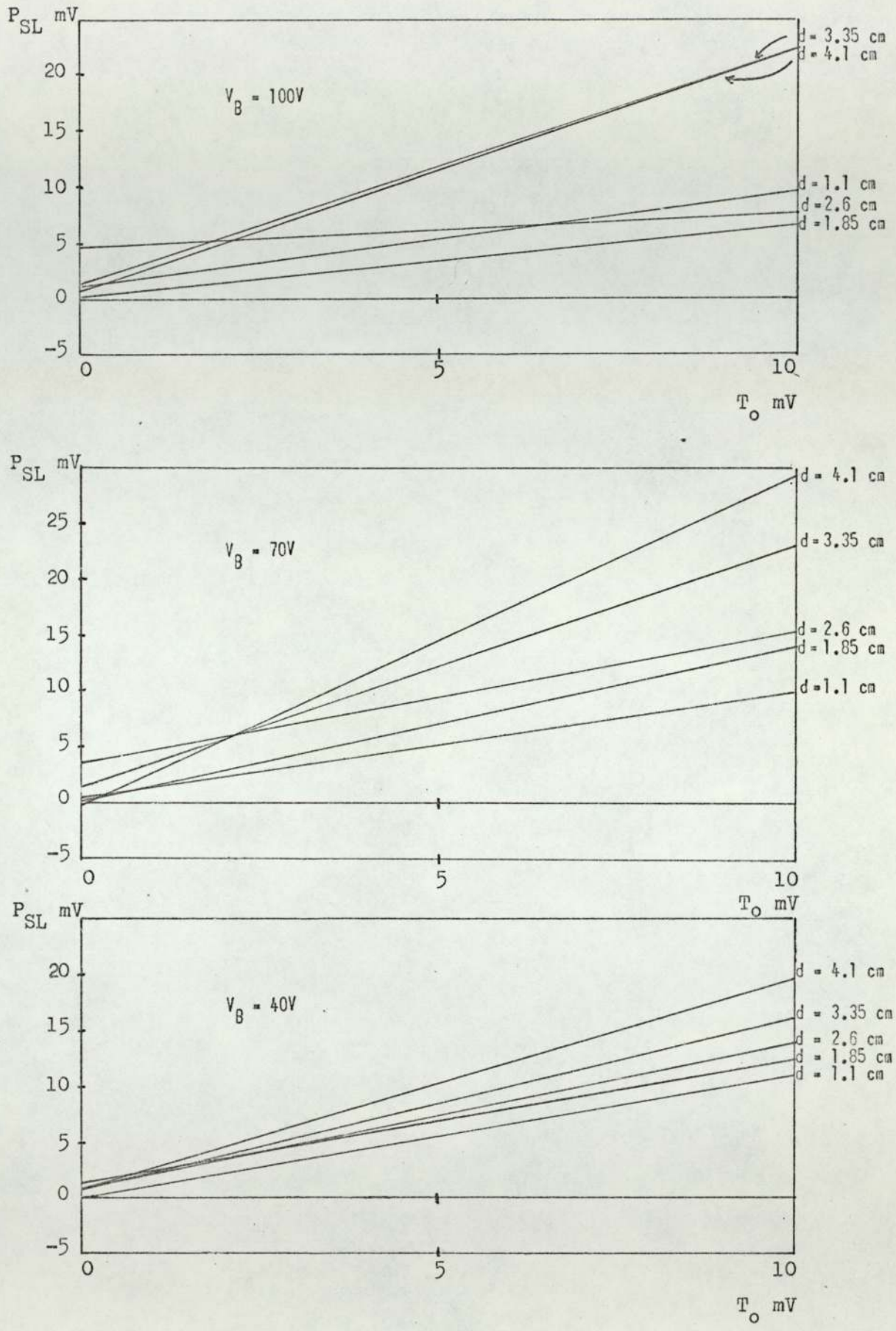

Fig. 126. Linear best fit for P_{SL} vs T_o for X = $V^{\tau}(S-L)$

horizontal plane the error in balance is small for small values of d and $\frac{dP}{dT_o}$ is close to unity for d = 1.1 cm in all cases. Apart from $V^{\tau}(S-L)$ in no case does $\frac{dP}{dT_o}$ become less than unity implying that T_o is either equal to or less than P (except for $V^{\tau}(S-L)$).

None of these temperature dependent parameters have the free jet temperatures as a reference temperature and the convective heat transfer coefficients between the two thermo-couples in the WIS jet (displaced in the y direction) are likely to be closer than between either thermo-couple and one in the free jet. Thus any radiation effects will be small for this reason but there could still be a geometrical effect which would increase with d. If perfect black body conditions prevailed then under true Z.N.H.T. conditions, i.e. when the free and WIS jets were both equal to P, the radiation effects would disappear.

As d increases the significance of radiation leakage from between the plates increases and the thermo-couple at y = 5 cm will intercept a smaller radiation flux than that at y = 0 cm. This will tend to reduce the temperature of the thermo-couple at y = 5 cm to below that at y = 0 cm. The effect will be compensated for to a certain extent in the smaller convective heat transfer coefficient associated with the thermo-couple at y = 5 cm.

As for the unheated free jets the effect of increasing d will be to decrease the average temperature of the WIS jet and also decrease the average value of $\frac{dT}{dy}$ (i.e. the temperature gradient along the WIS jet in the y direction).

Because the air temperatures involved in these Z.N.H.T. scans are considerably higher than those of the unheated free jet scans (and because $\frac{dT}{dy}$ is lower for the higher free jet temperatures for a given

value of P) the effects of turbulent mixing with cooler air will be correspondingly more significant.

An inspection of the vertical scans with the free jet temperatures approaching P shows that $\frac{dT}{dy}$ in fact becomes negative. This negative gradient increases slightly as V_B decreases. However, the significance of d is very much greater, with $\frac{-dT}{dy}$ increasing with d as well as the temperature becoming very turbulent.

This turbulent mixing effect is probably the most significant factor in influencing errors in balance.

The plots for $V^{\tau}(S-L)$ show the same sort of trend of increasing error in balance with d as existed with $V^{\tau}L$ and $V^{\tau}S$.

Table 7 shows the residual standard deviation for these plots involving measurements made in the vertical plane.

As with the residual standard deviations associated with $V^{\theta}L$, $V^{\theta}S$, $V^{\theta}(L-S)$ and $F(1+2)$, for $V^{\tau}L$, $V^{\tau}S$ and $V^{\tau}(S-L)$, the lower residual standard deviations tend to correspond with the low values of d. As d is increased further, however, there is little correlation between residual standard deviation and d. This may partly be due to the effects of temperature turbulence.

THE VARIATION OF WIS JET TEMPERATURE WITH CORRESPONDING FREE JET TEMPERATURE

In the last section errors in balance for the different forms of X and combinations of V_B and d were examined. The purpose of this heated free jet mode of operation was to predict surface temperature by measuring air temperature (in this case the free jet temperature) under balance conditions. Thus the smaller the error in balance, the more accurate the prediction.

TABLE 7

RESIDUAL STANDARD DEVIATIONS ON T_o FOR MEASUREMENTS MADE IN THE VERTICAL PLANE

V_B=100 V	d=1.1 cm	d=1.85 cm	d=2.6 cm	d=3.35 cm	d=4.1 cm
$V^{\tau}L$	206	72	270	807	3012
$V^{\tau}S$	228	225	1057	287	1997
$V^{\tau}(L-S)$	728	848	3809	2156	1126

V_B=70 V	d=1.1 cm	d=1.85 cm	d=2.6 cm	d=3.35 cm	d=4.1 cm
$V^{\tau}L$	51	152	229	632	835
$V^{\tau}S$	267	210	363	1631	1797
$V^{\tau}(L-S)$	438	1418	3273	2466	1301

V_B=40 V	d=1.1 cm	d=1.85 cm	d=2.6 cm	d=3.35 cm	d=4.1 cm
$V^{\tau}L$	237	133	1467	857	1871
$V^{\tau}S$	165	311	429	1165	962
$V^{\tau}(L-S)$	170	763	567	1291	876

All R.S.D's are expressed in terms of mV x 10^{-3}

An alternative procedure would have been to measure WIS jet temperature under balance conditions and predict surface temperature from this measurement. In fact this has been effectively done in the last section for $_{V}\theta_{L}$ and $_{V}\theta_{S}$ where the free jet temperature forms the reference temperature in X.

It has been indicated, however, that for the other temperature dependent parameters a balance does not necessarily imply an equality between the free and WIS jet temperatures. The temperature differential between the free and corresponding WIS jets at balance will therefore be examined for one or two of the temperature dependent parameters. Since any such temperature differentials are likely to increase with surface temperature P the following discussion will be confined to relatively large measured values of P.

Figs. 127-129 show the variation of large WIS jet temperature $\frac{E_1+E_2}{2}$ with corresponding free jet temperature for V_B = 100 V, 70 V and 40 V and values of d = 1.1 cm, 2.6 cm and 4.1 cm.

The surface temperature corresponding to each curve is denoted by $_{ave}P_L$. This relates to the large WIS jet and represents the average of five nominally equal surface temperatures each corresponding to a specific plot point for a given value of d and V_B. The values of P_L within each set of five all lay within about 1% of the corresponding average $_{ave}P_L$.

An examination of Figs. 127-129 in conjunction with the linear best fit plot of P vs T_o for $_{V}\tau_{L}$ will show that for the values of $_{ave}P_L$ dealt with the temperature differentials between the free and WIS jets at balance are negligible when d = 1.1 cm for all three values of V_B.

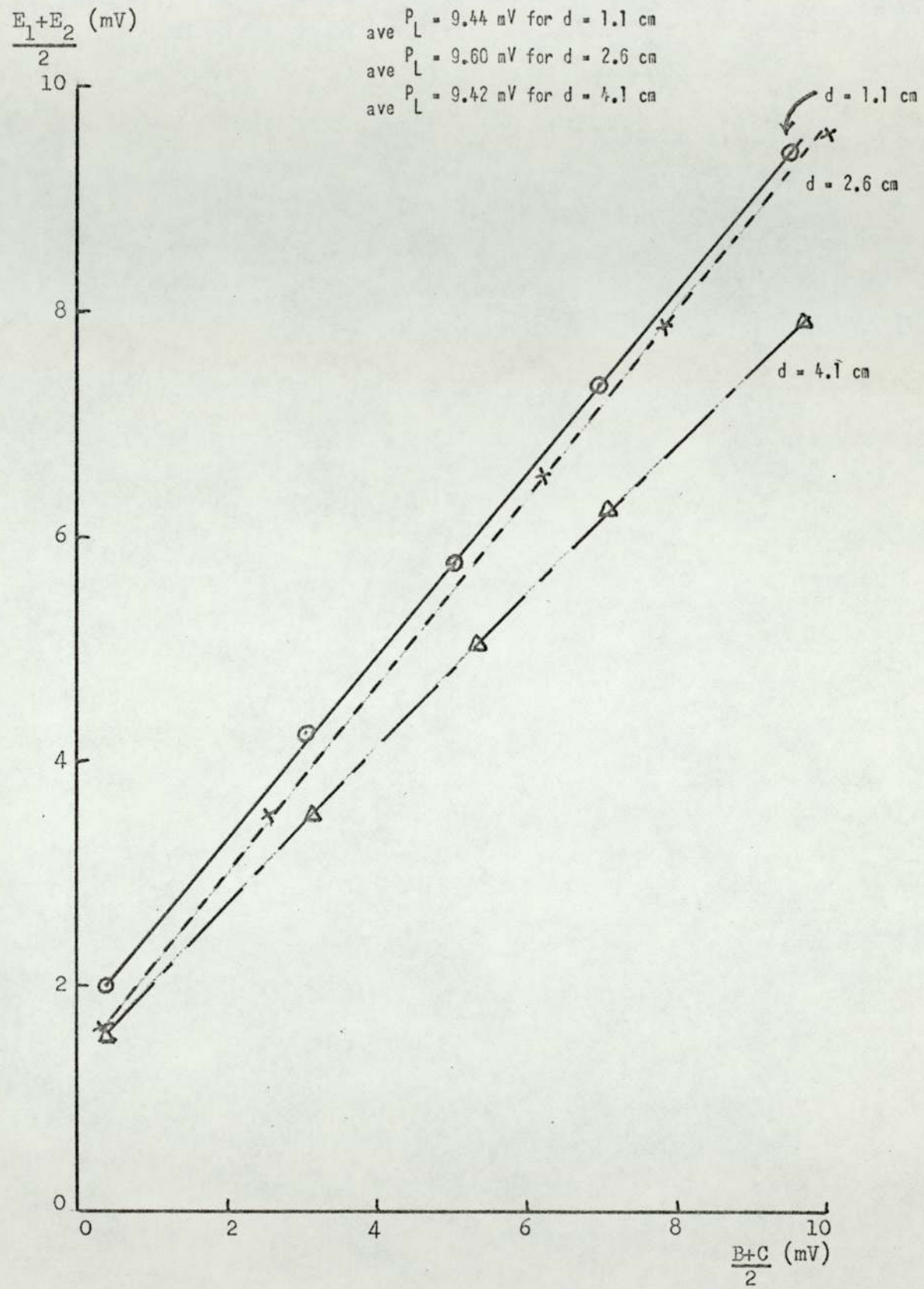

Fig. 127. Variation of $\frac{E_1+E_2}{2}$ with $\frac{B+C}{2}$ for V_B = 100V

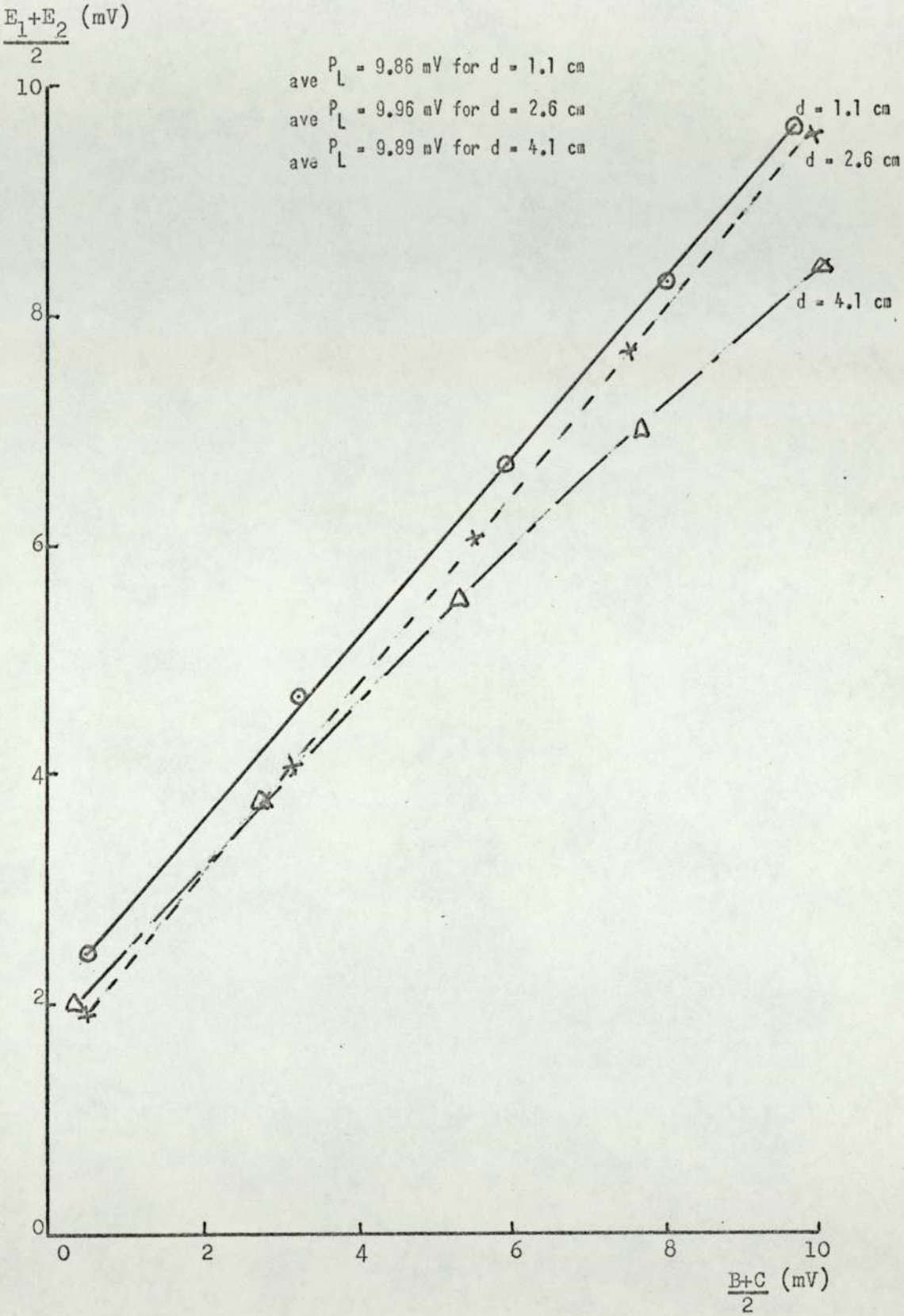

Fig. 128. Variation of $\frac{E_1+E_2}{2}$ with $\frac{B+C}{2}$ for V_B = 70V

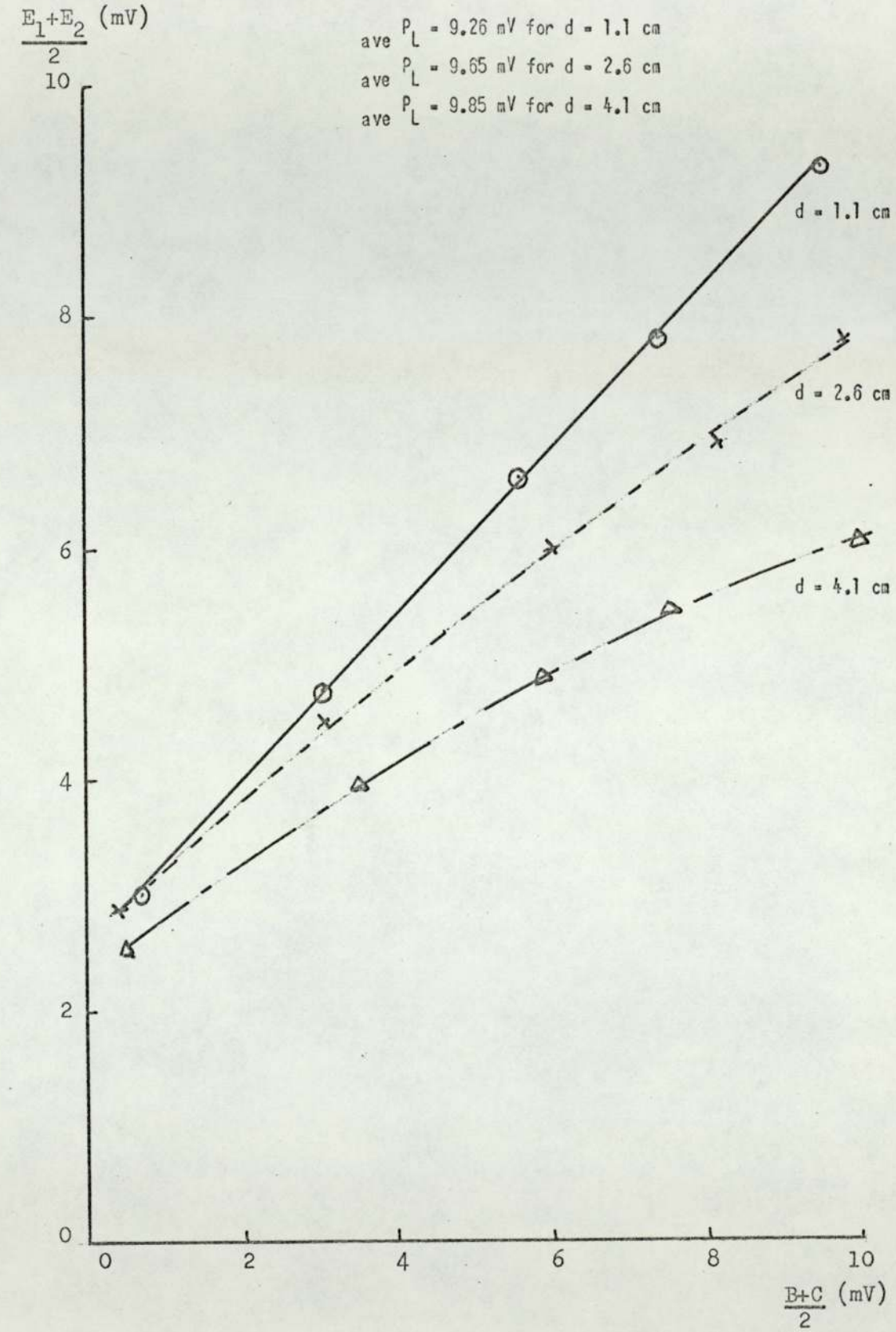

Fig. 129. Variation of $\frac{E_1+E_2}{2}$ with $\frac{B+C}{2}$ for V_B = 40V

For d = 2.6 cm and V_B = 100 V and 40 V the free jet temperatures are higher than the corresponding WIS jet temperatures at balance but for V_B = 70 V this differential is negligible.

For d = 4.1 cm and V_B = 70 V and 40 V the WIS jet temperatures at balance are lower than those of the corresponding free jets but for V_B = 100 V the WIS jet temperatures are higher than the latter.

The highest temperature differential observed corresponds to V_B = 100 V and d = 4.1 cm where the WIS jet has a temperature of about 10% greater than the corresponding free jet at balance.

Since it is found in practice that the average free jet temperature, $\frac{A+B+C}{3}$ is approximately equal to the corresponding average $\frac{B+C}{2}$ the curves in Figs. 127-129 may be used to estimate the trends in temperature differential between the free and WIS jets for $V^{\theta}(L-S)$.

Using these curves, therefore, in conjunction with the linear best fit plots of P vs T_o for $V^{\theta}(L-S)$ it was found that, once again, the differentials, at balance were negligible for d = 1.1 cm. This differential was also negligible for V_B = 100 V and d = 4.1 cm in contrast to $V^{\tau}L$ for these values of V_B and d.

All other combinations of V_B and d gave rise to free jet temperatures at balance higher than the corresponding WIS jet temperatures. For $V^{\theta}(L-S)$ the maximum temperature differential between the free and WIS jets at balance corresponded to V_B = 40 V and d = 4.1 cm where the free jet temperature was almost 20% higher than the corresponding WIS jet temperature. It is interesting to note that for this parameter with V_B = 100 V the maximum differential corresponded to a free jet temperature only 3% higher than the WIS jet temperature at balance.

The trends observed for $_{V}\theta_{(L-S)}$ will be similar for $F_{(1+2)}$.

Although the curves of WIS jet temperature vs corresponding free jet temperature have not been shown for the small WIS jet the general trends of these curves are similar to those for the large WIS jet. Thus it would be expected that the small values of d will again represent negligible temperature differentials between the free and WIS jets at balance in those temperature dependent parameters involving the small WIS jet, e.g. $_{V}T_{S}$.

To summarise, therefore, it may be concluded that negligible temperature differentials between the free and WIS jets at balance will exist for the small values of d irrespective of the value of V_B and the form of X. This of course, is consistent with the small temperature attenuation in the free and WIS jets for small values of d. For $_{V}\theta_{(L-S)}$ apart from those instances when this differential was negligible the free jet temperature at balance was always higher than the corresponding WIS jet temperature. This was also true for $_{V}T_{L}$ apart from the two exceptions where the WIS jet had a higher temperature than the corresponding free jet.

CHAPTER 11

DISCUSSION AND CONCLUSIONS

The principles underlying various non-contact temperature measuring methods have been examined, emphasis being placed on radiation pyrometry. Such methods are vulnerable to emissivity errors and various ways (some very sophisticated) of minimizing these errors have been discussed.

An attempt has been made by the author to eliminate these errors, or at least reduce their significance appreciably, by exploiting forced air convection instead of radiation in temperature measurement.

It has been seen that the former method gives rise to two modes of operation both involving passing air over the test surface. In one mode the air is initially unheated and the surface temperature is predicted from a measurement of the increase in air temperature due to heat transfer from the surface. The alternative mode involves preheating the air in order to effect a state of zero net heat transfer between the air and surface and predicting the latter's temperature from a measurement of the corresponding air temperature under these conditions.

The latter mode is absolute in that it does not require a calibration whereas the former mode involving initially unheated air does require a calibration.

The mode involving preheated air was successfully applied to the temperature measurement of 9-mm diameter stationary copper rod. Based on the original design a rig was constructed for the purpose

of measuring the temperature of continuously cast 9-mm diameter aluminium rod though at the time of writing the rig has not yet been installed. A similar design but employing the initially unheated air mode, is currently under construction for temperature measurement of extruded aluminium rod. Most of this thesis has been devoted to applying the method to temperature measurement of plane surfaces. This necessitated a different system geometry and it was appropriate to deliver air to the test surface by means of free jets.

It was found that the wall jet, i.e. the flow resulting from the impingement of a free jet directed normally onto a plane surface, was not, in itself amenable to exploitation in temperature measurement. This was due to the wall jet's small thickness and steep temperature gradients normal to the surface.

A different flow condition had to be synthesized therefore and it was found that when two wall jets were made to impinge the resulting flow condition the WIS jet, became potentially more suitable for exploitation in temperature measurement.

A simple theory was derived to describe the general structure of the WIS jet and from this a somewhat more rigorous theory was developed from which the WIS jet temperature characteristics were derived. These characteristics gave rise to several possible modes of operation of a temperature measuring device based on this forced air convection method and a theory underlying each has been developed.

It has been seen that a device may employ two or three free jets, these being heated or unheated and measurements may be made in either the horizontal or vertical planes.

Each of the above modes of operation gives rise to an associated temperature dependent parameter X with the aid of which

the surface temperature may be predicted.

A series of isothermal velocity scans was conducted involving three parallel, co-linear, asymmetrically displaced round free jets impinging normally onto a plane surface. The purpose of these was to derive the velocity characteristics appropriate to the above modes of operation and to assess the influence on these characteristics of a number of related variables.

This series of velocity scans was followed by a series of corresponding temperature scans using the same asymmetrical free jet distribution and system geometry.

The purpose of these was to derive the temperature characteristics existing between the free jet orifice plate and test surface and to assess again the influence of such variables as free jet velocity (V_B) and orifice plate - surface displacement (d) on these characteristics. For the unheated free jet mode a number of linear best fit plots of temperature dependent parameter X vs surface temperature P were generated for different values of V_B and d using data derived from the temperature characteristics.

It was found that for those parameters associated with measurements in the horizontal plane (i.e. $V^{\theta}L$, $V^{\theta}S$, $V^{\theta}L-S$ and $F_{(1+2)}$) the spread in $\frac{dX}{dP}$ was less than that for those associated with measurements in the vertical plane (i.e. $V^{\tau}L$, $V^{\tau}S$ and $V^{\tau}(S-L)$).

It has been shown that, although not usually as sensitive the temperature dependent parameters involving the highest free jet velocity (V_B = 100 V) are the least vulnerable to radiation effects since the convective heat transfer coefficient associated with the air temperature measuring thermo-couple is highest for this free jet velocity. Furthermore it has also been indicated that for these

measurements in the horizontal plane the temperature dependent parameters involving three free jets, i.e. $_{V}\theta_{(L-S)}$ and $F_{(1+2)}$ are less vulnerable to radiation effects than those involving two free jets, i.e. $_{V}\theta_{L}$, $_{V}\theta_{S}$. This is due to the smaller significance of differential convective heat transfer coefficients between the air temperature measuring thermo-couples in the former case.

It has been estimated that for thermo-couples of bead diameter 0.025 in. and emissivity 0.5 and a test surface of emissivity 0.1 (typical of oxidized aluminium) at a temperature 300°C the maximum radiation error (i.e. the radiation contribution to the temperature dependent parameter) is of the order of 15% for $_{V}\theta_{L}$ when V_B = 100 V but less than 2% for both $_{V}\theta_{(L-S)}$ and $F_{(1+2)}$ when V_B = 100 V. These figures are only approximate and are probably pessimistic but they do indicate the relative sensitivities of each parameter to radiation. These radiation effects may be further reduced by any of the following techniques:

(1) A reduction in the size of the thermo-couple bead.

(2) The inclusion of radiation shields.

(3) The measurement of air temperature with a suction pyrometer, this latter accelerating the flow round the thermo-couple resulting in an increased convective heat transfer coefficient.

Two surface velocity effects have been predicted to exist, one associated with a modification of the WIS jet flow characteristics and the other with a variation of convective heat transfer coefficient of the wall jet.

Taking both effects into account it is suggested that $_{V}\theta_{(L-S)}$ or $F_{(1+2)}$ will be less vulnerable to surface velocity effects than either $_{V}\theta_{L}$ or $_{V}\theta_{S}$.

It is seen, therefore, that for the device to operate in the unheated free jet mode the most suitable parameters to employ are either $F_{(1+2)}$ or $V^{\theta}_{(L-S)}$ both with V_B = 100 V. Since the former only requires two air temperature measuring thermo-couples, one in each of the WIS jets as opposed to four for $V^{\theta}_{(L-S)}$, $F_{(1+2)}$ is clearly the optimum parameter for the unheated free jet mode of operation.

It has been shown that so long as the surface roughness does not exceed approximately 0.01 in. its effect on temperature measurement will be insignificant.

Since this unheated free jet mode involves a certain amount of surface cooling it is best suited to measurement of moving surfaces or surfaces of fairly high thermal capacity.

A device based on the above recommendations has been constructed and used successfully to measure the temperature of continuously annealed 0.01 in. aluminium strip, this latter moving at approximately 300 ft per minute. It has been estimated that in this case the cooling effect of the device represents a reduction of strip temperature of less than 0.5%. Furthermore, the device was calibrated on a stationary surface and the effects of surface velocity of the strip have been estimated to give rise to an error in prediction of the order of 1%. This error is always positive, thus it can be easily calibrated out.

One point of caution is appropriate at this stage. It has been shown that the size of the temperature dependent parameter is proportional to the temperature differential between the impinging free jets and the surface, thus it is necessary to ensure that the free jet temperature is stabilized otherwise errors in surface

temperature prediction may arise.

The alternative mode of operation is that involving heated free jets. In this case the purpose of the air temperature measuring thermo-couples is twofold:

(1) To predict a condition of zero net heat transfer between the surface and air flowing over it.

(2) To predict surface temperature under these conditions.

In this mode, because the air and thermo-couple temperatures are close to those of the test surface and free jet orifice plate the effects of radiation will be very much lower than in the unheated free jet mode.

Any surface velocity effects arise from finite heat transfer from the surface to the wall jets. Since this heat transfer is negligible (and ideally should be zero) in this heated free jet mode these velocity effects will also be negligible.

The cooling of the surface will be negligible in this mode and the sensitivity to surface roughness even lower than the unheated free jet mode.

All temperature dependent parameters, X, give rise to small errors in balance (i.e. temperature differential between the surface and free jets when X = 0) for small values of d. This is consistent with the low temperature attenuation in the free and WIS jets for small values of d. In most cases the large values of d, i.e. 3.5 cm and 4.1 cm give rise to relatively large errors in balance.

It is recommended that if small values of d of the order of 1 cm are involved, then ${}_{V}\theta_{L}$ with V_B = 100 V would provide a suitable temperature dependent parameter to exploit in surface temperature measurement. In this case it would be appropriate

to locate the free jet orifices symmetrically about the centre of the orifice plate.

$_{V}\theta_{L}$ has the advantage of simplicity in implementation, it has the highest sensitivity to changes in surface temperature and its vulnerability to radiation from extraneous sources should be small.

If larger values of d are anticipated then a three free jet mode such as $F_{(1+2)}$ with V_B = 70 V is recommended. In this mode the error in balance is relatively small for all values of d. Note it is preferable in this case when large values of d are involved, i.e. of the order of 3 or 4 cm, to measure the free jet temperature rather than the WIS jet temperature at balance since this will give rise to higher accuracies in surface temperature prediction.

It has been seen, therefore, that the heated free jet mode of operation has several advantages over the unheated free jet mode. It is less sensitive to the effects of radiation, surface velocity and surface roughness and also produces negligible cooling of the test surface. It has the disadvantages, however, of requiring more peripheral equipment and because of the necessity to heat the free jets the measurement response time will be longer than that for the unheated free jet mode.

FUTURE WORK

More detailed experimental work is desirable to assess the exact significance on temperature measurement of the surface velocity in the unheated free jet mode with all forms of temperature dependent parameter considered.

The greatest scope for future work lies in examining

different types and configurations of free jets with the object of reducing still further the sensitivity of the predicted surface temperature to radiation and variations in d and also reducing the low frequency 'temperature turbulence' which gives rise to a relatively long measurement response time if the signal is integrated to remove this 'turbulence'.

It is hoped that this thesis has sown the seeds of a new method of non-contact temperature measurement exploiting forced air convection and guided by the results of these investigations it is anticipated that modifications, adaptions and improvements to the original designs will be made by myself and others.

APPENDIX A1

HOT WIRE ANNEMOMETER SIGNAL PROCESSING EQUIPMENT

Turbulent Mean Square Velocity Device for Measurement of Mean Square Value of the Fluctuating Component of the Annemometer Output (Corresponding to the Turbulent Component of Velocity)

The circuit for these measurements is shown in Fig. A1.1 and is built around an I.T.T. Type B54 indirectly heated thermistor.

This device consists of a thermistor bead surrounded by a small heater, both being contained in an evacuated glass capsule. When power is supplied to the heater (which is electrically insulated from the thermistor bead) it will heat up and reduce the thermistor resistance. The bead forms the active arm of a Wheatstone bridge, an inactive arm being formed by a matched thermistor of the same type, but with the heater disconnected. This latter is to minimize zero drift.

The bridge is initially balanced and when current flows in the heater of the active arm, an imbalance occurs proportional to the power dissipated in the heater. The heater resistance is only 100 Ω which presents too high a load for the constant temperature annemometer, thus a certain amount of impedance changing circuitry is included.

Mean Velocity Device for Measurement of the Mean Value of the Annemometer Output Signal Corresponding to the Mean Component of Velocity

This consists of a simple R.C. integrator followed by an emitter follower, see Fig. A1.1.

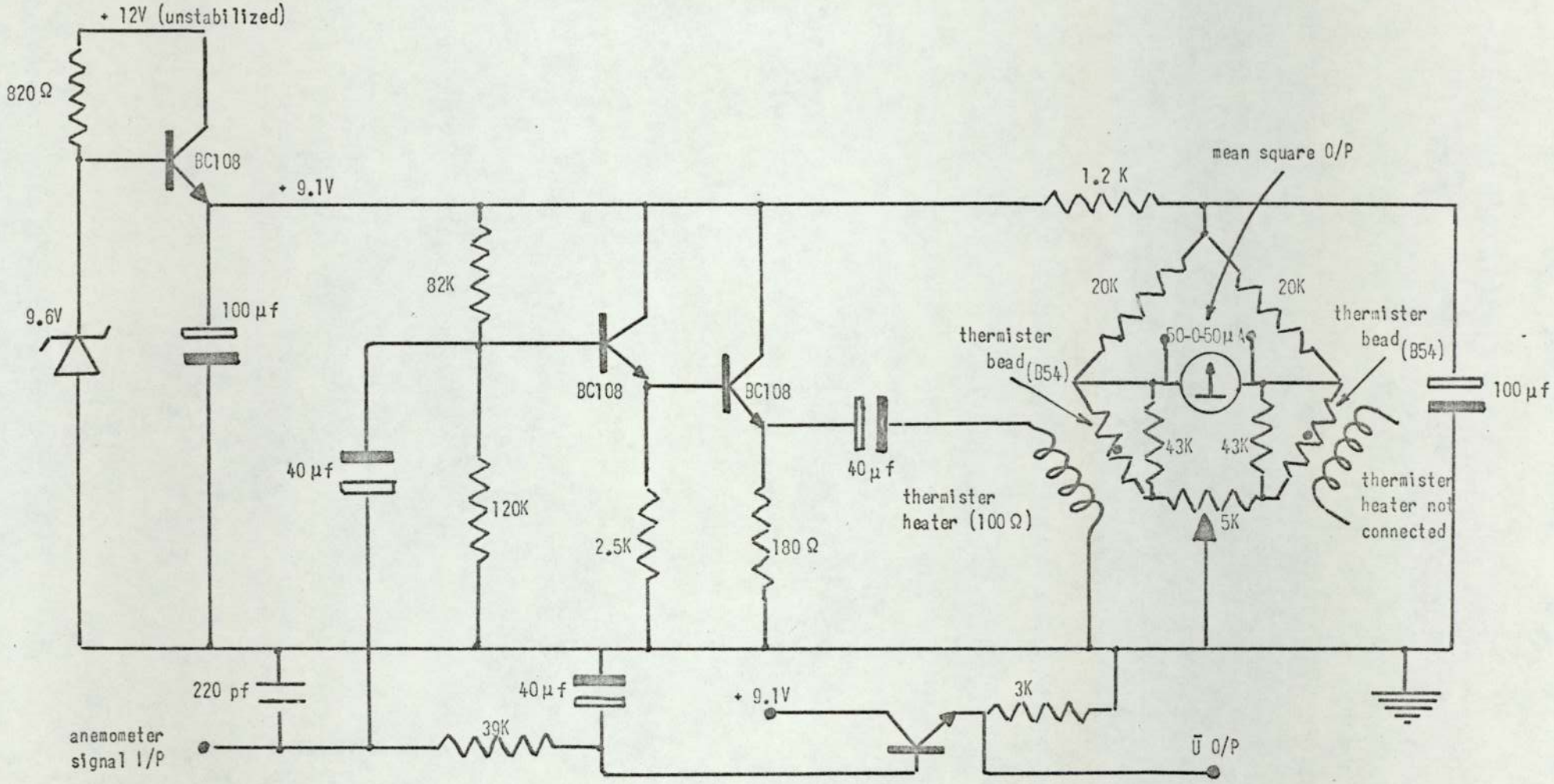

Fig. A1.1. Circuit for measuring mean square and mean velocities

THE DETERMINATION OF THE RISE AND FALL TIMES OF THE MEAN SQUARE AND MEAN VELOCITY PROCESSED SIGNALS

The Mean Square Velocity Rise Time and Fall Time

The mean square velocity signal was derived by measuring the power associated with the random fluctuations of the turbulent velocity. In order to gain more control over the levels this signal was simulated with a sine wave signal. Frequencies ranging from 15 Hz to 50 kHz were employed and the outputs corresponding to a range of step function inputs was recorded.

From a total of 52 measurements of the recorded output from the turbulent mean square measuring device a mean 'mean square' rise time was calculated to be 0.2775 minutes with a standard deviation of 0.0198 minutes.

From a total of 57 measurements of the recorded output a mean 'mean square' fall time was calculated to be 0.2812 minutes with a standard deviation of 0.0145 minutes.

The Mean Velocity Rise Time and Fall Time

The mean velocity signal was simulated with d.c. voltage levels of differing amplitude.

From a set of 36 step function inputs the mean 'mean' rise time was calculated to be 0.0994 minutes with a standard deviation of 0.0041 minutes. A similar set of 36 measurements gave rise to mean 'mean' fall time of 0.0994 minutes with a standard deviation of 0.0033 minutes.

A Method of Correcting Time Constant Errors Incurred in the Velocity Scans

As was indicated in the experimental section the horizontal, x,

scans were performed by displacing the hot wire sensor in 2-mm steps allowing 10 seconds to elapse between consecutive positions. Thus the annemometer output corresponding to a single displacement would take the form of a voltage step function, the amplitude of which would be proportional to the velocity difference between the two adjacent locations. This output voltage will, of course, have a fluctuating component if the flow is turbulent, see Fig.A1.2 for typical example.

The turbulent mean square velocity device, however, will isolate this component and it may be treated in exactly the same way as a d.c. voltage level when considering device response time.

Suppose a positive 'step' change in turbulent or mean velocity signal is applied to the appropriate signal processing device for sufficient time to allow the output to stabilize at some value A_o. Then if the same level is applied for some shorter time, t, (10 sec. in these experiments) then the device output A will be less than A_o by an amount depending upon the rise time constant of the device (see Fig.A1.3).

The value of A is given by:

$$A = A_o(1-\exp - \frac{t}{T_{rt}}) \quad \ldots\ldots\ldots\ldots\ldots\ldots\ldots\ldots\ldots \quad (A1.1)$$

where T_{rt} is the device rise time constant.

Similarly if a negative 'step' change is applied between the same levels, see Fig.A1.4, the value of A after time t will be given by:

$$A = A_o \exp - \frac{t}{T_{ft}} \quad \ldots\ldots\ldots\ldots\ldots\ldots\ldots\ldots\ldots \quad (A1.2)$$

where T_{ft} = device fall time constant.

If in this latter case A is measured from A_o then its value

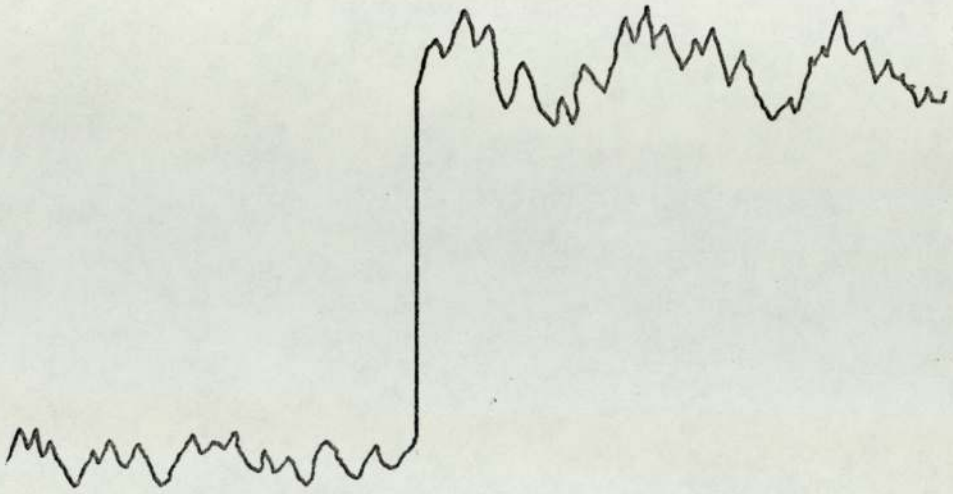

Fig. A1.2. Possible change in mean and turbulent velocity due to sensor movement

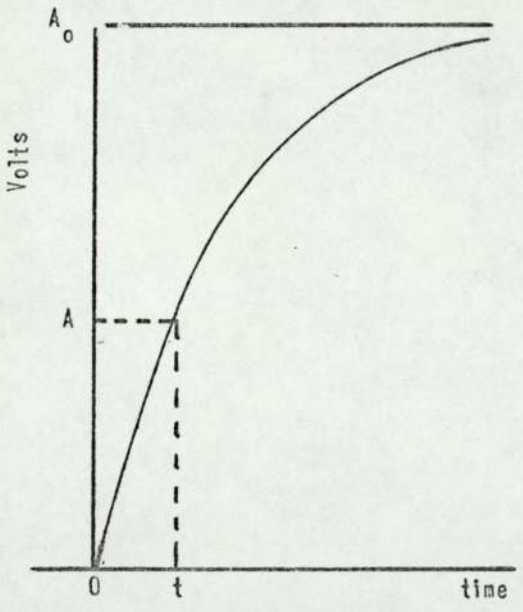

Fig. A1.3. Application of positive step input

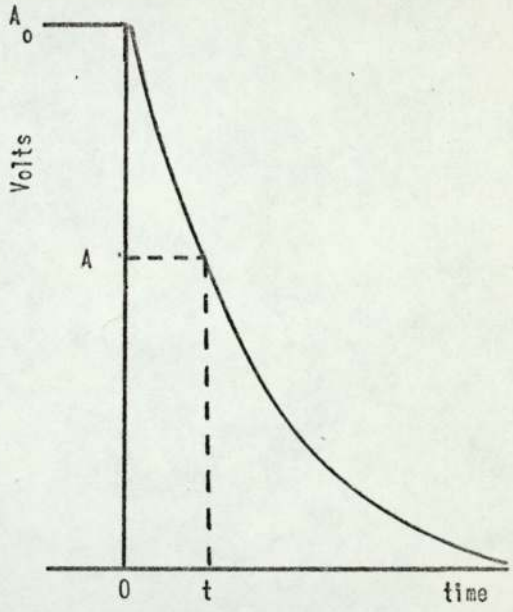

Fig. A1.4. Application of negative step input

can be expressed in the same form as (A1.1), thus:

$$A = A_o(1-\exp - \frac{t}{T_{ft}}) \quad \ldots\ldots\ldots\ldots\ldots\ldots\ldots\ldots\ldots\ldots \text{(A1.3)}$$

This form will be found useful in correcting negative going levels (see later).

Thus for a given value of T_{rt} or T_{ft} and t (10 sec.) A is directly proportional to A_o the constant of proportionality being the appropriate function in brackets.

In the correction procedure to follow, equation(A1.1)(for the correction of positive going levels) and (A1.3)(for the correction of negative going levels) will be used.

The values of the constants of proportionality in these equations have been calculated with the aid of the measured time constants. As would be expected these constants appropriate to the mean velocity rise and fall times are equal, their value being 0.81 (correct to second decimal place). For the mean square rise and fall times the corresponding proportionality constants are approximately equal with a value of 0.45 (correct to second decimal place). With the aid of these constants, corresponding straight line plots of A vs A_o have been drawn (see Fig. A1.5).

Time Constant Correction Procedure

Having provided the raw data from which to make these corrections, the actual procedure will now be examined.

Suppose the broken line curve shown in Fig. A1.6 corresponds to the measured mean square value of the turbulent component of velocity. Then with the appropriate choice of curve for the rise and fall times in Fig. A1.5 (the same curve with a slope of 0.45 will be used in this case) the procedure is as follows:

First the abscissa is divided up, so that each division corresponds to 10 seconds. These divisions are numbered consecutively.

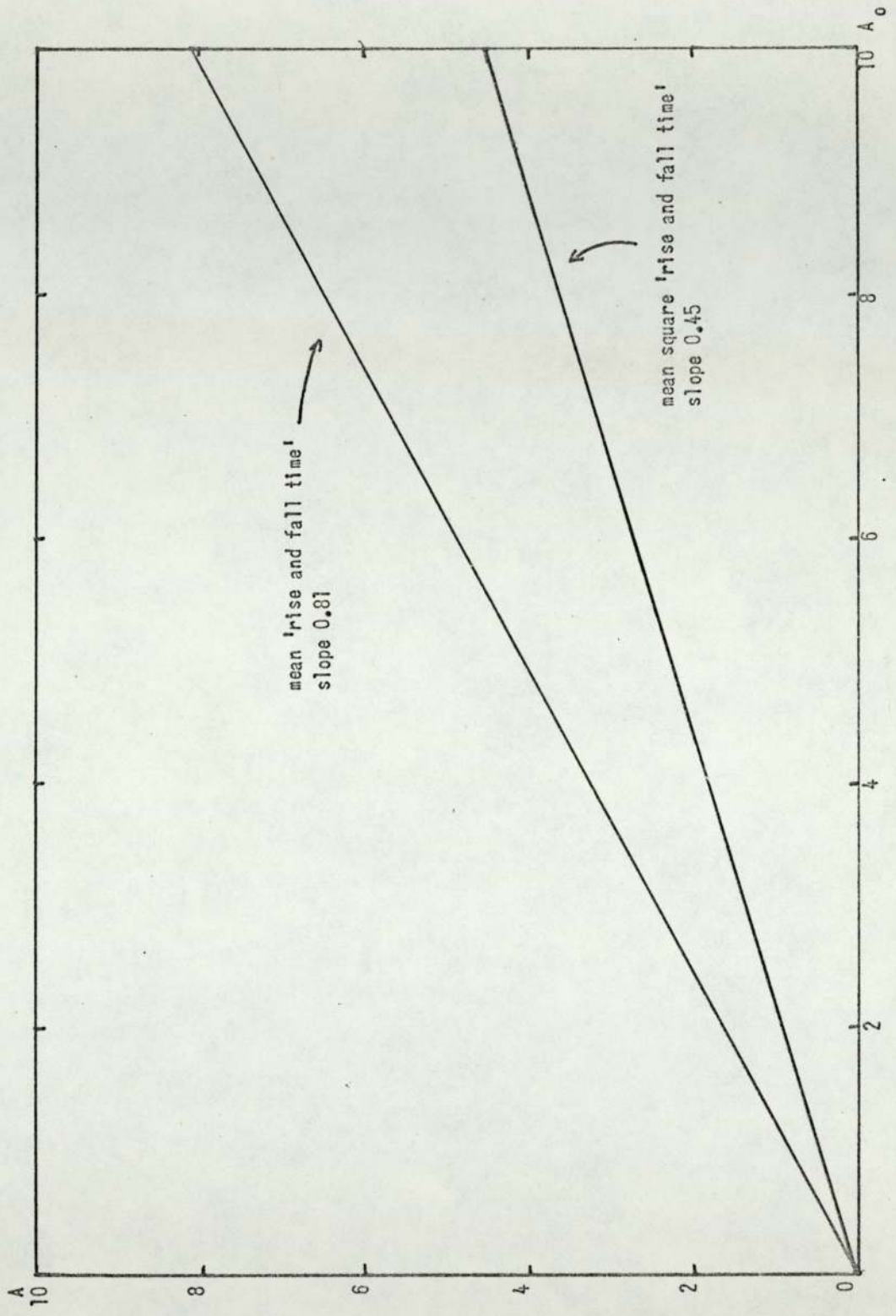

Fig. A1.5. Variation of A with A_o

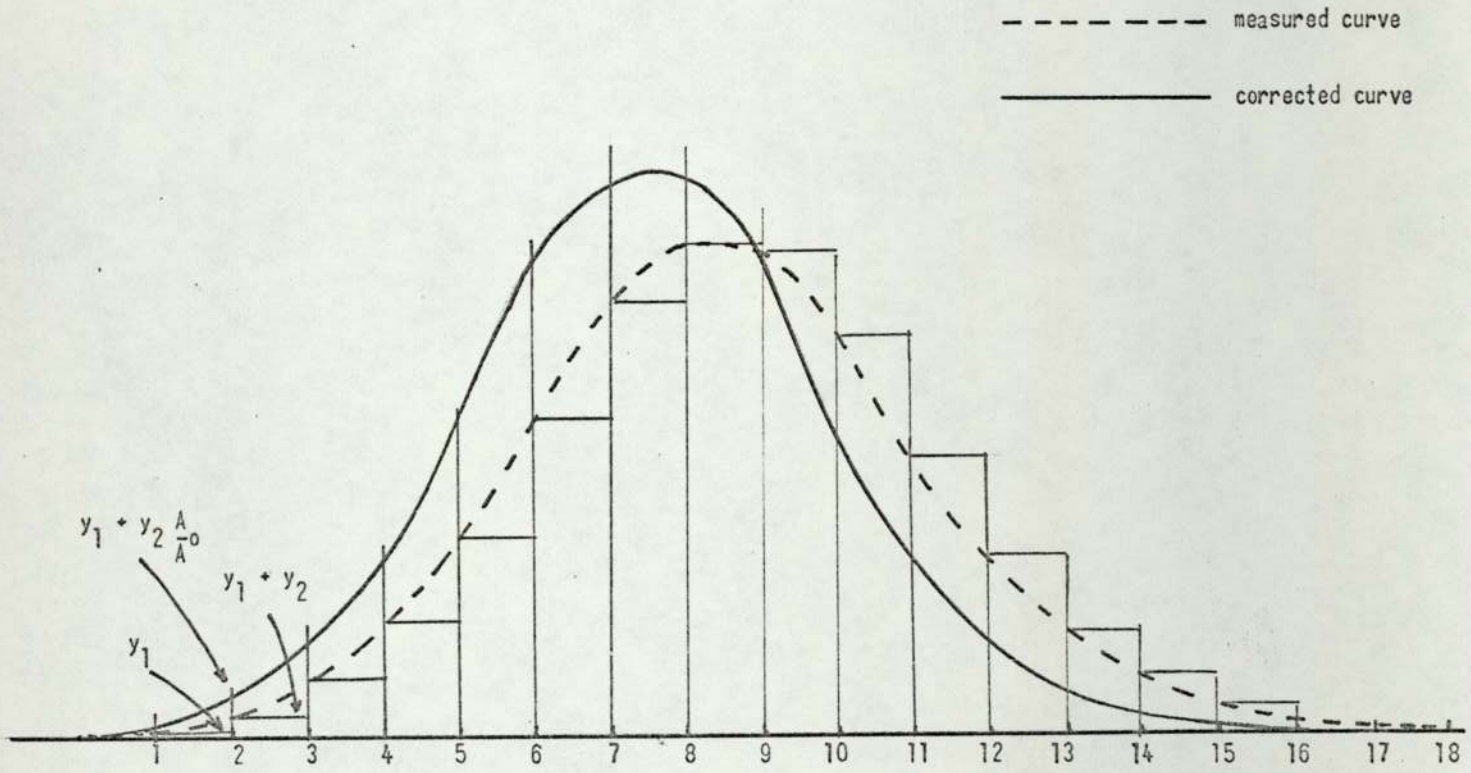

Fig. A1.6. Correction of time constant errors

(in this case it is found that 18 divisions are necessary, assuming each division corresponds to 10 seconds).

Normals are drawn through each numbered position of such a length to pass through the measured (broken line) curve. The correction is started from position 1.

The length of the normal, y_1, from the base line to the point at which it intercepts the measured curve, will be smaller than it would have been had the rise time been 0 (i.e. instantaneous response). By referring to the mean square 'rise and fall time' plot in Fig. A1.5 the value of A_o corresponding to A (i.e. y_1) may be found. A_o will be the corrected signal amplitude at position 1 and may be marked on the normal through position 1. (It is important to remember that the measured curve has been derived from a series of step velocities (in this case the turbulent component) giving rise to corresponding step voltages).

The corrected amplitude corresponding to position 2 is obtained by first drawing a horizontal line through the intercept of the normal through position 1 and the measured curve and the normal through position 2. This horizontal line provides the new base from which to correct the signal at position 2. Let the distance between this new base and the point of interception of the normal through position 2 and the measured curve be y_2. Then the corrected signal amplitude measured from the new base is again found from the mean square 'rise and fall time' plot in Fig. A1.5. In this case A represents y_2 and A_o the corrected value of y_2 which may be marked off on the normal through position 2 as before. Note the corrected signal amplitude at position 2 with respect to the original base line will be $y_1 + y_2 \frac{A_o}{A}$.

This procedure is repeated for each position until a corrected maximum is reached. From this point on corrections will be made in a similar way but in the negative going direction resulting in corrected signal amplitudes less than the corresponding uncorrected ones. The continuous curve in Fig. A1.6 shows the corrected curve resulting from the above procedure.

The correction procedure is exactly the same for the mean velocity signal profiles except that the mean 'rise and fall time' plot in Fig. A1.5 must be used in this case.

Fig. A1.7 shows an actual turbulent velocity scan (expressed in terms of turbulent mean square velocity device output voltage, V) before and after time constant correction. It is seen that for small rates of change output voltage $\frac{dV}{dt}$ (corresponding to velocity) the time constant error is small. For example for each of the WIS jets $\frac{dV}{dt}$ is fairly small. However, for the narrow turbulent annular zone surrounding the free jets $\frac{dV}{dt}$ is large, giving rise to corrected amplitudes considerably higher than the uncorrected peaks.

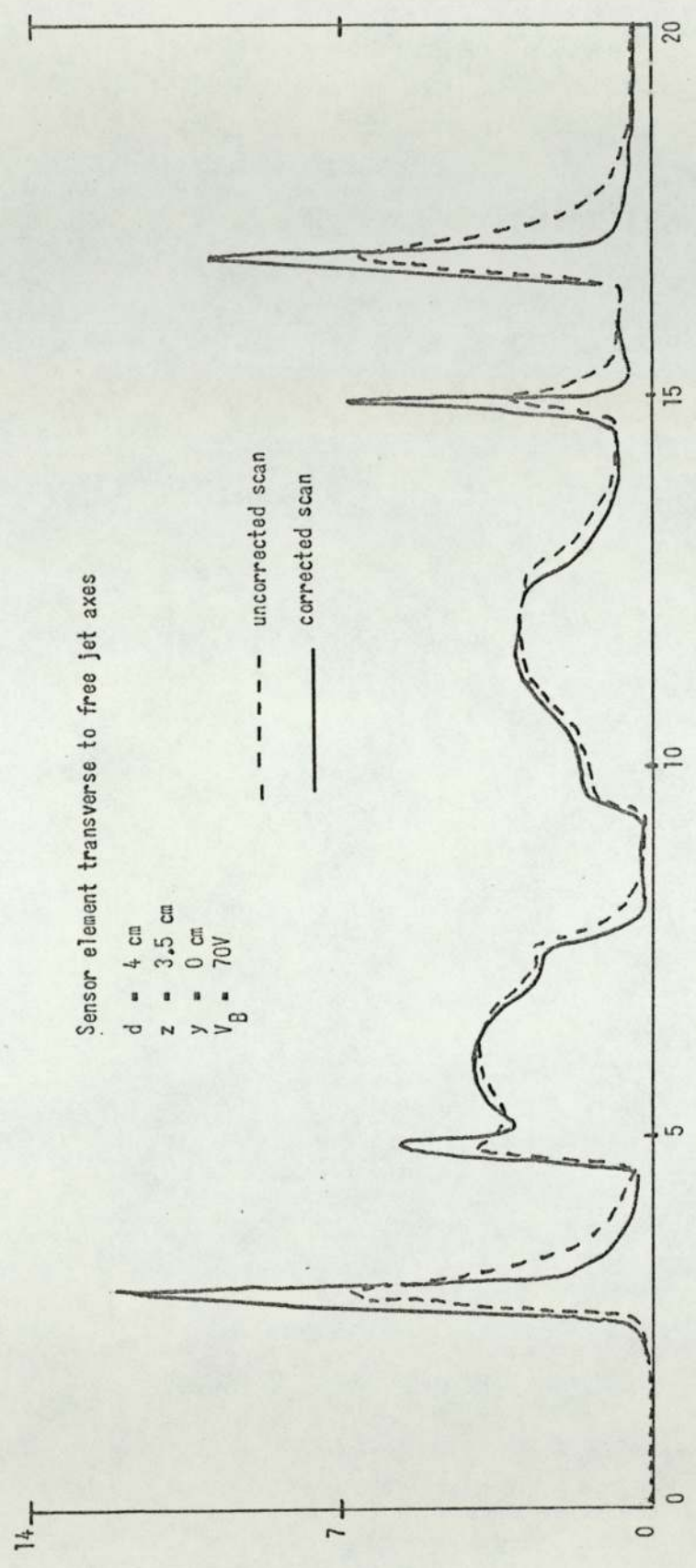

Fig. A1.7. Time constant correction for horizontal, turbulent mean square velocity, scan 11

APPENDIX A2

THE EFFECT OF SURFACE VELOCITY ON THE FLOW AND TEMPERATURE CHARACTERISTICS OF THE WIS JET

Effects Arising From a Modification of Flow Characteristics

No experimental work was carried out specifically to investigate this effect. However, this section will deal with, in a qualitative manner, a proposal (made by the author) of the possible influence of a modification of the flow characteristics (due to surface velocity effects) on the corresponding temperature characteristics.

Fig. A2.1 shows a typical velocity profile normal to the surface in a wall jet (solid curve).

Those regions of flow to the left of U_{max} will be decelerated due to the viscous drag by the wall, the effect becoming progressively greater as the wall is approached. Those regions to the right of U_{max} will be decelerated due to turbulent mixing with the adjacent still air.

Suppose now that the surface velocity is increased to some value U_s in the direction of flow. Then a velocity profile similar to the dotted curve in Fig. A2.1, will probably result. It can be seen that, although those regions in the laminar boundary layer very close to the surface will have increased in velocity by an amount approaching U_s the average velocity U_{ave} over the width of the wall jet will have increased by a much smaller amount δU_{ave}. It is this <u>average</u> velocity increase which is significant when considering surface velocity and its effect on the WIS jet temperature and velocity characteristics.

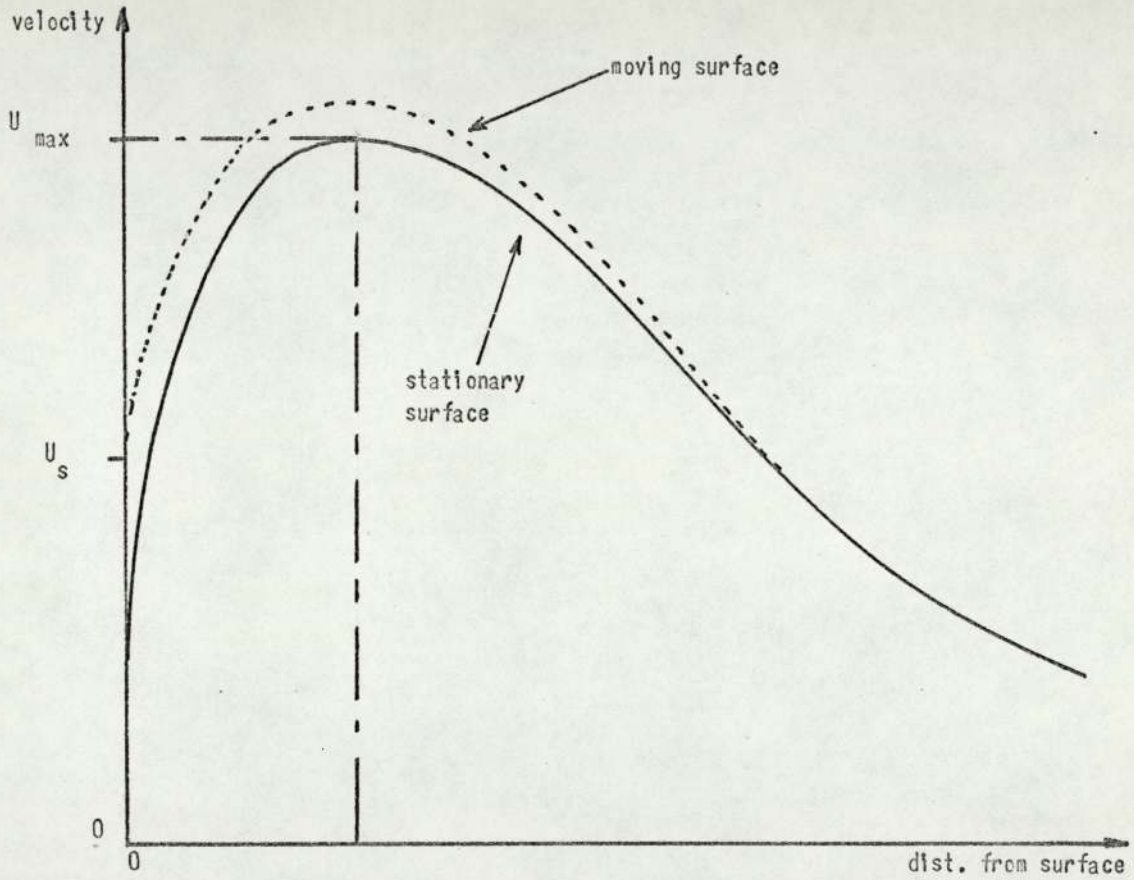

Fig. A2.1. Typical velocity profile normal to the surface in a wall jet

Note, because of the small influence of viscous drag by the surface on the outer, turbulent, layers of the wall jet, no significant increase in entrainment effects from the still air would be expected for surface velocities of the same order as the average flow velocity.

Consider now the effect of accelerating the surface from a velocity of zero to a velocity U_s in a direction parallel to the orifice plate P_o, but normal to O_1 O O_2 (see Fig. A2.2). Then the flow would acquire an average component of velocity δV_{ave} in this direction, the effect of which would be to deflect the flow along the solid lines to the dotted lines. (The non-linearity of these latter is due to the decrease in wall jet velocity with distance, from its origin.)

Fig. A2.3 shows the variation in the y direction of resolved component of WIS jet mean velocity in the z direction for a stationary surface (continuous line), and surface moving in the y positive direction at velocity U_s (broken line). It is seen that the effect of this acceleration is to shift the line of symmetry of the velocity profile from O to O'.

Since the component of wall jet velocity parallel to O_1 O O_2 in Fig. A2.2 is unaffected by the addition of the component δV_{ave} normal to O_1 O O_2 resulting from acceleration of the surface to velocity U_s the general shape of the WIS jet temperature profile in the y direction (shown with a continuous line for stationary surfaces and a broken line for the moving surface), should not alter. However, the line of symmetry will shift from O to some position in a y positive direction O' (see Fig. A2.4). The effect of this on a thermal sensor located at O would be to increase its

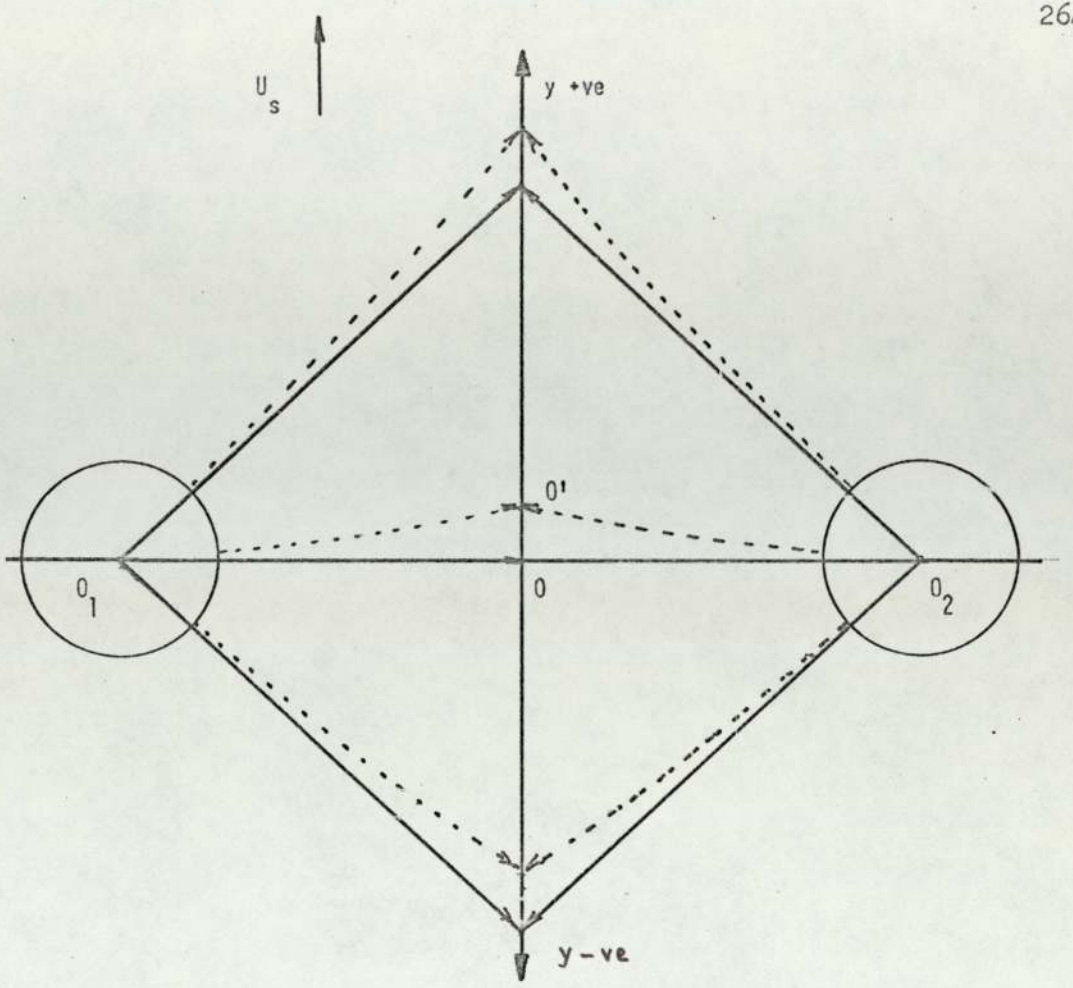

Fig. A2.2. Flow modification due to acceleration of surface from 0 to U_s

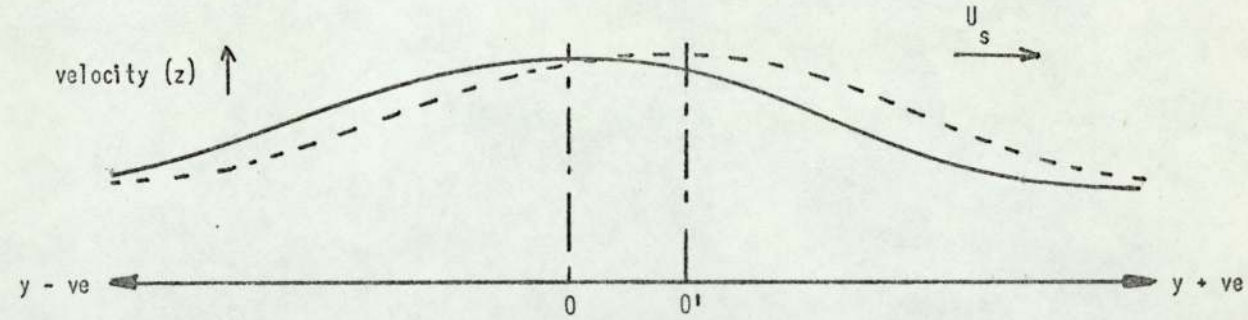

Fig. A2.3. Shift in mean velocity maximum due to acceleration of surface from 0 to U_s

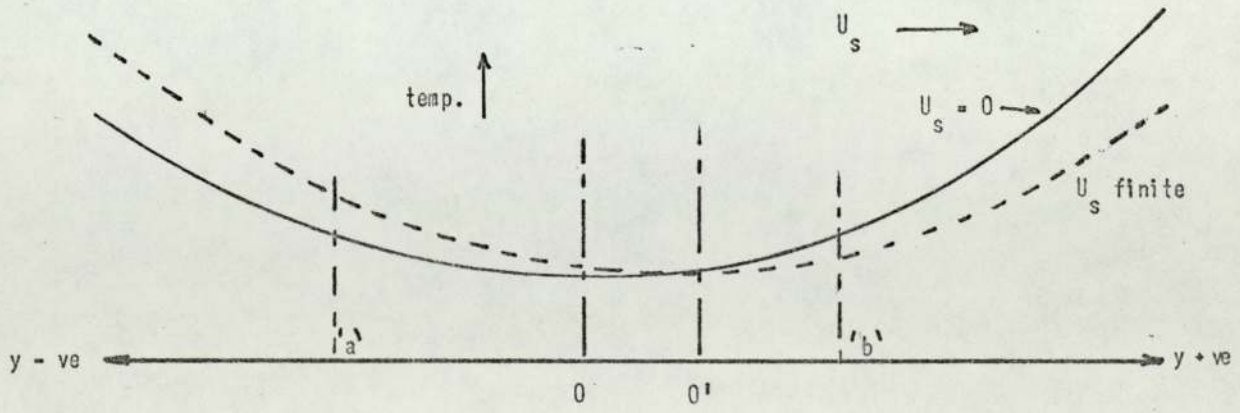

Fig. A2.4. Shift in temperature minimum due to acceleration of surface from 0 to U_s

temperature since it would now lie off the minimum of the dotted curve.

Because the rate of change of temperature with y is small for small values of y (see Theory, Chapter 4), it is expected that for surface velocities of the same order or less than the average flow velocity, the shift in minimum due to the addition of the component will represent a negligible change in thermal sensor temperature.

If this shift in mimimum is such that the change in sensor temperature is significant (corresponding to very high surface velocities compared to the flow velocity) then the following velocity compensating procedure may be adapted.

Two thermal sensors are located at 'a' and 'b' such that the two minima (one corresponding to zero velocity and the other velocity U_s) lie well within the normals through 'a' and 'b', By averaging the signal from each sensor (assuming them to have linear characteristics) a partial velocity compensation may be achieved since the shift in temperature minimum will increase the temperature of one thermal sensor but decrease the temperature of the other.

The errors in compensation still remaining after the application of the above procedure will increase with the departure from linearity of each profile at the points where the normals through 'a' and 'b' intercept.

Surface Velocity Effects on Temperature Measurements made in the Vertical Plane

In this case the thermal sensors are placed at two different locations, one at y = 0 cm and the other at y = 5 cm.

It can be seen from Fig. A2.5 that this system will tend to be even more vulnerable to surface velocity effects. Since a

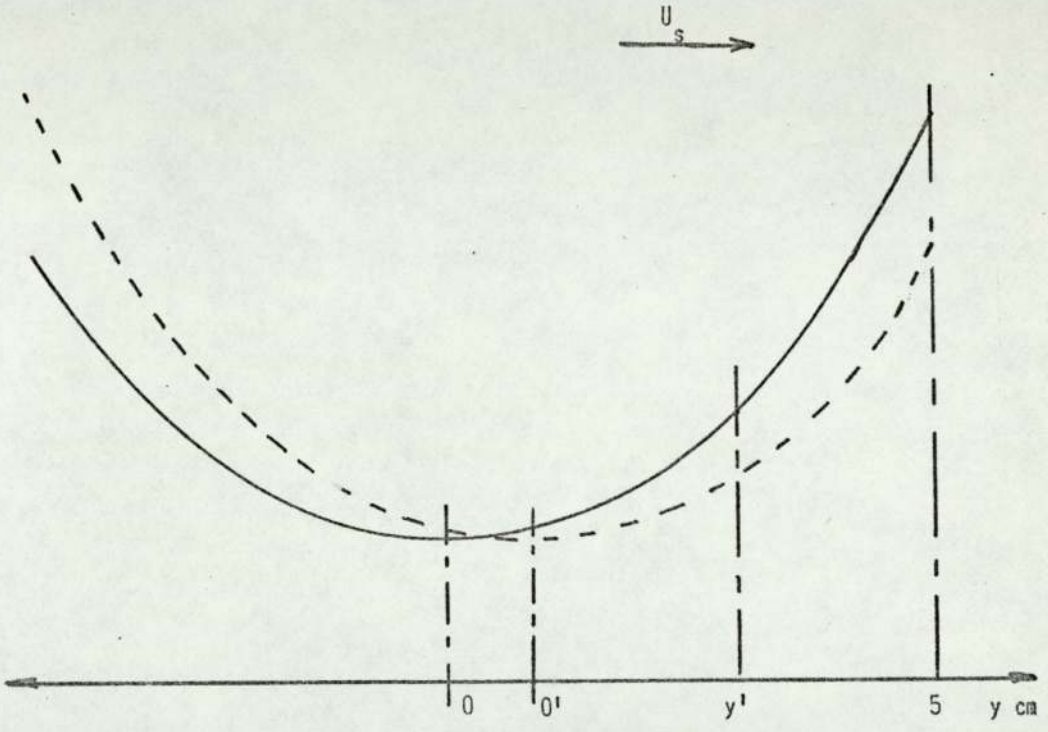

Fig. A2.5. Surface velocity effects on air temperature measurements made in the vertical plane

shift in temperature minima due to the addition of the component δV_{ave} will increase the temperature of one sensor but decrease the temperature of the other, since the temperature dependent parameter is based on the difference between these two temperatures, this shift will represent an error in measurement, the parameter indicating a temperature which is too low. If the surface velocity were in the opposite direction (i.e. y-ve) then the parameter would indicate too high a temperature.

If the thermal sensor at y = 0 cm were re-located at some position y' in Fig. A2.5 such that it lay on a more linear part of the profile, even after the shift in minimum as indicated, then the temperature dependent parameter would be more independent of velocity, since a shift in minimum would affect both thermal sensors in the same sense and by about the same amount (depending on the linearity of the characteristic).

Surface Velocity Effects on Temperature Measurement Involving Three Free Jets

This mode of operation will be partially self-compensating, since a shift of the minima in both the small and large WIS jets will change both thermal sensor temperatures in the same sense. A complete compensation will, however, not be achieved, because $\frac{dT}{dy}$ for the small WIS jet is higher than that for the large one, i.e. the temperature in the small WIS jet will vary more rapidly with y than that in the large WIS jet. However, since both thermal sensors are located at y = 0 cm where $\frac{dT}{dy}$ is zero for zero surface velocity, velocity effects should be small in this mode of operation (in as much as they are due to a modification of flow characteristics).

Effects Arising From Surface Velocity Parallel to the Line Joining the Free Jet Axes

Up to now the effects of surface velocity in a direction transverse to the line joining the free jet axes (i.e. the y direction) have been considered. However, if the surface velocity is parallel to this line (the x direction) then a different situation exists.

The same general lines of reasoning used above will apply to this case thus a detailed examination of the effects of surface velocity in the x direction will not be given here. A few general comments will, however, be made.

The significance of any velocity effects associated with a modification of the flow characteristics tends to increase with temperature gradient in a direction parallel to the velocity vector (i.e. $\frac{dT}{dx}$ in this case). Thus it would be expected that these velocity effects will decrease as d (hence z) increases since in general the value of $\frac{dT}{dx}$ in the WIS jets will decrease as z increases. (cf. the narrow WIS jet temperature peaks for small values of z.)

Surface Velocity Effects Using Heated Free Jets in the Z.N.H.T. Mode

In this case all temperature gradients and temperature differences are very much less than in the unheated free jet mode, hence any surface velocity effects will be correspondingly reduced.

SURFACE VELOCITY EFFECTS ARISING FROM CHANGES IN CONVECTIVE HEAT TRANSFER COEFFICIENT

If the relative velocity, U, between a wall jet and the surface over which it flows is increased by some velocity δU by accelerating the flow (w.r.t. some arbitrary zero, e.g. a jet orifice) by this amount a corresponding increase in Nusselt, Nu, (dimensionless

convective heat transfer coefficient) will occur since Nu α U^x where x is positive but less than unity. One of the effects of accelerating the wall jet flow is to increase its turbulence. This increased turbulence will be partly responsible for the increased value of Nu.

Suppose now that the above increase in relative velocity, δU, is created by accelerating the surface in the opposite sense to the flow velocity this latter remaining unchanged. In this case since the influence of the surface, arising from viscous drag on the fluid in contact with it, is small in the outer turbulent regions of flow then the corresponding increase in turbulence in these regions would be expected to be small. This would result in a smaller variation of Nu with velocity than was indicated above when the increase in relative velocity arose from an acceleration of the flow.

On the assumption that this modification of convective heat transfer coefficient due to surface velocity changes is significant its effect on temperature measurement will now be examined.

Surface Velocity Effects Arising From Movement in a Direction Transverse to the Line Joining the Free Jet Axes

Suppose the mean wall jet velocity to be U and the surface velocity U_s (see Fig. A2.6)then the resultant relative velocity U_R between the surface and the wall jet will be $(U^2+U_s^2)^{\frac{1}{2}}$.

It can be seen that if U_s is small compared to U then because U_R depends on the squares of these components the significance of U_s will be small as far as affecting, Nu, is concerned. Note even if U_s were equal to U which would increase the resultant to $\sqrt{2}$ U. because Nu is $\propto U^x$ where x is less than unity the corresponding increase in Nu will be less than $\sqrt{2}$ times the value when $U_s = 0$. The net effect of this increase in convective heat transfer

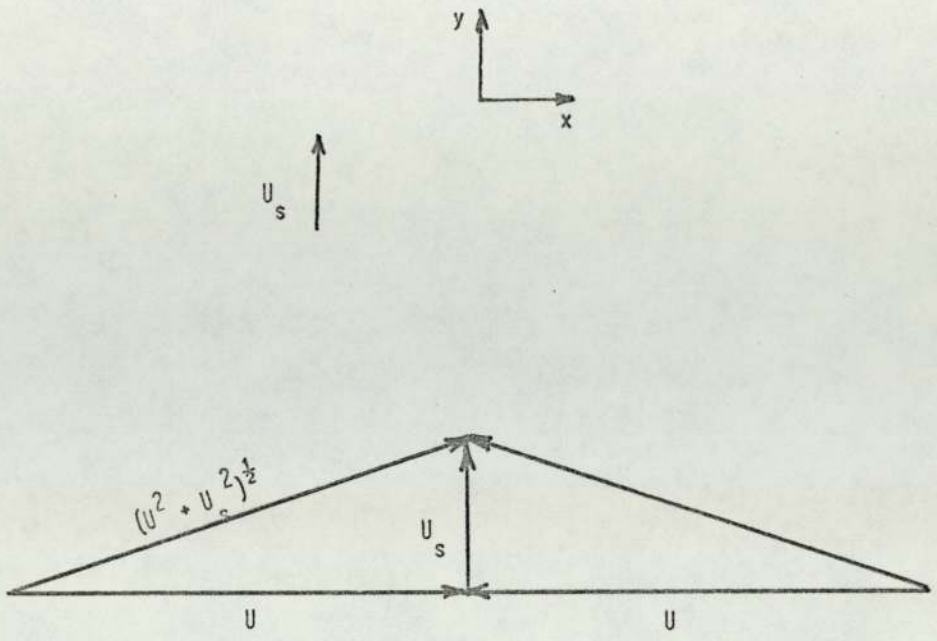

Fig. A2.6. Surface movement in direction transverse to the line joining the free jet axes

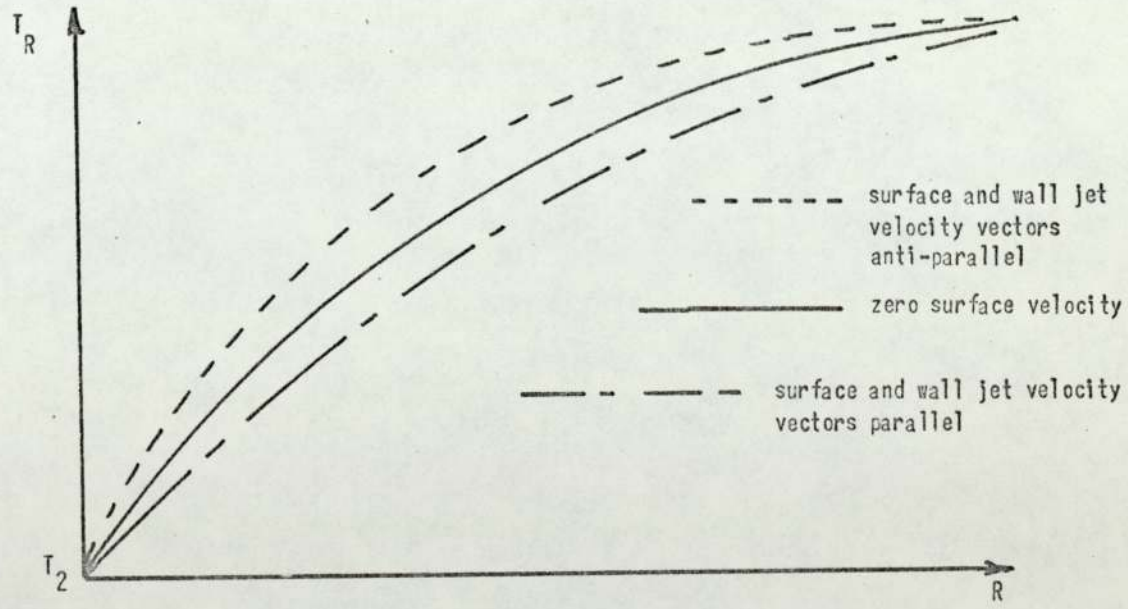

Fig. A2.7. Surface velocity effects arising from a change in convective heat transfer coefficient

coefficient is to increase the WIS jet temperature as well as the temperature gradient in the y (surface velocity) direction.

Measurements in the large WIS jet with the line joining the free jet axes transverse to the direction of surface movement indicated that for V_B = 100 V and a surface velocity increase from 500 ft/min. to 1200 ft/min. the corresponding increase in WIS jet temperature was approximately 3%.

Surface Velocity Effects Arising From Movement in a Direction Parallel to the Line Joining the Free Jet Axes

In this case the two wall jets from which the WIS jet is synthesized will give rise to different rates of heat transfer from the surface.

It can be seen from Fig. A2.7 that three curves are indicated. The middle curve corresponds to zero surface velocity, the lower curve corresponds to the surface and wall jet (as the latter approaches the impingement zone) moving in the same direction resulting in a reduced relative velocity between the two and the upper curve corresponds to the wall jet and surface moving in opposite directions resulting in an increased relative velocity between the two.

Since the WIS jet temperature depends on the average temperature of the corresponding wall jets just prior to impingement it can be seen from Fig. A2.7 that a certain amount of surface velocity compensation will result in this case.

Measurements made in the large WIS jet under the same conditions as existed when the line joining the free jet axes lay transverse to the surface velocity vector indicated an increase of 7% approximately in temperature.

It is likely that the small and large WIS jets will behave in a similar manner thus no significant improvement in surface velocity compensation would be expected when three free jets are employed as far as this 'convective heat transfer' effect is concerned.

All these surface velocity effects arise from a temperature differential between the surface and wall jets thus no significant effects would be expected under zero net heat transfer conditions where the free jets are heated to temperatures close to those of the surface.

APPENDIX A3

THE COOLING EFFECT OF THE FLOW ASSOCIATED WITH THE TEMPERATURE MEASURING DEVICE ON A HEATED, MOVING SURFACE

Since the heat transfer to the WIS jet from the surface will be negligible compared with that to the corresponding wall jet, the effect of the former will be neglected in the following discussion.

It is not intended to examine any subtle variations in heat transfer coefficient of the wall jet, but rather to obtain an approximate estimate of the average cooling effect by the wall jet on the surface.

Since heat transfer rates will be small at those regions outside the periphery of the orifice plate, their effect on surface cooling will be neglected.

It will be assumed that the surface moves in a direction parallel to the orifice plate and is continuous in this direction. The surface will also be assumed to move in such a manner that any one part of it, having once passed under the wall jet, will not be exposed to the latter's cooling influence subsequently unless that part is reheated.

Entrainment cooling in the wall jet will be neglected and equilibrium conditions will be assumed to prevail throughout.

Consider a single round free jet impinging normally onto the surface and forming a radial wall jet. Let δt be the average temperature differential between the origin O and a point on the circumference at a radial distance r (see Fig. A3.1).

Let $\dot{V}$ be the volume flow rate of the wall jet, ρ_a the density of air, ${}_aC_p$ the specific heat of air at constant pressure.

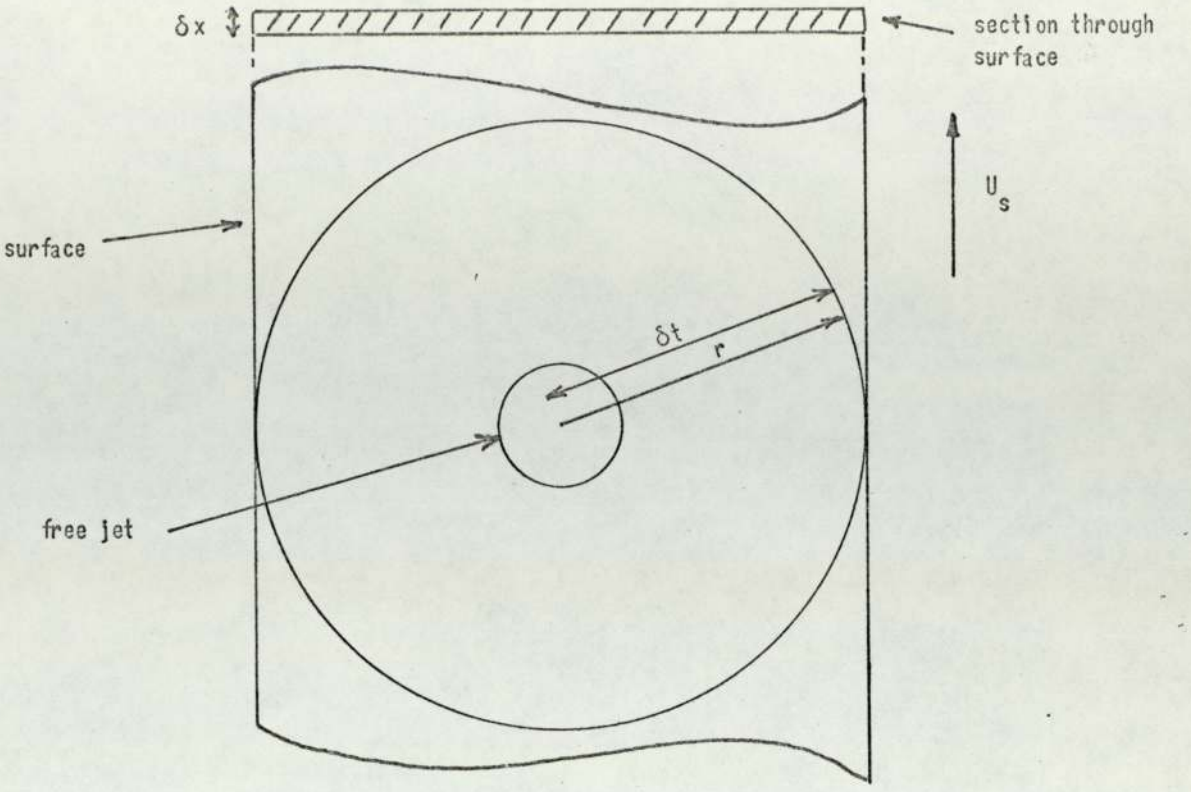

Fig. A3.1. Cooling of the surface by the flow associated with the temperature measuring device

Then the average rate of heat extraction by the wall jet from that area of the surface bounded by the circumference at radius r is given by:

$$\dot{V}\rho_a \, a C_p \, \delta t \qquad \text{..... (A3.1)}$$

Let C_s represent the total thermal capacity associated with that area of the surface which passes under the wall jet (within the specified limits) in unit time. Assuming the change in surface temperature, δT_s, due to this wall jet perturbation to be small compared to the absolute surface temperature then this change will be given by:

$$\delta T_s = \frac{\dot{V}\rho_a \, C_p \, \delta t}{C_s} \qquad \text{..... (A3.2)}$$

Suppose the surface concerned is that of a body of rectangular section normal to the plane of the surface.

Then C_s is given by:

$$2r \, \delta x \rho_s C_p \, U_s \qquad \text{..... (A3.3)}$$

where $2r\,\delta x$ = cross sectional area of that part of the body defined by the wall jet of diameter $2r$, δx being the thickness of the body.

U_s = surface velocity.

ρ_s = density of body.

${}_sC_p$ = specific heat of body.

In this case δT_s is given by:

$$\delta T_s = \frac{\dot{V}\rho_a C_p \delta t}{2r\,\delta x \rho_s {}_sC_p U_s} \qquad \text{..... (A3.4)}$$

This expression will be evaluated for a typical case of continuously annealed aluminium strip where:

$\delta x = 2.5 \times 10^{-2}$ cm

$U_s = 150$ cm/sec.

for $V_B = 100$ V, $\dot{V} \sim 3000$ cc/sec.

For unheated free jets $\delta t = 170^{\circ}C$ corresponding to a strip temperature of approximately $500^{\circ}C$ also from the dimensions of the sensing device.

$r = 10$ cm

Using the standard values of density and specific heat for aluminium and air it is found that equation (A3.4) gives rise to a value of δT_s of approximately $2^{\circ}C$.

Note this figure of $2^{\circ}C$ is a worst case estimate corresponding to the highest free jet velocity (i.e. $V_B = 100$ V) employed in these experiments.

If either the strip thickness and/or the speed are increased then this value of $2^{\circ}C$ will decrease accordingly. Also if the free jet flow rate is reduced this $2^{\circ}C$ surface temperature perturbation will be reduced. Note the above discussion has been appropriate to unheated free jets. If the heated free jet mode is used in which

the free jet and wall jet temperatures are close to that of the surface then any surface temperature perturbation will be negligible.

APPENDIX A4

THE EFFECTS OF SURFACE ROUGHNESS ON THE TEMPERATURE AND VELOCITY CHARACTERISTICS OF THE WIS JET

The temperature and velocity characteristics of the WIS jet are dependent upon those of the constituent wall jets. Thus any modification of the latter will influence the WIS jet characteristics.

It is therefore appropriate to examine the effects of surface roughness on the wall jet.

It has been indicated that a wall jet has a two-component structure in that it has similar characteristics to a free jet in the outer turbulent regions, but in the inner regions its characteristics are similar to those of a boundary layer, there being a thin laminar sub-layer close to the surface.

So long as the surface protuberances do not penetrate the laminar sub-layer then they will not affect either the heat transfer or fluid flow and the surface will behave as though it were perfectly smooth.

Schlichting (46, 47) has found that the 'admissible roughness' k_{ad} (i.e. the maximum height of the protuberances beyond which their existence becomes significant as far as their effect on heat transfer and fluid flow is concerned) is a function of kinematic viscosity ν $ft^2 sec^{-1}$ and flow velocity U_∞ $ft\ sec^{-1}$ where:

$$k_{ad} = \frac{100\nu}{U_\infty} \quad ft$$

This expression was derived for fluid flowing over a surface where U_∞ $ft\ sec^{-1}$ represents the free stream velocity, i.e. the velocity at a distance from the surface where the effects of viscous drag by the latter becomes negligible.

However, if U_∞ is replaced by U_{max} where U_{max} is the maximum wall jet velocity (see section on 'The Wall Jet', Chapter 3), then Schlichting's expression should give a good approximation to admissible roughness for wall jet flow.

Now U_{max} for free jet velocities of the order of 2000 ft per min. (the maximum involved in these experiments) will probably be of the order of 1000 ft per min. Also $\nu \simeq 1.6 \times 10^{-4}$ ft^2 sec.$^{-1}$. Thus for the maximum velocities involved in these experiments corresponding to $V_B = 100$ V:

$$k_{ad} \sim 10^{-2} \text{ inches}$$

Thus if the surface roughness gives rise to protuberances in excess of this value, their existence will be significant.

Plots A4.1 and A4.2 show electron microscope photographs of the surface which was involved in all the experiments in this thesis.

It is difficult to deduce the exact height of the protuberances from these plates but they are certainly less than 10^{-3} inches and hence well within the 'admissible roughness limit' of approximately 10^{-2} inches.

Thus it can be seen that there were no surface roughness effects prevailing in these experiments, i.e. the surfaces may be regarded as perfectly smooth and any variations in roughness below the calculated value of 10^{-2} inches will not be significant.

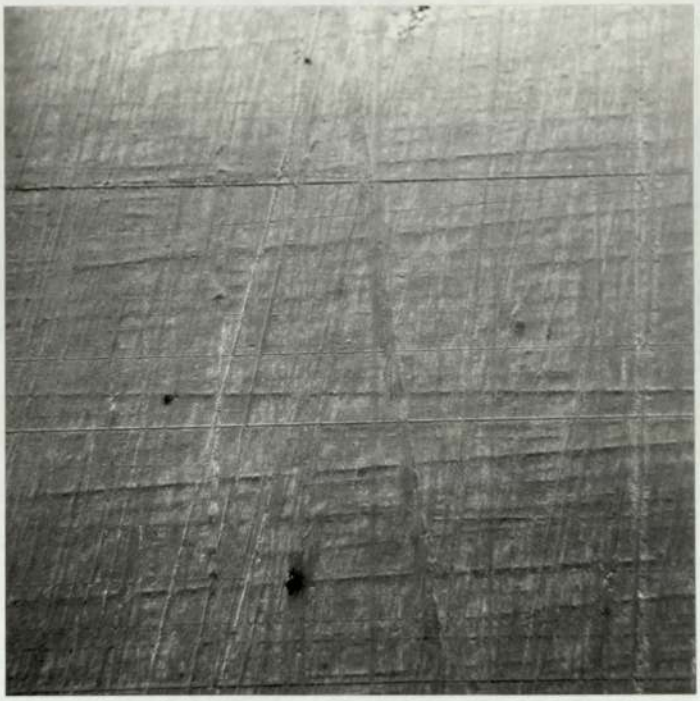

x 50

Plate A4.1. Electron beam angle = 45° to surface.

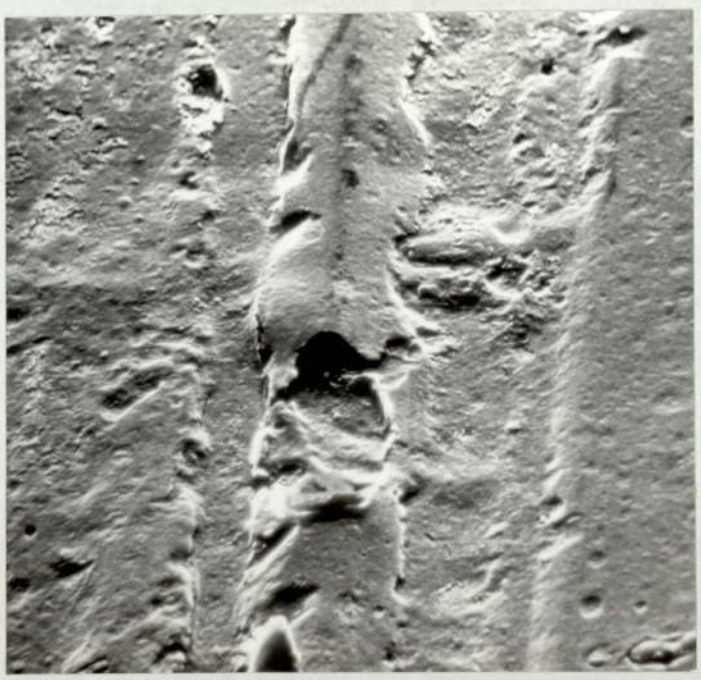

x 2000

Plate A4.2. Electron beam angle = 45° to surface.

Electron microscope photographs of replicas of the surface used for the velocity and temperature studies.

APPENDIX A5

CATALOGUE OF VELOCITY SCANS PERFORMED IN THE HORIZONTAL, x, DIRECTION

All scans indicated employed the asymmetrical free jet distribution.

d = 4 cm

Sensor element transverse to free jet axes

V_B = 100 V

Scan	y cm	z cm
1	0	3.5
2	5	3.5
3	10	3.5
4	0	2
5	5	2
6	10	2
7	0	1
8	0	3
9	5	3
10	10	3

V_B = 70 V

Scan	y cm	z cm
11	0	3.5
12	5	3.5
13	10	3.5
14	0	3
15	5	3
16	10	3
17	0	2
18	5	2
19	10	2
20	0	1

V_B = 40 V

Scan	y cm	z cm
21	0	3.5
22	5	3.5
23	10	3.5
24	0	3
25	5	3
26	10	3
27	0	2
28	5	2
29	10	2
30	0	1

Sensor element parallel to free jet axes

V_B = 100 V

Scan	y cm	z cm
31	0	3.5
32	5	3.5
33	10	3.5
34	0	3
35	5	3
36	10	3
37	0	2
38	5	2
39	10	2
40	0	1

V_B = 70 V

Scan	y cm	z cm
41	0	3.5
42	5	3.5
43	10	3.5
44	0	3
45	5	3
46	10	3
47	0	2
48	5	2
49	10	2
50	0	1

V_B = 40 V

Scan	y cm	z cm
51	0	3.5
52	5	3.5
53	10	3.5
54	0	3
55	5	3
56	10	3
57	0	2
58	5	2
59	10	2
60	0	1

d = 2.5 cm

Sensor element transverse to free jet axes

V_B = 100 V

Scan	y cm	z cm
61	0	2
62	5	2
63	10	2
64	0	1.5
65	5	1.5
66	10	1.5
67	0	1.25
68	5	1.25
69	10	1.25
70	0	1

V_B = 70 V

Scan	y cm	z cm
71	0	2
72	5	2
73	10	2
74	0	1.5
75	5	1.5
76	10	1.5
77	0	1.25
78	5	1.25
79	10	1.25
80	0	1

V_B = 40 V

Scan	y cm	z cm
81	0	2
82	5	2
83	10	2
84	0	1.5
85	5	1.5
86	10	1.5
87	0	1.25
88	5	1.25
89	10	1.25
90	0	1
91	5	1

Sensor element parallel to free jet axes

V_B = 100 V

Scan	y cm	z cm
92	0	2
93	5	2
94	10	2
95	0	1.5
96	5	1.5
97	10	1.5
98	0	1.25
99	5	1.25
100	10	1.25
101	0	1

V_B = 70 V

Scan	y cm	z cm
102	0	2
103	5	2
104	10	2
105	0	1.5
106	5	1.5
107	10	1.5
108	0	1.25
109	5	1.25
110	10	1.25
111	0	1

V_B = 40 V

Scan	y cm	z cm
112	0	2
113	5	2
114	10	2
115	0	1.5
116	5	1.5
117	10	1.5
118	0	1.25
119	5	1.25
120	10	1.25
121	0	1

d = 1 cm

Sensor element transverse to free jet axes

V_B = 100 V

Scan	y cm	z cm
122	0	0.5
123	5	0.5
124	10	0.5

V_B = 70 V

Scan	y cm	z cm
125	0	0.5
126	5	0.5
127	10	0.5

V_B = 40 V

Scan	y cm	z cm
128	0	0.5
129	5	0.5
130	10	0.5

Sensor element parallel to free jet axes

V_B = 100 V

Scan	y cm	z cm
131	0	0.5
132	5	0.5
133	10	0.5

V_B = 70 V

Scan	y cm	z cm
134	0	0.5
135	5	0.5
136	10	0.5

V_B = 40 V

Scan	y cm	z cm
137	0	0.5
138	5	0.5
139	10	0.5

CATALOGUE OF TEMPERATURE SCANS IN THE HORIZONTAL, x, AND VERTICAL, y, DIRECTIONS

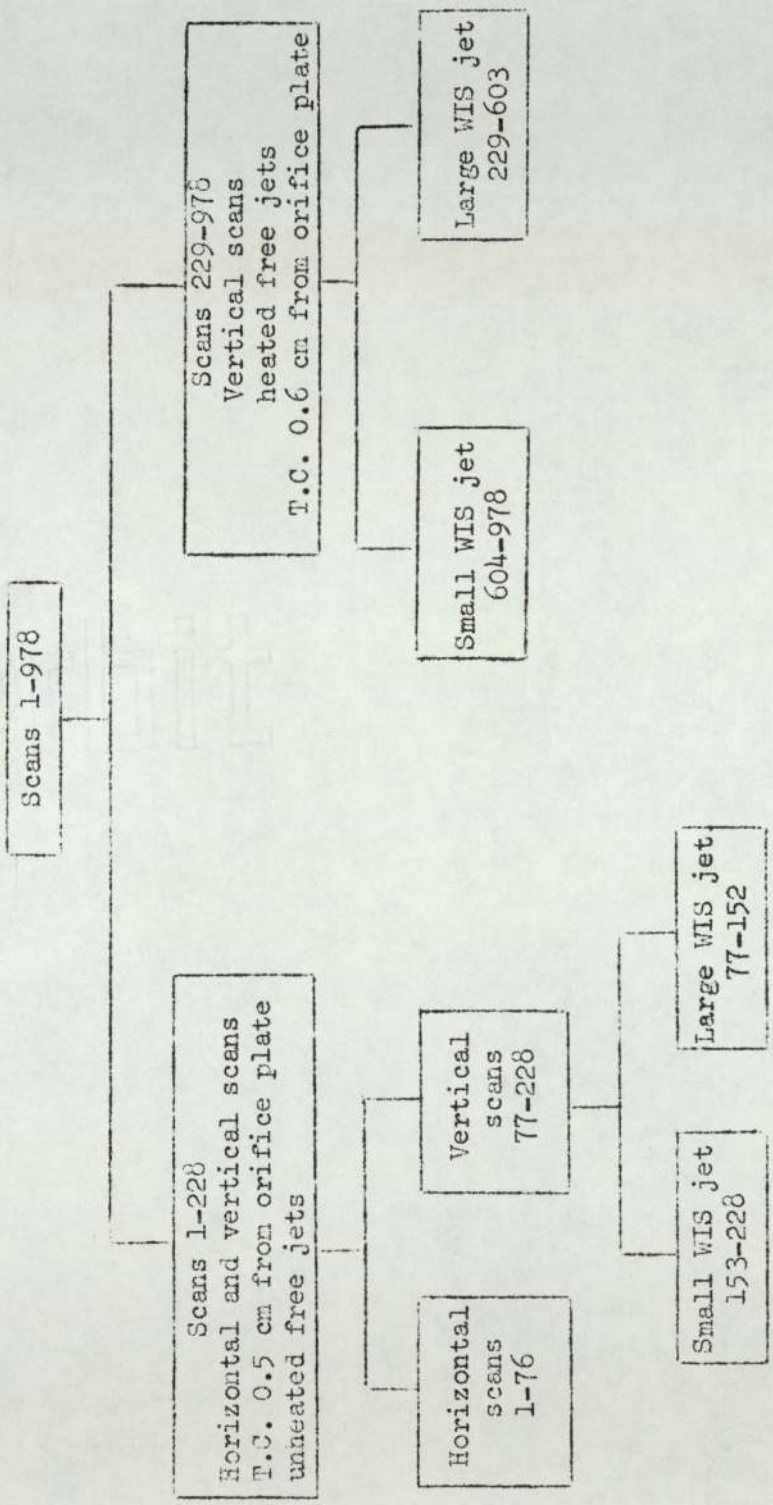

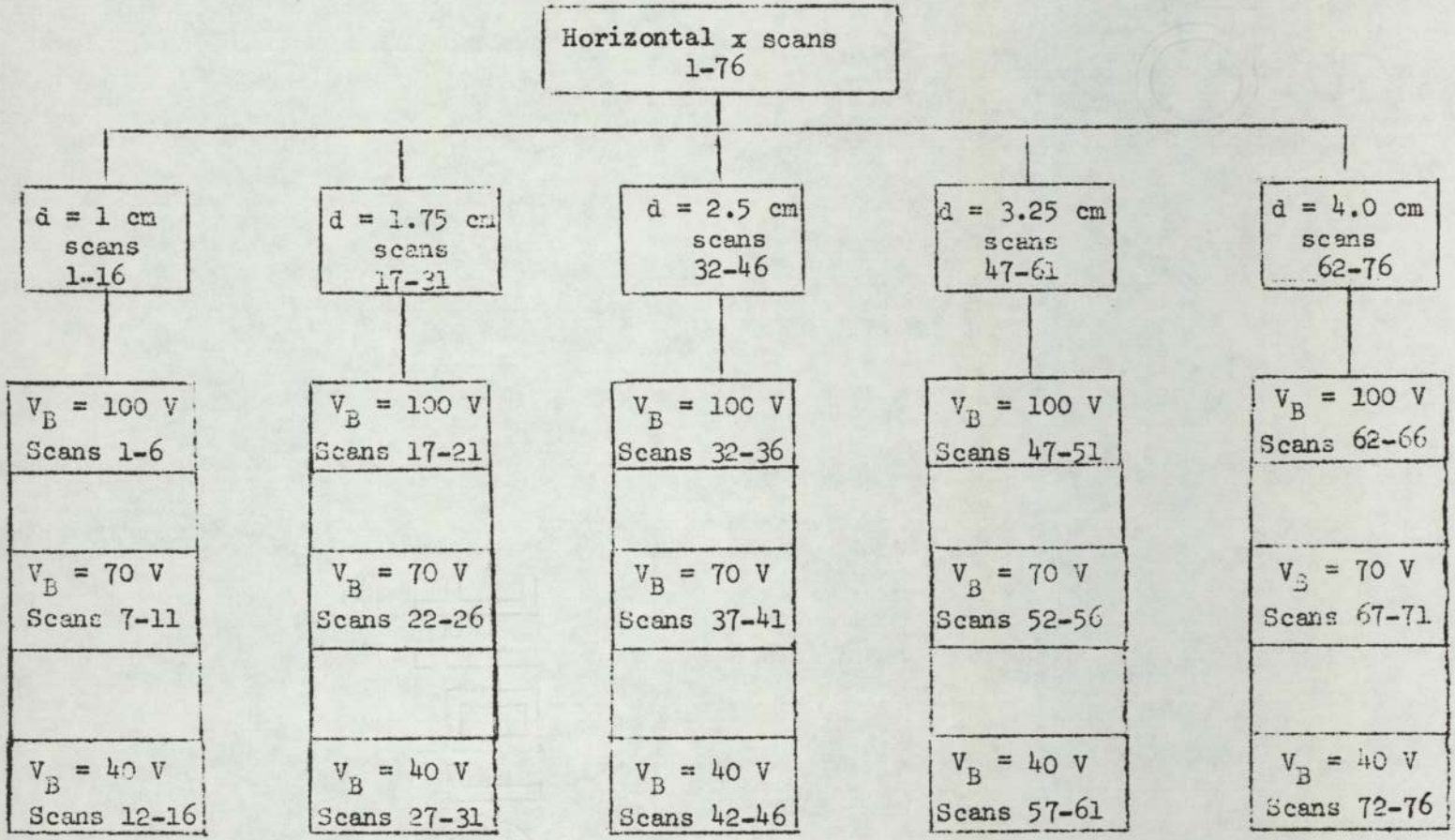
Horizontal x scans
1-76
d = 1 cm
scans
1-16
d = 1.75 cm
scans
17-31
d = 2.5 cm
scans
32-46
d = 3.25 cm
scans
47-61
d = 4.0 cm
scans
62-76
V_B = 100 V
Scans 1-6
V_B = 70 V
Scans 7-11
V_B = 40 V
Scans 12-16
V_B = 100 V
Scans 17-21
V_B = 70 V
Scans 22-26
V_B = 40 V
Scans 27-31
V_B = 100 V
Scans 32-36
V_B = 70 V
Scans 37-41
V_B = 40 V
Scans 42-46
V_B = 100 V
Scans 47-51
V_B = 70 V
Scans 52-56
V_B = 40 V
Scans 57-61
V_B = 100 V
Scans 62-66
V_B = 70 V
Scans 67-71
V_B = 40 V
Scans 72-76

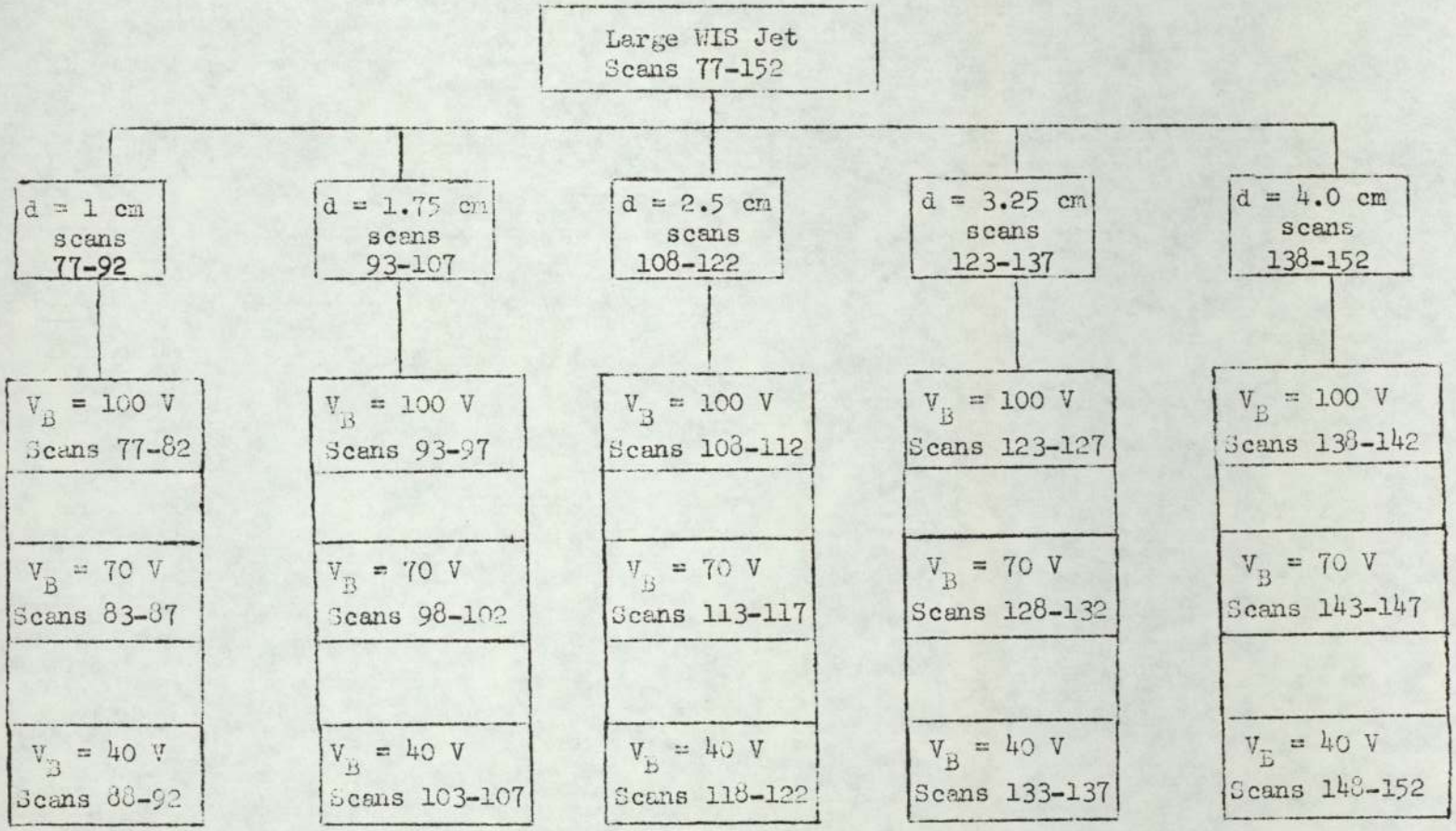
Large WIS Jet
Scans 77-152
d = 1 cm
scans
77-92
d = 1.75 cm
scans
93-107
d = 2.5 cm
scans
108-122
d = 3.25 cm
scans
123-137
d = 4.0 cm
scans
138-152
V_B = 100 V
Scans 77-82
V_B = 70 V
Scans 83-87
V_B = 40 V
Scans 88-92
V_B = 100 V
Scans 93-97
V_B = 70 V
Scans 98-102
V_B = 40 V
Scans 103-107
V_B = 100 V
Scans 108-112
V_B = 70 V
Scans 113-117
V_B = 40 V
Scans 118-122
V_B = 100 V
Scans 123-127
V_B = 70 V
Scans 128-132
V_B = 40 V
Scans 133-137
V_B = 100 V
Scans 138-142
V_B = 70 V
Scans 143-147
V_B = 40 V
Scans 148-152

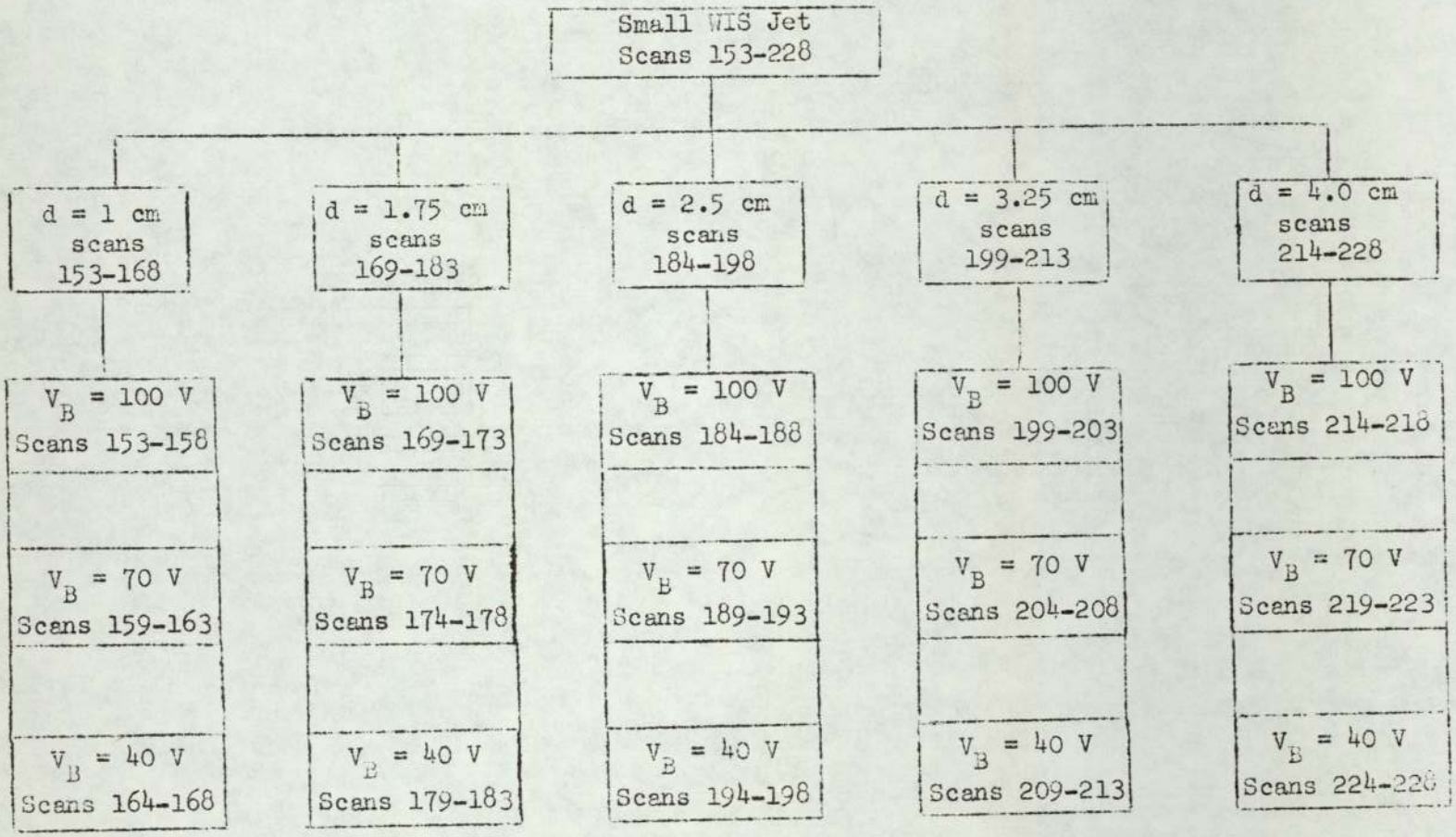
Small WIS Jet
Scans 153-228
d = 1 cm
scans
153-168
d = 1.75 cm
scans
169-183
d = 2.5 cm
scans
184-198
d = 3.25 cm
scans
199-213
d = 4.0 cm
scans
214-228
V_B = 100 V
Scans 153-158
V_B = 70 V
Scans 159-163
V_B = 40 V
Scans 164-168
V_B = 100 V
Scans 169-173
V_B = 70 V
Scans 174-178
V_B = 40 V
Scans 179-183
V_B = 100 V
Scans 184-188
V_B = 70 V
Scans 189-193
V_B = 40 V
Scans 194-198
V_B = 100 V
Scans 199-203
V_B = 70 V
Scans 204-208
V_B = 40 V
Scans 209-213
V_B = 100 V
Scans 214-218
V_B = 70 V
Scans 219-223
V_B = 40 V
Scans 224-228

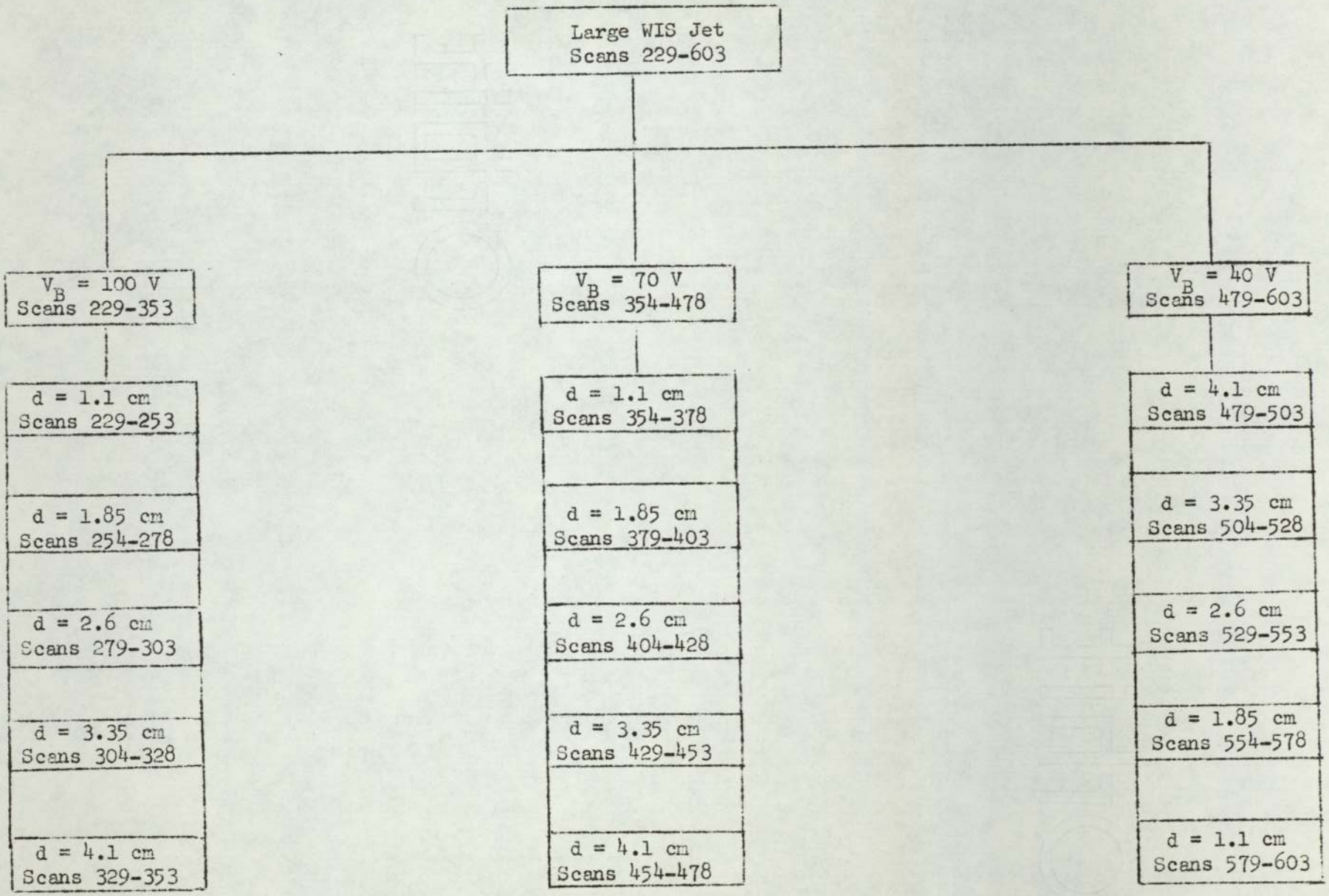
Large WIS Jet
Scans 229-603
V_B = 100 V
Scans 229-353
V_B = 70 V
Scans 354-478
V_B = 40 V
Scans 479-603
d = 1.1 cm
Scans 229-253
d = 1.85 cm
Scans 254-278
d = 2.6 cm
Scans 279-303
d = 3.35 cm
Scans 304-328
d = 4.1 cm
Scans 329-353
d = 1.1 cm
Scans 354-378
d = 1.85 cm
Scans 379-403
d = 2.6 cm
Scans 404-428
d = 3.35 cm
Scans 429-453
d = 4.1 cm
Scans 454-478
d = 4.1 cm
Scans 479-503
d = 3.35 cm
Scans 504-528
d = 2.6 cm
Scans 529-553
d = 1.85 cm
Scans 554-578
d = 1.1 cm
Scans 579-603

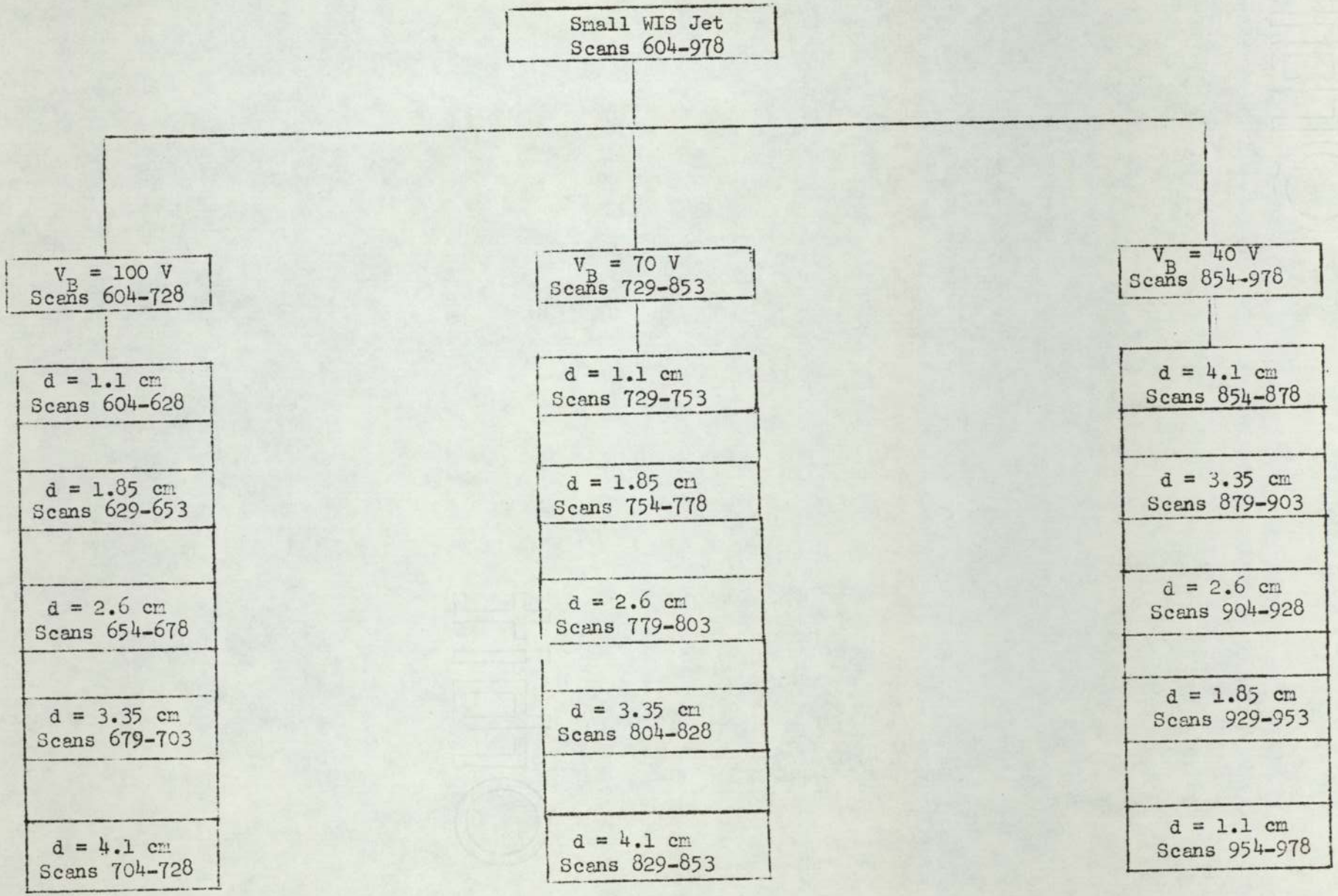
Small WIS Jet
Scans 604-978
V_B = 100 V
Scans 604-728
d = 1.1 cm
Scans 604-628
d = 1.85 cm
Scans 629-653
d = 2.6 cm
Scans 654-678
d = 3.35 cm
Scans 679-703
d = 4.1 cm
Scans 704-728
V_B = 70 V
Scans 729-853
d = 1.1 cm
Scans 729-753
d = 1.85 cm
Scans 754-778
d = 2.6 cm
Scans 779-803
d = 3.35 cm
Scans 804-828
d = 4.1 cm
Scans 829-853
V_B = 40 V
Scans 854-978
d = 4.1 cm
Scans 854-878
d = 3.35 cm
Scans 879-903
d = 2.6 cm
Scans 904-928
d = 1.85 cm
Scans 929-953
d = 1.1 cm
Scans 954-978

CATALOGUE OF TEMPERATURE SCANS PERFORMED IN THE z DIRECTION

In this section the following nomenclature will be used:

A', B', C' correspond to the free jets J_A, J_B and J_C respectively and represent the temperatures measured close to their respective axes.

D_o = Small WIS jet temperature at y = 0 cm.

D_5 = Small WIS jet temperature at y = 5 cm.

E_o = Large WIS jet temperature at y = 0 cm.

E_5 = Large WIS jet temperature at y = 5 cm.

All scans employed surface temperatures, T_s of approximately 270°C.

Unlike the other temperature scans (i.e. horizontal and vertical) the range in these z scans varied with d thus it is appropriate to quote this range in the following Tables.

Three levels of free jet temperature were employed:

(1) Unheated free jets, T_1,

(2) free jets heated to approximately $T_s/2$, T_2,

(3) free jets heated to approximately T_s, T_3.

d = 4.1 cm

Scan range - z = 5 mm ± 35 mm

	T_3			T_2			T_1		
	V_B volts			V_B volts			V_B volts		
	100	70	40	100	70	40	100	70	40
A'	1z	8z	15z	22z	29z	36z	43z	50z	57z
D_o	2z	9z	16z	23z	30z	37z	44z	51z	58z
B'	3z	10z	17z	24z	31z	38z	45z	52z	59z
E_o	4z	11z	18z	25z	32z	39z	46z	53z	60z
C'	5z	12z	19z	26z	33z	40z	47z	54z	61z
E_5	6z	13z	20z	27z	34z	41z	48z	55z	62z
D_5	7z	14z	21z	28z	35z	42z	49z	56z	63z

d = 2.6 cm

Scan range - z = 5 mm ⇆ 20 mm

	T_3			T_2			T_1		
	V_B volts			V_B volts			V_B volts		
	100	70	40	100	70	40	100	70	40
A'	64z	71z	78z	85z	92z	99z	106z	113z	120z
D_o	65z	72z	79z	86z	93z	100z	107z	114z	121z
B'	66z	73z	80z	87z	94z	101z	108z	115z	122z
E_o	67z	74z	81z	88z	85z	102z	109z	116z	123z
C'	68z	75z	82z	89z	96z	103z	110z	117z	124z
E_5	69z	76z	83z	90z	97z	104z	111z	118z	125z
D_5	70z	77z	84z	91z	98z	105z	112z	119z	126z

d = 1.6 cm

Scan range - z = 5 mm ⇆ 10 mm

	T_3			T_2			T_1		
	V_B volts			V_B volts			V_B volts		
	100	70	40	100	70	40	100	70	40
A'	127z	134z	141z	148z	155z	162z	169z	176z	183z
D_o	128z	135z	142z	149z	156z	163z	170z	177z	184z
B'	129z	136z	143z	150z	157z	164z	171z	178z	185z
E_o	130z	137z	144z	151z	158z	165z	172z	179z	186z
C'	131z	138z	145z	152z	159z	166z	173z	180z	187z
E_5	132z	139z	146z	153z	160z	167z	174z	181z	188z
D_5	133z	140z	147z	154z	161z	168z	175z	182z	189z

REFERENCES

(1) Reynolds, P.M. Measurement of aluminium extrusion temperatures: collaborative Works' trials of a commercial lead sulphide-cell instrument. J. Inst. Metals, 1966, 94, 379.

(2) Black, P.J.S. A pyrometer for the continuous measurement of the temperature of aluminium extrusions. J. Inst. Metals, 1966, 94, 384.

(3) Brånemark, P.I., Nilsson, K. Thermographic and microvascular studies of peripheral circulation. Bibliotheca Radiologica, 1969, 5, 129.

(4) Lloyd-Williams, K., Lloyd-Williams, F.J., Handley, R.S. Infra-red thermometry in clinical practice. Lancet, 2, 958. 1960

(5) Watmough, D.J., Oliver, R. The emission of infra-red radiation from the human skin - Implications for clinical thermography. Brit. J. of Radiology, 1969, 42, 411.

(6) Herzfeld, C.M. (ed.). Temperature: its measurement and control in science and industry. Vol. 3, Part 2. Applied Methods and Instruments. New York Reinhold: London: Chapman and Hall, 1962, p. 1005.

(7) Wolfe, H.C. (ed.). Temperature: its measurement and control in science and industry, Vol. 2. New York Reinhold: London: Chapman and Hall, 1955, p. 320.

(8) Mouly, R.J. Temperature measurement with eddy current. See ref. 6. p. 1009.

(9) Dobbs, E.R., and Llewellyn, J.D. Generation of ultrasonic waves without using a transducer - Non-destructive testing. p. 49, February 1971.

(10) Fam, S.S., Lynnworth, L.C., Carnevale, E.H. Ultrasonic thermometry - Instruments and control systems. Oct. 1969. p. 107.

(11) Hornbaker, D.R. and Dieter, R. The convective null-heat-balance concept for non-contact temperature measurements of sheets, rolls, fibres and wire. A paper presented at the "Fifth Symposium on Temperature - its Measurement and Control in Science and Industry". June 21-24, 1971, Washington, D.C.

(12) McFee, J.H., Marcus, P.M. and Estermann, I. Possible application of molecular beam techniques to the measurement of surface temperatures. Rev. Sci. Instrum., 1960, 31 (9), pp. 1013-1014.

(13) McAdams, W.H. Heat transmission. 3rd edn. London, New York and Toronto: McGraw-Hill, 1954.

(14) Reynolds, P.M. A review of multicolour pyrometry for temperatures below 1500°C. Brit. J. Appl. Phys., 1964, 15, p. 579.

(15) Reynolds, P.M. Emissivity errors of infra-red pyrometers in relation to spectral response. Brit. J. Appl. Phys., Aug. 1961, 12, pp. 401-405.

(16) Harmer, J.D., and Watts, B.N. Infra-red radiation pyrometer. J. Sci. Instrum., 1955, 32, 167.

(17) Herzfeld, C.M. (ed.). Temperature: its measurement and control in science and industry. 3, Part 1. Basic concepts, standards and methods. New York Reinhold, London: Chapman and Hall, 1962, p. 538.

(18) Reynolds, P.M. Minimising emissivity errors in radiation pyrometry. B.N.F.M.R.A. Research Report (Confidential) A1511, Jan. 1965.

(19) Ackerman, S. See ref. 6, p. 839.

(20) Land, T., Barber, R. Soc. Glass Technology, 1954, 38, 45.

(21) Reynolds, P.M. Industrial trials of a reflecting-wedge radiation pyrometer for measuring the temperature of aluminium. B.N.F.M.R.A. Research Report (Confidential) A1374, Feb. 1962.

(22) Kelsall, D. An automatic emissivity-compensated radiation pyrometer. J. Sci. Instrum., 1963, 40, 1.

(23) Murray, T.P. Polaradiometer - a new instrument for temperature measurement. Rev. Sci. Instrum., June 1967, 38, 6, 791.

(24) Arago, F. Chem. et Phys., 27 (2), p. 89, 1824.

(25) Pyatt, E.C. Some considerations of the errors of brightness and two-colour types of spectral radiation pyrometers. Brit. J. Appl. Phys., 1954, 5, 264-268.

(26) Kostkowski, H.J. and Lee, R.D. See ref.17, p. 449.

(27) Pyatt, E.C. A brightness temperature pyrometer using a photo-conductive cell. J. Sci. Instrum., 1952, 29 (4), pp. 125-127.

(28) Lord, J.S. See ref. 6. p. 865.

(29) Glauert, M.B. The wall jet. J. of Fluid Mech., 1, 525, 1956.

(30) Bakke, P. An experimental investigation of a wall jet. J. of Fluid Mech., 2, Part 5, 467, July 1957.

(31) Seban, R. and Back, L. Velocity and temperature profiles in a wall jet. Int. J. Heat and Mass Transfer, 3, pp. 255 to 265, 1961.

(32) McAdams, W.H. Heat transmission. McGraw-Hill, 3rd Edition, 1954, p. 465.

(33) Gardon, R., Cobonpue, J. Heat transfer between a flat plate and jets of air impinging on it. International developments in heat transfer. Proc. of the 1961-62 International Heat Transfer Conference of the A.S.M.E. pp. 454-460.

(34) Freidman, S.J., Mueller, A.C. Heat transfer to flat surfaces. Proc. General Discussion on Heat Transfer. Inst. Mech. Engrs., London, 1951 (pp. 138-142).

(35) Vickers, J.M.F. "Heat transfer coefficients between fluid jets and normal surfaces". Industrial and Engineering Chemistry, 51, pp.967-972, 1959.

(36) PAI, S.I. Fluid dynamics of jets. D. Van Nostrand Co. Inc., New York, Toronto, London, 1954.

(37) Squire, H.B. The round laminar jet. Quart. J. Mech. and Appl. Maths., Vol. IV, Pt. 3, pp. 322-329, 1951.

(38) Schlichting, H. Boundary layer theory. 4th edn. McGraw Hill, New York, 1960, pp. 681-707.

(39) Baron, T., Alexander, L.G. Momentum, mass, and heat transfer in free jets. Chem. Eng. Prog., April 1951, pp. 181-185.

(40) Bradshaw, P. An introduction to turbulence and its measurement. First edn. 1971. Pergamon Press: Oxford.

(41) Bradshaw, P. Experimental fluid dynamics. Second edn. 1970. Pergamon Press: Oxford.

(42) King, L.V. "On the convection of a heat transfer from small cylinders in a stream of fluid". Phil. Trans. Roy. Soc., London, Ser. A, 214, 1914.

(43) Collis, D.C. and Williams, M.J. "Two-dimensional convection from heated wires at low Reynolds numbers". J. Fluid Mechanics, 6, 1959.

(44) McAdams, W.H. Heat transmission. 3rd edn. McGraw-Hill. pp. 265-266.

(45) Perry, K.P. Heat transfer by convection from a hot gas to a plane surface. Proc. Inst. Mech. Engrs., 1954, pp. 775-780.

(46) Schlichting, H. Boundary layer theory. 4th edn. McGraw-Hill, New York, 1960, pp. 610-625.

(47) Hsu, S.T. Engineering Heat Transfer. D. Van Nostrand Co., Inc. Toronto, New York, London. pp. 269-270.

ACKNOWLEDGEMENTS

I should like to thank Dr. W.E.J. Neal, Senior Tutor in Physics at The University of Aston in Birmingham, for his valuable advice and guidance throughout the preparation of this thesis.

I should also like to thank Alcan International Limited: Banbury for providing the facilities with which to undertake these investigations.

Thanks are also due to the secretarial staff of Alcan International for their willing help and co-operation in preparing the final draft, the staff of the Photographic and Printing department of this Company and Mr. G.E.G. Tucker, Head of Alcan International Computing Department for his co-operation in computing the numerous temperature dependent parameters involved in this thesis.

Finally, I should like to thank my wife for typing the initial draft and for all her encouragement throughout its preparation.